AEC RESEARCH AND DEVELOPMENT REPORT

ORNL-1535
Special
49A

DECLASSIFIED

CLASSIFICATION CHANGED TO:

BY AUTHORITY OF:

BY:

THERMODYNAMIC AND HEAT TRANSFER ANALYSIS
OF THE
AIRCRAFT REACTOR EXPERIMENT

Bernard Lubarsky
NATIONAL ADVISORY COMMITTEE FOR AERONAUTICS

B. L. Greenstreet
AIRCRAFT NUCLEAR PROPULSION DIVISION
OAK RIDGE NATIONAL LABORATORY

ORNL-1535

Contract No. W-7405-eng-26

THERMODYNAMIC AND HEAT TRANSFER ANALYSIS
OF THE
AIRCRAFT REACTOR EXPERIMENT

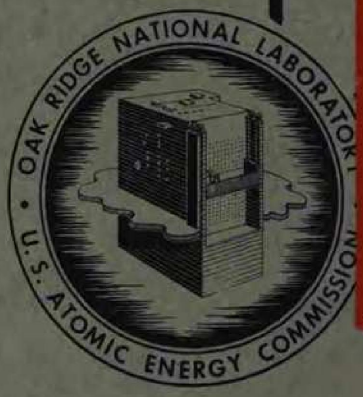Bernard Lubarsky
NATIONAL ADVISORY COMMITTEE FOR AERONAUTICS

B. L. Greenstreet
AIRCRAFT NUCLEAR PROPULSION DIVISION
OAK RIDGE NATIONAL LABORATORY

DATE ISSUED

AUG 1 0 1953

ORNL 1535
Special

INTERNAL DISTRIBUTION

EXTERNAL DISTRIBUTION

FOREWORD

The Aircraft Reactor Experiment utilizes the circulating fluoride-fuel as the primary reactor coolant. It is necessary, however, to employ an additional coolant whose primary function is to cool the reflector and pressure shell. Although liquid sodium will be used as the reflector coolant, the use of NaK had been assumed during the preceding year. Consequently, a considerable amount of consistent, detailed data on the performance characteristics for the reactor system using NaK as the reflector coolant has been assembled. These data are presented in this report. A sufficient number of calculations based upon the use of sodium has been made to assure that the performance with sodium will not deviate significantly from that calculated for NaK. Sodium is being used in preference to NaK because it can be more easily sealed at the pump shaft.

CONTENTS

Chapter 1

INTRODUCTION

The Aircraft Reactor Experiment (ARE) is an experimental, high-temperature, circulating-fuel reactor being constructed by the Aircraft Nuclear Propulsion Division of the Oak Ridge National Laboratory. The fuel is a mixture of fused fluorides, including uranium tetrafluoride; the moderator is beryllium oxide; and the structural material is Inconel. Figure 1 shows a schematic diagram of the reactor, the heat disposal equipment, and the other process equipment necessary to the operation of the reactor; also shown in Fig. 1 are the design-point pressures, temperatures, and flows at various points in the system. This report contains a summary of the more pertinent analytical investigations of thermodynamic and heat transfer properties of the ARE.

Considerably more investigations have been carried out than have been presented; the investigations omitted fall in one of the following categories:

1. investigations relating to systems and items of equipment not actually used in the ARE,

2. investigations relating to systems and items of equipment used in the ARE but with different fluids than those actually used,

3. investigations in which estimated fuel properties were used that were found to be incorrect when additional experimental determinations of fuel properties were made,

4. routine calculations of temperatures and pressures at various points of the system that were of interest only to the detail designer.

For convenience, the investigations are presented as they relate to the following subdivisions of the ARE:

Reactor
Fuel heat disposal system
Reflector coolant heat disposal system
Control rod cooling system
Preheating and monitoring system
Helium supply and vent system
Fill and dump system

The physical properties of the materials used in the reactor are given in Table 1.

TABLE 1. PROPERTIES OF MATERIALS

MATERIAL	THERMAL CONDUCTIVITY $[\text{Btu/hr·ft}^2\ (^\circ\text{F/ft})]$	VISCOSITY (lb/hr·ft)	SPECIFIC HEAT (Btu/lb·$^\circ$F)	DENSITY (lb/ft^3)	REFERENCE*
1. Air	0.0156 at 90.3°F 0.0180 at 190.3°F	4.54×10^{-2} at 90.3°F 5.15×10^{-2} at 190.3°F	0.2399 at 90.3°F 0.2409 at 190.3°F	0.0722 at 90.3°F 0.0611 at 190.3°F	1
2. Aluminum	116 at 64°F 119 at 212°F		0.2220 at 32°F 0.2297 at 212°F	168.5 at 68°F	2
3. Beryllium oxide	0.84 at 1100°F 0.73 at 1300°F 0.68 at 1500°F		0.46 at 1100°F 0.48 at 1300°F 0.50 at 1500°F	142 at 68°F (Porosity –23%) 177 at 68°F (Porosity –0%)	3
4. Copper	222 at 64°F 220 at 212°F		0.1008 at 30°F 0.1014 at 212°F	555.0 at 68°F	2
5. Fused fluorides	1.5	30.3 at 1150°F 21.8 at 1325°F 16.5 at 1500°F	0.26	187	
6. Helium	0.0885 at 100°F 0.1250 at 550°F 0.1650 at 1200°F	0.050 at 100°F 0.075 at 550°F 0.101 at 1200°F	1.24	0.0098 at 100°F 0.0054 at 550°F 0.0033 at 1200°F	4 and 2
7. Inconel	12.4 at 1200°F 13.1 at 1472°F		0.109 at 77 to 212°F	530	5
8. Insulation (cf., chap. 6)					
9. NaK	14.10 at 212°F 15.38 at 752°F	0.496 at 752°F 0.353 at 1292°F	0.210 at 752°F 0.209 at 1112°F 0.213 at 1472°F	48.4 at 752°F 46.1 at 1022°F 43.9 at 1292°F	6
10. Stainless steel	10.4 at 300°F 15.7 at 1500°F		0.1178 at 212°F 0.1519 at 752°F	489 at 32°F	7 and 8
11. Steel	26 at 212°F 21 at 1112°F		0.1178 at 212°F 0.1519 at 752°F	489 at 32°F	8
12. Water	0.343 at 32°F 0.363 at 100°F 0.393 at 200°F	2.43 at 68°F 1.59 at 104°F 1.13 at 140°F	0.99947 at 68°F 0.99869 at 104°F 1.00007 at 140°F	62.36 at 68°F 62.35 at 104°F 62.26 at 140°F	9

*The references are given at the end of this report.

Fig. 1. Reactor and Heat Disposal Equipment.

REACTOR

PRESSURE PULSE RESULTING FROM A SUDDEN CHANGE IN REACTIVITY

The self-controlling features of the ARE are due to the expansion of the fuel with increasing temperature. A transient increase in reactivity produces an attendant increase in temperature that increases the volume of the fuel. Since the reactor has a relatively fixed volume, some of the fuel is forced out of the core and the reactivity is reduced. The entire process occurs in a very short time, and therefore it is necessary to know what pressures will be set up in the fuel tubes when the fuel is rapidly forced out of the core. Figure 2 shows the reactor and connecting piping to the surge tanks. The fuel can expand out of the reactor in either direction, but since the path to the surge tank in one direction (upstream) is considerably shorter than in the other, it will be assumed that all the excess fuel takes the shorter path to the surge tank (this is a conservative simplification). Further assumptions that have been made are:

1. The fuel is incompressible.

2. The pressure pulse is of sufficiently short duration that the fuel in the external piping remains essentially fixed in temperature.

3. The temperature and power variations in the reactor core will be neglected; all the reactor fuel is assumed to be at the mean reactor temperature, and the power generation in the fuel is always equal to the mean power generation.

4. The effects of the pressure pulse on the fuel pumps will be neglected. Precisely what effect this pulse would have on the pumps is unknown, but the pulse will probably be of sufficiently short duration that no permanent damage will be done.

Figure 3a is a schematic diagram of the system to be analyzed. There are two, distinct cases to consider:

the reactor in which the temperature and the density of the fuel change with time and the external piping in which the temperature and density of the fuel are constant. The reactor will be considered first (Fig. 3b). The impulse-momentum equation for any section is

$$(1) \qquad - F \, dt = d(mv) \quad,$$

where
F = differential force on fuel volume, lb,
t = time, sec,
m = mass in fuel volume, slugs,
v = velocity of fuel volume, ft/sec.

For a fuel volume of cross section A, thickness dx, and position x,

$$(2) \qquad m = \rho A \, \Delta x \quad,$$

where
ρ = mass density, slugs/ft^3,
A = tube cross-sectional area, ft^2,
x = distance along the tube measured from the reactor outlet, ft.

Since the fuel is incompressible, all the incremental fuel volume being generated between zero and x by increasing temperature must pass across x (on the way to the reactor inlet and thence to the surge tank) as rapidly as the incremental volume is being generated. The rate at which incremental volume is being generated between zero and x is

$$(3) \qquad \frac{dV}{dt} = \beta A x \frac{d\theta}{dt} \, ,$$

where
V = volume from x = 0 to any arbitrary x, ft^3,
β = coefficient of volumetric expansion, per °F,
θ = fuel temperature, °F.

Since the rate at which the incremental volume is being generated must be equal to the rate at which the volume is crossing x,

(4)
$$\bar{v}A = \beta A x \frac{d\theta}{dt}$$

$$\bar{v} = v - v_0 = \beta x \frac{d\theta}{dt} \quad ,$$

where $\bar{v}$ is the incremental velocity $(v - v_0)$ in ft/sec and the subscript 0 refers to conditions at time zero.

The impulse-momentum equation, Eq. 1, may be rewritten for the volume $A \triangle x$ as

(5)
$$-\triangle F = m \frac{dv}{dt} + v \frac{dm}{dt} \quad .$$

Differentiating Eqs. 2 and 4 gives

(6)
$$\frac{dm}{dt} = A \triangle x \frac{d\rho}{dt}$$

and

(7)
$$\frac{dv}{dt} = \frac{d\bar{v}}{dt} = \beta x \frac{d^2\theta}{dt^2} \quad ,$$

and substituting Eqs. 2, 4, 6, and 7 in Eq. 5 gives

(8)
$$-\triangle F = \rho A \triangle x \beta x \frac{d^2\theta}{dt^2}$$

$$+ \left(\beta x \frac{d\theta}{dt} + v_0 \right) A \triangle x \frac{d\rho}{dt}$$

or

$$-\frac{\triangle F}{\triangle x} = A \left[\beta x \left(\rho \frac{d^2\theta}{dt^2} + \frac{d\rho}{dt} \frac{d\theta}{dt} \right) + v_0 \frac{d\rho}{dt} \right] \quad .$$

Dividing both sides by A and letting $\triangle x$ approach zero gives

(9)
$$-\frac{1}{A} \frac{dF}{dx} = -\frac{dP}{dx} = \beta x \left(\rho \frac{d^2\theta}{dt^2} \right.$$

$$\left. + \frac{d\rho}{dt} \frac{d\theta}{dt} \right) + v_0 \frac{d\rho}{dt} \quad ,$$

where P is pressure in lb/ft^2. The mass density, ρ, may be expressed in terms of the temperature:

(10)
$$\rho = \frac{\rho_0}{1 + \beta(\theta - \theta_0)} \quad .$$

Differentiating Eq. 10 gives

(11)
$$\frac{d\rho}{dt} = -\frac{\rho_0 \beta \frac{d\theta}{dt}}{[1 + \beta(\theta - \theta_0)]^2} \quad .$$

Substituting Eqs. 10 and 11 in Eq. 9 gives

(12)
$$-\frac{d\rho}{dx} = \beta x \left\{ \frac{\rho_0 \frac{d^2\theta}{dt^2}}{1 + \beta(\theta - \theta_0)} \right.$$

$$\left. - \frac{\rho_0 \beta \left(\frac{d\theta}{dt} \right)^2}{[1 + \beta(\theta - \theta_0)]^2} \right\}$$

$$- \frac{v_0 \rho_0 \beta \frac{d\theta}{dt}}{[1 + \beta(\theta - \theta_0)]^2} \quad .$$

Integrating Eq. 12 from $x = 0$ to $x = L$ and rearranging slightly gives

(13)
$$P_m - P_L = \frac{\beta \rho_0 L^2}{2(1 - \beta\theta_0 + \beta\theta)} \left[\frac{d^2\theta}{dt^2} \right.$$

$$\left. - \frac{\beta \left(\frac{d\theta}{dt} \right)^2 + \frac{v_0}{L} \frac{d\theta}{dt}}{1 - \beta\theta_0 + \beta\theta} \right] \quad ,$$

where the subscript m refers to conditions at $x = 0$ and the subscript L refers to conditions at $x = L$. Equation 13 with L set equal to the length of the reactor tubes gives the variations with time of the pressure differential across the reactor core.

For the external piping (Fig. 3c), where the temperature of the fuel is assumed constant, Eqs. 1, 2, and 5 are valid. However, Eq. 3 is not valid, because no incremental volume is generated in the external piping. The external piping, however, must pass all the incremental volume generated

Fig. 2. Fuel Circuit.

MANIFOLD, 2 IN PARALLEL
(EQUIVALENT TO 6 ft OF 2-in. IPS
PLUS 22 ft OF 2-in. IPS)

PUMP   SURGE
        TANK

9 ft OF 1½-in.-OD IPS
2 IN PARALLEL

REACTOR
39 ft OF 1.235-in.-OD x
0.060-in.-WALL IPS
6 IN PARALLEL

PUMP   SURGE
        TANK

(a)

ΔX

X=0   (b)

ΔX

X=0   (c)
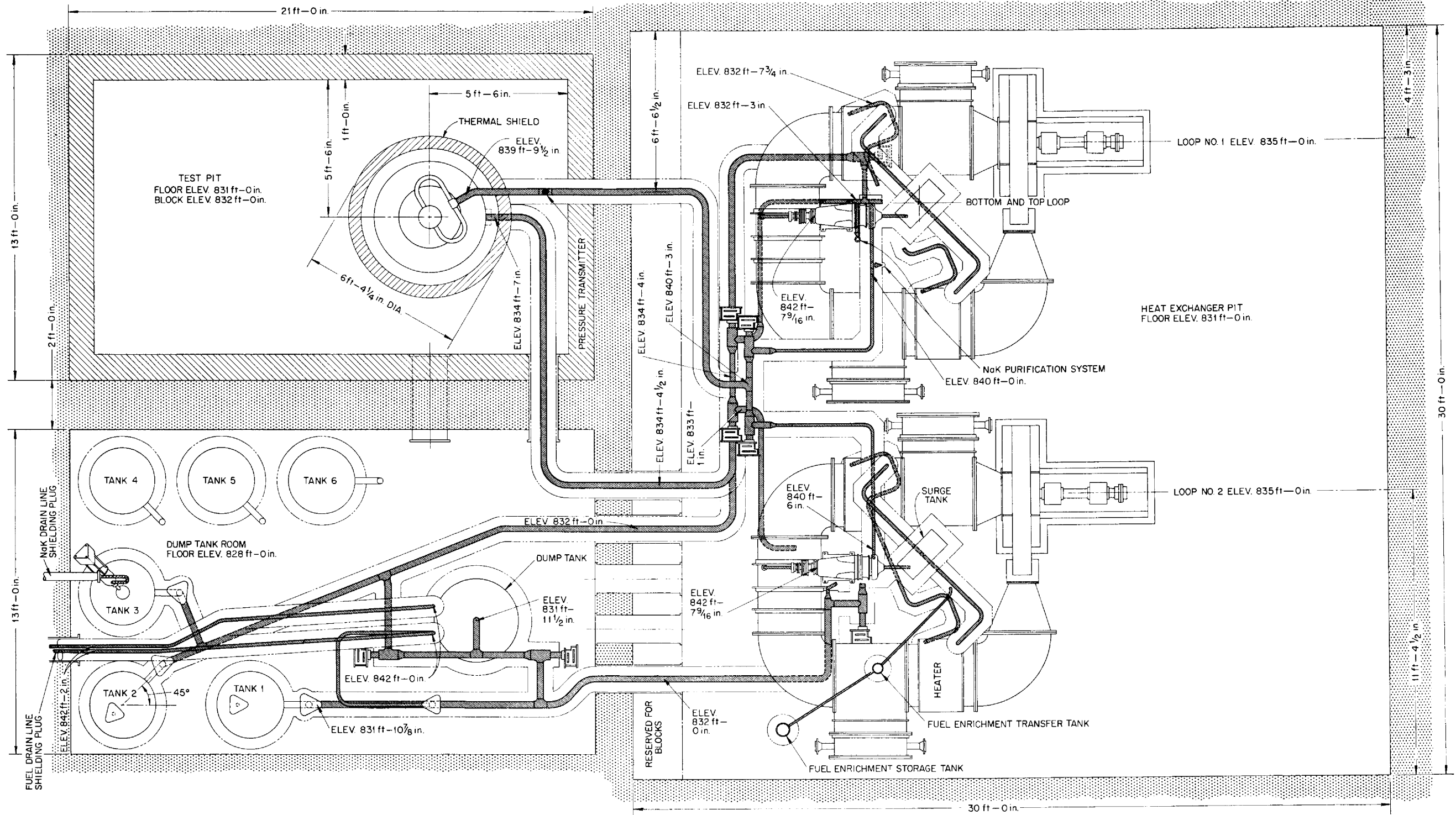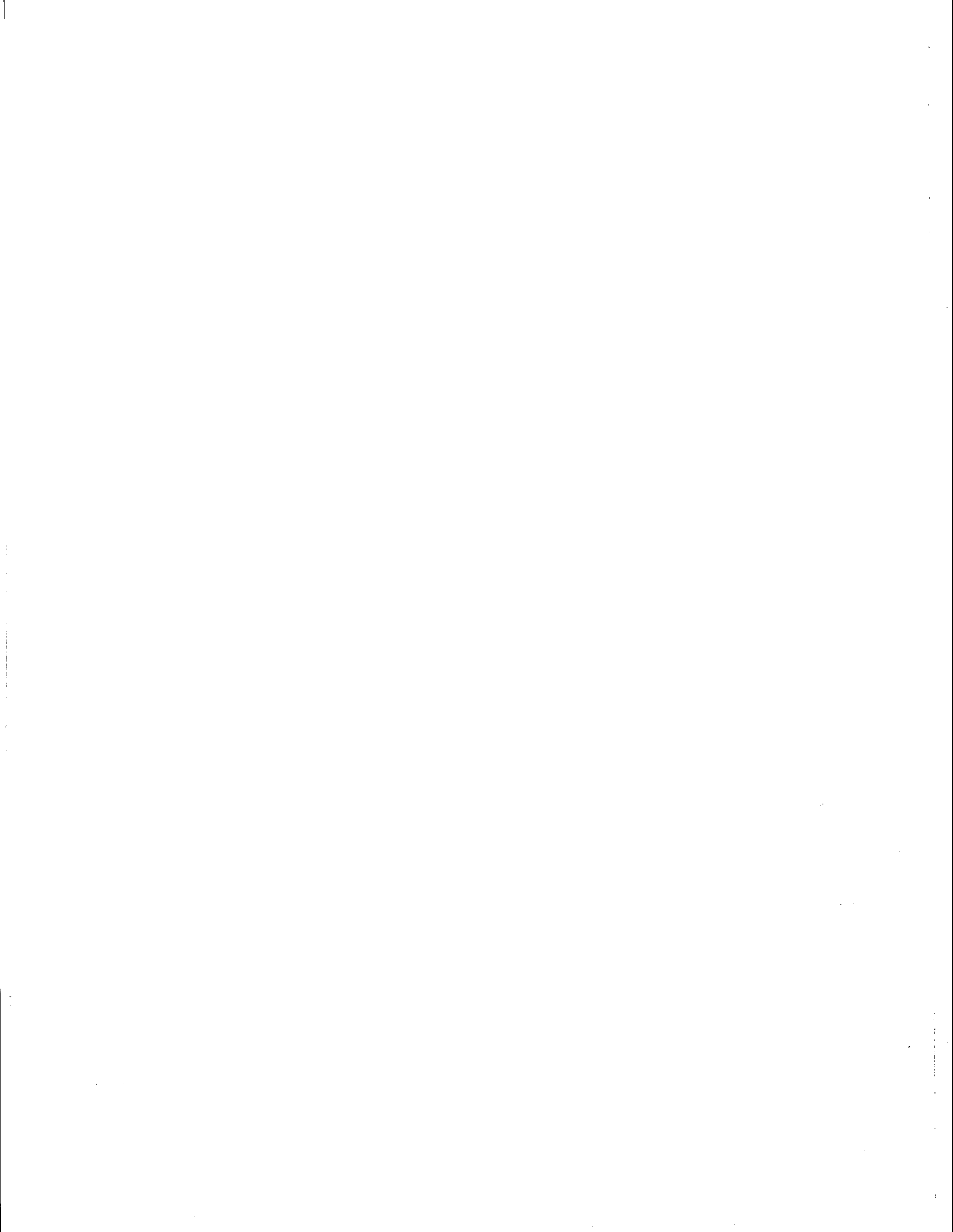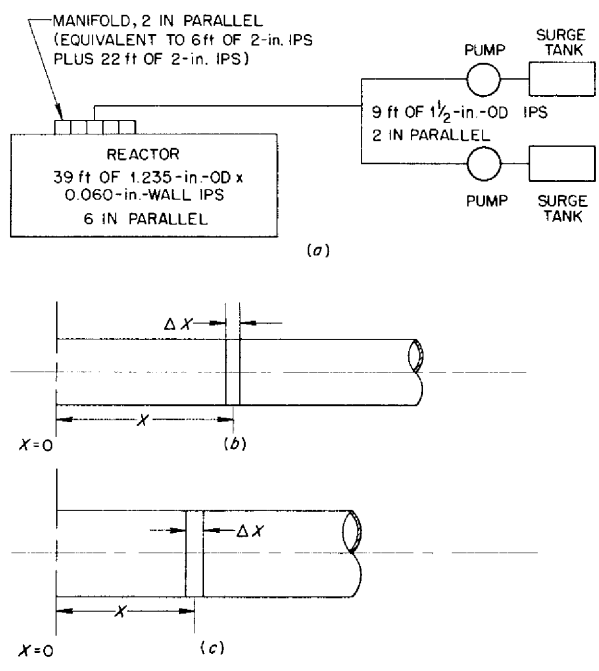
Fig. 3. Reactor and Connecting Piping to Surge Tank. (a) Schematic diagram of system. (b) Internal reactor piping. (c) External piping.

in the core, and therefore Eq. 4 may be rewritten for the external piping:

$$(14) \qquad \bar{v}'A' = \beta V_c \frac{d\theta}{dt} ,$$

$$\bar{v}' = v' - v'_0 = \frac{\beta V_c}{A'} \frac{d\theta}{dt} ,$$

where V_c is the fuel volume in the reactor core in ft^3 and the prime refers to values in the external piping. Equation 6, of course, becomes

$$(15) \qquad \frac{dm}{dt} = 0 ,$$

and Eq. 7 becomes

$$(16) \qquad \frac{dv'}{dt} = \frac{\beta V_c}{A'} \frac{d^2\theta}{dt^2} .$$

Substituting Eqs. 2, 14, 15, and 16 in Eq. 5 gives

$$(17) \qquad -\Delta F' = \rho'A' \, \Delta x \, \frac{\beta V_c}{A'} \frac{d^2\theta}{dt^2} .$$

Since ρ' is constant and equal to ρ_0, Eq. 17 may be rewritten as

$$(18) \qquad -\frac{1}{A'} \frac{\Delta F'}{\Delta x} = -\frac{\Delta P'}{\Delta x} = \frac{\rho_0 \beta V_c}{A'} \frac{d^2\theta}{dt^2} ,$$

or, by letting Δx approach zero,

$$-\frac{dP'}{dx} = \frac{\rho_0 \beta V_c}{A'} \frac{d^2\theta}{dt^2} .$$

Integrating Eq. 18 from $x = 0$ to $x = L'$ gives

$$(19) \qquad P_{\pi}' - P_{L'} = \frac{\rho_0 \beta V_c L'}{A'} \frac{d^2\theta}{dt^2} .$$

Equation 19 with L' set equal to the length of a run of external piping gives the variation with time of the pressure differential across the piping.

In addition to the pressure differential set up by the inertia of the fuel (Eqs. 13 and 19), there are pressure differentials resulting from the change in friction pressure drop associated with change in velocity. These pressure differentials may be evaluated by methods similar to those used above, except that the impulse-momentum equation (Eqs. 1 and 5) is replaced by the customary Fanning equation for the friction pressure drop:

$$(20) \qquad \frac{dP_f}{dx} = \frac{4f}{D} \frac{\rho v^2 - \rho_0 v_0^2}{2} ,$$

where

P_f = change in friction pressure drop, lb/ft^2,
f = friction factor,
D = tube diameter, ft.

Substituting Eqs. 4 and 10 for the reactor core into Eq. 20 gives

$$(21) \qquad \frac{dP_f}{dx} = \frac{2f}{D} \left[\frac{\rho_0 \left(\beta x \frac{d\theta}{dt} + v_0 \right)^2}{1 + \beta(\theta - \theta_0)} - \rho_0 v_0^2 \right]$$

9

or

$$\frac{dP_f}{dx} = \frac{2f\rho_0}{D} \left[\frac{\beta^2 x^2 \left(\frac{d\theta}{dt}\right)^2 + 2\beta x v_0 \frac{d\theta}{dt} + v_0^2}{1 + \beta(\theta - \theta_0)} - v_0^2 \right] .$$

Integrating with respect to x from $x = 0$ to $x = L$ gives

$$(22) \qquad (P_f)_m - (P_f)_L = -\frac{2f\rho_0}{D} \left[\frac{\frac{\beta^2 L^3}{3} \left(\frac{d\theta}{dt}\right)^2 + \beta L^2 v_0 \frac{d\theta}{dt} + v_0^2 L}{1 + \beta(\theta - \theta_0)} - v_0^2 L \right] .$$

Since the equivalent length of piping for friction pressure drop calculations is longer than the actual length to account for bends, exits, entrances, etc., the change in friction pressure drop in the core calculated by using Eq. 22 must be corrected:

$$(23) \quad [(P_f)_m - (P_f)_L]_{corrected}$$

$$= \frac{L_{eq}}{L} [(P_f)_m - (P_f)_L] ,$$

where L_{eq} is the equivalent length for the friction pressure drop, ft.

The change in friction pressure drop in the external piping is calculated in the following manner. Equation 20 is valid, and substituting Eq. 14 in Eq. 20 and noting that $\rho' = \rho_0$ gives

$$(24) \quad \frac{dP_f'}{dx} = \frac{2f'\rho_0}{D'} \left[\left(\frac{\beta V_c \frac{d\theta}{dt}}{A'}\right)^2 \right.$$

$$\left. + \frac{2\beta V_c v_0' \frac{d\theta}{dt}}{A'} \right] .$$

Integrating from $x = 0$ to $x = L'$ gives

$$(25) \quad (P_f')_m - (P_f')_L$$

$$= \frac{2f\rho_0 L'}{D} \left[\left(\frac{\beta V_c \frac{d\theta}{dt}}{A'}\right)^2 + 2v_0' \frac{\beta V_c \frac{d\theta}{dt}}{A'} \right]$$

and

$$(26) \quad [(P_f')_m - (P_f')_L]_{corrected}$$

$$= \frac{L_{eq}'}{L'} [(P_f')_m - (P_f')_L] .$$

Hence, if the variations of θ, $d\theta/dt$, and $d^2\theta/dt^2$ with time are known, the total pressure pulse can be calculated because all other quantities are known. The variation of the temperature and its first two derivatives with respect to time, as a result of a 0.5% step increase in reactivity, were evaluated on an electronic analog computer. The results are shown in Fig. 4. The other constants required for the evaluation of the pressure pulse are:

$A = 0.0407$ ft^2 (6 tubes in parallel, 1.255 in. OD by 0.060-in. wall),

$\beta = 8 \times 10^{-5}$ per °F,

$v_0 = -3.70$ ft/sec,

$\rho_0 = 5.81$ slugs/ft^3,

$\theta_0 = 1325$°F,

$L = 42$ ft,

$A' = 0.0233$ ft^2 (1 pipe, 2 in. IPS), 0.0283 ft^2 (2 pipes in parallel, 1 1/2 in. IPS),

$v_0' = -6.45, -5.31$ ft/sec,

$V_c = 1.71$ ft^3,

$L' = 28, 9$ ft,

$D = 0.0929$ ft,

$f = 0.0075,$

$L_{eq} = 52$ ft

$D' = 0.1721, 0.1341$ ft,

$f' = 0.0058, 0.0062,$

$L_{eq}' = 43, 15$ ft.
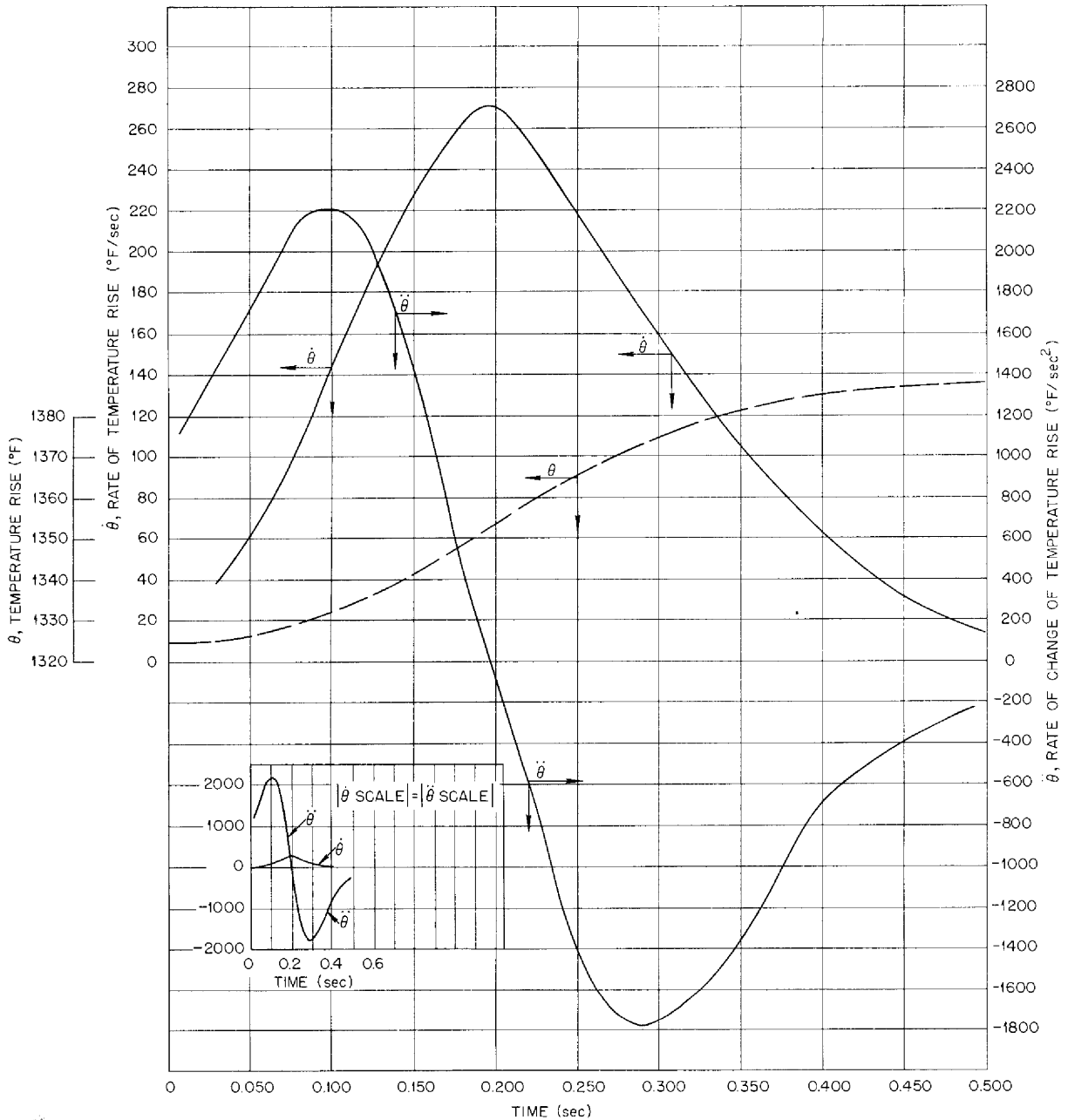
Fig. 4. **Temperature Rise, Rate of Temperature Rise, and Rate of Change of Temperature Rise vs. Time,** $\Delta k / k$ **= 0.005.** Data from ARE simulator.

The final results of the evaluation of Eqs. 13, 19, 23, and 26 are shown in Fig. 5, where the incremental pressure at the reactor outlet (position of maximum incremental pressure) is plotted against time. The maximum incremental pressure encountered is about 27 psi, and it occurs about 100 msec after the introduction of the step increase in reactivity.

CORE POWER DISTRIBUTION

The power distribution in the ARE reactor was estimated theoretically,

11
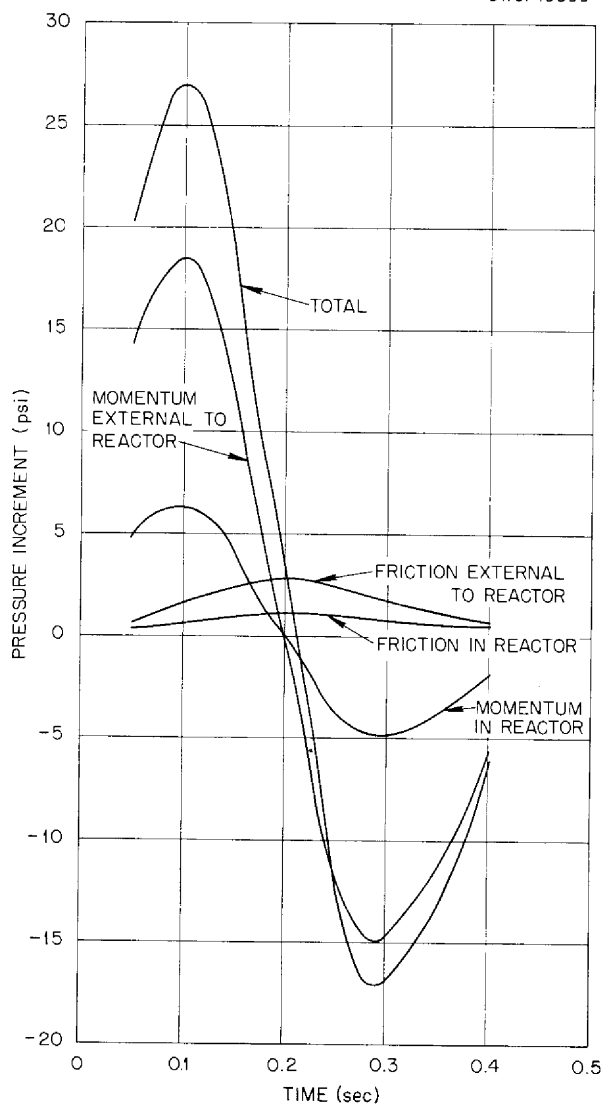
Fig. 5.   Incremental Pressure at Reactor Outlet as a Result of a $\Delta k/k$ of 0.005 vs. Time.

and the estimate was checked experi-
mentally by the physics groups of the
Laboratory.   The power distributions
used in the calculations in this
report are presented in Figs. 6, 7, and
8.   Figure 6 shows the variation of
fission heat generated in the fuel with
distance from reactor center; Fig. 7
shows the variation of neutron heating
of the moderator; Fig. 8 shows the
variation of gamma heating (average,
based on the assumption that the
reactor is homogenized).   The maximum
and average values of the fission,
neutron, and gamma heating are given
in Table 2.
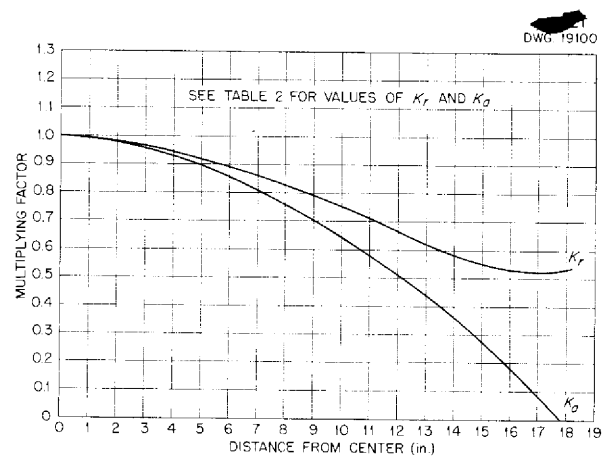
Fig. 6.   Fission Heat Generated in Fuel as a Function of Distance from Reactor Center.
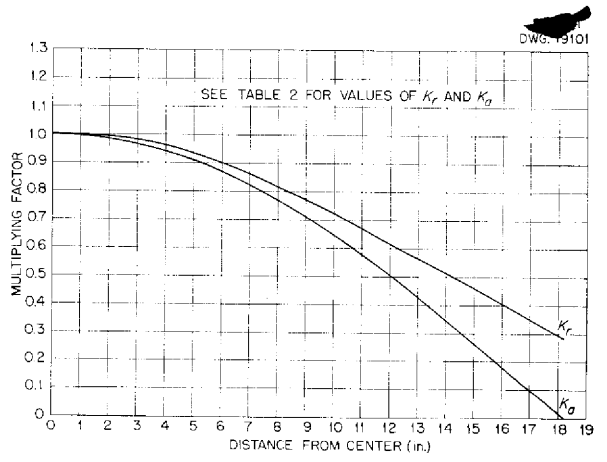
Fig. 7. Neutron Heating of Moderator as a Function of Distance from Reactor Center.
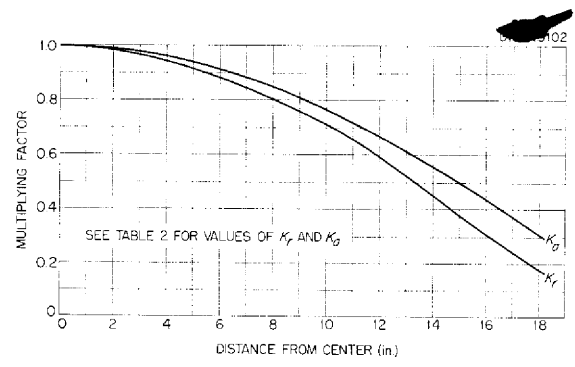
Fig. 8. Gamma Heating as a Function of Distance from Reactor Center.

12

TABLE 2. MAXIMUM AND AVERAGE VALUES OF FISSION, NEUTRON, AND GAMMA HEATING IN THE ARE

TYPE OF HEATING	MAXIMUM HEATING (kw/in.^{3})	AVERAGE HEATING (kw/in.^{3})	AXIAL MAXIMUM-TO-AVERAGE RATIO, K_a	RADIAL MAXIMUM-TO-AVERAGE RATIO, K_r
Fission (in fuel only)	2.78	1.22	1.55	1.48
Neutron (in moderator only)	0.012	0.0052	1.55	1.66
Gamma (average for homogenized reactor)	0.024	0.011	1.32	1.82

TEMPERATURE PROFILE IN A TYPICAL SECTION OF THE CORE LATTICE

Heat is removed from the moderator region of the reactor core by the fuel (Fig. 9). In a case in which no heat is transferred across the outer surface of a column of beryllium oxide blocks, the heat removed by the fuel flowing in the tube through this column would be the heat generated within the fuel, the metal of the tube, the NaK filling the gap between the tube and the column of blocks, and the blocks. For this hypothetical case, the temperature profile existing between the center line of the fuel tube and the outer periphery of the blocks can be calculated.

In the actual case, heat is transferred into the rod holes, through the "boundary" between the moderator and the reflector, and through the upper and lower surfaces of the moderator region. Thus, the calculated temperature profile has no meaning other than to show the maximum temperature gradients that can exist in the components of the moderator region. For the hypothetical case, the maximum temperature gradients will exist at the point of maximum heat generation. Therefore, for the temperature profile calculations, heat generation rates corresponding to the maximum values expected in the reactor core were used.

If the heat generated in a hollow cylinder is transferred through the inner surface, the temperature gradient between the outer and inner surfaces of the cylinder is given by

$$(27) \quad \Delta T = \frac{G}{2k} \left[\frac{1}{2} \left(r_i^2 - r_o^2 \right) + r_o^2 \ln \frac{r_o}{r_i} \right] ,$$

where
ΔT = temperature difference, °F,
G = heat generation rate, Btu/sec·ft^3,
k = thermal conductivity, Btu/sec·ft^2 (°F/ft),
r_i = inner radius, ft,
r_o = outer radius, ft.

On the other hand, the temperature gradient necessary for the transfer of heat across the hollow cylinder is

$$(28) \quad \Delta T = \frac{Q_t}{\dfrac{k}{\tau} A_m} ,$$

$$A_m = \frac{2\pi(r_o - r_i)}{\ln \dfrac{r_o}{r_i}} ,$$

where
Q_t = heat transferred per foot of length, Btu/sec,
τ = thickness $(r_o - r_i)$, ft,
A_m = mean area per foot of length, ft^2.

13

DWG 16336A

REGULATING ROD ASSEMBLY
SAFETY ROD GUIDE SLEEVE
SAFETY ROD ASSEMBLY
TUBE EXTENSION
THERMAL SHIELD CAP
THERMAL SHIELD TOP
FUEL INLET MANIFOLD

THERMOCOUPLE LAYOUT
CORE ASSEMBLY
REFLECTOR COOLANT TUBES
FUEL TUBES
PRESSURE SHELL
BOTTOM HEADER
THERMAL SHIELD CAP

TOP HEADER
TOP TUBE SHEET
HEATERS
BeO MODERATOR AND REFLECTOR
THERMAL SHIELD ASSEMBLY
BOTTOM TUBE SHEET
STUD
SUPPORT ASSEMBLY
FUEL OUTLET MANIFOLD
THERMAL SHIELD BOTTOM

80 1/2 in. REF.
23 5/8 in. REF.

SUPPORT ASSEMBLY
HELIUM MANIFOLD

0 2 4 6 8 12 16
SCALE IN INCHES

ASSEMBLY SEQUENCE

STEP 1: ASSEMBLE REACTOR ASSEMBLY TO HELIUM MANIFOLD TUBES.
STEP 2: SET THERMAL SHIELD CAP AND THERMAL SHIELD BOTTOM IN PLACE AND SLIP TUBES THROUGH.
STEP 3: INSULATE MANIFOLD TOP AND BRAZE TO TUBES.
STEP 3a: INSERT SPRING AND SHOCK TUBE.
STEP 3b: ASSEMBLE AND ADJUST ORIFICES
STEP 3c: COMPLETE MANIFOLD.
STEP 4: ASSEMBLE REACTOR ASSEMBLY WITH SUPPORT ASSEMBLY.
STEP 5: ASSEMBLE STUD WITH REACTOR ASSEMBLY AND SUPPORT ASSEMBLY.
STEP 6: ASSEMBLE THERMAL SHIELD CAP WITH HELIUM MANIFOLD.
STEP 7: ASSEMBLE THERMAL SHIELD CAP LOOSELY WITH COOLANT LINE ANNULUS OF REACTOR ASSEMBLY.
STEP 8: WELD TUBE EXTENSION TO SAFETY ROD GUIDE SLEEVE AND INSTRUMENT GUIDE SLEEVE, 6 REQ'D.
STEP 9: CONNECT ALL PIPING.

STEP 10: TEST PER TESTING SCHEDULE.
STEP 11: INSTALL HEATERS, CONNECT AND TEST.
STEP 11a: INSTALL THERMOCOUPLE LAYOUT.
STEP 12: ASSEMBLE THERMAL SHIELD BOTTOM.
STEP 13: ASSEMBLE BALANCE OF THERMAL SHIELD ASSEMBLY, THERMAL SHIELD TOP AND THERMAL SHIELD CAP AND WELD CLOSED.
STEP 14: SEAL ALL JOINTS OF ASSEMBLY OF THERMAL SHIELD ASSEMBLY, THERMAL SHIELD CAP, THERMAL SHIELD BOTTOM, THERMAL SHIELD TOP AND THERMAL SHIELD CAP WITH INSULATING CEMENT, J-M NO. 400 OR EQUIVALENT.
STEP 15: INSULATE HELIUM MANIFOLD WITH 2-in. LAYER J-M SPONGE FELTED INSULATION, SEAL ALL JOINTS WITH INSULATING CEMENT, J-M NO. 400 OR EQUIVALENT.
STEP 16: SEE OPERATING PROCEDURE.

Fig. 9.   Vertical Cross Section of Reactor.

Therefore, when heat is both transferred across and generated within a hollow cylinder,

$$(29) \quad \Delta T = \frac{Q_t}{\frac{k}{\tau} A_m} + \frac{G}{2k} \left[\frac{1}{2} (r_i^2 - r_o^2) + r_o^2 \ln \frac{r_o}{r_i} \right].$$

The temperature at any radius in a hollow cylinder in which there is internal heat generation and the heat is transferred through the inner surface is given by

$$(30) \quad T = \frac{G}{2k} \left[\frac{1}{2} (r_i^2 - r^2) + r_o^2 \ln \frac{r}{r_i} \right] + T_i ,$$

where

T = temperature at any radius r, °F,
r = any radius within the cylinder, ft,
T_i = temperature at r_i, °F.

The heat generated per foot of length of the cylinder can be calculated from

$$(31) \quad Q = G\pi(r_o^2 - r_i^2) ,$$

where Q is the heat generated per foot of length, Btu/sec.

The calculations of temperatures and temperature differences were made from the following data for beryllium oxide, NaK, and the metal tube.

Beryllium Oxide Block. The beryllium oxide block is hexagonal in cross section (3.73 in. across flats). For simplicity in calculation, the block was assumed to be a circular cylinder of equivalent cross-sectional area, with an outside radius of 1.960 in. and an inside radius of 0.630 inch. The temperature difference between the outer and inner surfaces is due entirely to internal heat generation. Therefore,

$$\Delta T = \frac{G}{2k} \left[\frac{1}{2} (r_i^2 - r_o^2) + r_o^2 \ln \frac{r_o}{r_i} \right].$$

NaK. The outer and inner radii of the NaK annulus, measured from the center of the cylinder, are 0.630 and 0.618 in., respectively. Since the NaK is nearly stagnant, the temperature gradient through the NaK is

$$\Delta T = \frac{Q_t}{\frac{k}{\tau} A_m} + \frac{G}{2k} \left[\frac{1}{2} (r_i^2 - r_o^2) + r_o^2 \ln \frac{r_o}{r_i} \right] ,$$

where Q_t is the heat generated in the beryllium oxide.

Metal Tube. The outside radius of the metal tube is 0.618 in., and the inside radius is 0.558 inch. The expression for the temperature gradient in the tube is the same as that for NaK, except that Q_t is the heat generated in the beryllium oxide plus the heat generated in the NaK.

The amount of heat generation in the fuel is proportional to the length of time the fuel resides in the reactor core. Thus high-velocity fuel will have less heat generated within it than fuel flowing at a low velocity and, correspondingly, its temperature will be lower. Upon looking at the velocity profile of fuel flowing in a fuel tube, it is seen that the maximum velocity is at the center and that the minimum velocity is at the tube wall. From this, it can be seen that a temperature gradient will exist between the outer surface and the center of the fuel. This temperature gradient can be determined, and the expression $(T_o - T_{mm})/Gr_o^2$, in which T_o is the temperature of the outer surface of the fuel, °F, and T_{mm} is the temperature of the fuel at the center of the tube, °F, has been plotted as a function of Reynolds' and Prandtl's moduli by Poppendiek and Palmer.[10] The fuel also has a temperature gradient between the center and outer surface, which is given by

$$\Delta T = \frac{Q_t}{hA} ,$$

$$h = 0.023 \frac{k}{D} N_R^{0.8} N_{Pr}^{0.4} ,$$

15

where

  h = coefficient of heat transfer by convection, Btu/sec·ft^2·°F,

  A = area of the inside surface of the metal tube per foot of length, ft^2,

  D = hydraulic diameter of the fuel tube, ft,

  N_R = Reynolds' modulus,

  N_{Pr} = Prandtl's modulus,

  Q_t = heat generated in the beryllium oxide plus the heat generated in the NaK plus the heat generated in the metal tube.

From this it is seen that the total temperature gradient in the fuel is

$$\Delta T = \frac{Q_t}{hA} + \Delta T \text{ (resulting from internal heat generation).}$$

For the fuel, the physical characteristics are:

Radius, r_o	0.558 in.
Temperature, T	1170°F
Viscosity, μ	8.27 x 10^{-3} lb/sec·ft
Density, ρ	187 lb/ft^3

Specific heat, c_p	0.26 Btu/lb·°F
Thermal conductivity, k	4.17 x 10^{-4} Btu/sec·ft^2 (°F/ft)

The following are the maximum expected heat generation rates for the various components:

COMPONENT	G (Btu/sec·ft^3)
BeO	62.21
NaK	41.47
Metal tube	41.47
Fuel	4838

The results of the calculations of temperature differences for the various components are:

COMPONENT	ΔT (°F)
Fuel	81.08
Metal tube	22.97
NaK	3.08
BeO	108.00
Total	215.13

Thus the maximum temperature is 1170 + 215 = 1385°F. A plot of temperature vs. distance from fuel tube center is shown on Fig. 10.

DWG. 19103
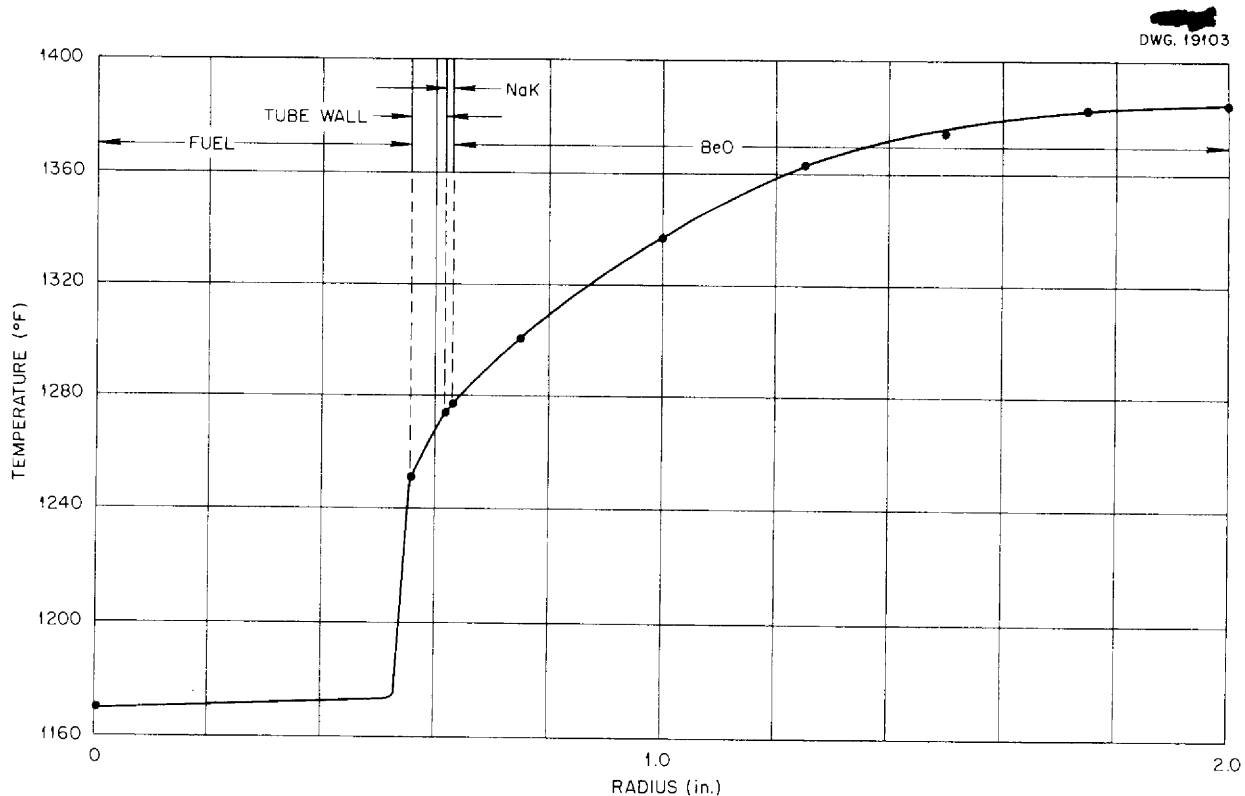
Fig. 10.   Temperature Profile in Core Lattice.

FLOW OF REFLECTOR COOLANT THROUGH CORE

In the ARE, the pressure shell, the moderator, and the thimbles of the control rod and instrument holes are cooled by the circulation of NaK. The NaK circuit (reflector coolant circuit) is shown in Fig. 1.

The coolant enters the pressure shell at the bottom, flows through the lattice, and leaves at the top (Fig. 9). The flow through the core lattice is divided among the annulus between the outer periphery of the reflector and moderator can and the pressure shell, the tubes leading through the reflector blocks, and the annuli around the rod and instrument holes. For adequate cooling of the moderator and pressure shell, it is necessary to have only a minimum amount of coolant flowing in the annuli around the rod and instrument holes. The additional heat that must be removed from the thimbles will be carried away by the helium that cools the rods and instruments. To obtain this minimum flow, orifice plates (Fig. 11) were placed in the annuli.

There will be a pressure drop in the fluid when it enters the pressure shell because of expansion, and when it leaves there will be a further pressure drop because of contraction. In the spaces between the tube sheets and the pressure shell above and below the core lattice, which will act as plenum chambers, the coolant velocity will be effectively zero. Thus the pressure drop in these regions will be very small. The pressure drop in the coolant flowing through the core lattice will be due to contraction, friction, and expansion. Since the pressure drop of the fluid inside the pressure shell is due almost entirely to that in the core lattice, the flow through the various paths will be directly proportional to the respective resistances of the paths.

The loss in pressure by contraction is given by

$$(32) \qquad \Delta P_c = k_c \frac{\rho v_1^2}{2g} \,,$$

where k_c is a constant given by McAdams (cf., p. 122 of ref. 11); the expansion pressure drop is given by

$$(33) \qquad \Delta P_e = \frac{\rho (v_1 - v_2)^2}{2g} \; ;$$

and the friction pressure drop for turbulent flow in either a tube or an annulus is given by

$$(34) \qquad \Delta P_f = 4f \frac{L}{D} \frac{\rho v^2}{2g} \,.$$

The equation for the friction factor is

$$(35) \qquad f = \frac{0.046}{N_R^{0.2}} \,.$$

The meanings and units of the symbols used in Eqs. 32 through 35 are:

ΔP = pressure drop, lb/ft^2,

f = friction factor, dimensionless,

L = length, ft,

D = hydraulic diameter, ft,

ρ = density, lb/ft^3,

v = average velocity, ft/sec,

g = gravitational acceleration, 32.2 ft/sec^2,

k_c = constant, dimensionless,

v_1 = average linear velocity upstream, ft/sec,

v_2 = average linear velocity downstream, ft/sec,

N_R = Reynolds' number.

The subscripts have the following meanings:

c = contraction,

e = expansion,

f = friction.

All the annuli around the control rod and instrument holes have the same dimensions: the outside diameter, D_o, is 3.652 in. and the inside diameter, D_i, is 3.000 inches. There are two instrument holes, three safety rods, and one regulating rod; thus there are six holes and six corresponding annuli. Where the NaK enters at the bottom of the annuli (Fig. 9), there are orifice plates (Fig. 11). These orifice plates reduce the outside diameters of the annuli to 3.140 in.; the length of each orifice plate is 1.00 in.; and the length of the remainder of each annulus is 35.25 inches. The annulus
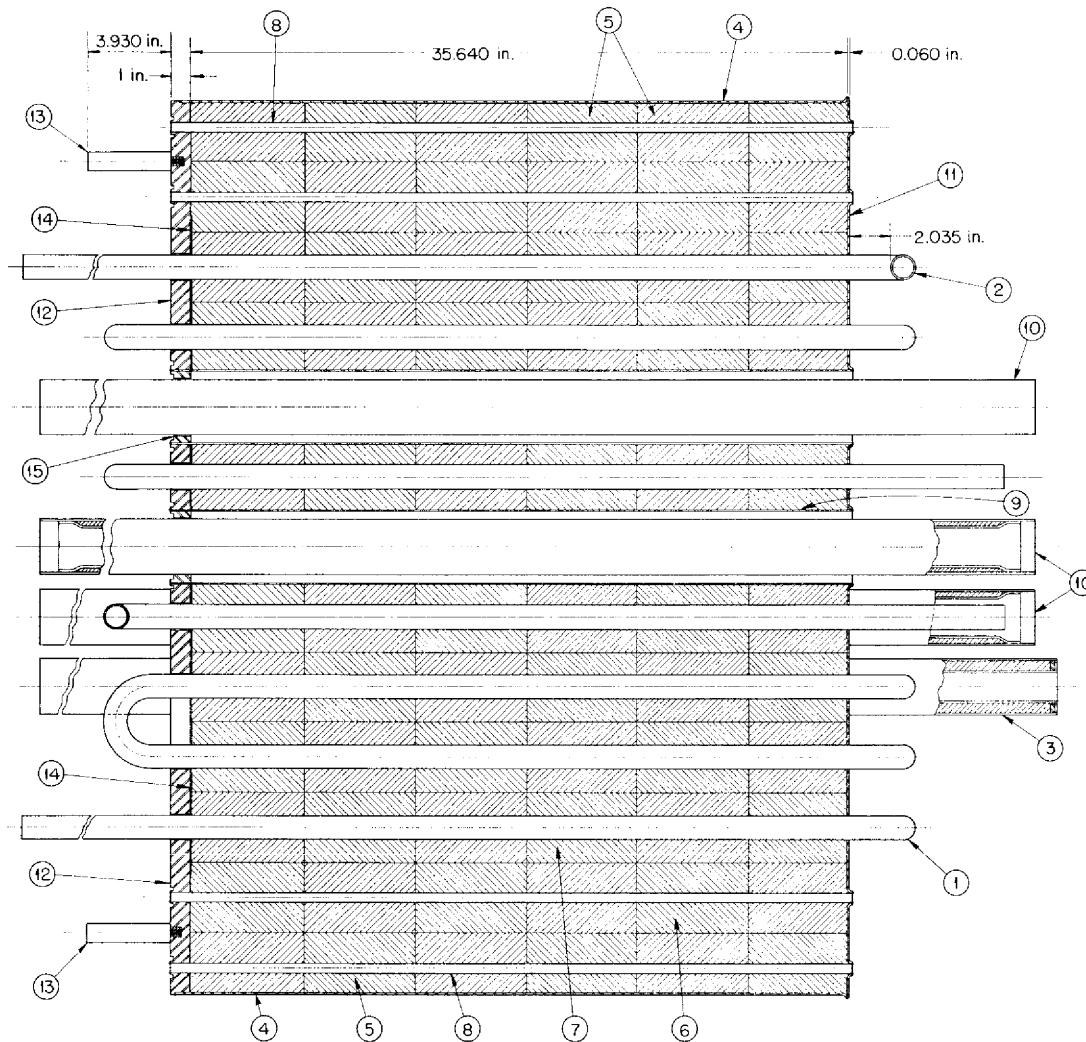
PARTS LIST

1   INCONEL TUBE COIL A
2   INCONEL TUBE COIL B
3   INCONEL INSTRUMENT TUBE SUB-ASSEMBLY
4   INCONEL CAN
5   BeO REFLECTOR EDGE BLOCK
6   BeO REFLECTOR BLOCK
7   BeO CORE BLOCK
8   INCONEL REFLECTOR COOLANT TUBES
9   INCONEL CORE SLEEVE
10 INCONEL SAFETY ROD GUIDE SLEEVE
11 INCONEL TOP TUBE SHEET
12 INCONEL BOTTOM TUBE SHEET
13 INCONEL SUPPORT STUDS
14 INCONEL SPACER
15 INCONEL ORIFICE PLATE

ASSEMBLY SEQUENCE

STEP 1: WELD ITEMS 8, 9 AND 15 TO ITEM 12,
         9 AND 15 WELDED TOGETHER TO ITEM 12
STEP 2: ASSEMBLE ITEM 13 WITH ITEM 12
STEP 3: ASSEMBLE ITEMS 1 AND 2 WITH ITEM 12,
         THEN ITEM 14 WITH ITEMS 1, 2 AND 8
STEP 4: ASSEMBLE ITEM 7 WITH ITEMS 1 AND 2
STEP 5: ASSEMBLE ITEM 6 WITH ITEM 8
STEP 6: ASSEMBLE ITEM 5
STEP 7: ASSEMBLE AND WELD ITEM 4 TO ITEM 12
STEP 8: WELD ITEMS 8 AND 9 TO ITEM 11
STEP 9: WELD ITEM 4 TO ITEM 11

Fig. 11.   Core and Reflector Assembly Elevation Section.

between the pressure shell and the outer periphery of the moderator can has an outside diameter of 48.57 in.; the gap width is 1/16 in.; and the path length through this annulus is 36.25 inches.

In the reflector region, there are 79 tubes, one through each column of beryllium oxide blocks. Each of these has an inside diameter of 0.49 in., and is 36.25 in. long.

The coolant is carried to and from the pressure shell by 2 1/2-in. schedule-40 pipe. Since the NaK flowing through the reactor pressure shell and core lattice is almost isothermal, the physical properties were considered to be constant. The values of density and viscosity used were, respectively,

$$\rho = 44.5 \text{ lb/ft}^3$$

and

$$\mu = 0.36 \text{ lb/hr} \cdot \text{ft} .$$

By using Eqs. 32 and 33, the inlet and outlet losses of the pressure shell were calculated to be

$$\Delta P \text{ (inlet)} = 156.3 \text{ lb/ft}^2$$

and

$$\Delta P \text{ (outlet)} = 78.15 \text{ lb/ft}^2 .$$

From Eqs. 32 through 35 and the assumption that the distribution of flow through the core lattice depends only on the relative resistance of each path, the distribution of flow was found, by trial and error, to be:

PATH	FLOW RATE (ft^3/sec)
Large annulus	0.108
Tubes through reflector	0.272
Six annuli	0.120

The pressure drop through the lattice, which is the loss in pressure experienced by the fluid flowing through one path, was found to be

$$\Delta P = 19.49 \text{ lb/ft}^2 .$$

If the pressure drop in the spaces above and below the core lattice is neglected, the total pressure drop is

$$\Delta P = 253.9 \text{ lb/ft}^2$$
$$= 1.76 \text{ lb/in.}^2 .$$

HEAT REMOVAL BY THE REFLECTOR COOLANT

A cross section of the reactor is shown in Fig. 9; a plan view is shown in Fig. 12. Molten NaK is circulated through the reactor to remove the heat generated in the reflector and to cool the pressure shell and the walls of rod and instrument holes. In passing through the reactor, heat is removed from the following sources in the reactor by the NaK:

1. heat generated in the reflector,
2. heat generated in the pressure shell,
3. heat generated in the NaK,
4. heat transferred from the reactor core
   a. through the serpentine elbows,
   b. through the tube sheets,
   c. through the "boundary" between the core and the reflector,
   d. through the walls of the rod and instrument holes.

The NaK in the interstices of the moderator blocks in both the reactor core and reflector is almost stagnant and, for the purposes of the following calculations, is assumed to be entirely stagnant. It is assumed that the electric heaters on the pressure shell add sufficient heat to the system to just balance the heat loss to the environment; therefore it is also assumed that there is no net heat flow across the outside of the pressure shell.

Heat Generated in the Reflector. The following values for gamma and neutron heating of the reflector were obtained from the section on "Core Power Distribution."

Gamma Heat Generation:

Peak gamma heating (at center of core), Btu/sec·in.[3]	0.023
Ratio of maximum gamma heating at a radius of 18 in. to peak gamma heating	0.20
Maximum gamma heating at a radius of 24 in.	0.0
Ratio of maximum gamma heating at any radius to average gamma heating at the same radius	1.32

DWG.E-A-1A

THERMAL SHIELD ASSEMBLY

PRESSURE SHELL
TOP HEAD ASSEMBLY

FUEL OUTLET
MANIFOLD

SAFETY ROD
EXTENSION GUIDE

INSTRUMENT TUBE
EXTENSION GUIDE

INCHES
0 3 6 9 12 15
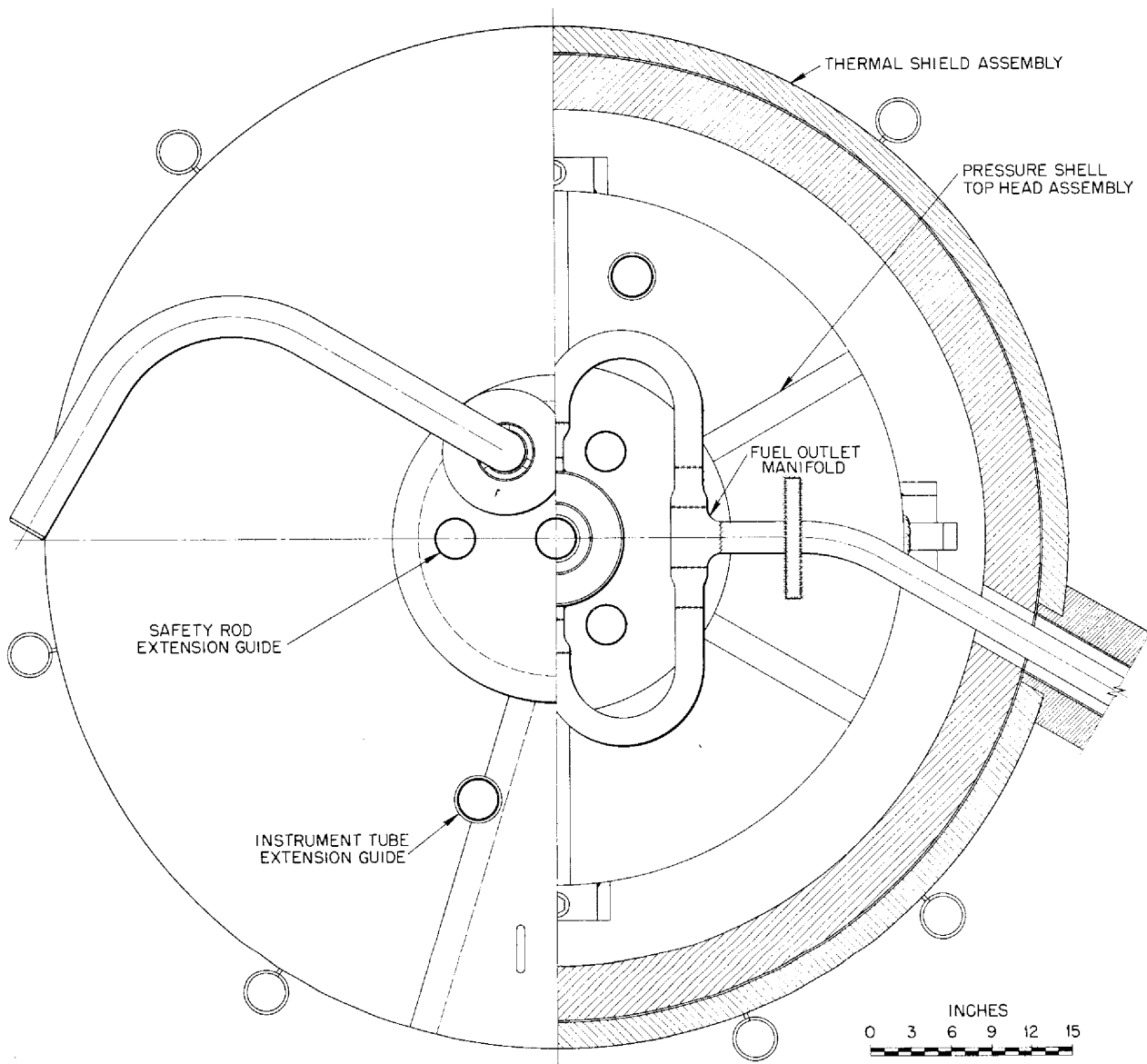
Fig. 12. Plan View of Reactor.

Neutron Heat Generation:

Peak neutron heating in beryllium oxide (at center of core), Btu/sec·in.^{3}	0.011
Ratio of maximum neutron heating at a radius of 18 in. to peak neutron heating	0.30
Neutron heating of the reflector at a radius of 22 1/2 in.	0.0
Ratio of maximum neutron heating at any radius to average neutron heating at the same radius	1.55

Neutron heating occurs only in the beryllium oxide, which constitutes about 78.5% of the reactor.

It is assumed that within the reflector the gamma and the neutron heat generation vary linearly with radial distance. That this assumption is fairly valid may be observed from Figs. 7 and 8. The following equations for the average gamma and neutron heat generation at any radius within the reflector can be written:

(36) $\quad q_\gamma = 0.00460 - 0.000767 \, (R - 18)$,
$$18 \leq R \leq 24,$$

(37) $\quad q_n = 0.00260 - 0.000575 \, (R - 18)$,
$$18 \leq R \leq 22.5 ,$$

(38) $\quad q_n = 0$, $\quad R > 22.5$,

where
q = heat generation, Btu/sec·in.^{3},
R = radius, inches.

The total heat generation, Q, is

(39) $\quad Q_\gamma = \int_{18}^{24} [0.00460$
$$- 0.000767 \, (R - 18)] \; 2\pi R \; dR$$
$$= 40.7 \text{ Btu/sec} ,$$

(40) $\quad Q_n = \int_{18}^{22.5} [0.00210$
$$- 0.000467 \, (R - 18)] \; 2\pi R \; dR$$
$$= 9.5 \text{ Btu/sec} ,$$

(41) $\quad Q = Q_\gamma + Q_n = 50.2 \text{ Btu/sec}$.

The heat generated in the reflector is removed by the NaK through various interfaces; the temperature limitations of the beryllium oxide and associated structure are sufficiently far above the NaK temperature that temperature patterns in the reflector need not be calculated.

Heat Generated in the Pressure Shell.
The heat generated in the Inconel pressure shell is due to gamma attenuation and fast-neutron scattering. The actual variation of heat generation with position in the top head is shown in Fig. 13. The curve may be approximated by the exponential relationship

(42) $\quad q' = 13,200 \; e^{-9.20x}$,

where
q' = heat generation, Btu/hr·ft^3,
x = distance from inside surface, ft.

The heat generation in the bottom head and barrel is actually less than this, but to be conservative, it is assumed that the curve may be used. The total heat generation, Q, in a flat plate of thickness τ is given by

(43) $\quad Q = \int_0^\tau 13,200 \; e^{-9.20x} \; dx$
$$= 1450 \; (1 - e^{-9.20\tau}) ,$$

where τ is in feet.

The Inconel pressure shell is constructed of 2-in.-thick plate reinforced to 4 in. in thickness at critical locations in the heads. Evaluation of Eq. 43 for thicknesses, τ, of 1/6 and 1/3 ft gives
$$Q = 1135 \text{ Btu/hr·ft}^2$$
and
$$Q = 1380 \text{ Btu/hr·ft}^2 ,$$
respectively.

If the barrel is treated as a flat plate, the total area of the 2-in.-thick material is 72.5 ft^2, and the total area of the 4-in.-thick material is 9.5 ft^2. Therefore the total heat generation is 95,300 Btu/hr, or 26.5 Btu/sec. This value is probably high, but because Fig. 13 is approximate, a conservative value is desirable.

Temperature of Pressure Shell.
Inasmuch as the allowable design stress in the pressure shell is a function of the pressure shell temperature, the temperature pattern in the pressure shell head (the most critical portion of the pressure shell from the standpoint of both stress and temperature) must be calculated.

The pressure shell will be treated as a flat plate in which there is internal heat generation. One side of the plate is insulated and the other side is cooled by circulating NaK.

The differential equation, then, is:

(44) $\quad \dfrac{d^2\theta}{dx^2} = -\dfrac{q'}{k}$,

where
q' = heat generation, Btu/hr·ft^3 = $13,200 \; e^{-9.20x}$,
$\theta = T_x - T_{NaK}$,
T_x = temperature in pressure shell at position x,
T_{NaK} = temperature of NaK,
k = thermal conductivity of Inconel = 11 Btu/hr·ft^2 (°F/ft),
x = distance from inside surface, ft.

The boundary conditions are:
$$\frac{d\theta}{dx} = 0 , \quad \text{at } x = \tau ,$$
$$\frac{d\theta}{dx} = \frac{h}{k} \theta , \quad \text{at } x = 0 ,$$

* TOTAL HEATING SHOULD BE INCREASED
APPROXIMATELY 10% TO ALLOW FOR
FAST-NEUTRON SCATTERING

TOTAL HEATING *

2.5-Mev GAMMA (CORE)

7-Mev GAMMA (CORE)

CAPTURE GAMMAS

CAPTURE PLUS INDUCED ACTIVITY FROM GAMMAS IN SHELL

HEAT (watts/cm³)

THICKNESS OF SHELL (cm)
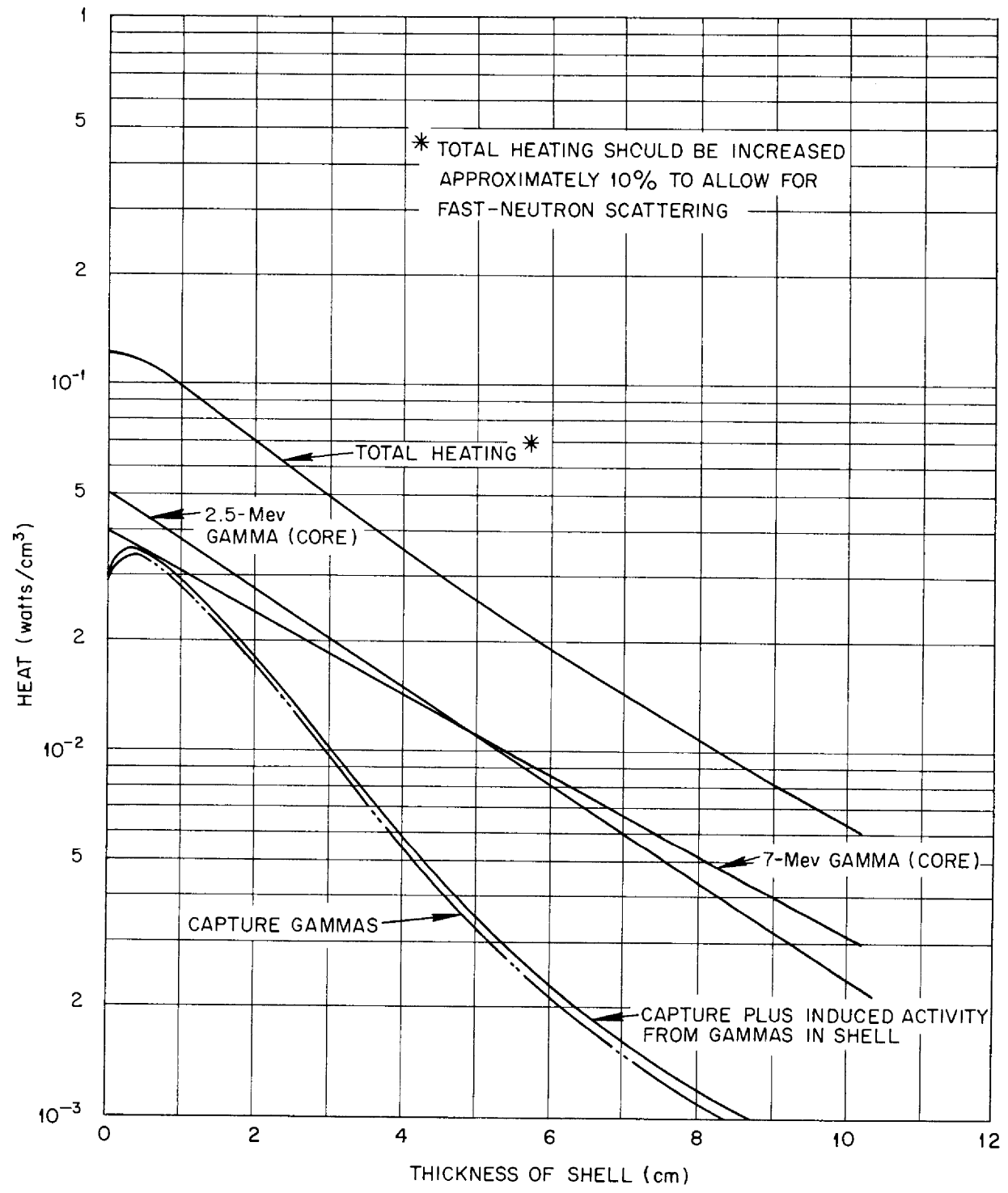
Fig. 13.   Heat Generated in Pressure Shell at 3-Megawatt Power Level.

where h is the heat transfer coefficient of NaK in Btu/hr·ft²·°F. The heat transfer coefficient, h, may be calculated by the following formula:

$$(45) \qquad h = \frac{k_{NaK}}{D} (5.8 + 0.02 \, Pe^{0.8}) ,$$

where

k_{NaK} = thermal conductivity of NaK,

D = NaK passage equivalent diameter,

Pe = Peclet's number for NaK.

To assure a conservative value for the heat transfer coefficient, the hydraulic diameter of the NaK passage without the tube elbows was used as the equivalent diameter of the NaK passage. The diameter and other values are

D = 0.667 ft,

k_{NaK} = 16.0 Btu/hr·ft² (°F/ft),

Pe = 148, using a velocity of 0.1 ft/sec (cf., chap. 2, "Flow of Reflector Coolant Through Core").

Therefore

h = 166 Btu/hr·ft²·°F.

The differential equations and boundary conditions thus become

$$(46) \qquad \frac{d^2\theta}{dx^2} = 1200 \, e^{-9.20x}$$

and

$$(47) \qquad \frac{d\theta}{dx} = 0 , \qquad \text{at } x = \tau ,$$

$$(48) \qquad \frac{d\theta}{dx} = 15.1 \, \theta , \qquad \text{at } x = 0 .$$

The solution is, of course, obvious:

$$(49) \qquad \frac{d\theta}{dx} = 130.5 \, e^{-9.20x} + c_1 ,$$

where, from Eq. 47,

$$c_1 = -130.5 \, e^{-9.20\tau} ,$$

and therefore

$$\frac{d\theta}{dx} = 130.5 \, (e^{-9.20x} - e^{-9.20\tau}) ,$$

$$(50) \qquad \theta = -14.19 \, e^{-9.20x}$$

$$- 130.5 \, x \, e^{-9.20\tau} + c_2$$

$$c_2 = 8.64 \, (1 - e^{-9.20x}) + 14.19$$

$$\theta = 14.19 \, (1 - e^{-9.20x})$$

$$- 130.5 \, x \, e^{-9.20\tau}$$

$$+ 8.64 \, (1 - e^{-9.20x}) .$$

The temperature at $x = \tau$, which is, of course, the maximum temperature difference, can be determined:

$$(51) \qquad \theta_\tau = 22.83 \, (1 - e^{-9.20\tau})$$

$$- 130.5 \, \tau \, e^{-9.20\tau} .$$

For τ = 2 in., θ = 13.2°F; for τ = 4 in., θ = 19.8°F.

As a check on the calculation,

$$\theta_{x=0} = 8.64 \, (1 - e^{-9.20\tau})$$

$$= 6.78 , \quad \text{for } \tau = 1/6 \text{ ft} ,$$

$$= 8.23 , \quad \text{for } \tau = 1/3 \text{ ft} ,$$

$$h\theta_{x=0} = 166 \; \theta_{x=0}$$

$$= 1130 , \quad \text{for } \tau = 1/6 \text{ ft} ,$$

$$= 1370 , \quad \text{for } \tau = 1/3 \text{ ft} .$$

These values check very closely the heat generated per square foot in the two different sections. The pressure shell, therefore, will be about 5 to 20°F hotter than the NaK.

Heat Generated in the NaK. The calculation of heat generation in the NaK in the reactor circuit is rather complex, and only a gross estimate of the heat generation is available. The maximum heat generation in the NaK will probably be of the order of 10 Btu/sec·ft³, with the average heat generation being of the order of 3 Btu/sec·ft³. Since there is approximately 10 ft³ of NaK in the pressure shell, the total heat generation in the NaK will be of the order of 30 Btu/sec.

The total heat added to the reflector coolant circuit by heat generation in the reflector, pressure shell, and NaK is

Q = 50.2 + 26.5 + 30 = 106.7 Btu/sec .

This heat addition is independent of NaK temperature.

Heat Transferred from the Reactor Core. Heat is transferred to the NaK in the reflector coolant circuit from the reactor core. The boundaries

23

across which the heat is transferred are the serpentine elbows, the tube sheets, the boundary between the core and the reflector, and the walls of the rod and instrument holes.

Serpentine Elbows. The fuel tubes are wound as serpentine coils that pass through the core 11 times (Fig. 9); there are six tubes in parallel. There are therefore sixty 180-deg bends or elbows between the core and the pressure shell, 30 above the core and 30 below it. In addition, between the core and the pressure shell, there are six straight sections at the inlet of the tubes and six straight sections at the outlet. The length of the 180-deg elbows is 8.5 in. for the elbows above the core and 6.5 in. for elbows below the core; the straight sections are 4 in. long above the core and 3 in. long below it. The tubes have an outside diameter of 1.235 in. and 0.060-in. walls. The total length of the bends and the internal and external areas of the bends are

$$L = 30 \left(\frac{6.5}{12} + \frac{8.5}{12} \right) + 6 \left(\frac{4}{12} + \frac{3}{12} \right)$$

$$= 41.0 \text{ ft },$$

$$A_{ext} = 41.0 \times \pi \times \frac{1.235}{12} = 13.3 \text{ ft}^2 ,$$

$$A_{int} = 41.0 \times \pi \times \frac{1.235 - 0.120}{12}$$

$$= 12.0 \text{ ft}^2 .$$

The fuel-side heat transfer coefficient can be calculated by first calculating the heat transfer coefficient for a straight pipe and correcting for the effect of the bend:

$$(52) \qquad h_f = h'_f \left(1 + 3.5 \frac{D_i}{D_H} \right) ,$$

where

h_f = fuel-side heat transfer coefficient, Btu/sec·°F,
h'_f = heat transfer coefficient in a straight section, Btu/sec·ft²·°F,
D_i = tube inside diameter,
D_H = bend diameter,

$$h_f = h'_f \left(1 + 3.5 \frac{1.115}{3.75} \right) = 2.04 \, h'_f ;$$

$$(53) \qquad h'_f = 0.027 \left(\frac{k}{D} \right)_f \text{Re}_f^{0.8} \, \text{Pr}_f^{1/3} \left(\frac{\mu}{\mu_s} \right)_f^{0.14}$$

where

Re_f = Reynolds' number for fuel
= 10,600,
Pr_f = Prandtl's number for fuel
= 3.78,
$\left(\dfrac{\mu}{\mu_s} \right)_f^{0.14}$ = 0.96,
$\left(\dfrac{k}{D} \right)_f$ = 0.00449.

Therefore

h'_f = 0.303 Btu/sec·ft²·°F,
h_f = 0.618 Btu/sec·ft²·°F,
$(hA)_f$ = 7.42 Btu/sec·°F,
$\left(\dfrac{1}{hA} \right)_f$ = 0.135.

The value of the NaK-side heat transfer coefficient is somewhat in doubt because very little work has been done on the heat transfer coefficient of liquid metals flowing across round tubes. For an approximation, the formula for flow inside a round tube will be used, with the outside diameter of the tube being considered as the equivalent diameter:

$$(54) \qquad h_{NaK} = \left(\frac{k}{D} \right)_{NaK} \left(7 + 0.025 \, \text{Pe}_{NaK}^{0.8} \right) ,$$

where

Pe_{NaK} = Peclet's number for NaK
= 22.9,
$\left(\dfrac{k}{D} \right)_{NaK}$ = 0.0432.

Therefore

h_{NaK} = 0.316,
$(hA)_{NaK}$ = 4.20 Btu/sec·°F,
$\left(\dfrac{1}{hA} \right)_{NaK}$ = 0.238.

The tube wall resistance is

$$(55) \qquad \left(\frac{1}{hA} \right)_{metal} = \frac{\ln \dfrac{D_o}{D}}{2\pi kL} = 0.130 ,$$

where D_o is the outside diameter; and

the over-all resistance is

$$(56) \quad \left(\frac{1}{hA}\right) = \left(\frac{1}{hA}\right)_f + \left(\frac{1}{hA}\right)_{NaK}$$
$$+ \left(\frac{1}{hA}\right)_{metal} = 0.503 \ .$$

For the calculation of the effective temperature difference between the fuel and the NaK it is assumed that the NaK temperature is constant and is the same as the mean temperature of the NaK in the core. This simplifying assumption leads to some inaccuracies in the calculation of the heat transferred to the NaK; however, in view of the extremely complex flow of the NaK through the reactor, it is doubtful whether any approximation would be more valid. Since the variation in the fuel temperature from 1150 to 1500°F is due primarily to heating in the core, the arithmetic-average temperature difference between the NaK and the fuel should be used.

The arithmetic-average elbow temperature is about 1330°F. The effective temperature difference and the heat rejected to the NaK through the serpentine elbows are given in the following tabulation for various mean temperatures:

MEAN NaK TEMPERATURE (°F)	AVERAGE TEMPERATURE DIFFERENCE (°F)	HEAT REJECTED TO NaK (Btu/sec)
1300	30	60
1200	130	258
1075	255	507
1000	330	656
800	530	1054

Tube Sheets. The tube sheets are the metal plates at the upper and lower boundaries of the core through which the fuel tubes pass (Fig. 9). Figure 14 shows a cross section of a typical fuel tube and its associated moderator blocks and tube sheet section. Heat is generated in the moderator and transferred to the fuel and the NaK; in addition, heat flows from the fuel to the NaK through the moderator blocks. The differential equation and boundary conditions for the two-dimensional

system shown in Fig. 14 are given in the following:

$$(57) \quad \frac{\partial^2 \theta}{\partial x^2} + \frac{\partial^2 \theta}{\partial y^2} = -\frac{q'}{k} \ ,$$

where

θ = $T - T_{NaK}$, °F,

T = temperature at any point (x, y), °F,

T_{NaK} = temperature of the NaK, °F,

q' = heat generation in moderator, Btu/sec·ft³,

k = thermal conductivity of moderator, Btu/sec·ft² (°F/ft).

DWG.19104
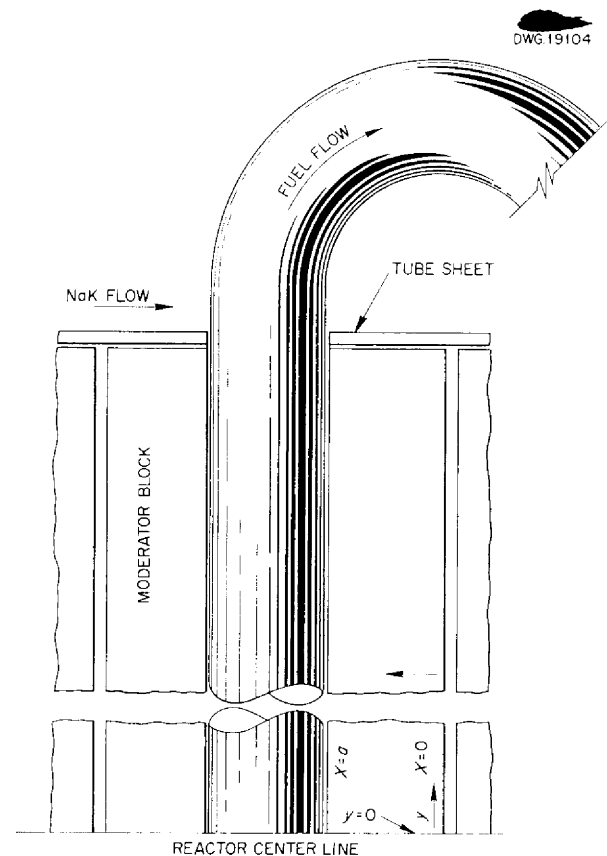
Fig. 14. Cross Section of Moderator Block Showing Tube Sheet and Fuel Tube.

The heat generation in the moderator block is assumed to be constant in the x direction and to vary in the y direction in accordance with the axial moderator heating curve found in the section on power distribution. The

boundary conditions are

$$(58) \qquad \frac{\partial \theta}{\partial x} = 0 , \qquad \text{at } x = 0 ,$$

$$(59) \qquad \frac{\partial \theta}{\partial y} = 0 , \qquad \text{at } y = 0 ,$$

$$(60) \qquad \frac{\partial \theta}{\partial x} = - \frac{h_f}{k} \left(\theta + T_{NaK} - T_s \right) ,$$
$$\text{at } x = a ,$$

$$(61) \qquad \frac{\partial \theta}{\partial y} = - \frac{h_{NaK}}{k} \theta , \qquad \text{at } y = b .$$

No closed or series solution for this boundary value problem could be readily found; consequently, solutions to specific numerical problems were undertaken by the relaxation method. Figure 15 shows the temperature pattern across the tube sheet face of a typical moderator block, as found by this method, for several NaK temperatures. The heat loss from the section of the tube sheet adjacent to one fuel tube and moderator block and the total heat loss from both tube sheets, which is 132 times the loss from one of the sections, are tabulated in the following:

NaK TEMPERATURE (°F)	HEAT LOSS PER SECTION (Btu/sec)	TOTAL HEAT LOSS (Btu/sec)
900	1.86	246
1075	1.15	150
1250	0.25	33

Boundary Between Core and Reflector. The fuel tubes at the periphery of the core (near the reflector) are at a considerably higher temperature than the reflector, and they transfer heat into the reflector through the beryllium oxide blocks. An estimate of the heat transferred into the NaK circuit by this method has been made. The system of fuel tubes, NaK tubes, and beryllium oxide blocks was simplified and considered as a hollow beryllium oxide cylinder with internal heat generation in which the inner surface is washed by fuel and the outer surface is washed by NaK. The actual heat transfer coefficients of the fuel and the NaK in the tubes were calculated and, from these coefficients, hypothetical heat transfer coefficients on the sides of the cylinder were computed so that
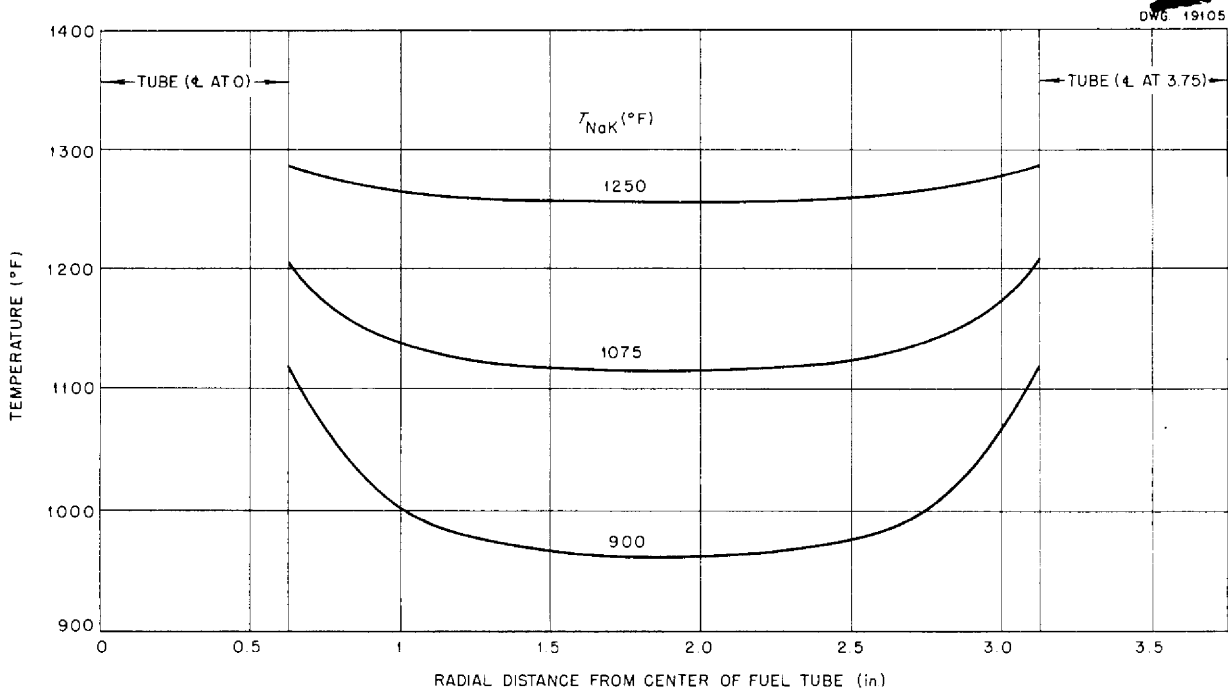
$$(62) \qquad h^*A^* = hA ,$$

Fig. 15. Temperature Pattern Across Tube Sheet Face.

where

h^* = actual heat transfer coefficient, Btu/sec·ft^2·°F,

A^* = actual heat transfer area, ft^2,

h = hypothetical heat transfer coefficient, Btu/sec·ft^2·°F,

A = hypothetical heat transfer area, ft^2.

The mean radius of the peripheral fuel tube circle is about 15 in. and there are 29 tubes; the mean radius of the inner circumference of the NaK tubes is about 18 1/2 in. and there are 35 tubes; and the reactor core is 36 in. in height. Therefore the actual heat transfer areas are

$$(63) \qquad A^* = \pi D L N ,$$

$$A_f^* = 25.8 \text{ ft}^2 ,$$

$$A_{NaK}^* = 11.86 \text{ ft}^2 ;$$

and the hypothetical heat transfer areas are

$$(64) \qquad A = 2 \pi r L ,$$

$$A_f = 23.6 \text{ ft}^2 ,$$

$$A_{NaK} = 29.1 \text{ ft}^2 ,$$

where

D = tube inside diameter, ft,

L = tube length, ft,

N = number of tubes,

r = average radius of tube circle, ft.

The heat transfer coefficients in the tubes are found as follows:

1. For the fuel tubes

$$(65) \quad h_f^* = 0.027 \frac{k_f}{D_f} \text{Re}_f^{0.8} \text{Pr}_f^{1/3} \left(\frac{\mu}{\mu_s}\right)_f^{0.14} ,$$

where

k_f = thermal conductivity of fuel, Btu/sec·ft^2 (°F/ft),

Re_f = Reynolds' number for fuel,

Pr_f = Prandtl's number for fuel,

$\left(\dfrac{\mu}{\mu_s}\right)_f$ = ratio of viscosity of fuel at bulk temperature to viscosity at surface temperature.

For a fuel velocity of 3.7 ft/sec and a D_f of 0.09285 ft, the values of the terms in Eq. 65 are

$$\text{Re}_f = 13,450 ,$$

$$\text{Pr}_f = 2.98 ,$$

$$\left(\frac{\mu}{\mu_s}\right)_f^{0.14} = 1 ,$$

$$h_f^* = 0.373 .$$

2. For the NaK tubes

$$(66) \quad h_{NaK}^* = \frac{k_{NaK}}{D_{NaK}} (7.0 + 0.025 \, \text{Pe}_{NaK}^{0.8}) ,$$

where Pe_{NaK} is Peclet's number for NaK. For a NaK velocity of 3.0 ft/sec and a D_{NaK} of 0.03582 ft, the values of the terms in Eq. 66 are

$$\text{Pe}_{NaK} = 236.4 ,$$

$$h_{NaK}^* = 1.093 .$$

The hypothetical heat transfer coefficients are therefore

$$h_f = \frac{h_f^* A_f^*}{A_f} = 0.408$$

and

$$h_{NaK} = \frac{h_{NaK}^* A_{NaK}^*}{A_{NaK}} = 0.446 .$$

The differential equation for steady-state heat conduction with internal heat generation is

$$(67) \qquad \nabla^2 T = -\frac{q'}{k_{BeO}} ,$$

where

T = temperature at any point in the BeO, °F,

q' = internal heat generation, Btu/sec·ft^3,

k_{BeO} = thermal conductivity of BeO, Btu/sec·ft^2 (°F/ft).

Although q' varies with radial distance and k_{BeO} varies with temperature, both will be assumed constant and equal to their average values. This simplifying assumption undoubtedly results in some error and the following solutions, accordingly, are only estimates:

$$q' = 7.74 \text{ Btu/sec·ft}^3 ,$$

and

$$k_{BeO} = 0.0054 \ \text{Btu/sec} \cdot \text{ft}^2 \ (^\circ F/\text{ft}) \ .$$

The solution of the differential equation for the infinite cylinder case is

$$(68) \qquad \frac{dT}{dr} = -717 + \frac{c_1}{r} \ ,$$

$$(69) \quad T = -358.5 \ r^2 + c_1 \ \ln r + c_2 \ ,$$

where r is the radial distance from the center of the core in feet and c_1 and c_2 are arbitrary constants. The boundary conditions are

$$(70) \quad \frac{dT}{dr} = - \frac{h_f}{k_{BeO}} \ (1460 - T) \ ,$$

$$\text{at } r = 1.25 \text{ ft}$$

(the mean fuel temperature in the peripheral tubes is 1460°F),

$$(71) \quad \frac{dT}{dr} = - \frac{h_{NaK}}{k_{BeO}} \ (T - T_{NaK}) \ ,$$

$$\text{at } r = 1.5417 \text{ ft}$$

(T_{NaK} is the mean NaK temperature). The values of c_1 and c_2 are obtained by using the boundary conditions:

$$(72) \quad c_1 = 4.3823 \ T_{NaK} - 5008.53$$

and

$$(73) \quad c_2 = 3072.71 - 0.93146 \ T_{NaK}$$

(the solution requires that many significant figures be carried). The temperature differences at the BeO-to-fuel and BeO-to-NaK interfaces and the heat removed from the fuel and added to the NaK are given in Table 3. It is obvious from the data in Table 3 that heat is transferred from the fuel to the NaK and that all the heat generated in the beryllium oxide goes into the NaK. A simple check of the numerical work, by the method of superposition, is therefore possible:

$$(74) \qquad Q_{BeO} = q' \pi (r_{NaK}^2 - r_f^2) L$$
$$= 59.5 \text{ Btu/sec,}$$

θ_{BeO} = temperature difference across the beryllium

oxide resulting from internal heat generation only = 61.1°F,

$$\left(\frac{1}{hA} \right)_f = 0.1039 \ ,$$

$$\left(\frac{1}{hA} \right)_{NaK} = 0.0771 \ ,$$

$$\left(\frac{1}{hA} \right)_{BeO} = 2.060 \ ,$$

$$\left(\frac{1}{hA} \right)_{f-NaK} = 2.241 \ .$$

The fuel-to-NaK temperature differences for the various NaK temperatures are given in Table 4. As can be seen, the results agree quite well with the results given in Table 3.

A portion of the heat transferred to the NaK comes from heat generated in the beryllium oxide in the reflector, as previously discussed. It is therefore necessary to subtract from the heat transferred to the NaK an amount equal to

$$Q = 7.74 \ \pi \left[\left(\frac{18.5}{12} \right)^2 - \left(\frac{18.0}{12} \right)^2 \right] \times 3 = 4.65 \text{ Btu/sec} \ .$$

The net heat added to the NaK is then

T_{NaK}	$(Q_{NaK})_{net}$
800	322
1000	233
1075	199
1200	143
1300	99

Walls of the Rod and Instrument Holes. There are six vertical holes through the reactor core and pressure shell to admit control rods and nuclear instruments (Fig. 16). In each hole there are three concentric tubes (Fig. 17); NaK flows through the passage between the outer two

TABLE 3. TEMPERATURE DIFFERENCES AND HEAT TRANSFERRED AT THE BeO-TO-FUEL AND BeO-TO-NaK INTERFACES

T_{NaK} (°F)	TEMPERATURE DIFFERENCE (°F)		Q_f [a]	Q_{NaK} [b]	$Q_{BeO} = Q_{NaK} + Q_f$ [c]
	BeO-to-Fuel	BeO-to-NaK			
800	−27.77	25.20	−267.4	326.7	59.3
1000	−18.49	18.31	−178.0	237.4	59.4
1075	−15.01	15.73	−144.5	203.9	59.4
1200	−9.21	11.42	−88.7	148.0	59.3
1300	−4.57	7.97	−44.0	103.3	59.3

[a] Q_f = heat transferred to the fuel, Btu/sec.

[b] Q_{NaK} = heat transferred to the NaK, Btu/sec.

[c] Q_{BeO} = heat generated in BeO, Btu/sec.

TABLE 4. TEMPERATURE DIFFERENCES AND HEAT TRANSFERRED AT THE FUEL-TO-NaK INTERFACE

T_{NaK} (°F)	TEMPERATURE DIFFERENCE FUEL-TO-NaK, θ_{f-NaK} (°F)	$\theta_{f-NaK} - \theta_{BeO}$ (°F)	$Q_f = (hA)_{f-NaK}(\theta_{f-NaK} - \theta_{BeO})$ (Btu/sec)	$Q_{NaK} = -Q_f + Q_{BeO}$ (Btu/sec)
800	660	598.9	−267.2	326.7
1000	460	398.9	−178.0	237.5
1075	385	323.9	−144.5	204.0
1200	260	198.9	−88.7	148.2
1300	160	98.9	−44.1	103.6

tubes and removes the heat that would otherwise be transmitted to the hole from the reactor; the passage between the inner two tubes is packed with insulation; helium flows inside the inner tube and cools the rod or instrument and the inner tube wall. Heat is therefore added to the NaK from the reactor and removed from the NaK by the helium. Since the two instrument holes are located in the reflector and the heat addition to the NaK from the reflector has already been accounted for in the calculation of heat generated in the reflector, only the heat added to the NaK in the four control rod holes remains to be calculated. The calculation of the heat removed from the NaK by the helium in the six holes can be found in chap. 5, "Rod and Instrument Cooling System."

Each rod hole through the reactor is surrounded by six beryllium oxide blocks, each of which contains a fuel tube (Fig. 16). The mean fuel temperature in the fuel tubes is about 1200°F. As a simplification (similar to that used in the calculation of heat transfer across the boundary of the core and reflector), the holes and associated structure were considered as a hollow beryllium oxide cylinder with internal heat generation and with the inner surface washed by NaK and the outer surface washed by fuel.
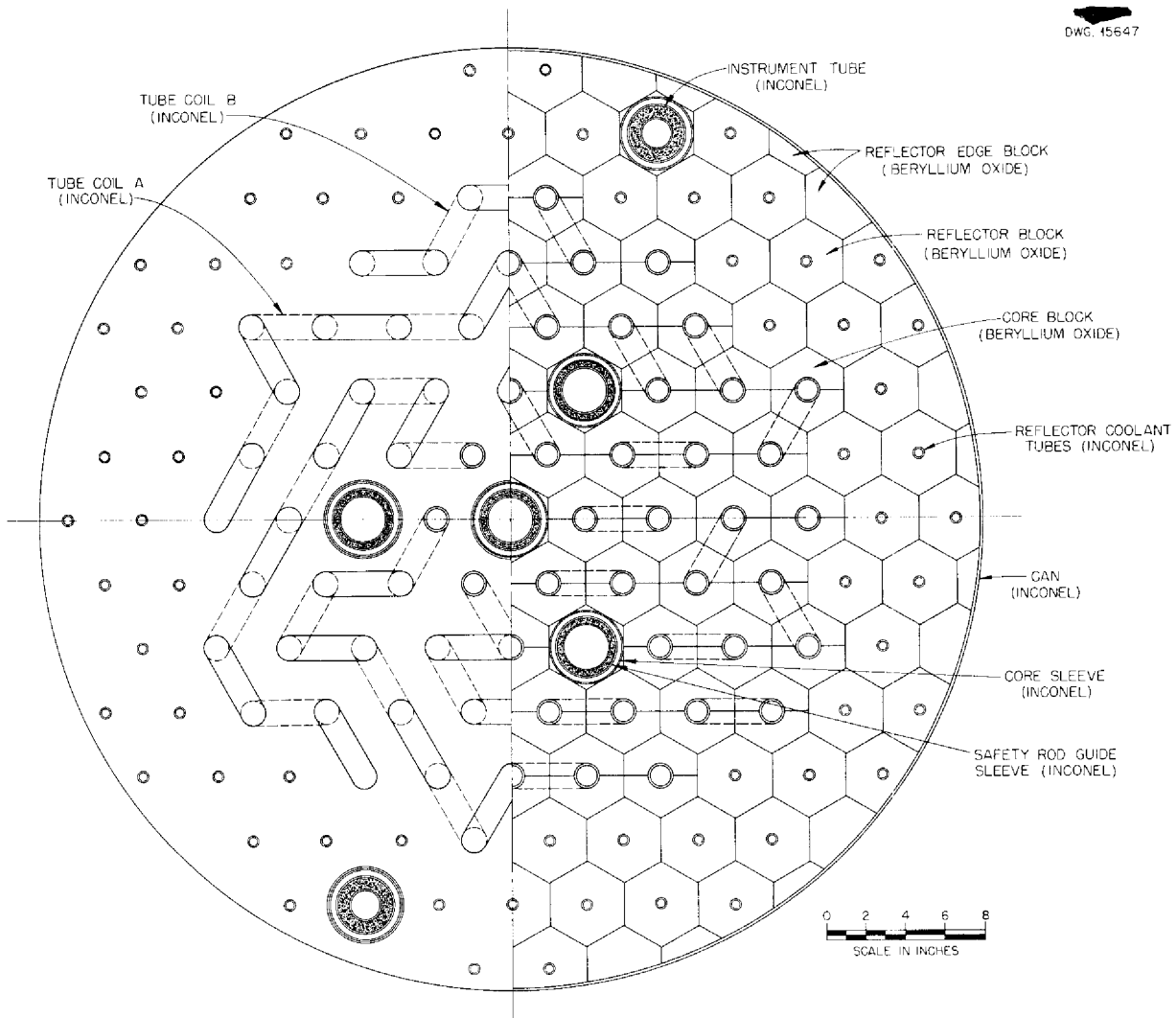
Fig. 16. Plan View of Reactor Core Lattice.

There is some overlapping of fuel tubes in the sense that some of the tubes are members of the tube sets encircling more than one rod hole. This effect was neglected inasmuch as the heat added to the NaK in the rod holes is considerably smaller in magnitude than the heat added elsewhere and, hence, a rough estimate of the heat addition is all that is necessary. The actual heat transfer coefficient in the fuel tubes was calculated and, from this coefficient, a hypothetical heat transfer coefficient on the side of the cylinder was computed so that:

$$(75) \qquad h^*A^* = hA \ ,$$

where

h^* = actual heat transfer coefficient, $\text{Btu/sec} \cdot \text{ft}^2 \cdot {}^{\circ}\text{F}$,

A^* = actual heat transfer area, ft^2,

h = hypothetical heat transfer coefficient, $\text{Btu/sec} \cdot \text{ft}^2 \cdot {}^{\circ}\text{F}$,

A = hypothetical heat transfer area, ft^2.

The inside radius of the outer NaK-containing tube is 1.826 in.; the mean radius of the fuel tube circle is 3.75 in.; and the height of the reactor core is 36 inches. The heat transfer coefficients and
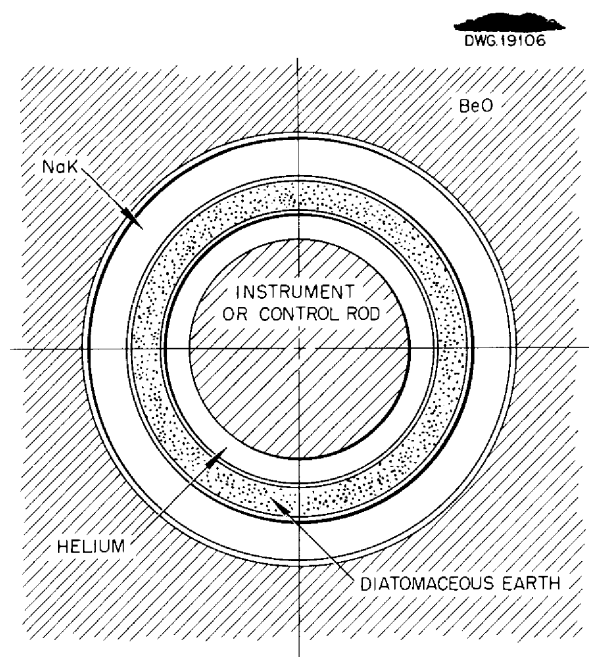
Fig. 17. Cross Section of Helium Passage and Sleeve.

areas are therefore:

1. For the NaK annulus

$$(76) \qquad A_{NaK} = A^*_{NaK} = \pi D_{NaK} L ,$$

$$(77) \quad h_{NaK} = h^*_{NaK}$$

$$= \frac{k_{NaK}}{D_{NaK}} \left(5.8 + 0.020 \, Pe_{NaK}^{0.8} \right) ,$$

where

D = equivalent diameter, ft,
L = length of reactor core, ft,
k = thermal conductivity, Btu/sec·ft^2 (°F/ft),
Pe = Pelcet's number.

For a NaK velocity of 0.81 ft/sec, an $A_{NaK} = A^*_{NaK}$ of 2.87 ft^2, and a D_{NaK} of 0.0543 ft, the values of the terms in Eqs. 76 and 77 are

$$Pe_{NaK} = 97.4 ,$$

$$h_{NaK} = h^*_{NaK} = 0.530 \, Btu/sec \cdot ft^2 \cdot °F .$$

2. For the fuel tubes

$$(78) \qquad A^*_f = \pi D_f L N_f ,$$

$$(79) \qquad A_f = 2\pi r_f L ,$$

$$(80) \quad h^*_f$$

$$= 0.027 \, \frac{k_f}{D_f} \, Re_f^{0.8} \, Pr_f^{1/3} \left(\frac{\mu}{\mu_s} \right)_f^{0.14} ,$$

where

N = number of tubes,
r = mean radius, ft,
Re = Reynolds' number,
Pr = Prandtl's number,

$\left(\dfrac{\mu}{\mu_s} \right)_f$ = ratio of viscosity of fuel at bulk temperature to viscosity at surface temperature.

For a fuel velocity of 3.7 ft/sec, an A^*_f of 5.25 ft^2, an A_f of 5.90 ft^2, and a D_f of 0.09285 ft, the values of the terms in Eqs. 78, 79, and 80 are

$$Re = 7970 ,$$

$$Pr = 5.02 ,$$

$$\left(\frac{\mu}{\mu_s} \right)_f^{0.14} = 1 ,$$

$$h^*_f = 0.294 \, Btu/sec \cdot ft^2 \cdot °F ,$$

$$h_f = 0.262 \, Btu/sec \cdot ft^2 \cdot °F .$$

The differential equation for steady-state heat conduction with internal heat generation is

$$(81) \qquad \nabla^2 T = - \frac{q'}{k_{BeO}} ,$$

where

q' = internal heat generation, Btu/sec·ft^3,
k_{BeO} = thermal conductivity of BeO, Btu/sec·ft^2 (°F/ft).

Although q' varies with radial distance and k_{BeO} varies with temperature, both will be assumed constant and equal to their average values. This is done for simplicity and undoubtedly results in solutions that are only approximate. The values are

$$q' = 39.8 \, Btu/sec \cdot ft^3$$

and

$$k_{BeO} = 0.0058 \, Btu/sec \cdot ft^2 \, (°F/ft) .$$

The solution of the differential

31

equation for the infinite cylinder case is

$$(82) \qquad \frac{dT}{dr} = 3431 \, r + \frac{c_1}{r} ,$$

$$(83) \quad T = 1715.5 \, r^2 + c_1 \ln r + c_2 ,$$

where

T = temperature, °F,
r = radial distance from center of core, ft,
c_1 and c_2 = arbitrary constants.

The boundary conditions are

$$(84) \qquad \frac{dT}{dr} = \frac{h_{NaK}}{k_{BeO}} (T - T_{NaK}) ,$$

at $r = 0.15217$ ft,

$$(85) \qquad \frac{dT}{dr} = \frac{-h_f}{k_{BeO}} (T - 1200) ,$$

at $r = 0.13250$ ft (the mean fuel temperature is approximately 1200°F). Solving for c_1 and c_2 by using the boundary condition gives

$$(86) \quad c_1 = 1573.87 - 1.1596 \, T_{NaK} ,$$

$$(87) \quad c_2 = 3110.40 - 1.2666 \, T_{NaK}$$

(the solution requires that many significant figures be carried).

The temperature differences at the BeO-to-NaK and BeO-to-fuel interfaces and the heat added to the NaK and to the fuel are given in Table 5. The values given in Table 5 are for one of the four rod holes. A check of some of the numerical work, by the method of superposition, is possible:

$$Q_{BeO} = q' \pi (r_f^2 - r_{NaK}^2) L = 27.9 \text{ Btu/sec} .$$

The temperature difference from the fuel to the NaK across the beryllium oxide because of internal heat generation only is 131.7°F when all the generated heat enters the NaK, and −88.8°F when all the generated heat enters the fuel.

The resistance to heat transfer between the NaK and the fuel is

$$\left(\frac{1}{hA} \right)_{NaK} = 0.6574 ,$$

$$\left(\frac{1}{hA} \right)_{f} = 0.6475 ,$$

$$\left(\frac{1}{hA} \right)_{BeO} = 6.5818 ,$$

$$\left(\frac{1}{hA} \right)_{f-NaK} = 7.887 .$$

The fuel-to-NaK temperature differences for the various NaK temperatures are given in Table 6. As can be seen, the results agree quite well with the results given in Table 5.

TABLE 5. TEMPERATURE DIFFERENCES AND HEAT TRANSFERRED AT THE BeO-TO-NaK AND BeO-TO-FUEL INTERFACES

T_{NaK} (°F)	TEMPERATURE DIFFERENCE (°F)		Q_{NaK} [a]	Q_f [b]	$Q_{BeO} = Q_{NaK} - Q_f$ [c]
	BeO-to-NaK	BeO-to-Fuel			
800	40.74	−22.01	61.97	−33.97	28.00
1000	24.06	−5.57	36.60	−8.60	28.00
1075	17.80	0.60	27.08	0.93	28.01
1200	7.38	10.87	11.23	16.78	28.01
1300	−0.96	19.09	−1.46	29.47	28.01

[a] Q_{NaK} = heat transferred to NaK, Btu/sec.

[b] Q_f = heat transferred to the fuel, Btu/sec.

[c] Q_{BeO} = heat generated in BeO, Btu/sec.

T_{NaK} (°F)	$\theta_{f\text{-}NaK}$ (°F)	GENERATED HEAT ENTERS	$\theta_{f\text{-}NaK} - \theta_{BeO}$ (°F)	Q_f (Btu/sec)	Q_{NaK} (Btu/sec)
800	400	NaK	268.3	−34.0	62.0
1000	200	NaK	68.3	−8.7	36.6
1075	100	NaK and fuel			
1200	0	NaK and fuel			
1300	−100	Fuel	−11.3	+29.3	−1.4

The heat removed from the NaK by the helium flowing through the rod holes is calculated in chap. 5, "Rod and Instrument Cooling System," for the various rods and instruments.

Summary. A plot of the heat added to the NaK circuit vs. the mean NaK temperatures for the various sources of heat addition is shown in Fig. 18. A plot of the net heat that must be removed from the NaK in the reflector coolant heat exchangers vs. the mean NaK temperature is shown in Fig. 19. By cross-plotting these two figures, the mean NaK temperature is obtained; the cross-plot is shown in Fig. 19. The mean NaK temperature is about 1172°F, and at that temperature, 640 Btu/sec (675 kw) is removed from the reactor by the reflector cooling system. The minimum and maximum NaK temperatures are about 1105 and 1235°F, respectively (Fig. 1). The maximum pressure-shell temperature is about 20°F greater than the maximum NaK temperature (see previous work in this section) and is therefore about 1255°F.

PRESSURE DROP IN FUEL MANIFOLDS AND CORE TUBES

The fuel flows from the heat exchangers through the surge tanks and pumps and into the inlet manifold of the reactor, where it is distributed into the six parallel passes through the core lattice. Upon leaving the core lattice, the fuel enters the outlet manifold. From the outlet manifold, the fuel is returned to the

heat exchangers. For a fuller understanding of the circuit, see Figs. 1 and 9. The problem is to determine the pressure drop (or drops) of the
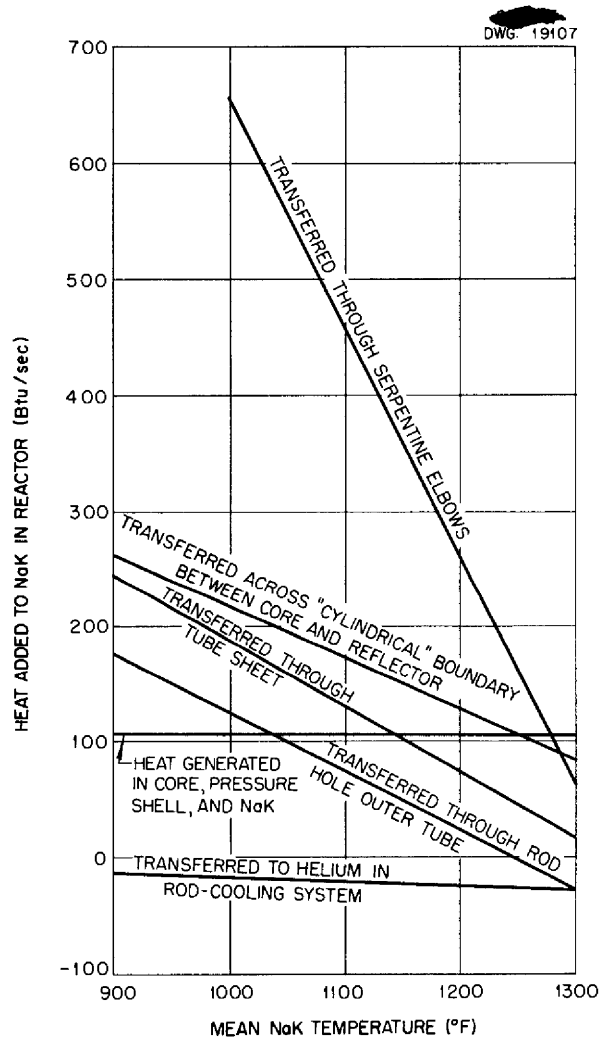
Fig. 18.   Heat Removed by NaK.
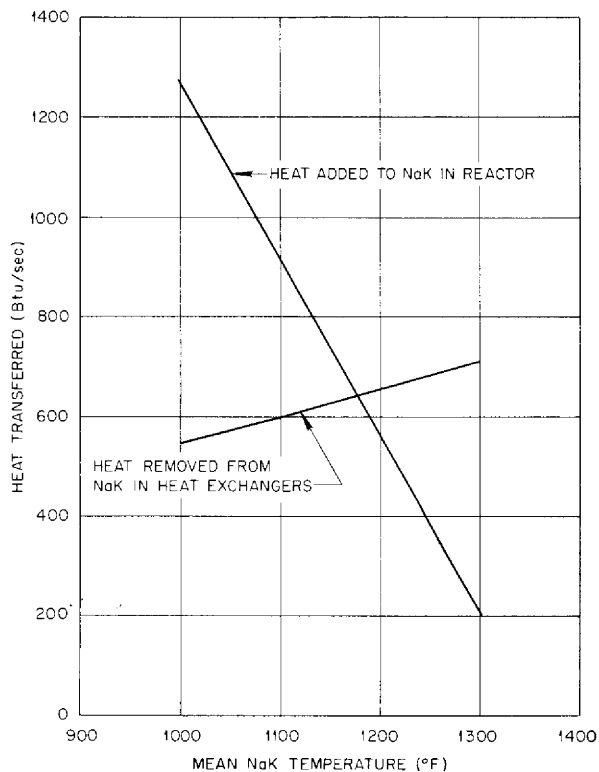
Fig. 19. Heat Added to and Removed from NaK vs. Temperature.

fuel from the time it enters the inlet manifold until it leaves the outlet manifold.

The pressure drop of the fuel in flowing through the inlet manifold, core lattice, and outlet manifold is due to five factors: friction, curvature of the tubes or pipes, contraction losses, expansion losses, and losses in the pipe fittings and square elbows. The formula for loss in pressure because of friction is

$$(88) \qquad \Delta P_f = 4f \frac{L}{D} \frac{\rho v^2}{2g},$$

where f is the friction factor given by $f = 0.046/N_R^{0.2}$ for turbulent flow.[11] The curvature loss is given more simply by

$$(89) \qquad \Delta P_c = k_c \frac{\rho v^2}{2g}.$$

In this expression, k_c is a constant that is taken from the curves of Cox,

Glen, and Germano (cf., p. 191 and 193 of ref. 12). The expression for contraction loss is very similar to that for curvature;

$$(90) \qquad \Delta P_x = k \frac{\rho v_1^2}{2g},$$

where k is a constant that is dependent upon the ratio of the smaller area to the larger. Values for k are found in the work of McAdams (cf., p. 122 of ref. 11). The loss caused by expansion is determined from

$$(91) \qquad \Delta P_y = \rho \frac{(v_1 - v_2)^2}{2g}.$$

The pressure drop in a fitting or square elbow is calculated by using the friction drop equation and replacing L by L_e; that is,

$$(92) \qquad \Delta P_F = 4f \frac{L_e}{D} \frac{\rho v^2}{2g}.$$

The L_e's for square elbows and various fittings are given in ref. 13; they depend upon the tube or pipe size. The symbols used in the equations above have the following meanings and units:

ΔP = pressure drop, lb/ft^2,
f = friction factor, dimensionless,
L = length, ft,
D = hydraulic diameter, ft,
ρ = density, lb/ft^3,
v = average velocity given by ft^3 of fluid per second/ft^2 of cross section, ft/sec,
g = gravitational acceleration, $32.2\ ft/sec^2$,
k = constant, dimensionless,
k_c = constant, dimensionless,
v_1 = average linear velocity upstream, ft/sec,
v_2 = average linear velocity downstream, ft/sec,
L_e = equivalent length of straight pipe, ft,
N_R = Reynolds' number.

The subscripts have the following meanings:

f = friction,
c = curvature,
x = contraction,

34

y = expansion,
e = equivalent,
F = fitting.

In the pressure drop calculations, it was assumed that the flow of fuel would be equally distributed between the six passes through the core. Although this is a reasonable assumption, it is not quite true, as will be demonstrated by the calculated data.

The same value of density was used throughout the calculation, but the viscosities corresponded to the mean temperatures in the inlet manifold, core lattice, and outlet manifold. The properties used were:

Density, ρ 187 lb/ft^3

Viscosity, μ
  Inlet manifold   12.5 cp
  Core lattice   9.0 cp
  Outlet manifold   6.8 cp

The flow rate of the fuel was considered to be 0.150 cfs. Figure 20 shows sketches of the inlet and outlet manifolds. In this figure, the outlets of the inlet manifold are numbered 1 to 6 and the inlets of the outlet manifold are numbered correspondingly. Thus outlet 1 of the inlet manifold is connected by a tube to inlet 1 of the outlet manifold, etc., and the fluid paths from the entrance tee of the inlet manifold to the exit tee of the outlet manifold are given designations such as "1-1." The geometries of the two manifolds are shown in Figs. 21 and 22. The pressure drops in these manifolds were calculated by using Eqs. 88 through 92.

The tubes carrying the fuel through the core lattice are often referred to as "serpentine" tubes because each tube has 10 bends and 11 straight lengths. For each tube the equivalent straight length is

$$L = 42.20 \text{ ft}.$$

The pressure drop for each path through the system being considered was easily calculated by using the equal flow rate assumption and Eqs. 88 and 89.

The results are tabulated in Table 7. Of course, as can be seen, the flow will not be distributed equally among the six parallel paths through the core lattice. In fact, the flow rate may vary as much as 2.5%. Thus a maximum temperature difference of the order of 9°F may exist in the fuel exit temperatures from the various tubes.

DWG. 19109

INLET MANIFOLD

OUTLET MANIFOLD

Fig. 20. Fuel Manifolds.

DWG. E-A-1-1-3 B

INCONEL CONCENTRIC
REDUCER 1½ x 1-in. IPS

INCONEL LEG
1½-in. IPS SCH 40

INCONEL LEG
1-in. IPS SCH 40

54 in.

15,000-in. R

60°

60°

60°

45°

30°

45°

60°

60°

60°

60°

INCONEL WELDING COLLAR

INCONEL STRAIGHT TEE
2 x 2 x 2-in. IPS

INCONEL LEG
2-in. IPS SCH 40

INCONEL CASING TUBE
3½-in. OD x 1/16-in. WALL

INCONEL OUTLET LINE
2-in. IPS SCH 40

INCONEL CONCENTRIC
REDUCER 2 x 1½-in. IPS

REF
3 in.

REF
2½ in.

A

A

INCONEL LEG
1-in. IPS SCH 40

INCONEL LEG
1½-in. IPS SCH 40

4.188 in.

1/16 in.

1/8 in.

INCONEL
WELDING COLLAR

1.049-in. D REAM TO
1.053-in. AFTER WELDING

$\frac{2.360}{2.365}$ -in. D

SECTION A-A

19 in.

22½°

7½-in. R

24 in.

50°

Fig. 21. Fuel Outlet Manifold.

INLET LINE 1½ IPS SCH 40 PIPE

4 7/8 R

ECCENTRIC REDUCER
1½ IPS — 1 IPS

INLET LEG
1 IPS SCH 40 PIPE

REDUCER 2 IPS — 1½ IPS

TEE 2 x 2 x 2

INLET LINE 2 IPS SCH 40 PIPE

10½

7

DIA
7.500

30°

30°

7½ R

COVER REMOVED
IN THIS VIEW

4 7/8 REF

10½

54

4 7/8 R

21

COVER

BODY

INLET LINE

TEE

INLET LINE

SLEEVE

NOTES:
ALL DIMENSIONS ARE IN INCHES.
ALL MATERIAL IS INCONEL.
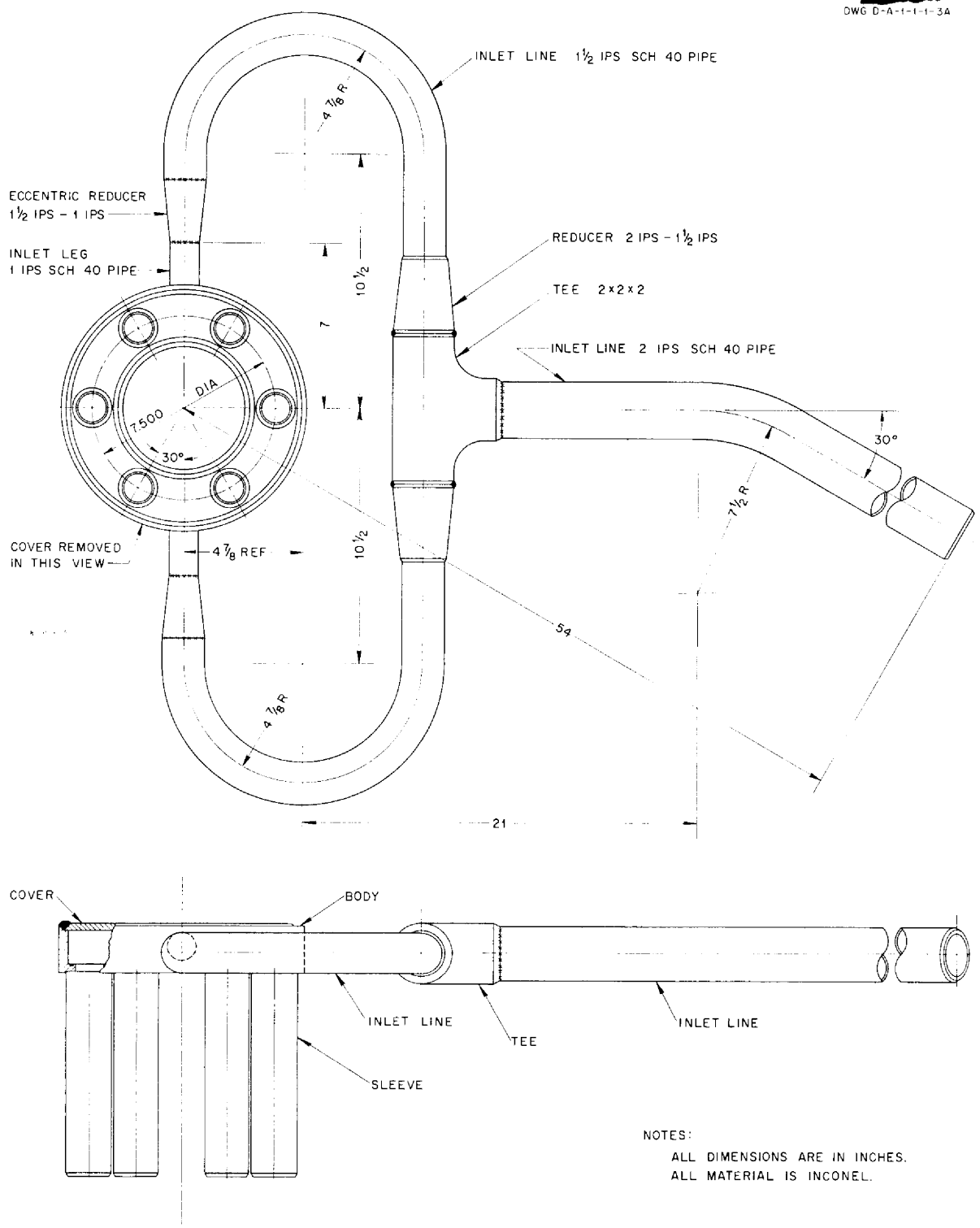
Fig. 22.   Fuel Inlet Manifold.

37

TABLE 7. PRESSURE DROP IN FUEL MANIFOLDS AND CORE TUBES

PATH	PRESSURE DROPS (lb/ft^2)			TOTAL PRESSURE DROP	
	Inlet Manifold	Serpentine Tubes	Outlet Manifold	In lb/ft^2	In lb/ft^2
1-1	627.7	613.0	172.5	1413	9.81
2-2	605.7	613.0	155.7	1374	9.54
3-3	627.7	613.0	155.7	1396	9.70
4-4	627.7	613.0	172.5	1413	9.81
5-5	605.7	613.0	121.0	1340	9.30
6-6	627.7	613.0	121.0	1362	9.46

TEMPERATURE GRADIENTS IN THERMAL SLEEVES

The fuel tubes pass through the pressure shell heads in the manner shown schematically in Fig. 23a. The sleeve connecting the pressure shell and fuel tube is at the pressure shell temperature at one end and at the fuel tube temperature at the other end. At the fuel tube outlet, the fuel tubes are at 1500°F; the pressure shell temperature at this point is difficult to determine, but it is probably not less than 1150°F. The sleeve gains heat from the fuel tube through the NaK between the tube and sleeve; the NaK is assumed to be stagnant. Heat lost by the sleeve to the surrounding helium atmosphere may be neglected because the helium is at about 1200°F. The problem was simplified by considering the sleeve, the fuel tube, and the NaK between the sleeve and the fuel tube as a single cylindrical tube. The temperature was assumed to be constant across any cross section of this cylindrical tube, and an average thermal conductivity for the tube was used. (The conductivities of NaK and Inconel are nearly equal.) The differential equation governing the flow of heat in the sleeve is (Fig. 23b)

$$(93) \qquad -ka \frac{d^2 T}{dx^2} = hc(1500 - T) \, ,$$

where

k = thermal conductivity of the composite tube, Btu/hr·ft^2 (°F/ft),

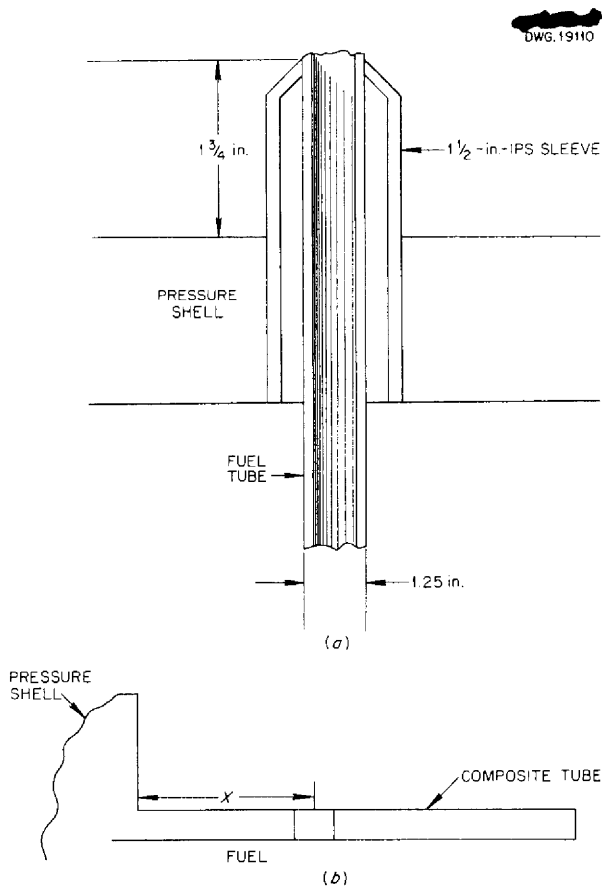a = cross-sectional area of the composite tube, ft^2,

Fig. 23. Thermal Sleeve.

T = temperature, °F,
x = distance from pressure shell, ft,
h = fuel heat transfer coefficient, Btu/hr·ft²·°F,
c = circumference of inside of fuel tube, ft.

The boundary conditions are

(94) $T = 1150°F$,   at $x = 0$,

(95) $T = 1500°F$,   at $x = 0.1146$.

The fuel heat transfer coefficient may be evaluated by using the following formula:

$$(96) \quad h = 0.027 \frac{k}{D} Re^{0.8} Pr^{1/3} \left(\frac{\mu}{\mu_s}\right)^{0.14} ,$$

where

k = thermal conductivity of the fuel, Btu/hr·ft² (°F/ft),
D = fuel tube inner diameter, ft,
Re = Reynolds' number for the fuel,
Pr = Prandtl's number for the fuel,
$\dfrac{\mu}{\mu_s}$ = ratio of fuel viscosity at bulk temperature to fuel viscosity at surface temperature.

For this case,
$k = 1.5$ Btu/hr·ft² (°F/ft),
$D = 0.0929$ ft,
$Re = 14,100$,
$Pr = 2.85$,
$\left(\dfrac{\mu}{\mu_s}\right)^{0.14} = 0.965$
$h = 1250$ Btu/hr·ft²·°F.

In Eq. 93,
$k = 13.7$ Btu/hr·ft² (°F/ft),
$a = 0.0129$ ft²,
$c = 0.422$ ft;

therefore

$$(97) \quad \frac{d^2 T}{dx^2} - 2980 \, T = -4.48 \times 10^6 .$$

The solution of Eq. 97 is

(98) $T = c_1 e^{54.6x} + c_2 e^{-54.6x} + 1500$.

The first boundary condition, Eq. 94, gives

(99) $c_1 + c_2 = -350$.

The second boundary condition, Eq. 95, gives

(100) $520 \, c_1 + 0.001923 \, c_2 = 0$.

Therefore

$$c_1 = 0.001294$$

and

$$c_2 = -350 .$$

Thus Eq. 98 becomes

(101) $T = 0.001294 \, e^{54.6x}$
$- 350 \, e^{-54.6x} + 1500$,

and the first derivative of T with respect to x is

(102) $\dfrac{dT}{dx} = 0.07065 \, e^{54.6x}$
$+ 19,110 \, e^{-54.6x}$.

Plots of Eqs. 101 and 102 are shown in Fig. 24. The maximum temperature gradient is about 1600°F per inch.

Temperature in Fuel Tube Elbows as a Result of Afterheat of Residual Fuel. There is a possibility of fuel remaining in the U bends of the reactor fuel tubes after dumping. This residual fuel will rise in temperature because of internal heat generation, and it is desirable to know the maximum temperature that will be attained. Since the activity of the fuel decreases with time after shutdown, an equilibrium will be reached when the heat generation rate is the same as the rate of the heat loss. Once this equilibrium has been reached, the fuel temperature will decrease.

The total heat generation rate of the fuel is given in another portion of this report. From this, the heat generation rate of the fuel in a U bend is

$$(103) \quad Q = \frac{\text{volume of fuel in U bend}}{\text{total fuel volume}} \times Q_f ,$$

where
Q = heat generation rate, Btu/sec
Q_f = total heat generation rate of fuel, Btu/sec.

The temperature rise in the U bend will be greatest when the reflector coolant system is filled with helium (Fig. 9). Under this condition, heat is removed from the tube by free convection and radiation. The free
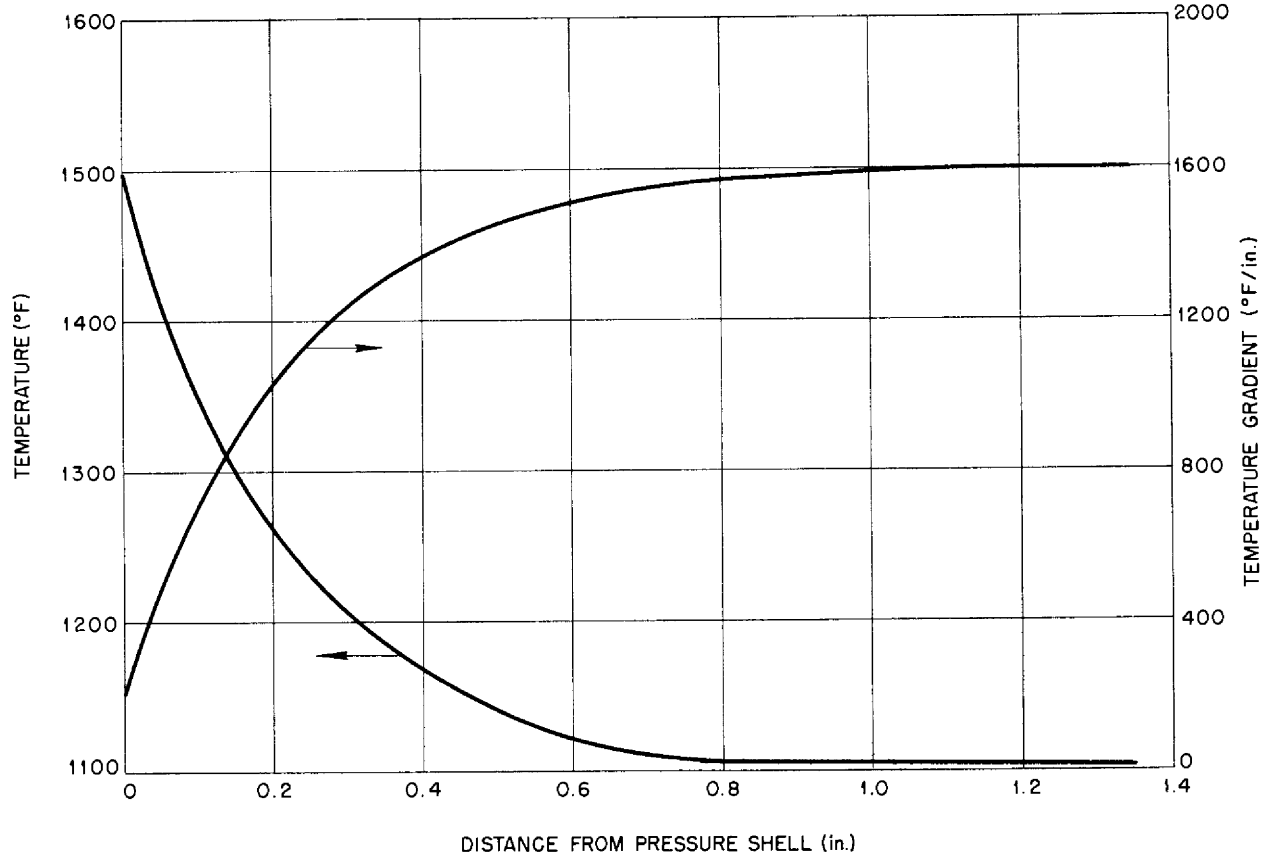
Fig. 24. Temperature and Temperature Gradient in Thermal Sleeve vs. Distance from Pressure Shell.

convection loss is

$$(104) \qquad q_c = hA\theta \ ,$$

where

q_c = heat transferred, Btu/sec,
h = free convection heat transfer coefficient, Btu/sec·ft^2·°F,
A = surface area of tube, ft^2,
θ = temperature difference between the surface of the tube and the helium, °F.

The radiation loss is given by

$$(105) \qquad q_R = \frac{0.173}{3600} \times A$$
$$\times \ \epsilon \left[\left(\frac{T_{tube}}{100} \right)^4 - \left(\frac{T_{sink}}{100} \right)^4 \right] \ ,$$

where

ϵ = radiation emissivity, dimensionless,
T_{tube} = absolute temperature of the surface of the tube, °R,

T_{sink} = absolute temperature of the sink (surrounding material), °R.

The total heat loss is

$$(106) \qquad q = q_c + q_R \ .$$

Jakob has given Nusselt's number (cf., p. 525, Fig. 25-1, of ref. 14) as a function of the product of Grashof's and Prandtl's numbers. The value of Nusselt's number for the existing helium conditions was taken from Jakob's work, and the free-convection heat transfer coefficient was determined.

The temperature change of the fuel and the metal of the tube per unit time is

$$(107) \qquad \Delta T = \frac{Q - q}{\Sigma w c_p} \ ,$$

where

ΔT = temperature change, °F/sec,

$\Sigma w c_p$ = summation of heat capacities of fuel and metal of tube, Btu/°F,

w = weight of material, lb,

c_p = specific heat of material, Btu/lb·°F.

The data required to make the calculations are listed in the following tabulation; only the portion of the tube that is below the tube sheet is considered:

1. For the metal tube,

Area, A	0.226 ft^2
Volume of metal	1.86 in.^{3}
Density, ρ	0.307 lb/in.^{3}
Specific heat, c_p	0.11 Btu/lb·°F

2. For the fuel,

Volume of fuel	4.74×10^{-3} ft^3
Density, ρ	187 lb/ft^3
Specific heat, c_p	0.26 Btu/lb·°F
Total fuel volume of entire system	7.75 ft^3

The temperatures of the fuel at various times after shutdown were calculated by numerical methods for sink temperatures of 1200 and 1300°F. The calculated data for the two sink temperatures are given in Fig. 25.
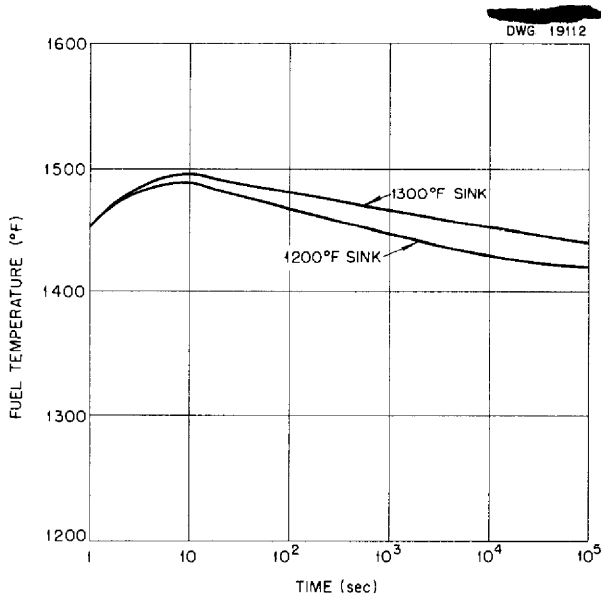

Fig. 25. Temperature of Fuel at Various Times after Shutdown with Fuel Remaining in U Bend.

FORMATION OF NONPLUGGING SOLIDS IN FUEL TUBE IN THE EVENT OF A SMALL LEAK

In the event of a small leak in a fuel tube, it is possible that the NaK entering the fuel tube will precipitate solids that will adhere to the walls of the fuel tube. This deposit can build up to appreciable thickness before causing any measurable change in the flow through the fuel tube. The temperatures which might exist in such a deposit were calculated by treating the solid deposit as a flat plate, with internal heat generation, cooled on one side by the flowing fuel. The differential equation and boundary conditions governing the heat flow are

$$(108) \qquad \frac{d^2\theta}{dx^2} = -\frac{q'}{k} \, ,$$

$$(109) \qquad \frac{d\theta}{dx} = 0 \, , \quad \text{at } x = 0 \, ,$$

$$(110) \qquad -k\frac{d\theta}{dx} = h\theta \, , \quad \text{at } x = \tau \, ,$$

where

θ = temperature difference between a point in the solid and the flowing fuel, °F,

x = distance from tube wall, ft,

q' = internal heat generation, Btu/hr·ft^3,

k = thermal conductivity of fuel, Btu/hr·ft^2 (°F/ft),

τ = thickness of solid deposit, ft,

h = heat transfer coefficient from solid to flowing fuel, Btu/hr·ft^2 (°F/ft).

The heat transfer coefficient is given by

$$(111) \qquad h = 0.027 \frac{k}{D} \text{Re}^{0.8} \text{Pr}^{1/3} \left(\frac{\mu}{\mu_s}\right)^{0.14} \, ,$$

where

D = equivalent diameter, ft,

Re = Reynolds' number,

Pr = Prandtl's number,

$\dfrac{\mu}{\mu_s}$ = ratio of viscosity at bulk temperature to viscosity at surface temperature.

Two cases will be considered; a tube near the inlet where the fuel temperature is about 1170°F and the internal heat generation is 1.64×10^7 Btu/hr·ft³ on the reactor center line, and a tube near the outlet where the fuel temperature is about 1490°F and the internal heat generation is about 0.85×10^7 Btu/hr·ft³ on the reactor center line:

Fuel temperature, °F	1170	1490
Internal heat generation, Btu/hr·ft³	1.64×10^7	0.85×10^7
Equivalent diameter, ft	0.0929	0.0929
Reynolds' number	7700	14,100
Prandtl's number	5.20	2.85
$\left(\dfrac{\mu}{\mu_s}\right)^{0.14}$	0.97	0.97
Heat transfer coefficient, Btu/hr·ft²·°F	945	1260

The solution of the differential equation, Eq. 108, is

$$(112) \qquad \frac{d\theta}{dx} = -\frac{q'x}{k} + c_1 \; ,$$

$$(113) \qquad \theta = -\frac{q'x^2}{2k} + c_1 x + c_2 \; .$$

The boundary conditions, Eqs. 109 and 110, give

$$(114) \qquad c_1 = 0 \; ,$$

$$(115) \qquad c_2 = \frac{q'\tau^2}{2k} + \frac{q'\tau}{h} \; ,$$

and Eq. 113 becomes

$$(116) \qquad \theta = \frac{q'}{2k}(\tau^2 - x^2) + \frac{q'\tau}{h} \; .$$

The maximum temperature in the solid occurs at $x = 0$; therefore

$$(117) \qquad T_{max} = \theta_{max} + T_f = \frac{q'\tau^2}{2k} + \frac{q'\tau}{h} + T_f \; ,$$

where

T_{max} = maximum temperature in the solid, °F,

T_f = temperature of the flowing fuel, °F.

A tabulation of values of some of the terms of Eq. 117 for values of τ of 0.1 and 0.2 in. is presented below:

T_f, °F	1170		1490	
τ, in.	0.1	0.2	0.1	0.2
$\dfrac{q'\tau^2}{2k}$, °F	380	1418	197	787
$\dfrac{q'\tau}{h}$, °F	145	289	56	112
T_{max}, °F	1694	2878	1743	2388

The values for the maximum temperatures of the solid indicate that unless the solids found when NaK and fuel are mixed have a lower melting point than that of Inconel there is danger that a small leak might result in the formation of a solid deposit which would reach a high enough temperature to melt the Inconel tube wall.

Chapter 3
FUEL HEAT DISPOSAL SYSTEM

PERFORMANCE OF FUEL HEAT DISPOSAL SYSTEM

Heat Transfer. The heat added to the fuel in the reactor is disposed of by circulating the fuel to a heat exchanger where it gives up its heat to helium. The hot helium is then passed through a heat exchanger where it gives up its heat to water. The fuel and helium recirculate; the water is dumped. There are actually four fuel-to-helium heat exchangers and four helium-to-water exchangers. These exchangers are arranged (Fig. 1) so that all four fuel-to-helium exchangers are in parallel on the fuel side and all four helium-to-water exchangers are in parallel on the water side. The helium circuits are arranged so that there are two parallel circuits and each circuit contains two fuel-to-helium and two helium-to-water exchangers in series (the exchangers alternate, of course). Figures 26 and 27 show the details of the two types of heat exchangers. The performance of the fuel heat disposal loop over a range of operating conditions is calculated below.

The fuel heat disposal system obeys the following relations:

$$(1) \qquad Q = W_f \; c_f \; (T'_f - T_f) \; ,$$

$$(2) \qquad Q = W_{He} \; c_{He} \; (T'_{He} - T_{He}) \; ,$$

$$(3) \qquad Q = W_w \; c_w \; (T'_w - T_w) \; ,$$

$$(4) \qquad Q = h_{f\text{-}He} \; A_{f\text{-}He} \; \theta_{f\text{-}He} \; ,$$

$$(5) \qquad Q = h_{He\text{-}w} \; A_{He\text{-}w} \; \theta_{He\text{-}w} \; ,$$

where

Q = heat transferred, Btu/sec,
W = weight flow, lb/sec,
T' = maximum temperature, °F,
T = minimum temperature, °F,
c = specific heat, Btu/lb·°F,
h = heat transfer coefficient, Btu/sec·ft^2·°F,
A = heat transfer area, ft^2,
θ = effective log mean temperature difference, °F,

and the subscripts refer to

f = fuel,
He = helium,
w = water,
f-He = fuel-to-helium heat exchanger,
He-w = helium-to-water heat exchanger.

The heat disposal system is operated with the following restraints and conditions:

1. The fuel flow is held fixed at 28.2 lb/sec.
2. The water outlet temperature is thermostatically controlled and held fixed at 135°F.
3. The water inlet temperature will vary with the time of year, but for this analysis it has been assumed to be fixed at 70°F.
4. The mean temperature of the fuel is fixed because the reactor is self-controlling to a constant mean temperature. The design mean temperature is 1325°F. Calculations were also carried out for mean temperatures of 1225 and 1425°F to give some indication of the effect of a change in mean fuel temperature.

The helium weight flow is the independent variable; the flow is controlled by variable speed hydraulic motors which drive the two helium blowers. The dependent variables are Q, W_w, T'_f, T_f, T'_{He}, and T_{He}. Thus there are six unknowns and six equations: the five equations listed above and the one inherent in the fourth condition, namely:

$$(6) \qquad \frac{T'_f + T_f}{2} = \text{a constant} \; .$$

Before these equations can be solved, the heat transfer coefficients and areas must be calculated for the two exchangers. The over-all hA's are

$$(7) \quad (hA)_{f\text{-}He}$$

$$= \left[\frac{1}{(hA)_f} + \frac{1}{(hA)_{He}} + \frac{1}{(hA)_m} \right]^{-1}_{f\text{-}He}$$
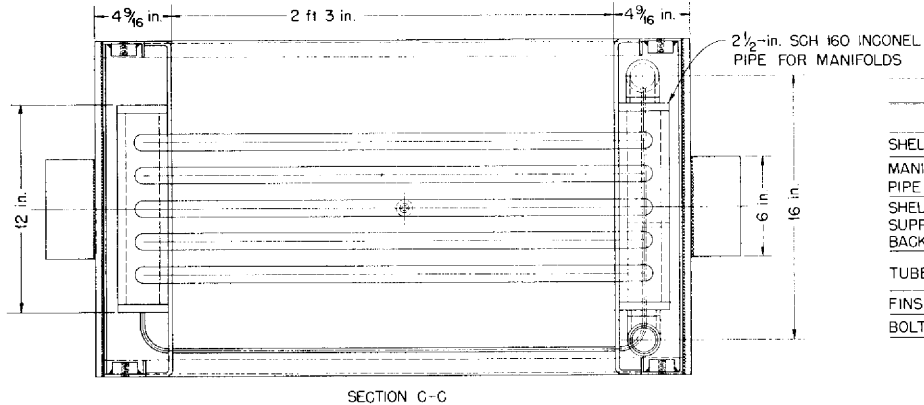
43

DWG. A-3-1-21A

MATERIAL AND MATERIAL SPECIFICATIONS

DESCRIPTION	MATERIAL	SPECIFICATION	QUALITY
SHELL, TUBE SUPPORT PLATES	STAINLESS STEEL	ASME-SA-240	GR S TYPE 304
MANIFOLD, WELD ELL AND PIPE	NICKEL, CHROME AND IRON	ASTM-B-167	INCONEL
SHELL SUPPORTS, MANIFOLD SUPPORTS, FLANGE BARS AND BACKING BARS	STAINLESS STEEL	COMMERCIAL	TYPE 304
TUBES	NICKEL, CHROME AND IRON	ASTM-B-167	INCONEL
FINS	STAINLESS STEEL		TYPE 304
BOLTS	STAINLESS STEEL	ASME-SA-193	GRADE B-8
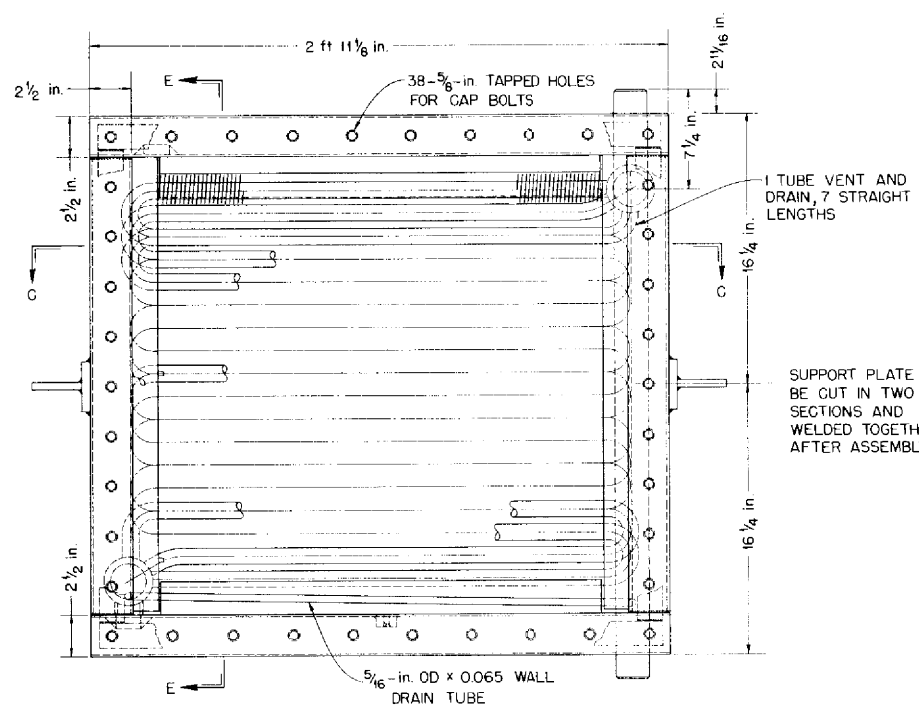
DESIGN DATA

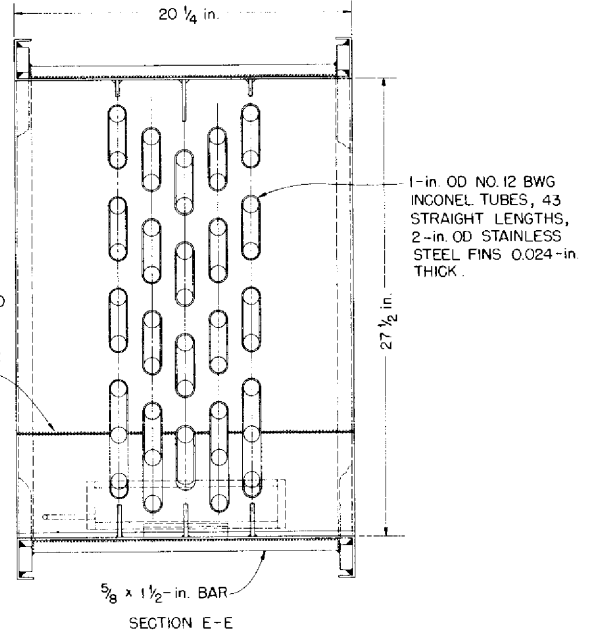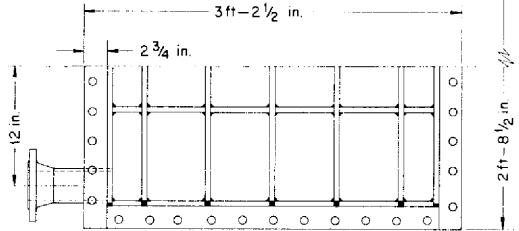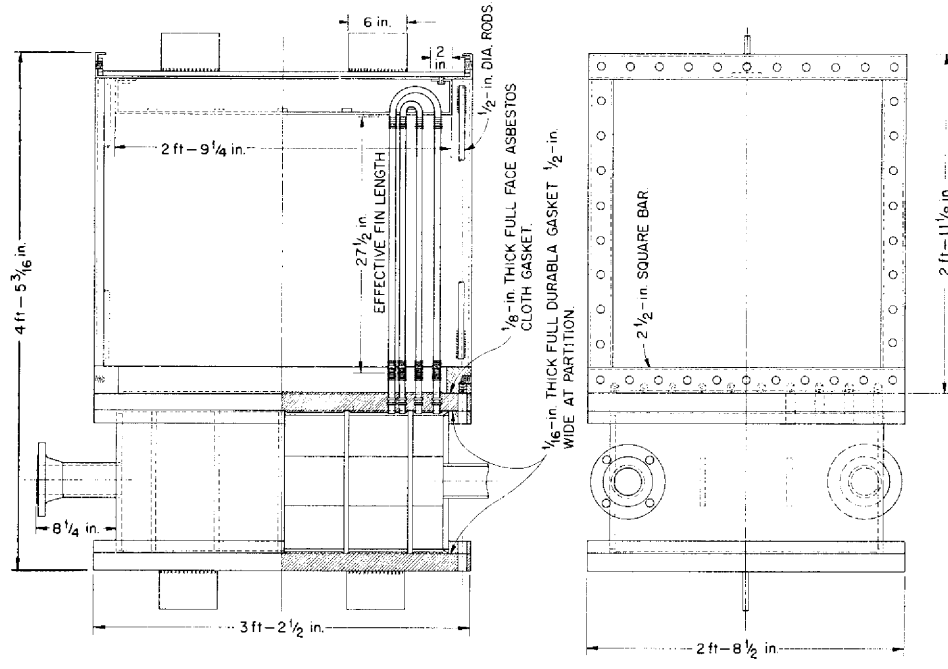|		
1.	DESIGN PRESSURE SHELL SIDE	6 in WATER
2.	DESIGN PRESSURE TUBE SIDE	25 psi
3.	DESIGN TEMPERATURE SHELL SIDE	1500 °F
4.	DESIGN TEMPERATURE TUBE SIDE	1500 °F
5.	HYDROSTATIC TEST PRESSURE TUBE SIDE	500 psi

Fig. 26. Fuel-to-Helium Heat Exchanger.

DESIGN DATA		
	SHELL	TUBES
DESIGN PRESSURE	6-in. H$_2$O	50 psi
DESIGN TEMPERATURE	1500 °F	340 °F

HALF VIEW OF STAT. HEAD WITH COVER REMOVED

FEET

MATERIAL AND MATERIAL SPECIFICATIONS

DESCRIPTION	MATERIAL	SPEC	QUALITY
SHELL FLANGE AT TUBE SHEET, GAS INLET FLANGE, SHELL AND SHELL COVER PLATE, BLANKING-OFF PLATE, TUBE SUPPORT BAR, BACKING-UP BAR.	STAINLESS STEEL	ASME SA-240 GR 5	TYPE S-304
STAT. HEAD PLATES, STAT. HEAD FLANGES, GAS OUTLET FLANGE, STAT. HEAD PARTITIONS, STAT. HEAD TIE PLATES, STAT. HEAD COVER PLATE, TUBE SHEET.	FIREBOX STEEL	ASME SA-285	GRADE C
3-in., 150 lb. WELDING NECK FLANGE.	FORGE STEEL	ASME SA-181	GRADE I
3-in. SCH. 40 PIPE.	SEAMLESS STEEL	ASME SA-106	GRADE A
TUBES, TUBE BENDS.	SEAMLESS STEEL	ASME SA-179	MIN WALL
FINS	COPPER	COMMERCIAL	
STAT. HEAD GASKETS.	DURABLA	COMMERCIAL	
SHELL GASKET SMEARED BOTH SIDES WITH PLASTISEAL.	ASBESTOS CLOTH	COMMERCIAL	
BOLTING FOR TUBE SHEET AND SHELL FLANGE.	STAINLESS STEEL	ASME SA-193 B8	
NUTS AT TUBE SHEET AND STAT. HEAD COVER PLATE.	BETH OIL QUENCH	ASME SA-194	CLASS 2H
BOLTING FOR STAT. HEAD COVER PLATE.	ALLOY STEEL		

Fig. 27. Helium-to-Water Heat Exchanger.

45

and

(8) $(hA)_{He-w}$

$$= \left[\frac{1}{(hA)_{He}} + \frac{1}{(hA)_w} + \frac{1}{(hA)_m} \right]^{-1}_{He-w} ,$$

where the subscript m refers to the metal of the tube wall.

The heat transfer coefficients of the fuel are calculated from the curve of ref. 11 (p. 193). The heat transfer coefficient of the water is

(9) $h_w = 0.027 \dfrac{k_w}{D_w} Re_w^{0.8} Pr_w^{1/3} \left(\dfrac{\mu}{\mu_s} \right)_w^{0.14}$

(Sieder-Tate relation[15]), where

k = thermal conductivity, Btu/sec·ft² (°F/ft),

D = equivalent diameter, ft,

Re = Reynolds' number,

Pr = Prandtl's number,

μ = viscosity at bulk temperature, lb/hr·ft,

μ_s = viscosity at surface temperature, lb/hr·ft.

The liquid-side areas are:

(10) $\qquad A_f = \pi D_f L_{f-He}$

and

(11) $\qquad A_w = \pi D_w L_{He-w}$,

where L is the total effective length of the heat exchanger tubes in feet.

The resistance of the metal is

(12) $\left[\dfrac{1}{(hA)_m} \right]_{f-He} = \dfrac{\ln \left(\dfrac{D_o}{D_f} \right)_{f-He}}{2\pi (k_m)_{f-He} \, L_{f-He}}$

and

(13) $\left[\dfrac{1}{(hA)_m} \right]_{He-w} = \dfrac{\ln \left(\dfrac{D_o}{D_f} \right)_{He-w}}{2\pi (k_m)_{He-w} \, L_{He-w}}$,

where D_o is tube outside diameter in feet.

The heat transfer coefficients on the gas side are taken from a corre-lation by Kern of data by Jameson and Tate and Cartinhour (cf., p. 555 of ref. 8). Kern's correlation curve may be approximated by the following equation:

(14) h_{He}

$$= 0.092 \dfrac{k_{He}}{D_{He}} Re_{He}^{0.723} Pr_{He}^{1/3} \left(\dfrac{\mu}{\mu_s} \right)_{He}^{0.14} ,$$

where D_{He} for the fin and tube con-figuration is defined as

(15) $\qquad D_{He} = \dfrac{2(A_o + A_f)}{\pi(\text{projected perimeter})}$,

where

A_o = tube outside bare area, ft²,

A_f = fin area, ft²,

and the projected perimeter is the sum of all the external distances in the plan view of the finned tubes (ft).

The mass velocity used in the Reynolds' number is computed from the free flow area in a single bank of tubes at right angles to the gas flow. The helium-side heat transfer area is

(16) $\qquad A_{He} = A_o + \eta_f A_f$,

where η_f is the fin efficiency.[16]

Table 8 lists the pertinent infor-mation obtained from the heat exchanger designs (Figs. 26 and 27) and Eqs. 7 through 16. Values are given for three different flow rates of helium and of water; curves were plotted from these values and used in the solution of Eqs. 1 through 6.

The data of Table 8 were used to solve the six simultaneous equations (Eqs. 1 through 6) for various values of the independent variable – helium weight flow. (Inasmuch as the water heat transfer coefficient is a function of the water flow rate, it was necessary to assume a water flow rate for each helium flow rate and solve the equations by iteration.) The results of the solution of Eqs. 1 through 6 are shown in Figs. 28 and 29, where the heat transferred, maximum fuel temper-ature, and maximum and minimum helium

TABLE 8. HEAT EXCHANGER DATA

	FUEL-TO-HELIUM HEAT EXCHANGER	HELIUM-TO-WATER HEAT EXCHANGER
Tube outside diameter, in.	1.0	0.625
Tube wall thickness, in.	0.109	0.049
Tube material	Inconel	Steel
Fin outside diameter, in.	2.0	0.75
Number of fins per inch	7	16
Fin thickness, in.	0.024	0.014
Fin material	Stainless steel	Copper
Tube transverse pitch, in.	2.75	2.25
Tube longitudinal pitch, in.	2.43	1.47
Number of tubes per exchanger	43	360
Number of tubes transverse to flow (per exchanger)	9	12
Exchanger height, in.	24.75	27.0
Exchanger width (also active tube length), in.	26.25	27.5
Total active tube length per exchanger, ft	93.65	825
Liquid flow area per exchanger, ft^2	0.01006 (First bank group*), 0.00671 (Second bank group*)	0.0545
Liquid flow rate per exchanger, lb/sec	7.05	10.61, 7.08, 3.54
Liquid velocity, ft/sec	3.74, 5.61	3.11, 2.08, 1.04
Reynolds' number	5890, 8840	19,000, 12,700, 6,340
Liquid heat transfer coefficient, Btu/sec·ft^2·°F	0.24, 0.38	0.27, 0.20, 0.11
Liquid heat transfer area per exchanger, ft^2	11.15, 8.02	114
$(hA)_{liquid}$ per exchanger, Btu/sec·°F	2.676, 3.048	30.8, 22.8, 12.5
Total	5.724	
$(1/hA)_{liquid}$ per exchanger, sec·°F/Btu	0.175	0.0325, 0.0439, 0.080
$(1/hA)_m$ per exchanger, sec·°F/Btu	0.137	0.00456
Helium-side equivalent diameter (D_{He}), in.	1.447	0.670
Helium free flow ratio	0.575	0.71
Helium flow area per exchanger, ft^2	2.60	3.66
Helium flow rate per exchanger, lb/sec	1.5, 1.0, 0.5	1.5, 1.0, 0.5
Helium Reynolds' number	4050, 2630, 1290	1330, 860, 420
Helium heat transfer coefficient, Btu/sec·ft^2·°F	0.0083, 0.0061, 0.0036	0.0080, 0.0059, 0.0035
Fin efficiency	0.37, 0.43, 0.55	1.0, 1.0, 1.0
Helium heat transfer area,** ft^2	115, 131, 162	402, 402, 402
$(hA)_{He}$ per exchanger, Btu/sec·°F	0.955, 0.800, 0.580	3.22, 2.37, 1.40
$(1/hA)_{He}$ per exchanger, sec·°F/Btu	1.05, 1.25, 1.72	0.310, 0.422, 0.714

*The liquid side of the fuel-to-helium heat exchanger is divided into two groups of tubes. The first bank group has three tubes in parallel and is connected in series with the second bank group, which has two tubes in parallel.

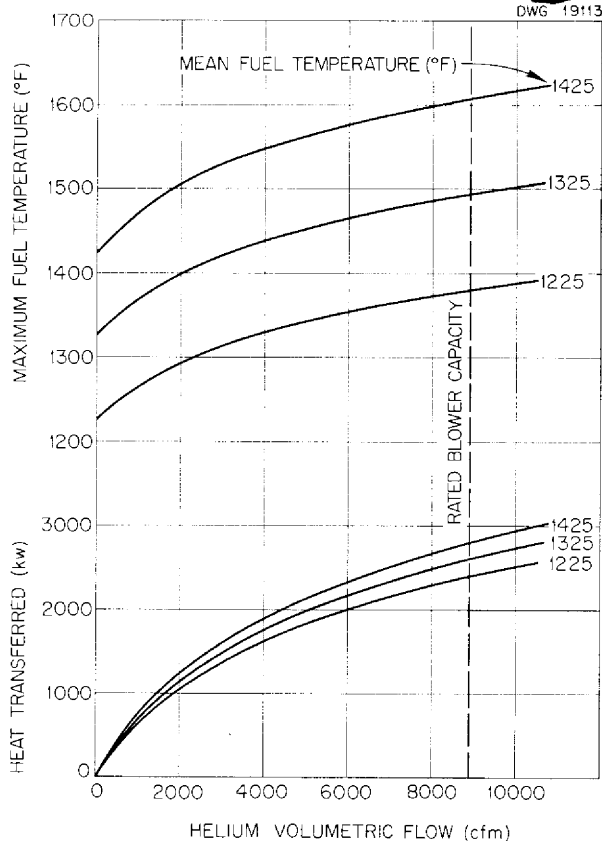**"Area" varies with helium flow rate because the fin efficiency varies with helium flow rate (cf., Eq. 16).

Fig. 28. Heat Transferred and Maximum Fuel Temperature vs. Helium Volumetric Flow.

Fig. 29. Maximum and Minimum Helium Temperature vs. Helium Volumetric Flow.

temperatures are plotted against helium volumetric flow for the three different values of mean fuel temperature investigated.

At design point, 700 kw is removed by the reflector coolant and rod cooling circuits. Therefore, 2300 kw is to be removed by the fuel.

Film Temperature. Because the fuel has a high melting point (about 970°F), the minimum fuel film temperature must be calculated to determine the situation with respect to freezing of the fuel film. The minimum fuel film temperature at any point may be calculated from the relation

$$(17) \qquad T_{f_{min}} = T_{f_{bulk}} - \frac{Q}{(hA)_f} ,$$

where

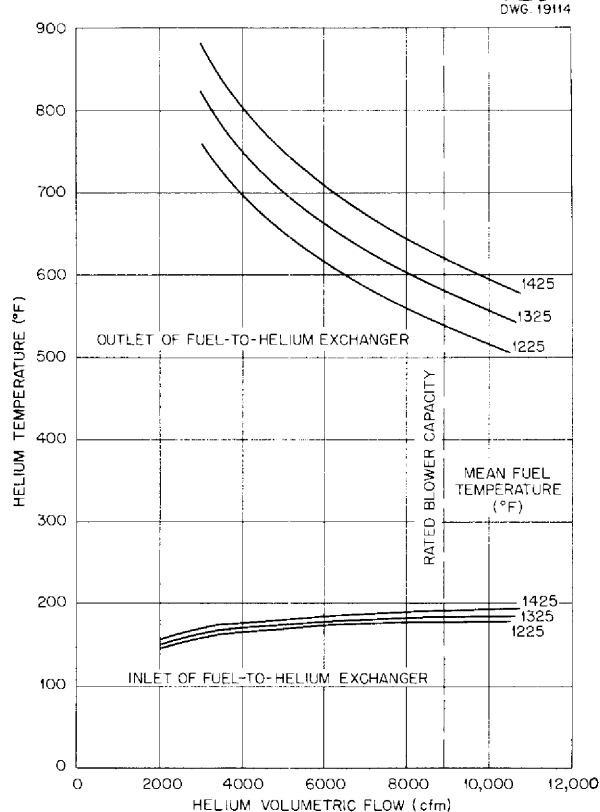$T_{f_{min}}$ = minimum fuel film temperature at the point in question, °F,

$T_{f_{bulk}}$ = bulk fuel temperature at the point in question, °F.

The other symbols mean the same as they did previously, except that the fuel heat transfer coefficient, h_f, must be evaluated locally, that is, at the point in question. Several critical points were investigated in the fuel-to-helium exchanger, and a plot of the lowest of the temperatures vs. helium volumetric flow (and various mean fuel temperatures) is shown in Fig. 30 a.

Pressure Drop. The pressure drops in the fuel and in the helium have been calculated for the exchangers. The fuel pressure drop was calculated by using the customary Fanning equation[11] for the straight sections, and the curves presented by Cox and Germano[12] for the bends, exists, and entrances. Since the fuel flow is constant and the properties do not vary substantially in the range of mean fuel temperatures considered, the

48
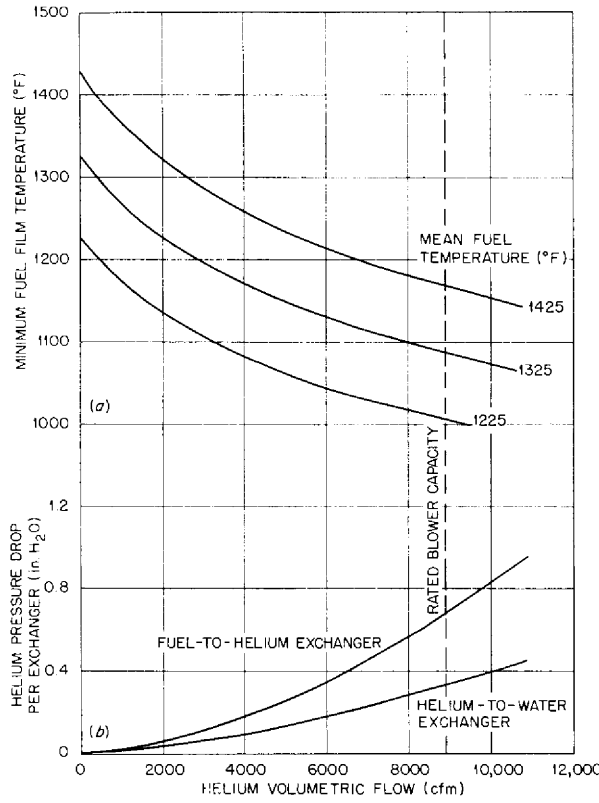
**Fig. 30. Minimum Fuel Film Tempera-
ture and Helium Pressure Drop vs.
Helium Volumetric Flow.**

fuel pressure drop is constant and
equal to about 17 psi.

The pressure drop in the helium
was calculated by the method given
by Gunter and Shaw:[17]

$$(18) \qquad \Delta P = 5.305 \times 10^{-10} \, \frac{f G_{He}^2 L_p}{D'_{He} \; s \left(\frac{\mu}{\mu_s}\right)_{He}^{0.14}} \left(\frac{D'_{He}}{S_t}\right)^{0.4} \left(\frac{S_l}{S_t}\right)^{0.6} ,$$

where

ΔP = pressure drop, in. of H_2O,

f = friction factor,

G_{He} = helium unit weight flow,
lb/sec·ft²,

L_p = length of helium flow path, ft,

s = average helium specific gravity,

S_t = transverse pitch, ft,

S_l = longitudinal pitch, ft,

μ = viscosity at bulk temperature,
lb/hr·ft,

μ_s = viscosity at surface tempera-
tures, lb/hr·ft,

D'_{He} = equivalent diameter (cf.,
Eq. 19), ft.

The equivalent diameter in the
Gunter-Shaw correlation is

$$(19) \qquad D'_{He} = \frac{4 \times \text{net free volume}}{A_f + A_o} ,$$

where A_f and A_o have the same meanings
as previously.

The values of D'_{He} are 0.0438 ft for
the fuel-to-helium exchangers and
0.1365 ft for the helium-to-water
exchangers. The friction factor, f,
which is a function of Reynolds'
number, is evaluated from the Gunter-
Shaw correlation. The helium pressure
drop is plotted against helium volu-
metric flow for both exchangers in
Fig. 30b. The helium pressure drop is
not greatly affected by the mean fuel
temperature, and thus the curves of
Fig. 30b are valid for the range of
mean fuel temperature considered.

The pressure drops in the fuel and
in the helium for the remainder of
the fuel and helium circuits have been
calculated by using the Fanning
equation and the Cox and Germano data.
Figure 1 shows the pressure at various
points in the fuel circuit. The fuel
pressure drop external to the heat
exchangers is 40 psi; the total fuel
pressure drop is 57 psi (Fig. 2 shows
the fuel piping). Figure 31 shows the
helium ducting for the fuel circuit.
The pressure drop external to the
heat exchangers and the total pressure
drop are plotted against helium volu-
metric flow in Fig. 32.

TEMPERATURE IN FUEL SYSTEM BECAUSE
OF AFTERHEAT IN THE EVENT OF
COMPLETE PUMP FAILURE

If there were a complete power
failure and all the fuel remained in

DUCT

ELBOW

ELBOW

He TO H₂O
HEAT EXCHANGER

HEAT BARRIER

FUEL TO He
HEAT EXCHANGER

He TO H₂O
HEAT EXCHANGER

HEAT BARRIER

TRANSITION PIECE

ELBOW

HELIUM BLOWER

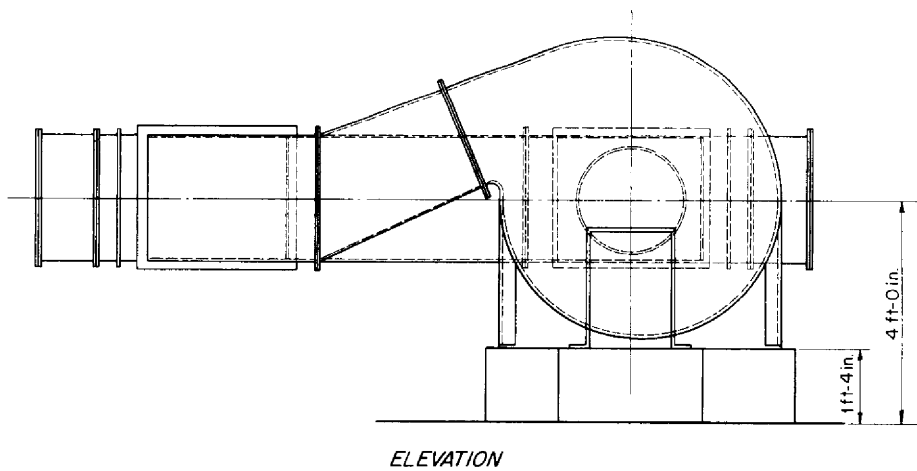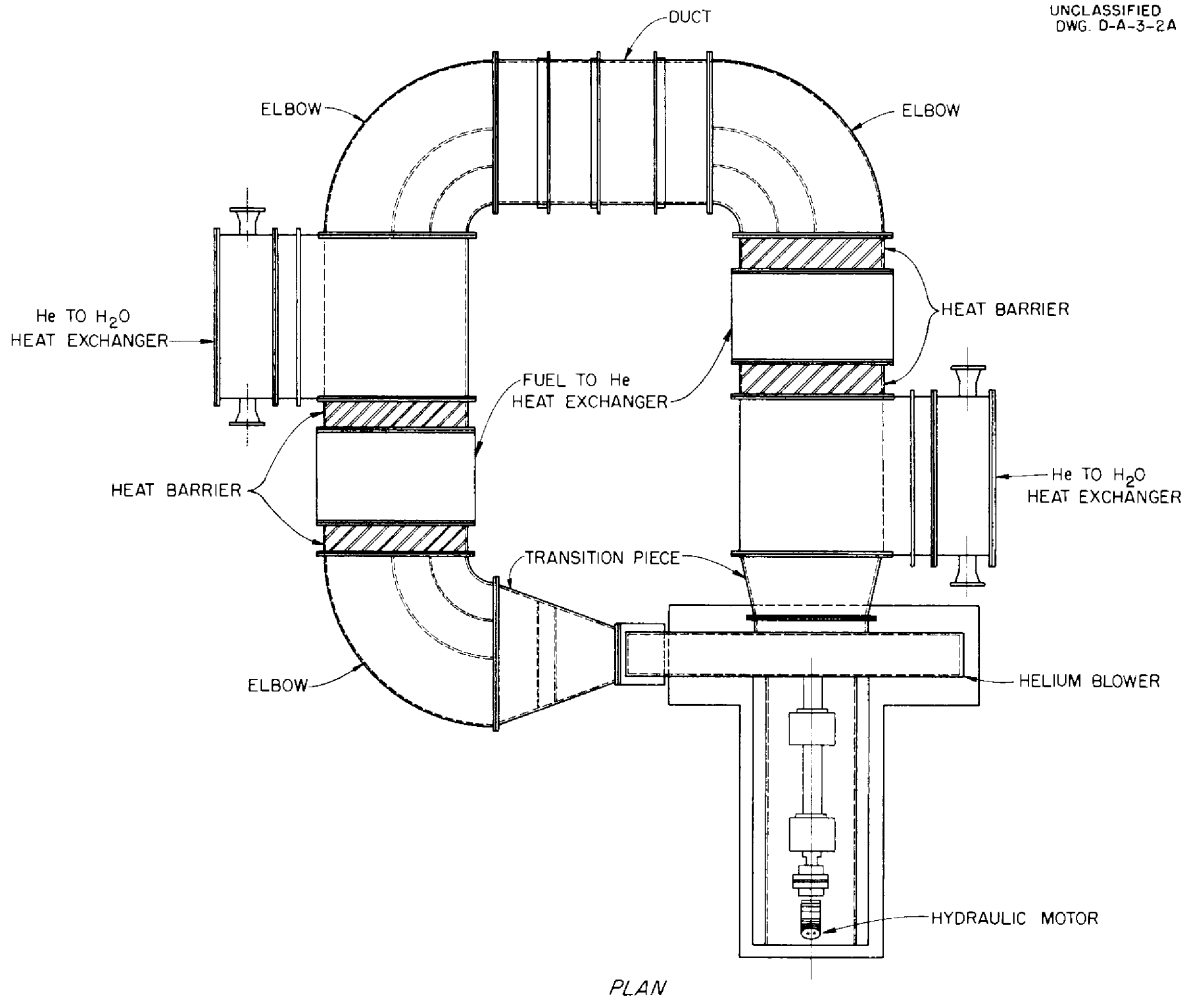HYDRAULIC MOTOR

PLAN

4 ft-0 in.

1 ft-4 in.

ELEVATION

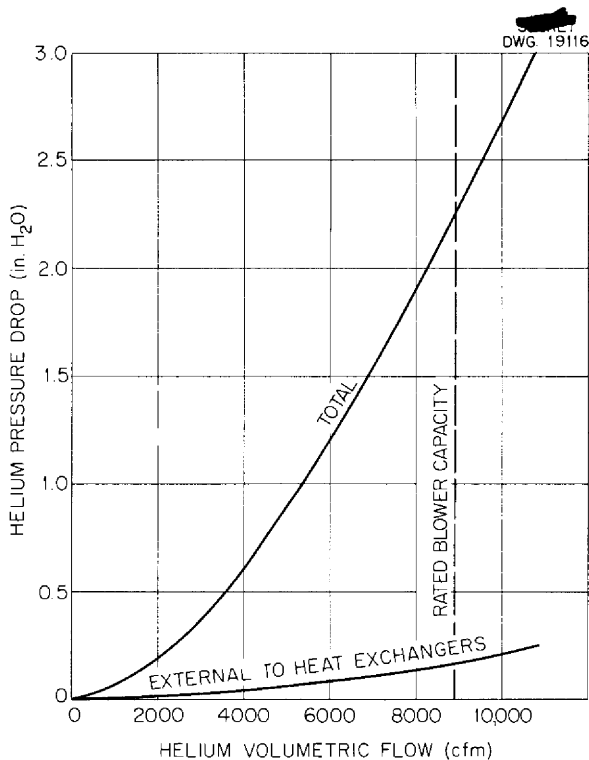**Fig. 31. Helium Loop for Fuel Circuit.**

Fig. 32. Helium Pressure Drop vs. Helium Volumetric Flow.

the system, it would be desirable to know the maximum temperature the fuel would attain (Fig. 1). The temperature rise in the fuel will be due to internal heat generation. However, since the heat generation rate decreases with time after shutdown, at some temperature an equilibrium will be reached between the heat generated and the heat lost from the system. The maximum fuel temperature will be attained at equilibrium. As soon as the maximum has been reached, the temperature will decrease.

The total heat generation rate of the fuel is given as a function of

time after shutdown in chap. 9. Heat is lost from the components of the fuel system by free convection to the helium in the pits and by thermal radiation to the equipment and walls. This heat loss is given in chap. 6.

The change in temperature of the fuel and metal of each fuel system component per unit time is

$$(20) \qquad \Delta T = \frac{Q_f - Q_l}{\Sigma w c_p}$$

and

$$(21) \quad Q = \frac{\text{volume of fuel in component}}{\text{total fuel volume}} \times Q_f \ ,$$

where

ΔT = temperature change, °F/sec,

Q_f = total heat generation rate in the fuel, Btu/sec,

Q = heat generation rate in the fuel in the component, Btu/sec,

Q_l = heat loss from the component, Btu/sec,

$\Sigma w c_p$ = heat capacity of component plus fuel, Btu/°F,

w = weight of material, lb,

c_p = specific heat of material, Btu/lb·°F.

The most critical points in the fuel system under the condition postulated are those with the smallest surface-to-volume ratio. The components in this category are the reactor (Fig. 9), the surge tanks (Fig. 33), and the 2-in. pipe lines.

Table 9 gives the data needed to calculate the temperature rise in these components.

TABLE 9. DATA FOR CALCULATION OF TEMPERATURE RISE OF VARIOUS COMPONENTS

COMPONENT	$\Sigma w c_p$ (Btu/sec)	FUEL VOLUME (ft^3)	TEMPERATURE AT FAILURE (°F)
Reactor	4166	1.96	1400
Surge tank	48.6	0.83	1150
2-in. pipe (per foot of length)	1.52	0.023	1500
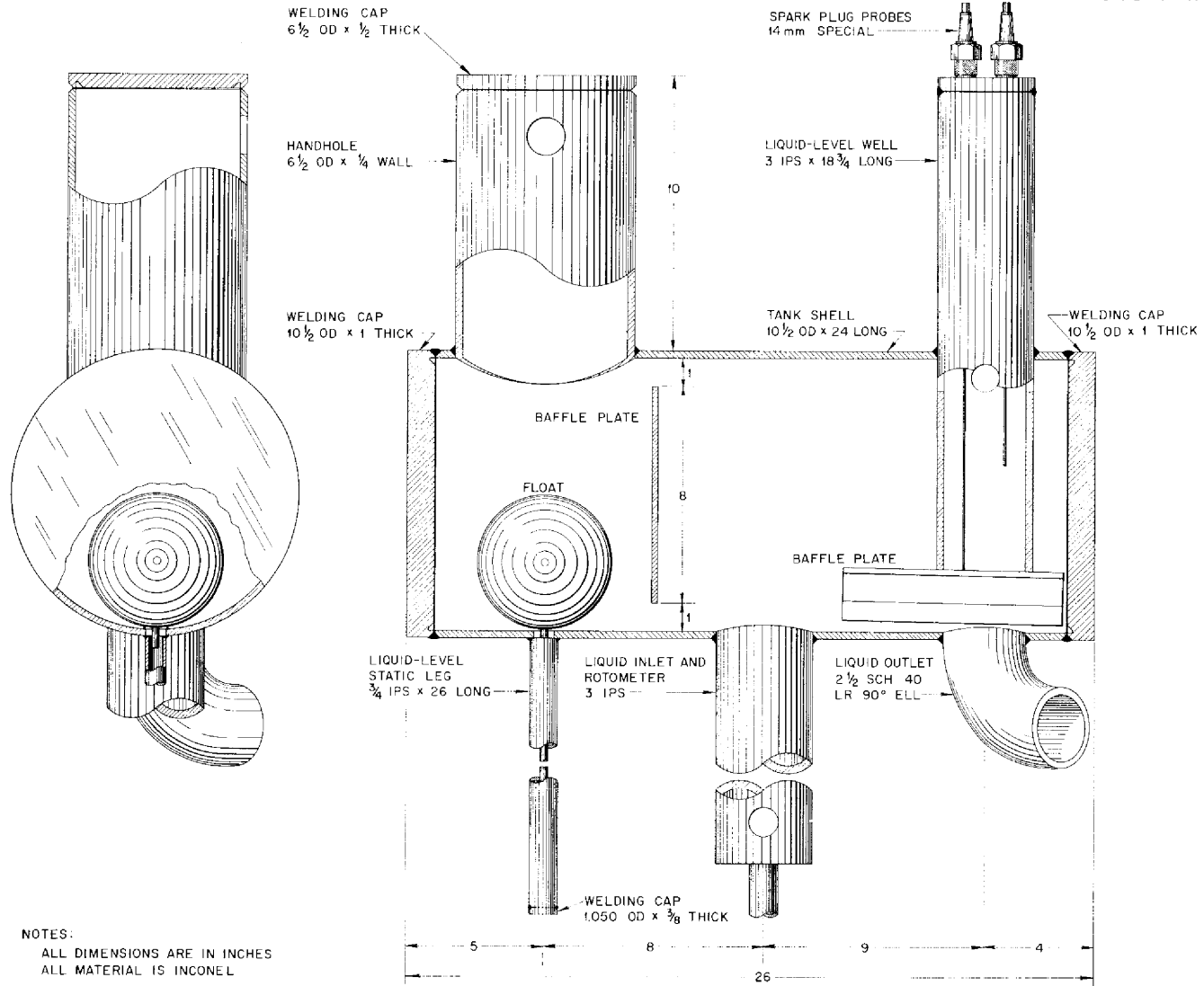
Fig. 33. Fuel Surge Tank.

For the metal

$$c_p = 0.11 \text{ Btu/lb} \cdot {}^\circ\text{F},$$
$$\rho = 0.307 \text{ lb/in.}^3,$$

and for the fuel

$$c_p = 0.26 \text{ Btu/lb} \cdot {}^\circ\text{F},$$
$$\rho = 187 \text{ lb/ft}^3.$$

The total volume of fuel in the system was taken to be 7.75 ft^3, and the sink temperature was taken as $130{}^\circ\text{F}$ or $590{}^\circ\text{R}$.

The maximum temperature to be expected in each component was calculated numerically by using Eqs. 20 and 21. The following results were obtained:

COMPONENT	MAXIMUM TEMPERATURE ($^\circ$F)
Reactor	1400
Surge tank	1900
2-in. pipe	1520

Curves of temperature vs. time after shutdown are shown in Fig. 34.

Fig. 34. Component Temperature vs. Time after Shutdown.

Chapter 4

REFLECTOR COOLANT HEAT DISPOSAL SYSTEM

The heat added to the reflector coolant (NaK) in the reactor is disposed of by circulating the NaK to a heat exchanger where it gives up its heat to helium. The hot helium is then passed through a h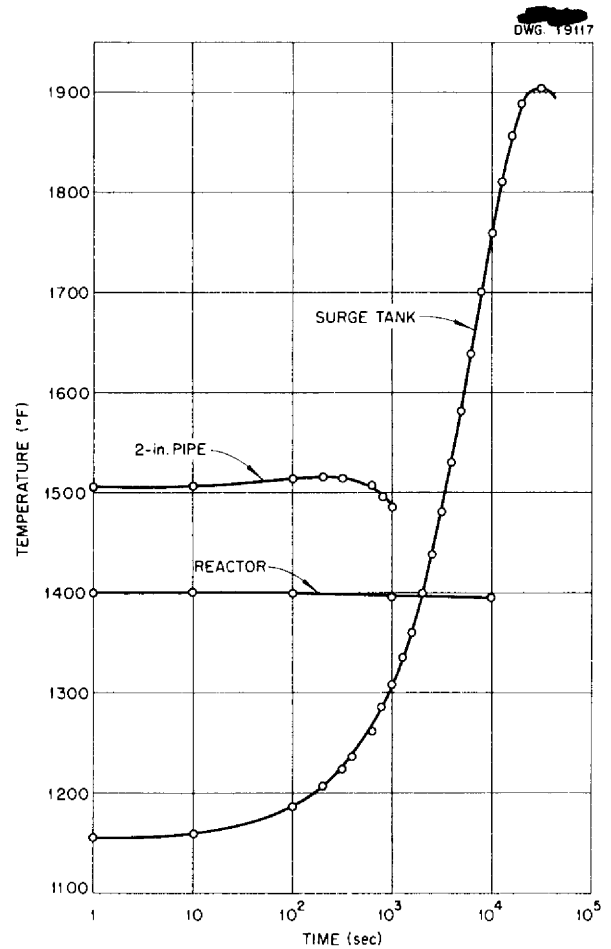eat exchanger where it gives up its heat to water. The NaK and helium recirculate; the water is dumped. There are two NaK-to-helium exchangers and two helium-to-water exchangers arranged (Fig. 1) so that the liquid sides of each pair of exchangers are in parallel. The helium circuit consists of two parallel circuits, and each circuit contains one NaK-to-helium and one helium-to-water heat exchanger in series. Figures 35 and 36 show the details of the two types of heat exchangers. The performance of the NaK heat disposal loop over a range of operating conditions is calculated below.

The NaK heat disposal system obeys the following relations:

(1) $\quad Q = W_{NaK} \, c_{NaK} \, (T'_{NaK} - T_{NaK})$,

(2) $\quad Q = W_{He} \, c_{He} \, (T'_{He} - T_{He})$,

(3) $\quad Q = W_w \, c_w \, (T'_w - T_w)$,

(4) $\quad Q = h_{NaK-He} \, A_{NaK-He} \, \theta_{NaK-He}$,

(5) $\quad Q = h_{He-w} \, A_{He-w} \, \theta_{He-w}$,

where

$\quad Q$ = heat transferred, Btu/sec,
$\quad W$ = weight flow, lb/sec,
$\quad T'$ = maximum temperature, °F,
$\quad T$ = minimum temperature, °F,
$\quad h$ = heat transfer coefficient, Btu/sec·ft² (°F/ft),
$\quad A$ = heat transfer area, ft²,
$\quad \theta$ = effective log mean temperature difference, °F,

and the subscripts refer to

$\quad$ NaK = NaK,
$\quad$ He = helium,
$\quad w$ = water,
$\quad$ NaK-He = NaK-to-helium heat exchanger,
$\quad$ He-w = helium-to-water heat exchanger.

The heat disposal system is operated with the following restraints and conditions:

1. The NaK flow is held fixed at 23 lb/sec.
2. The helium volumetric flow per exchanger is held fixed at 2000 cfm at blower inlet temperature. This fixes W_{He} once T_{He} is known.
3. The water outlet temperature is thermostatically controlled and is held fixed at 100°F.
4. The water inlet temperature will vary with the time of the year, but for this analysis it has been assumed to be fixed at 70°F.

The heat transferred is chosen as the independent variable in the system, since it is determined by the heat added to the NaK in the reactor. This leaves as dependent variables T'_{NaK}, T_{NaK}, T'_{He}, T_{He}, and W_w. There are therefore five unknowns and five equations (Eqs. 1 through 5). Before these equations can be solved, the heat transfer coefficients and areas must be calculated for the two heat exchangers.

The over-all hA's are:

(6) $\quad (hA)_{NaK-He}$

$$= \left[\frac{1}{(hA)_{NaK}} + \frac{1}{(hA)_{He}} + \frac{1}{(hA)_m} \right]^{-1}_{NaK-He}$$

and

(7) $\quad (hA)_{He-w}$

$$= \left[\frac{1}{(hA)_{He}} + \frac{1}{(hA)_w} + \frac{1}{(hA)_m} \right]^{-1}_{He-w} \, ,$$

where m refers to the metal of the tube wall.

The liquid-side heat transfer coefficients are:

(8) $\quad h_{NaK} = \dfrac{k_{NaK}}{D_{NaK}} (7.0 + 0.025 \, Pe^{0.8})$

SECTION A-A
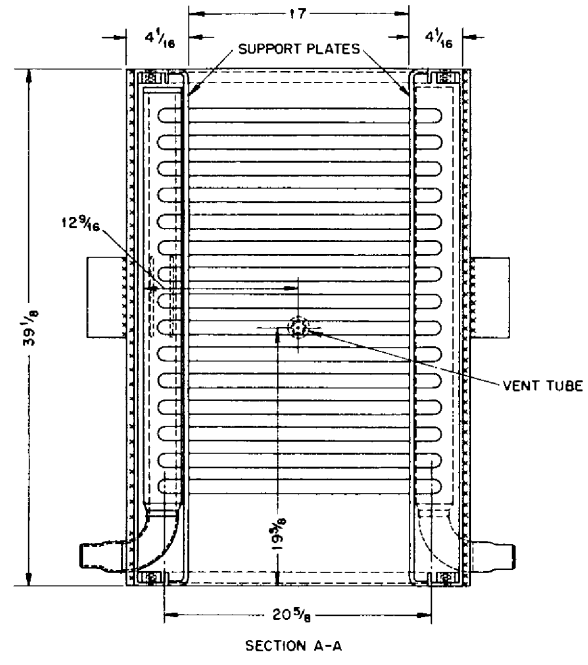
MATERIAL AND MATERIAL SPECIFICATIONS

PART	MATERIAL	SPECS.	QUALITY
SHELL, TUBE SUPPORT PLATES.	STEEL	ASTM A-283	GRADE C
MANIFOLD, WELD ELL, AND REDUCER.	NICKEL, CHROME, IRON	ASTM B-167	INCONEL
SHELL SUPPORTS, FLANGE BARS BACKING BARS AND AIR STOPS.	STEEL	ASTM A-283	GRADE C
TUBES	NICKEL, CHROME, IRON	ASTM B-167	INCONEL
MANIFOLD CAP AND TRANSITION.	NICKEL, CHROME, IRON	ASTM B-167	INCONEL
FINS	STAINLESS STEEL	TYPE 304	
MANIFOLD SUPPORTS	STAINLESS STEEL	TYPE 304	
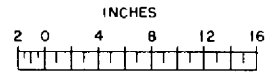
INCHES

NOTE: ALL DIMENSIONS IN INCHES.

SUPPORT PLATES

VENT TUBE

ELEVATION

SECTION C-C

Fig. 35.   NaK-to-Helium Heat Exchanger.

55

PLAN VIEW labels:

⅛-in. TH'K FULL FACE ASBESTOS CLOTH GASKET

½ × 1-in. BAR WELDED TO BLANKING-OFF PLATE

1 × ⅜-in. BARS WELDED TO BLANKING-OFF PLATE

¼-in. BLANKING-OFF PLATE

2 ft - 11⅛ in.

3 ft - 2⅝ in

2½ in.

20⅛ in.

2 ft - 10 9/16 in.

PLAN VIEW

SIDE ELEVATION labels:

⅛-in. TH'K FULL FACE ASBESTOS CLOTH GASKET

¼-in. DIA. VENT HOLE

1/32-in. TH'K DURABLA GASKET

2 ft - 1⅛ in.

9 7/16 in.

10 7/16 in.

1¼ in.

3 in.

21 in.

21⅜ in.

SIDE ELEVATION

2 ft 9⅝-in × ¼-in. × 2-in STIFFENING BAR

⅝ × 1½-in. BAR ALL AROUND OPENING BOTH SIDES

1/32-in. TH'K DURABLA GASKET

1½-in. 150-lb F.S. WELDING NECK FLANGE

¼-in. DIA DRAIN HOLE

MATERIAL AND MATERIAL SPECIFICATIONS			
DESCRIPTION	MATERIAL	SPECIFICATION	QUALITY
SHELL, SHELL COVER ℞, BLANKING-OFF ℞, TUBE SUPPORT BAR, BACKING-UP BARS FOR SHELL FLANGE, SHELL REINFORCING BARS, SHELL SUPPORT ℞, AIR BAFFLE BOX	STEEL	ASTM-A-283	GRADE C
STAT. HD. FLANGES, SUPP'T ℞'S, STAT. HD. PARTITIONS, STAT. HD. TIE ℞'S, STAT. HD. COVER ℞, TUBE SHEET STAT. HD. ℞'S	FIRE BOX STEEL	ASTM-A-285	GRADE C
1½-in. 150-lb WELDING NECK FLANGE	FORGE STEEL	ASTM-A-181	GRADE 1
1½-in. SCH. 40 PIPE	SEAMLESS STEEL	ASTM-A-106	GRADE A
TUBES	SEAMLESS STEEL	ASTM-A-179	MIN WALL
FINS	COPPER	COMMERCIAL	
STAT. HD. GASKETS	DURABLA	COMMERCIAL	
SHELL GASKET AT TUBE SHEET	⅛-in TH'K ASBESTOS CLOTH	COMMERCIAL	
TAP BOLTS AT BLANKING-OFF BAFFLE	ALLOY STEEL	COMMERCIAL	
BOLTING AT STAT. HD. AND TUBE SHEET	ALLOY STEEL	ASTM-A-193 B-7	125000 TS 105000 YP
TIE RODS, SPACERS AND NUTS	STEEL	COMMERCIAL	
NUTS AT TUBE SHEET AND COVER PLATE	BETH OIL QUENCH	ASTM-A-194	CLASS 2H

DESIGN DATA		
	SHELL	TUBES
DESIGN PRESSURE	6 in WATER	50 psi
DESIGN TEMPERATURE	1000°F	340°F
HYDROSTATIC TEST PRESSURE		75 psi
DESIGN TEMPERATURE AT TUBE SHEET	650°F	
MAXIMUM METAL TEMPERATURE, SHELL SIDE 900°F		

Fig. 36.   Helium-to-Water Heat Exchanger.

(Lyon equation[6]) and

$$(9) \quad h_w = 0.027 \frac{k_w}{D_w} \text{Re}_w^{0.8} \text{Pr}_w^{1/3} \left(\frac{\mu}{\mu_s}\right)_w^{0.14}$$

(Sieder-Tate equation[15]), where

k = thermal conductivity, Btu/sec·ft² (°F/ft),

D = equivalent diameter, ft,

Pe = Peclet's number,

Re = Reynolds' number,

Pr = Prandtl's number,

μ = viscosity at bulk temperature, lb/hr·ft,

μ_s = viscosity at surface temperature, lb/hr·ft.

The liquid-side areas are

$$(10) \quad A_{NaK} = \pi D_{NaK} L_{NaK-He}$$

and

$$(11) \quad A_w = \pi D_w L_{He-w} \quad,$$

where L is the total effective length of the heat exchanger tubes in feet.

The resistance of the metal is

$$(12) \quad \left[\frac{1}{(hA)_m}\right]_{NaK-He} = \frac{\ln\left(\frac{D_o}{D_{NaK}}\right)_{NaK-He}}{2\pi \left(k_m\right)_{NaK-He} L_{NaK-He}}$$

and

$$(13) \quad \left[\frac{1}{(hA)_m}\right]_{He-w} = \frac{\ln\left(\frac{D_o}{D_w}\right)_{He-w}}{2\pi \left(k_m\right)_{He-w} L_{He-w}} \quad,$$

where D_o is the tube diameter in feet.

The heat transfer coefficients on the gas side are calculated in a manner identical to that used for the fuel heat disposal system calculations (cf., Eqs. 14, 15, and 16 of chap. 3).

Table 10 contains a list of pertinent information obtained from heat exchanger designs (Figs. 35 and 36) and the heat transfer relations discussed above. Values are given for four different flow rates of helium and four different flow rates of water; curves were plotted from these values and used in the solution of Eqs. 1 through 5.

The data of Table 10 were used to solve the five simultaneous equations (Eqs. 1 through 5) for various values of the independent variable — heat

transferred. Inasmuch as the helium volumetric flow is constant (see restraint 2), the helium weight flow cannot be precisely determined until the helium temperature at the blower (T_{He}) is known. It was necessary therefore to assume a helium weight flow for each power and to solve the equations by iteration. The results of the solution of Eqs. 1 through 5 are shown in Figs. 37 and 38, in which the minimum and maximum NaK and helium temperatures are plotted against heat transferred. The mean NaK temperature is also shown in Fig. 37.

The pressure drops in the NaK and in the helium have been calculated for the exchangers. The NaK pressure drop was calculated with the use of the customary Fanning equation[11] for the
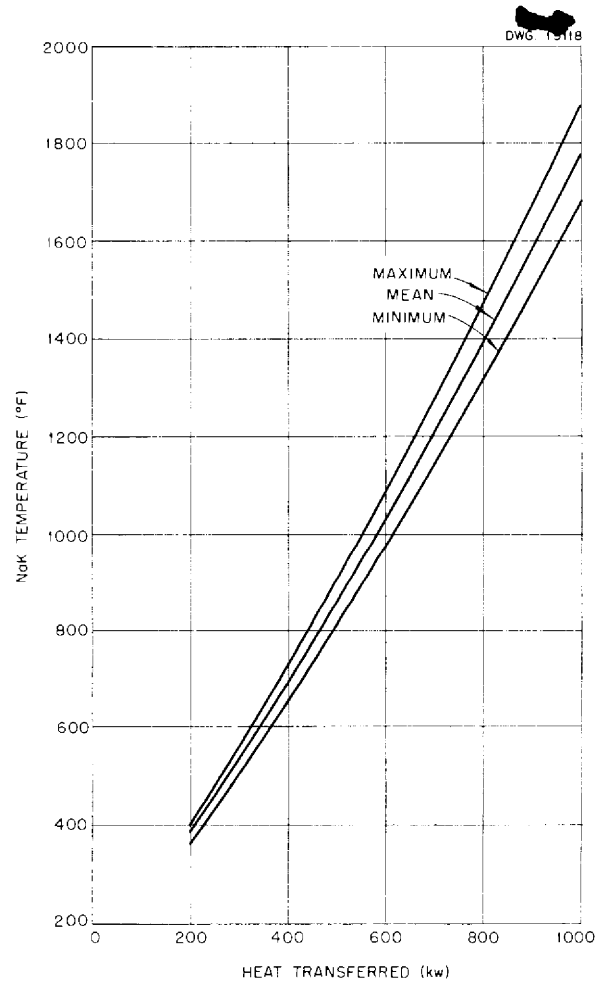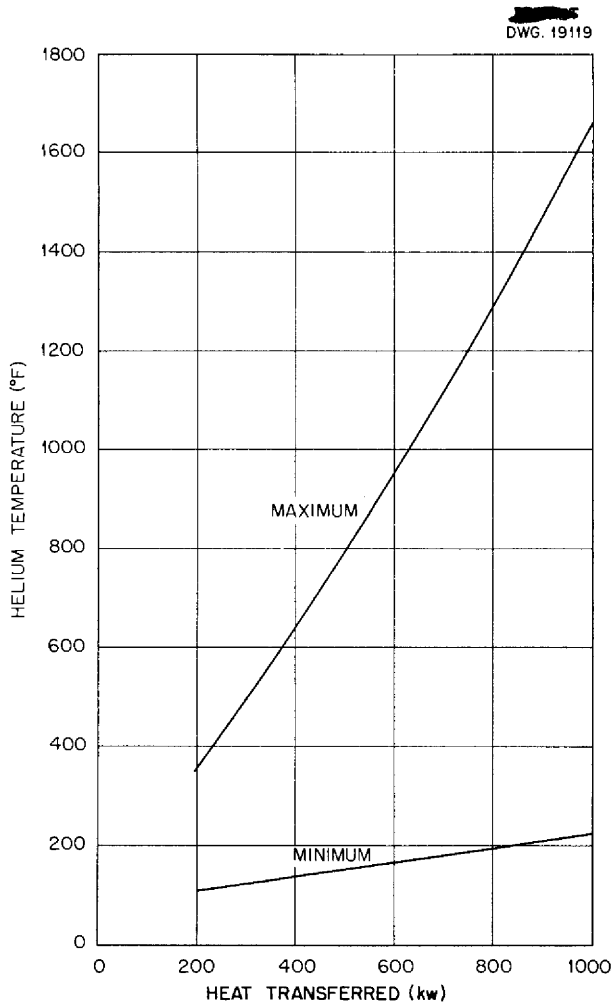

Fig. 37. NaK Temperatures vs. Heat Transferred in Heat Exchangers.
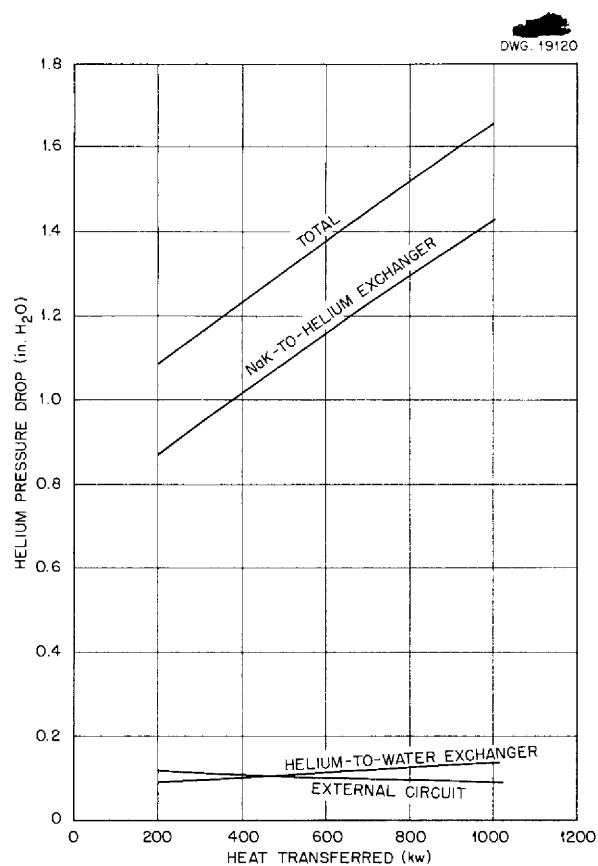
57

TABLE 10.   HEAT EXCHANGER DATA

	NaK-TO-HELIUM HEAT EXCHANGER	HELIUM-TO-WATER HEAT EXCHANGER
Tube outer diameter, in.	1.0	0.625
Tube wall thickness, in.	0.109	0.049
Tube material	Inconel	Steel
Fin outer diameter, in.	2.0	0.875
Number of fins per inch	7	12
Fin thickness, in.	0.024	0.010
Fin material	Stainless steel	Copper
Tube transverse pitch, ft	2.75	2.80
Tube longitudinal pitch, ft	2.43	1.684
Number of tubes per exchanger	75	180
Number of tubes transverse to flow (per exchanger)	5	6
Exchanger height, in.	13.75	16.8
Exchanger width (also active tube length), in.	16.25	17.0
Total active tube length, ft	101.6	255.1
Liquid flow area per exchanger, ft^2	0.0503	0.0273
Liquid flow rate per exchanger, lb/sec	11.5	16.67, 10.0, 6.67, 3.33
Liquid velocity, ft/sec	4.97	9.89, 5.40, 3.91, 1.96
Peclet's number	790	
Reynolds' number		49,300, 29,600, 19,700, 9,860
Liquid heat transfer coefficient, $Btu/sec \cdot ft^2 \cdot {}^\circ F$	0.830	0.610, 0.406, 0.290, 0.168
Liquid heat transfer area per exchanger, ft^2	20.8	35.2
$(hA)_{liquid}$ per exchanger, $Btu/sec \cdot {}^\circ F$	17.3	21.5, 14.3, 10.2, 5.92
$(1/hA)_{liquid}$ per exchanger, $sec \cdot {}^\circ F/Btu$	0.058	0.047, 0.070, 0.098, 0.169
$(1/hA)_m$ per exchanger, $sec \cdot {}^\circ F/Btu$	0.126	0.015
Helium-side equivalent diameter (D_{He}), in.	1.447	0.722
Helium free flow ratio	0.575	0.768
Helium flow area per exchanger, ft^2	0.893	1.524
Helium flow rate per exchanger, lb/sec	0.33, 0.22, 0.11	0.33, 0.22, 0.11
Helium Reynolds' number	2,230, 1,470, 720	650, 430, 210
Helium heat transfer coefficient, $Btu/sec \cdot ft^2 \cdot {}^\circ F$	0.0063, 0.0046, 0.0028	0.0051, 0.0038, 0.0023
Fin efficiency	0.43, 0.50, 0.60	1.0, 1.0, 1.0
Helium heat transfer area,* ft^2	142, 162, 190	187, 187, 187
$(hA)_{He}$ per exchanger, $Btu/sec \cdot {}^\circ F$	0.889, 0.743, 0.526	0.957, 0.709, 0.424
$(1/hA)_{He}$ per exchanger, $sec \cdot {}^\circ F/Btu$	1.12, 1.35, 1.90	1.04, 1.41, 2.36

*"Area" varies with helium flow rate because the fin efficiency varies with helium flow rate.

Fig. 38. Helium Temperatures vs. Heat Transferred in Heat Exchangers.

Fig. 39. Helium Pressure Drop vs. Heat Transferred.

straight sections and the curves presented by Cox and Germano[12] for the bends, exits, and entrances. Since the NaK flow is relatively constant, the NaK pressure drop is approximately constant and is equal to about 1 psi. The helium pressure drop is calculated in a manner identical to that used for calculating the helium pressure drop in the fuel system. The helium pressure drop is plotted against heat transferred in Fig. 39.

The pressure drops in the remainder of the NaK and the helium circuits have been calculated with the use of the Fanning equation and the Cox and Germano data. Figure 40 shows the NaK piping; Fig. 41 shows the helium ducting. The pressures at various points in the fuel circuit are shown in Fig. 1. The NaK pressure drop, exclusive of the heat exchangers, is 16 psi; the total NaK pressure drop is 17 psi. The helium pressure drop exclusive of the heat exchanger and the total helium pressure drop are plotted against heat transferred in Fig. 39.
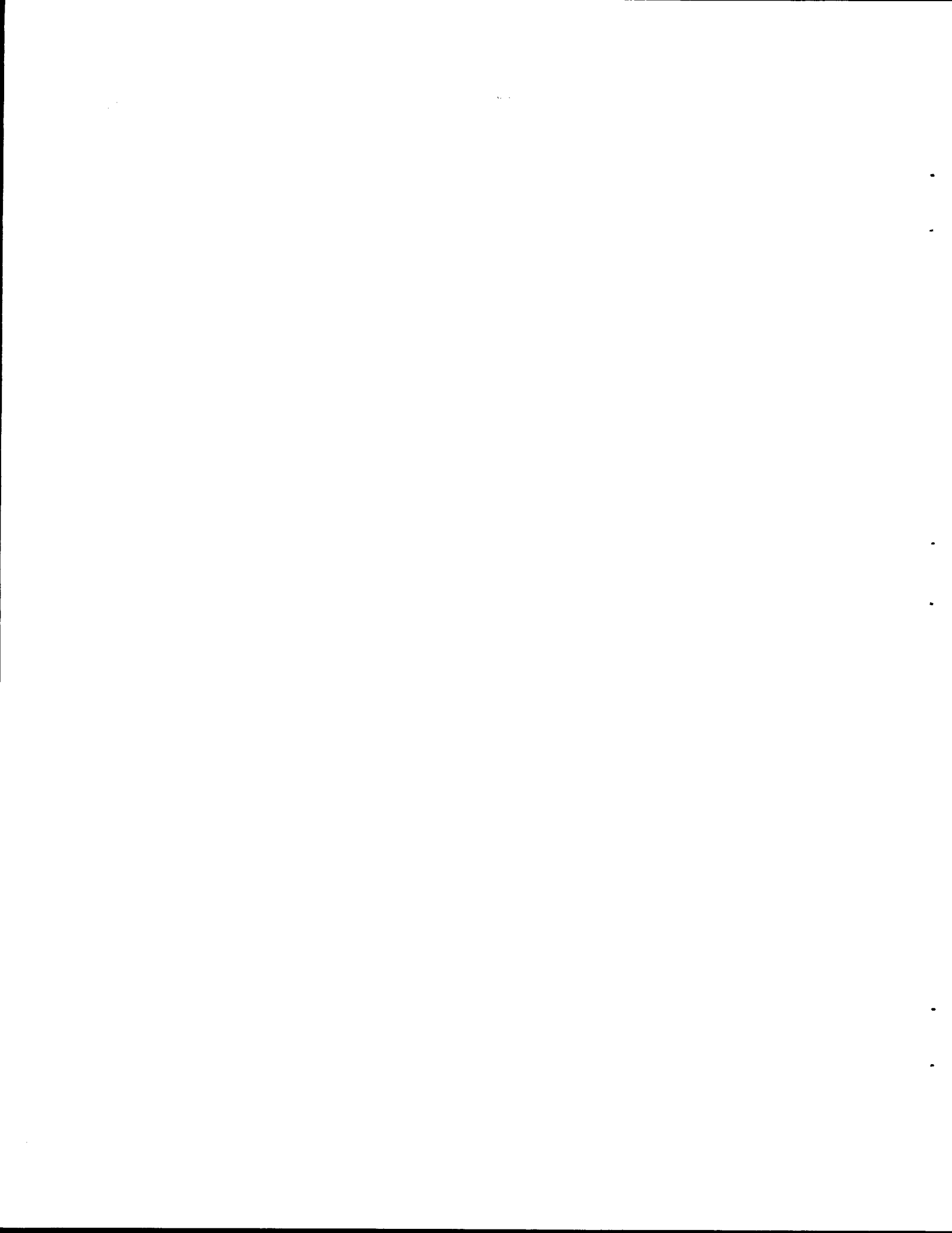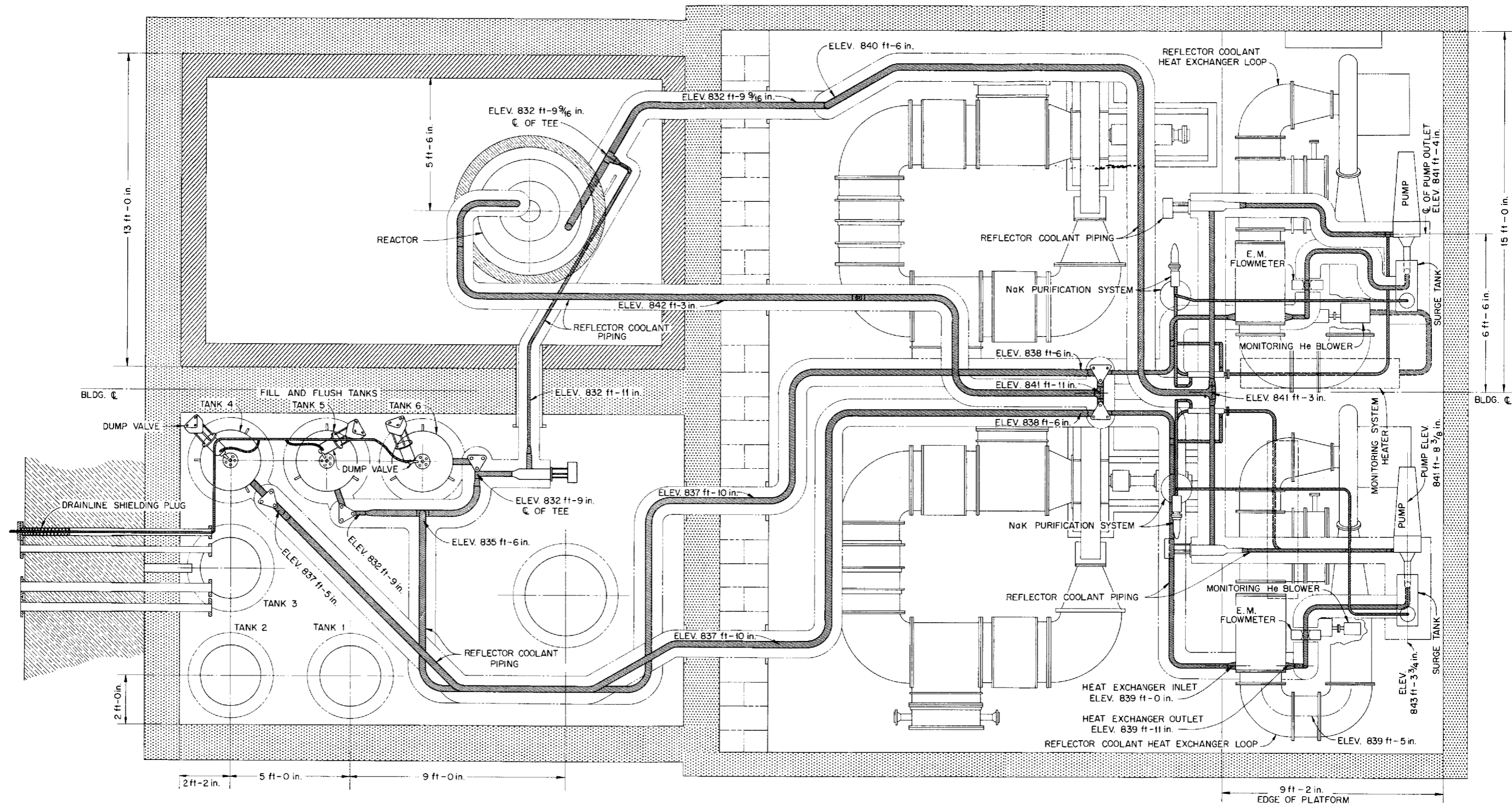
Fig. 40.   Reflector Coolant Piping.

14 ft -0⅜ in. REF.

10 ft -10⅝ in.

3 ft - 8⅛ in.

7 ft - 3½ in.

PLAN
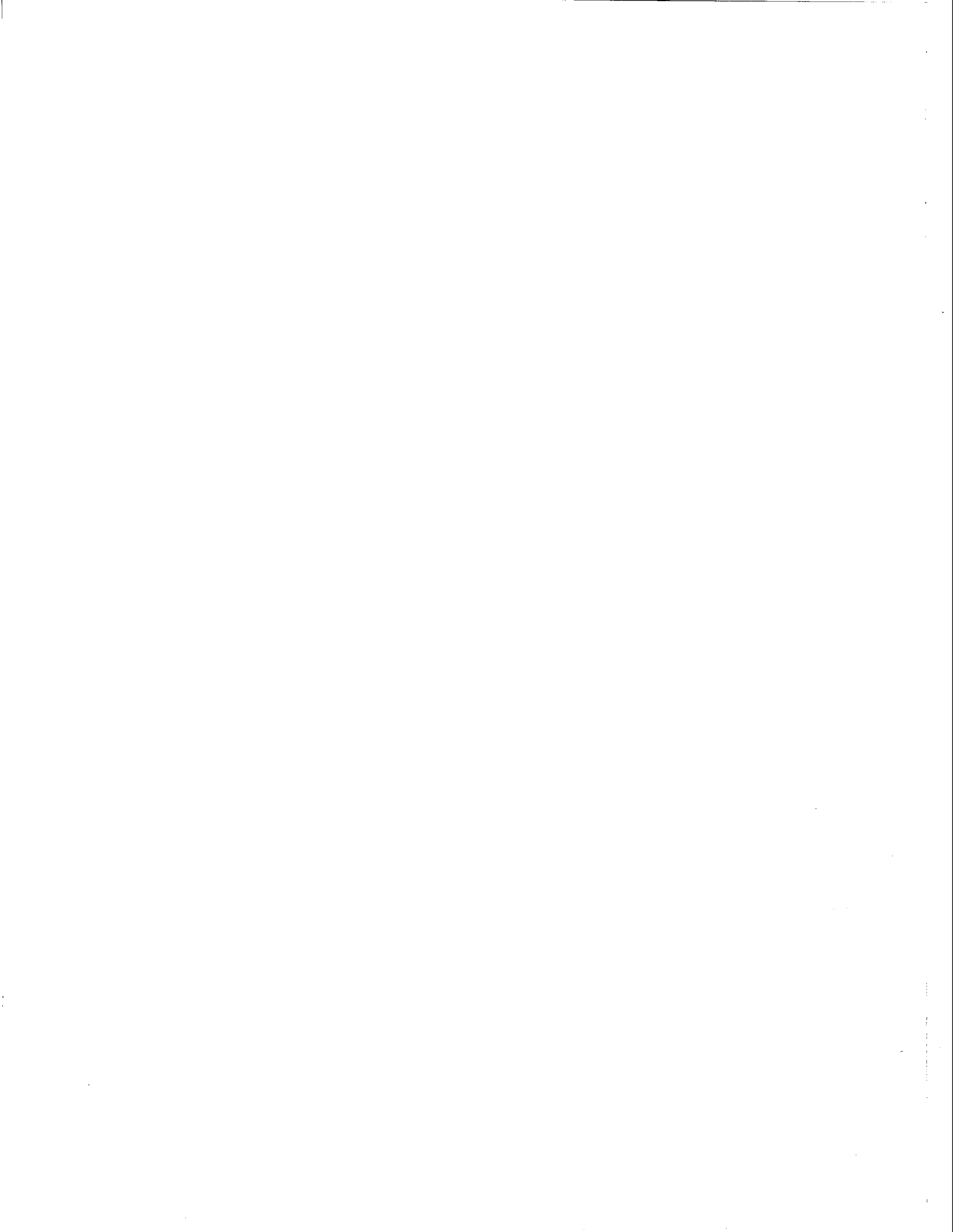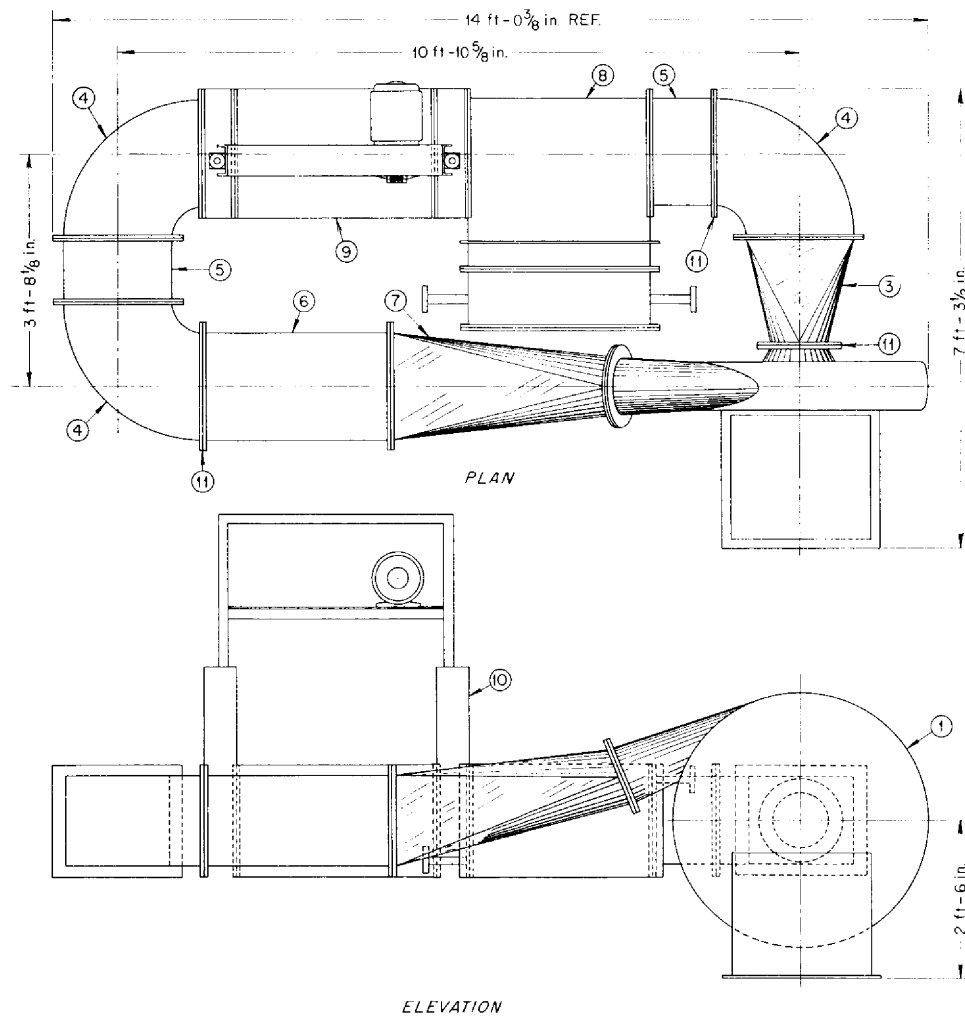
1   NO. 20-SM200 LAMSON BLOWER
2   VICKERS HYDRAULIC MOTOR
3   TRANSITION PIECE, 10-in ID TO 20⅛ × 16½ in.
4   90° ELBOW, 20⅛ × 16½ in.
5   DUCT, 20⅛ × 16½ × 11¾-in. LONG
6   DUCT, 20⅛ × 16½ in. × 3 ft-0-in. LONG
7   TRANSITION PIECE, 10-in ID TO 20⅛ × 16½ in.
8   GRISCOM-RUSSELL He TO H₂O HEAT EXCHANGER
9   GRISCOM-RUSSELL NaK TO He HEAT EXCHANGER
10 ORNL HEAT BARRIER
11 ASBESTOS GASKETS, REQUIRED DIA × 1/16 in. THICK
NOTE:
    ITEMS NO. 3, 4, 5, 6, AND 7 ARE SAE NO. 10-20.

ELEVATION

2 ft - 6 in.

8 in.   3 ft - 0 1/16 in.

END VIEW

Fig. 41.   Reflector Coolant Heat Exchanger Loop.

Chapter 5

ROD AND INSTRUMENT COOLING SYSTEM

COOLING OF THE CONTROL RODS AND INSTRUMENTS

There are six vertical holes in the reactor of the ARE (Fig. 16) into which a regulating rod, three safety rods, and two fission chambers can be lowered, when required. Helium is blown through the annular passages between the rods and instrument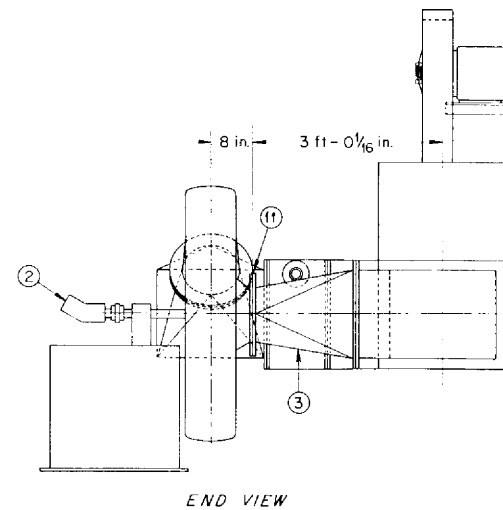s and the reactor to cool the various surfaces present. In the case of the rods, this cooling is desirable because the guide vanes on the rods slide in contact with the sleeve in the reactor; considerable uncertainty exists as to what would happen if this sliding contact were to be made at the high temperatures in the reactor. The instruments require cooling because the electrical insulators used in their construction emit false signals at temperatures above about 700°F. The rod and instrument cooling circuit consists of two blowers, each of 1000 cfm capacity, which blow helium through the annular passages in the reactor holes, and a heat exchanger which removes from the helium the heat picked up in the reactor holes. Although the blowers have a total capacity of 2000 cfm, they are operated so that the helium flow is 1000 cfm. Figure 1 shows a diagram of the rod and instrument cooling system. Figure 42 shows the dimensions of the helium passages through the reactor. Figure 17 shows a cross section of the helium passages and details of the sleeve in the reactor. This sleeve, as may be seen, is actually triple-walled. The helium passes between the inner wall and the rod or instrument in question. The space between the inner wall and the middle wall is packed with diatomaceous earth, which serves as thermal insulation between the reactor and the rod or instrument hole. NaK from the reflector coolant circuit flows between the middle and outer wall and provides some cooling because it is

colder than the surrounding sections of the reactor core. Since the 1000 cfm of helium available may be apportioned differently to the various holes, the cooling of the various holes was investigated for a range of helium flows. Also, at the time of the calculations, the mean NaK temperature was unknown and, consequently, a range of mean NaK temperatures was investigated. The cooling of the various rods and instruments will be considered separately and in the following order: safety rods, regulating rod, fission chambers. The division of the total flow among the different holes will be discussed last.

DWG. 19121
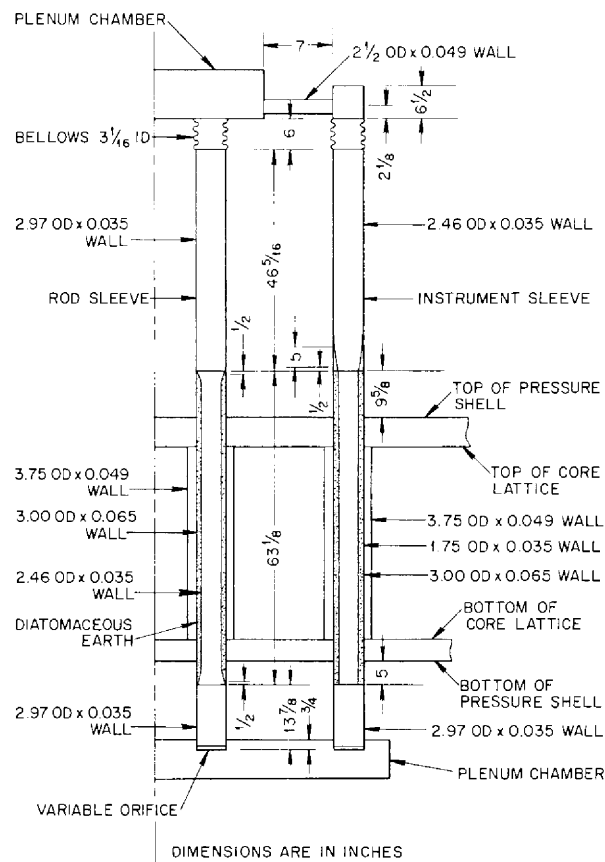
Fig. 42. Rod and Instrument Sleeves.

COOLING OF THE SAFETY RODS

During normal reactor operation, the safety rods are not in the reactor but are withdrawn into sleeves above the reactor. The safety rods themselves are in a cool area, and the only cooling problem, then, is that of cooling the sleeve in the reactor. The equations governing this process are quite straightforward and are listed below:

$$(1) \qquad Q = Wc_p \ (T'_{He} - T_{He}) \ ,$$

$$(2) \qquad Q = hA\theta + Q_r \ ,$$

$$(3) \quad hA = \left[\frac{1}{(hA)_{NaK}} + \frac{1}{(hA)_m} \right.$$
$$\left. + \frac{1}{(hA)_I} + \frac{1}{(hA)_n} + \frac{1}{(hA)_{He}} \right]^{-1} \ ,$$

where
- Q = heat transferred to helium, Btu/sec,
- W = weight flow of helium, lb/sec,
- c_p = specific heat of helium, Btu/lb·°F,
- T' = maximum temperature, °F,
- T = minimum temperature, °F,
- h = heat transfer coefficient, Btu/sec·ft² (°F/ft),
- A = heat transfer area, ft²,
- θ = effective log mean temperature difference between the NaK and the helium,
- Q_r = heat generated in the sleeve by nuclear radiation, Btu/sec,

and the subscripts
- He = helium,
- NaK = NaK,
- m = middle metal wall in sleeve,
- I = insulation (diatomaceous earth),
- n = inner metal wall.

The various terms in Eq. 3 may be evaluated as follows:

$$(4) \quad h_{NaK} = \frac{k_{NaK}}{D_{NaK}} \left(5.8 + 0.020 \ Pe^{0.8} \right) \ ,$$

where
- k = thermal conductivity, Btu/sec·ft² (°F/ft),
- D = equivalent diameter (four times hydraulic radius), ft,
- Pe = Peclet's number;

$$(5) \qquad A_{NaK} = d'_m \ h \ ,$$

where
- d' = tube outside diameter, ft,
- L = length of tube = height of pressure shell, ft;

$$(6) \qquad \frac{1}{(hA)_m} = \frac{\ln \dfrac{d'_m}{d_m}}{2\pi k_m L} \ ,$$

where
- d = tube inside diameter, ft;

$$(7) \qquad \frac{1}{(hA)_I} = \frac{\ln \dfrac{d_m}{d'_m}}{2\pi k_I L} \ ;$$

$$(8) \qquad \frac{1}{(hA)_n} = \frac{\ln \dfrac{d'_n}{d_n}}{2\pi k_n L} \ ;$$

$$(9) \quad h_{He} = 0.023 \ \frac{k_{He}}{D} \ Re^{0.8} \ Pr^{0.4} \ ,$$

$$\text{for } Re \geq 2100 \ ,$$

$$h_{He} = 1.86 \ \frac{k_{He}}{D_{He}} \ Re^{1/3} \ Pr^{1/3} \left(\frac{D_{He}}{L} \right)^{1/3} \ ,$$

$$\text{for } Re < 2100 \ ;$$

$$(10) \qquad A_{He} = \pi d_n L \ .$$

Equations 1 through 10 and the dimensions shown in Figs. 42 and 9 were used to calculate the exit temperature of the helium and the heat transferred to the helium; an inlet helium temperature of 150°F was assumed. The properties of helium were evaluated at the mean helium temperature. The range of helium weight flows considered was from 0.005 to 0.100 lb/sec, and the calculations were made for mean NaK temperatures of 1000, 1150, and 1300°F. The results of the computations are shown in Figs. 43, 44, and 45.

The maximum temperature of the sleeve wall can be calculated from the

Fig. 43. Safety Rod Cooling at a NaK Temperature of 1000°F.
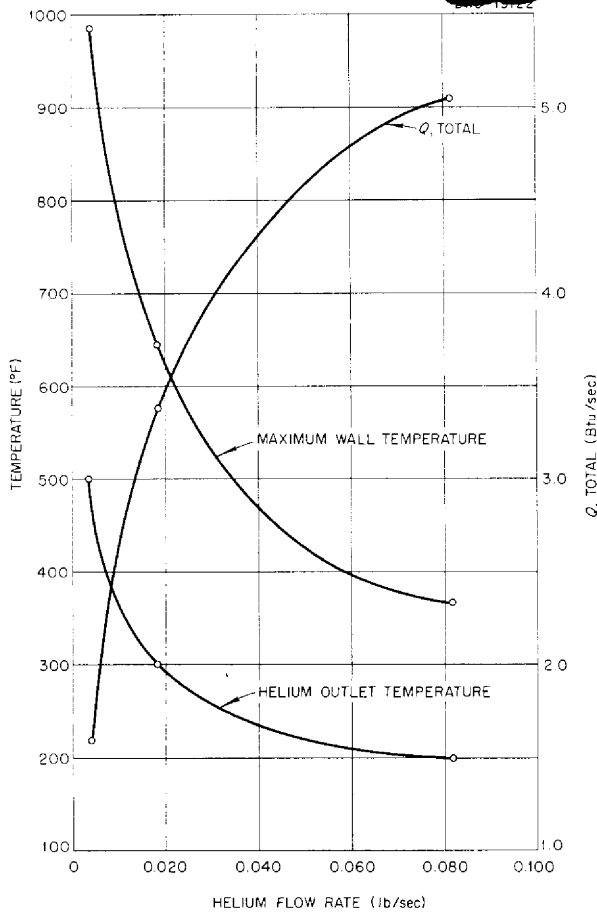
Fig. 44. Safety Rod Cooling at a NaK Temperature of 1150°F.

following equation:

$$(11) \qquad (T_n)_{max} = T'_{He} + \frac{Q}{(hA)_{He}} .$$

The helium heat transfer coefficient, h, in Eq. 11 is evaluated by means of Eq. 9, with the helium properties corresponding to the maximum helium temperature being used. The maximum wall temperature was evaluated by using Eq. 11, and the results are shown in Figs. 43, 44, and 45.

COOLING OF THE REGULATING ROD

During normal operation, the position of the regulating rod may vary from a position completely out of the reactor to a position where the midpoint of the stainless steel slug is coincident with the center line
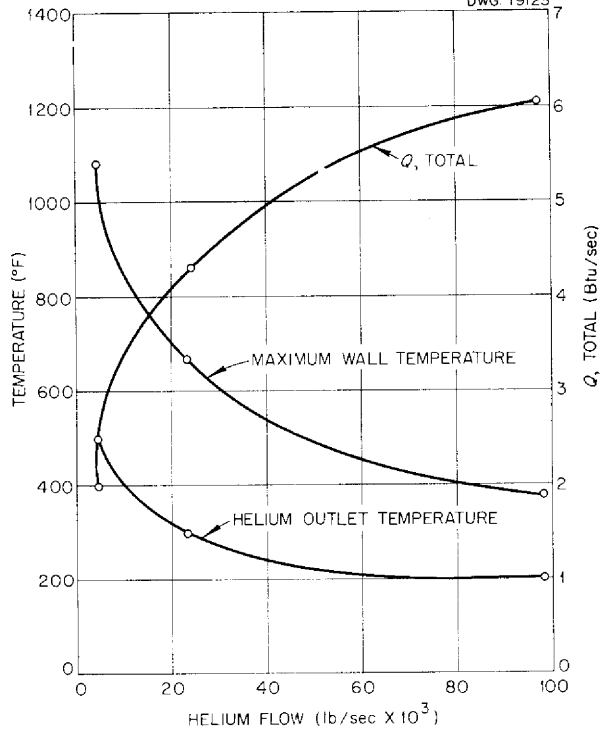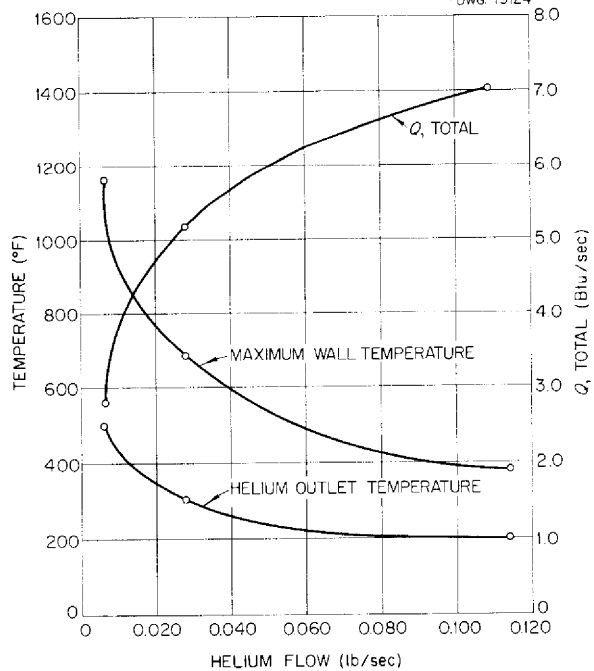
Fig. 45. Safety Rod Cooling at a NaK Temperature of 1300°F.

of the reactor. When the regulating rod is completely out of the reactor, the situation is exactly the same as that analyzed in the previous section on the safety rods, the triple-walled sleeve being identical for the two types of rods. When the regulating rod is in the reactor, the situation is more complex; the case of the regulating rod all the way into the reactor, which is the extreme condition, will be analyzed. The regulating rod hole will be divided into three sections in the reactor (Fig. 46). The top section of the rod hole is the section that contains the portion of the regulating rod which is in the reactor but contains no appreciable amount of neutron and gamma absorber. The middle section of the rod hole is the section that contains the portion of the regulating rod which contains
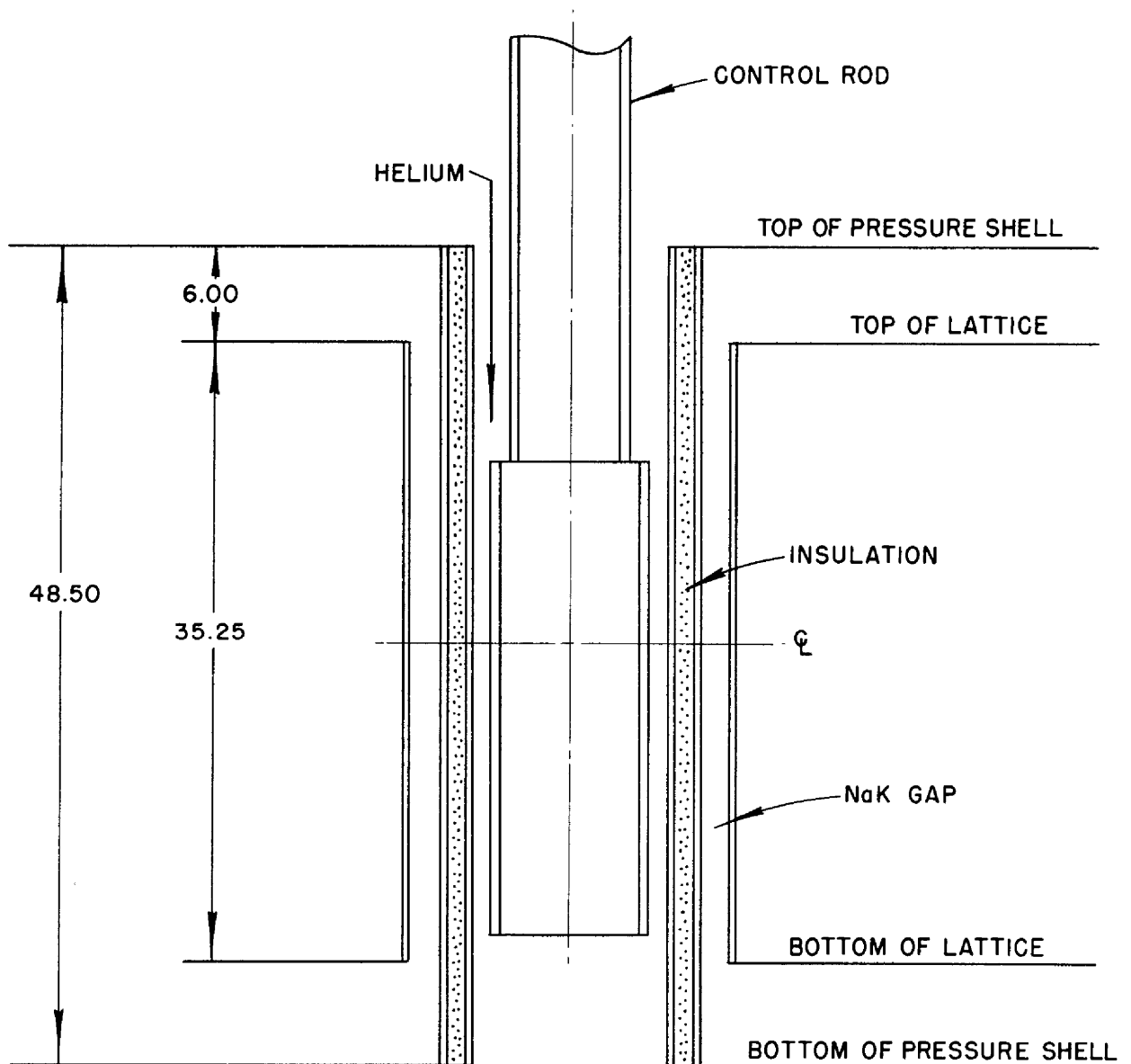
Fig. 46. Regulating Rod.

the heavy stainless steel slug. The bottom section of the rod hole is the section that contains no regulating rod. The equations governing the cooling process in the three sections of the rod hole are

$$(12) \quad Q_i = Wc_p \, (T'_{He} - T_{He})_i \,,$$
$$i = 1, 2, 3 \,,$$

where the symbols have the same meanings as given previously and the subscript i refers to the sections of the regulating rod hole:

1 = top section,
2 = middle section,
3 = bottom section;

$$(13) \quad Q_i = (hA\theta + Q_r + q)_i \,,$$

where

q = the heat which must be removed from the rod, Btu/sec;

$$(14) \quad q_i = (q_r + q_R)_i \,,$$

where

q_r = heat generated in the rod by nuclear radiation, Btu/sec,

q_R = heat transferred from the sleeve to the rod by thermal radiation, Btu/sec;

it may be noted that $(q_r)_{i=1} = 0$ and $q_{i=3} = 0$;

$$(15) \quad (hA)_i = \left[\frac{1}{(hA)_{NaK}} + \frac{1}{(hA)_m} \right.$$
$$\left. + \frac{1}{(hA)_I} + \frac{1}{(hA)_n} + \frac{1}{(hA)_{He}} \right]_i^{-1} \,,$$

where the various terms are evaluated exactly as the corresponding terms in Eq. 3;

$$(16) \quad (q_R)_i = \frac{0.173}{3600} \frac{a_i}{\dfrac{1}{\epsilon} + \left(\dfrac{a_i}{A_n}\right)\left(\dfrac{1}{\epsilon} - 1\right)} \left[\left(\frac{T_n + T'_n}{200}\right)^4 - \left(\frac{t + t'}{200}\right)^4 \right]_{i=1,2} \,,$$

$$(q_R)_{i=3} = 0 \,,$$

where

a = surface area of control rod, ft^2,
t' = maximum rod temperature, °F abs,
t = minimum rod temperature, °F abs,
ϵ = emissivity.

It may be noted that the arithmetical-average temperature is used in Eq. 16 to evaluate the heat transferred by thermal radiation. This is only an approximation, but a check has indicated that it is not too greatly in error. Equations 12 through 16 and the dimensions shown in Figs. 42, 46, and 47 were used to calculate for the various sections the exit temperature of the helium and the heat transferred to the helium; an inlet temperature to the rod hole of 150°F was assumed. The properties of helium were evaluated at the mean temperatures, and the values of Q_r and q_r are shown in Fig. 48. The range of helium weight flows considered was 0.015 to 0.025 lb/sec; average NaK temperatures of 1000, 1150, and 1300 were used, as before. The results of the calculations are shown in Figs. 49, 50, 51, and 52, which show the helium temperature and the heat transferred to the helium at the end of sections 2 and 3 plotted against helium flow for the various NaK temperatures.

The maximum temperature of the sleeve and the rod can be calculated from the following equations:

$$(17) \quad (T_n)_{max} = (T'_{He})_{i=3} + \left[\frac{Q}{(hA)_{He}} \right]_{i=3}$$

and

$$(18) \quad (t)_{max} = (T'_{He})_{i=2} + \left[\frac{Q}{(hA)_{He}} \right]_{i=2} \,.$$

Again, the helium heat transfer coefficients are evaluated locally.

The results of the evaluations of Eqs. 17 and 18 are also shown in Figs. 49, 50, and 51.

COOLING OF FISSION CHAMBERS

The fission chambers will be in the reactor core during startup of the

STAINLESS STEEL
REGULATING ROD NOSE

STAINLESS STEEL
CANNED DILUTED SLUGS

STAINLESS STEEL
ADAPTOR

$1\frac{1}{2}$-in. OD x 0.065-in. WALL x 170 in.
STAINLESS STEEL LOWER DRIVE TUBE

TACK WELD

WELD

TACK WELD

69.031 in.
68.969 in.

1.499-in.
1.497-in. DIA.

0.577 in.
0.547 in.

SNUG FIT WITH LOWER
DRIVE TUBE

MAKE FROM $1\frac{5}{8}$-in. OD x 0.312-in. WALL

$\frac{3}{8}$-in. DIA. HOLE

15°

1.265-in.
1.235-in. DIA.

WELD AND
GRIND FLUSH

0.125-in. MAX

0.765-in.
0.735-in.

$1\frac{5}{8}$-in. OD x $\frac{5}{16}$-in. WALL x 69-in.
STAINLESS STEEL UPPER DRIVE TUBE

1.140-in.
1.110-in.

Fig. 47.   Regulating Rod Assembly.

6.6 watts/linear in.

DIATOMACEOUS EARTH

SLEEVE
IN CORE REGION

56.2 watts/linear in.

4.0 watts/linear in.

CONTROL ROD

295 watts/linear in.

5.0 watts/linear in.

4.0 watts/linear in.

B_4C

SAFETY ROD

Fig. 48. Cross Sections of Sleeve, Control Rod, and Regulating Rod Showing Nuclear Heat Generation Rates.

reactor, but later they will be removed from the core entirely. For the following analysis, the fission chambers are considered as being in the core, which is the most extreme condition. Each instrument hole is divided into sections in much the same fashion as the regulating rod hole was divided. The top section of the hole is the portion which contains the fission chamber; the lower portion contains nothing (Fig. 53). The equations to be used in calculating the cooling requirements are

(19) $\quad Q_i = Wc_p (T'_{He} - T_{He})_i, \quad i = 1, 2,$

where the subscript i refers to

$\qquad 1 = $ top section

and

$\qquad 2 = $ bottom section;
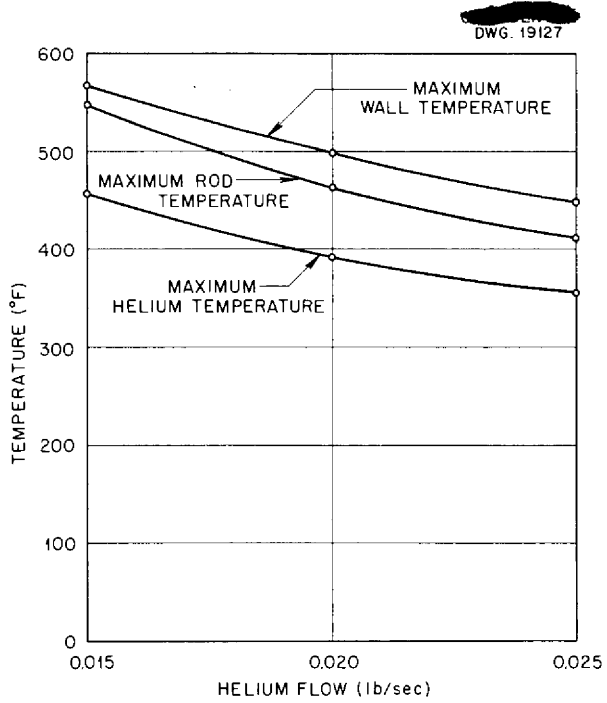
Fig. 49. Regulating Rod Cooling at a NaK Temperature of 1000°F.
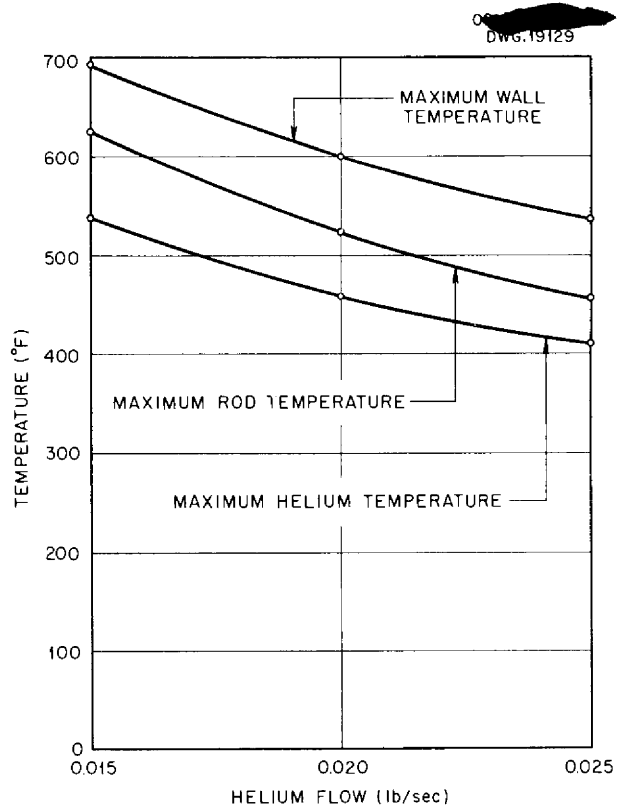
Fig. 51. Regulating Rod Cooling at a NaK Temperature of 1300°F.
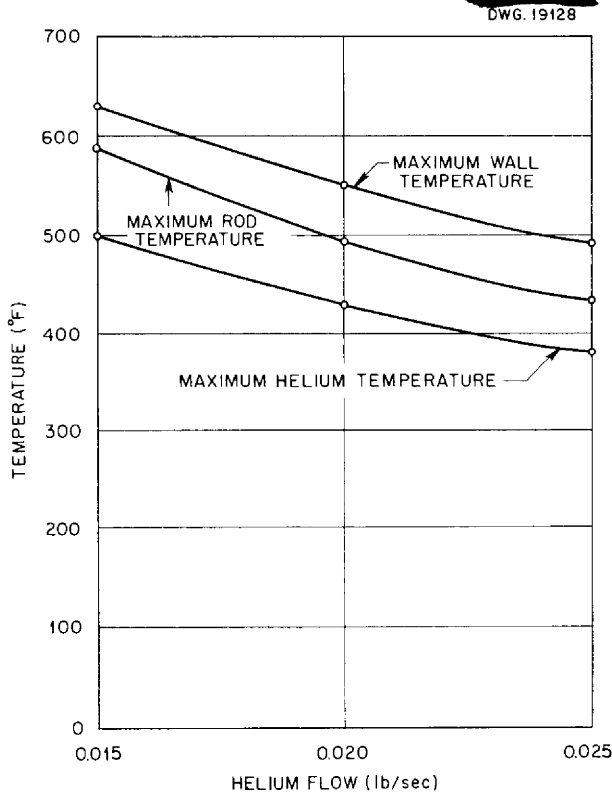
Fig. 50. Regulating Rod Cooling at a NaK Temperature of 1150°F.

Fig. 52. Regulating Rod Cooling at Various NaK Temperatures.

71

INSTRUMENT

HELIUM

TOP OF PRESSURE SHELL

6.00

TOP OF LATTICE

INSULATION

48.50

35.25

℄

NaK GAP

BOTTOM OF LATTICE

BOTTOM OF PRESSURE SHELL

Fig. 53.   Instrument Hole.

(20) $$Q_i = (hA\theta + q_R)_i \ ,$$

where the symbols have the same meanings as before;

(21) $$(hA)_i = \left[\frac{1}{(hA)_{NaK}} + \frac{1}{(hA)_m} + \frac{1}{(hA)_I} + \frac{1}{(hA)_n} + \frac{1}{(hA)_{He}} \right]^{-1}_i \ ,$$

where the various terms are also evaluated the same as in Eq. 3, except that the heat transfer coefficient in an annulus is given by

(22) $$h = 1.02 \frac{k_{He}}{D_{He}} Re^{0.45} \left(\frac{\mu}{\mu_s}\right)^{0.14} \left(\frac{D_{He}}{l}\right)^{0.4} \left(\frac{d_n}{d_f}\right)^{0.8} Gr^{0.05} \ , \quad \text{for } Re < 2100 \ ,$$

where

μ = dynamic viscosity evaluated at the mean temperature of helium, lb/sec·ft,

μ_s = dynamic viscosity evaluated at inner wall temperature, lb/sec·ft,

l = length of section, ft,

d_f = outside diameter of fission chamber, ft,

Gr = Grashof number;

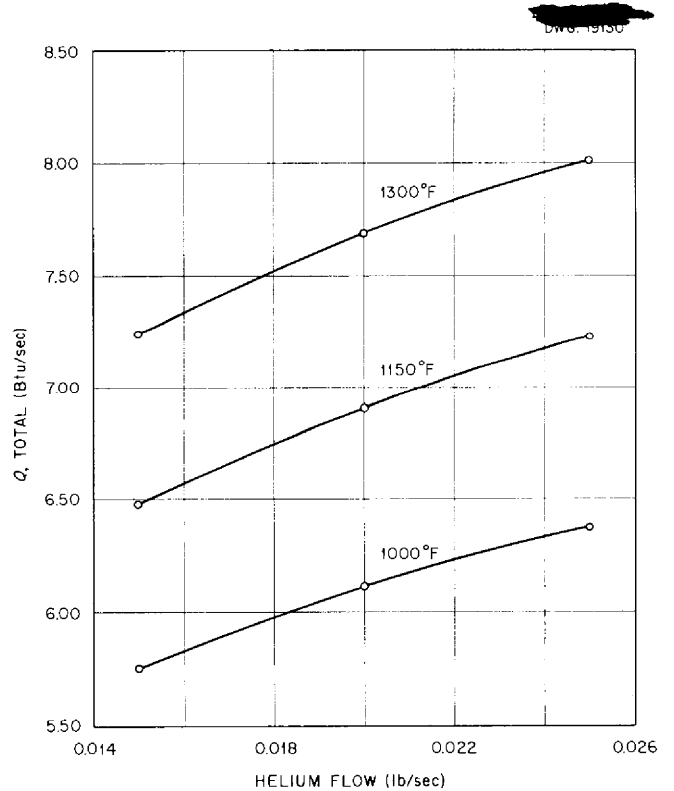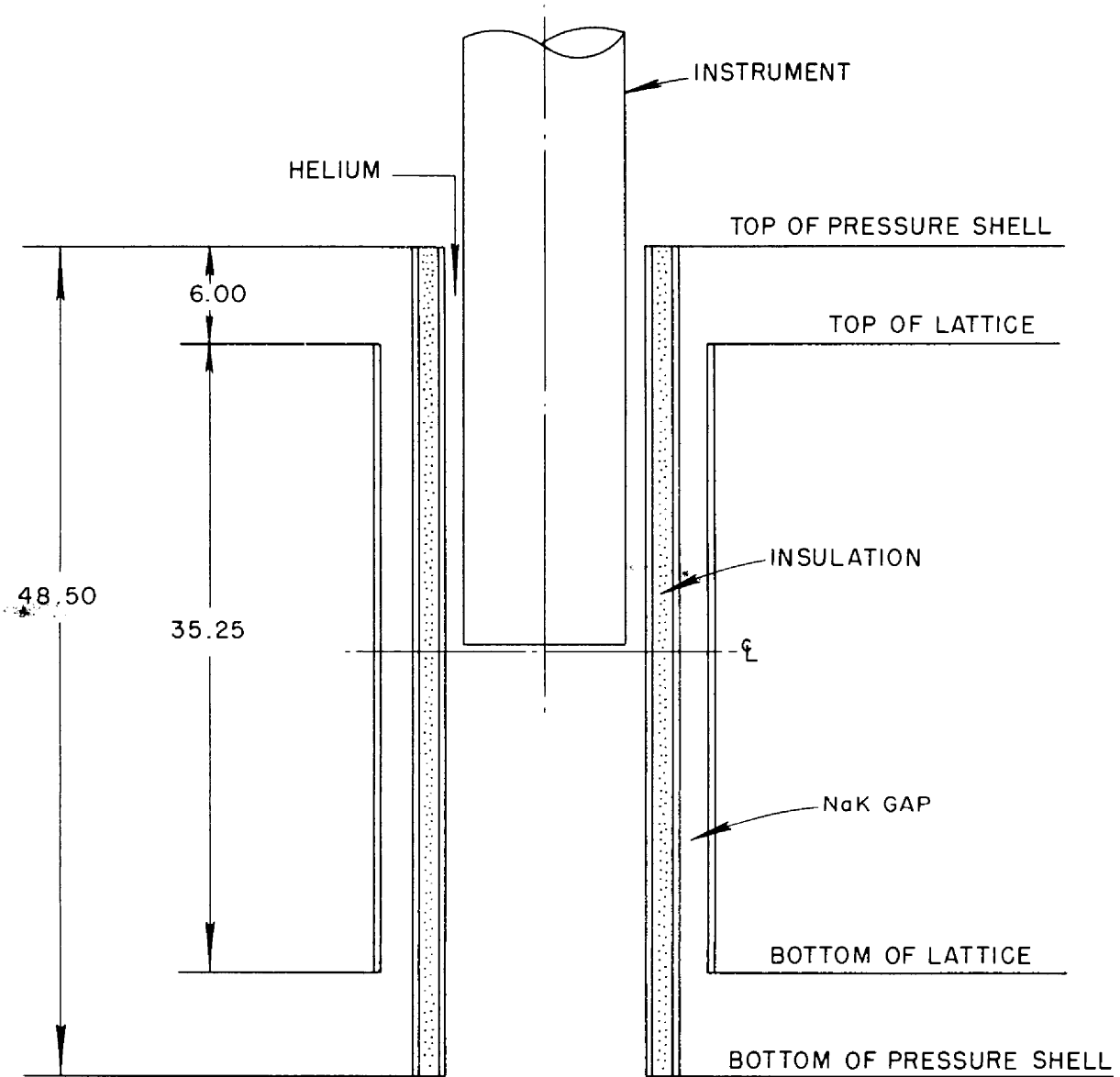(23) $$q_R = \frac{0.173}{3600} \frac{a_f}{\frac{1}{\epsilon_f} + \left(\frac{a_f}{A_n}\right)\left(\frac{1}{\epsilon} - 1\right)} \left[\left(\frac{T_n + T_n'}{200}\right)^4 - \left(\frac{t_f + t_f'}{200}\right)^4 \right] \ ,$$

where

a_f = surface area of fission chamber, ft²,

t_f = minimum fission chamber temperature, °F abs,

t_f' = maximum fission chamber temperature, °F abs,

ϵ_f = emissivity of fission chamber,

ϵ = emissivity of tube.

The cooling requirement calculations for the fission chambers are made with the assumption that the bottom of each instrument (excluding nose) is at the center line of the core. Also, the maximum temperature of the instrument is taken to be 600°F, and the inlet temperature of helium is taken to be 150°F. The outside diameter of the instrument is 1.25 in., and the

dimensions of the sleeve are shown in Fig. 42. The calculations are based on the same NaK temperatures as used before, and the results are given in Fig. 54.

Figure 55 shows the heat removed and the maximum temperature of the helium vs. helium flow rate for a NaK temperature of 1150°F.

HELIUM PRESSURE DROPS

The helium pressure drops in the safety rod, regulating rod, and instrument sleeves are calculated by

using various helium flows and a NaK temperature of 1170°F. The equations governing the pressure drops are

(24) $$\Delta P_f = 4f \frac{l}{D} \frac{\rho v^2}{2g} \ ,$$

(25) $$\Delta P_c = X \frac{\rho v^2}{2g} \ ,$$

(26) $$\Delta P_e = \frac{\rho(v_1 - v_2)^2}{2g} \ ,$$

(27) $$\Delta P_y = 4f \frac{l_e}{D} \frac{\rho v^2}{2g} \ .$$

The symbols have the following meanings and units:

ΔP = pressure drop, lb/ft²,

f = friction factor,

l = length of section, ft,

l_e = equivalent length, ft,

D = hydraulic diameter, ft,

v = average velocity, ft/sec,

g = gravitational acceleration, 32.2 ft/sec²,

X = constant, dimensionless,

73

v_1 = average linear velocity up-
   stream, ft/sec,
v_2 = average linear velocity down-
   stream, ft/sec.

The meanings of the subscripts are the
following:

f = friction,
c = contraction,
e = expansion,
y = elbow.

The friction factor, f, is given by

$$(28) \quad f = \frac{16}{Re} \ , \qquad \text{for Re} \leq 2100 \quad,$$

$$f = 0.0014 + \frac{0.125}{(Re)^{0.32}} \ ,$$

$$\text{for Re} > 2100 \quad.$$

However, for an annulus

$$(29) \quad f = \frac{6}{Re} \ , \qquad \text{for Re} \leq 2100 \ .$$

Values for X are given by McAdams
(cf., p. 122 of ref. 11), and l_e values
are taken from ref. 13.
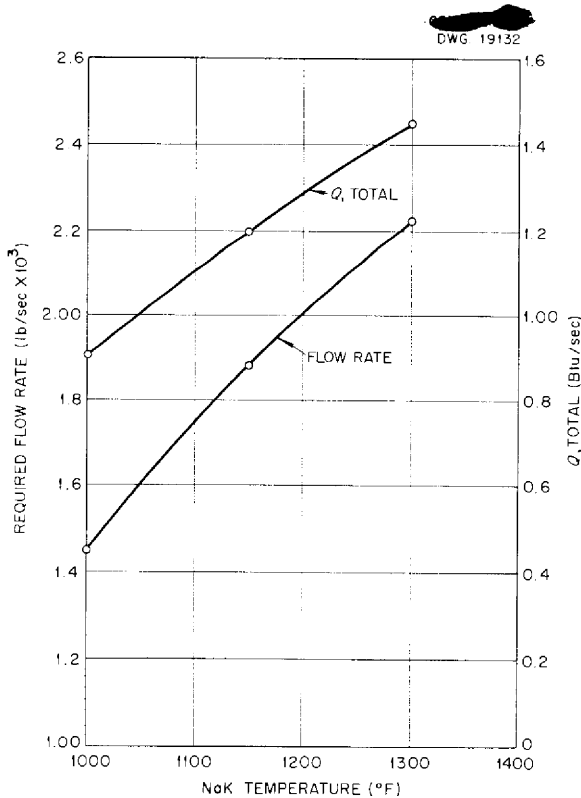
Each sleeve is equipped with a
variable orifice where it enters the
bottom chamber. However, the pressure
drops calculated here do not include
the pressure losses across these
orifices. The dimensions of the
sleeves are given in Fig. 42.

The lower end of the safety rod
will be 1 in. above the top of the
core lattice when the safety rod is
in the "full out" position. The
pressure drops were calculated for
the rod in this position with helium
flows varying from 0.005 to 0.090
lb/sec. The safety rod dimensions
are given in Fig. 56, and the results
of the calculations are given in Fig.
57.

The regulating-rod helium pressure
drops were calculated for the rod in
the "full in" and "full out" positions.
The "full out" position for this rod
was taken to be the same as that for

Fig. 54. Instrument Cooling.
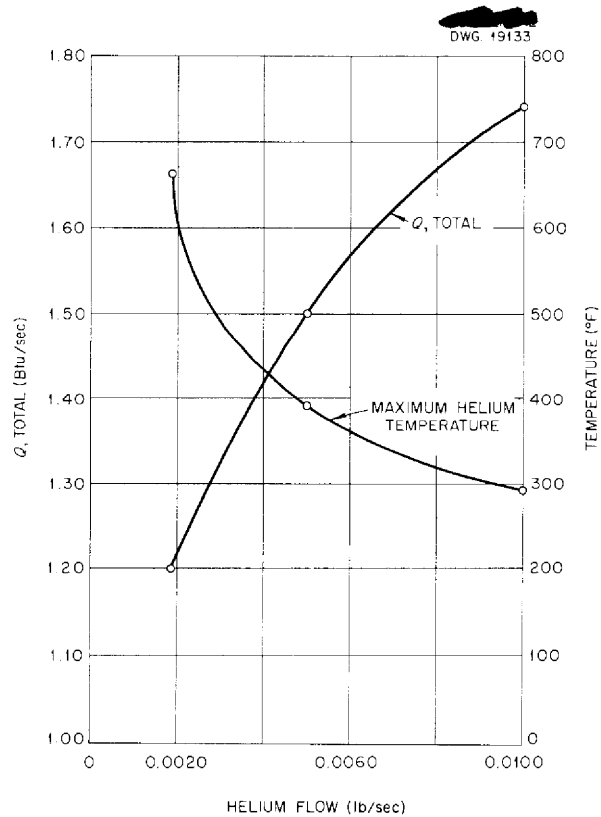
Fig. 55. Instrument Cooling with
Bottom of Instrument at Center Line of
Core and at a NaK Temperature of
1150°F.
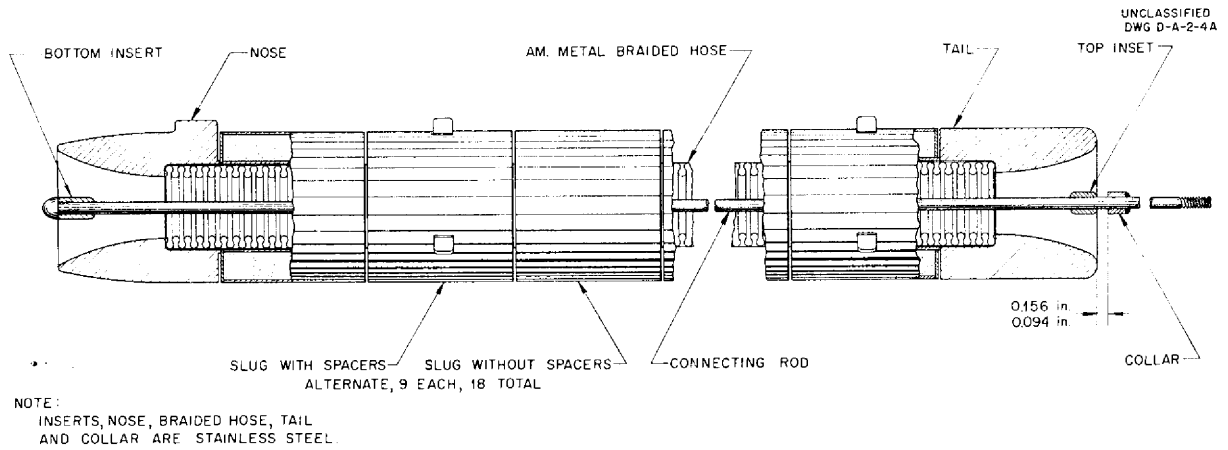
Fig. 56. Safety Rod Assembly.
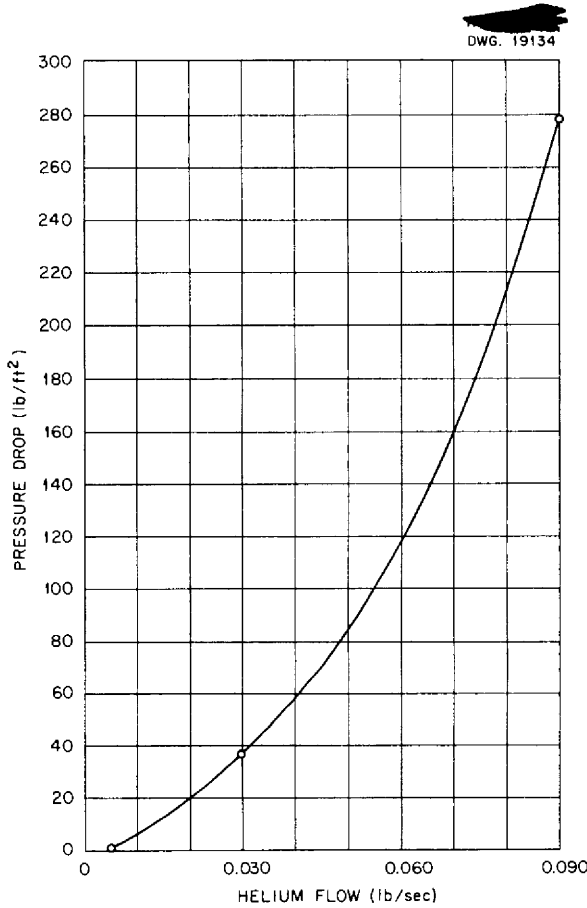
Fig. 57. Pressure Drop in Safety Rod Sleeve.

Fig. 58. Pressure Drop in Regulating Rod Sleeve.

the safety rod. Figure 58 gives the results of the pressure drop computations for flow rates from 0.015 to 0.025 lb/sec.

The helium pressure drops for the instrument hole were also calculated

for the instrument in the "full in" and in the "full out" positions. Here, the bottom of the instrument (excluding

nose) is 15 in. above the top of the pressure shell when the instrument is in the "full out" position. The flow rates used in these calculations ranged from 0.0015 to 0.0100 lb/sec. The results of the calculations are given in Fig. 59.

DIVISION OF FLOW OF HELIUM

The flow of the helium to the various holes is apportioned so that the minimum flow to the instrument in the "full in" position is 0.005 lb/sec, and the minimum flow to the regulating rod in the "full out" position is 0.034 lb/sec. The flow rates per hole for all combinations of regulating rod and instrument positions, with the safety rod out of the core, are given in Table 11.

PERFORMANCE OF ROD AND INSTRUMENT COOLING SYSTEM HEAT EXCHANGER

The control rods and nuclear instruments in the core of the ARE are cooled by helium, which gives up its heat in a helium-to-water exchanger (Fig. 60). The equations governing the performance of this heat exchanger are

$$(29) \qquad Q = W_{He} \, c_{p_{He}} \, (T'_{He} - T_{He}) \, ,$$

$$(30) \qquad Q = W_w \, c_{p_w} \, (T'_w - T_w) \, ,$$

$$(31) \qquad Q = hA\theta \, ,$$

where

Q = heat transferred, Btu/sec,
W = weight flow, lb/sec,
c_p = specific heat, Btu/lb·°F,
T' = maximum temperature, °F,
T = minimum temperature, °F,

h = over-all heat transfer coefficient, Btu/sec·ft^2·°F,
A = heat transfer area, ft^2,
θ = effective log mean temperature difference.

The heat exchanger operates under the following restraints and conditions:

1. The helium flow is 1000 cfm at blower temperature.
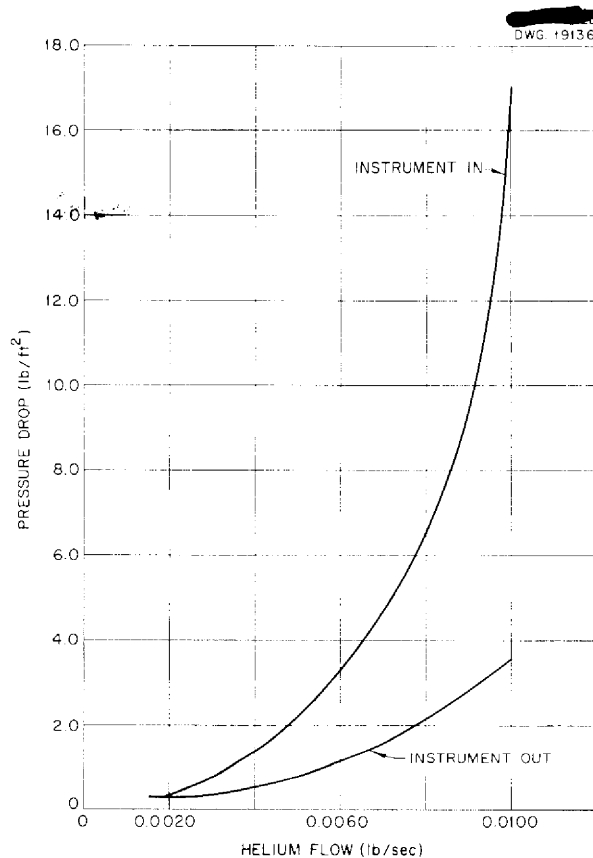
Fig. 59. Pressure Drop in Instrument Sleeve.

TABLE 11. HELIUM FLOW RATES IN ROD AND INSTRUMENT HOLES

POSITION				HELIUM FLOW (lb/sec)		
Regulating Rod		Instrument		Safety Rod	Regulating Rod	Instrument
Out	In	Out	In			
x		x		0.035	0.034	0.005
	x	x		0.037	0.026	0.005
	x		x	0.037	0.026	0.005
x		x		0.035	0.034	0.005
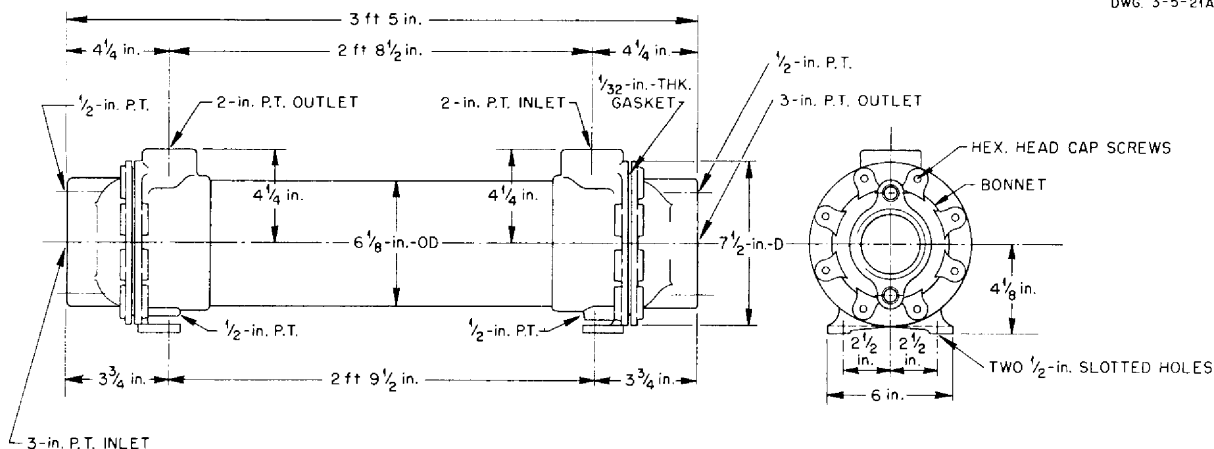
Fig. 60. Helium-to-Water Heat Exchanger.

2. The water outlet temperature is thermostatically controlled and is held fixed at 100°F.

$$(32) \quad hA = \left[\frac{1}{(hA)_{He}} + \frac{1}{(hA)_m} + \frac{1}{(hA)_w} \right]^{-1};$$

$$(33) \quad h_{He} = 1.86 \frac{k_{He}}{D_{He}} \left(\frac{\mu}{\mu_s} \right)_{He}^{0.14} Re_{He}^{1/3} Pr_{He}^{1/3} \left(\frac{D_{He}}{L} \right)^{1/3}$$

3. The water inlet temperature will vary with the season of the year, but has been assumed to be 70°F for this calculation.

The rod cooling system heat exchanger consists of three standard shell-and-tube heat exchangers arranged in parallel. The helium flows in the tubes, and the water flows across the outside of the tubes. The following are pertinent physical dimensions of the exchanger; all values are for one of three units:

Shell inside diameter, in.	6 1/8
Tube length, ft	3
Tube outside diameter, in.	0.375
Tube inside diameter, in.	0.319
Number of tubes	116
Surface area per tube (inside), ft^2	0.251
Surface area per tube (outside), ft^2	0.295
Surface area (inside), ft^2	29.1
Surface area (outside), ft^2	34.2
Baffle spacing, in.	2
Tube pitch (triangular pattern), in.	29/64

The heat transfer coefficient may be evaluated from the following equations:

(McAdams, p. 190 of ref. 11), where the calculation indicates that the helium flow is laminar;

$$(34) \quad h_w = \frac{k_w}{D_w} \left(\frac{\mu}{\mu_s} \right)_w^{0.14} Re_w^{0.55} Pr_w^{1/3}$$

(Kern, p. 137 of ref. 8), where

$$Re_w = \frac{G_w D_w}{\mu_w},$$

$$D_w = \frac{4 \times \text{free area}}{\text{wetted perimeter}} \quad \text{(free area measured in a plane perpendicular to the tubes)},$$

$$G_w = \frac{dCB}{p};$$

$$(35) \quad \left(\frac{1}{hA} \right)_m = \frac{2\pi k_m L}{\ln \frac{D_{He}}{D_w}},$$

where

k = thermal conductivity, Btu/sec·ft^2 (°F/ft),

77

D = equivalent diameter, ft,

μ = viscosity at bulk temperature, lb/hr·ft,

μ_s = viscosity at surface temperature, lb/hr·ft,

Re = Reynolds' number,

Pr = Prandtl's number,

L = tube length, ft,

G = unit weight flow, lb/hr·ft^2,

d = shell inside diameter, ft,

C = tube clearance, ft,

B = distance between baffles, ft,

p = tube pitch, ft,

and the subscripts

He = helium,

w = water.

The helium and water heat transfer areas are tabulated above: 29.1 and 34.2 ft^2 per one unit of three, respectively.

By using Eqs. 29 through 35 and noting that the large number of baffles on the shell side makes the effective log mean temperature difference almost equal to the log mean temperature difference for counterflow, the performance of the rod cooling system heat exchanger can be calculated. Figure 61 shows the result of such a calculation; the helium inlet and outlet temperatures are plotted against the heat transferred. Some of the pertinent information not shown in Fig. 60 is tabulated in Table 12.

The heat removed from the core in the rod cooling circuit, calculated in the first section of this chapter, is about 25 Btu/sec. From Fig. 61, it may be seen that the minimum and maximum temperatures in the rod cooling heat exchanger will be about 110 and 240°F, respectively. The helium will actually pick up a considerable amount of heat between the heat exchanger and the inlet to the reactor and, consequently, the inlet and outlet temperatures of the heat exchangers will be greater than those listed above. The inlet temperature to the reactor will be about 150°F.
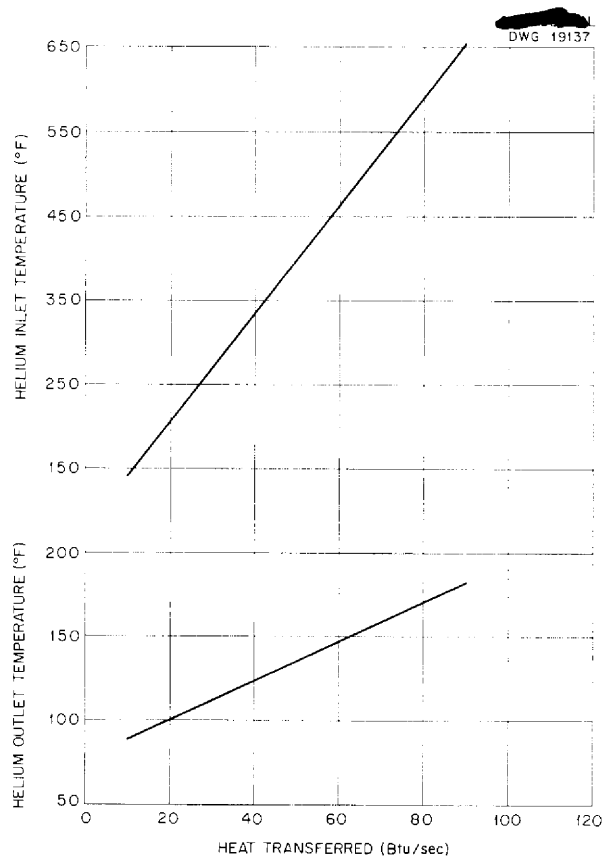
Fig. 61. Helium Inlet and Outlet Temperature vs. Heat Transferred.

TABLE 12. HEAT EXCHANGER DATA FOR HELIUM-TO-WATER HEAT EXCHANGER

Helium flow area (total), ft^2	0.246
Helium velocity, ft/sec	65
Helium Reynolds' number	950
Helium heat transfer coefficient, Btu/sec·ft^2·°F	0.0039
$(hA)_{He}$, Btu/sec·°F	0.344
Water weight flow, lb/sec	1.0, 2.0, 3.0
Water heat transfer coefficient, Btu/sec·ft^2·°F	0.13, 0.19, 0.24
$(hA)_w$, Btu/sec·°F	13.5, 19.8, 24.6
hA, Btu/sec·°F	3.01, 2.99, 2.98

Chapter 6
MONITORING AND PREHEAT SYSTEM

HEAT LOSS THROUGH INSULATION

The heat loss to the environment of the various pieces of equipment in the three ARE pits is complicated by the fact that the pits are filled with helium. The helium tends to replace the air in the pores of the insulation and thus to increase the thermal conductivity of the insulation. The following formula for the thermal conductivity of porous insulating materials was derived by Maxwell and reported by Jakob (cf., p. 85 of ref. 14):

$$(1) \quad k = k_s \frac{1 - \left(1 - \frac{ak_g}{k_s}\right)b}{1 + (a - 1)b} \quad ,$$

where

$$a = \frac{3k_s}{2k_s + k_g} \quad ,$$

$$b = \frac{V_g}{V_s + V_g} = 1 - \frac{V_s}{V_s + V_g} = 1 - \frac{\rho}{\rho_s} \quad ,$$

k = thermal conductivity, Btu/hr·ft^2 (°F/ft),

V = volume, ft^3,

ρ = density, lb/ft^3,

and the subscripts

s = solid,

g = gas.

The ARE uses three types of insulation; diatomaceous earth and Superex for high-temperature insulation, and felted Asbestos-Sponge for lower-temperature insulation. The properties of these insulations are given in Table 13. By using the data of Table 13 and mean thermal conductivities of 0.033 and 0.021 Btu/hr·ft^2 (°F/ft) for the air in the high- and low-temperature insulation, respectively, the thermal conductivity of the solid, k_s, can be determined from Eq. 1. Since k_s is known, k can be calculated for the case with helium in the pores by using 0.15 and 0.11 Btu/hr·ft^2 (°F/ft),

respectively, for the high- and low-temperature mean thermal conductivities of helium. The results of the calculations are tabulated in Table 14.

The insulation on the outside of the ARE piping and equipment is a combination of Superex and Asbestos-Sponge, and diatomaceous earth is used for insulation in the control rod cooling loop. The heat loss to the environment through the combination Superex and Asbestos-Sponge insulation may be calculated from the following equations:

1. For insulating cylindrical shapes (i.e., piping),

$$(2) \quad Q = \frac{2\pi k_s \theta_s}{\ln \frac{D_s}{D_s'}} \quad ,$$

$$(3) \quad Q = \frac{2\pi k_{a-s} \theta_{a-s}}{\ln \frac{D_{a-s}}{D_{a-s}'}} \quad ,$$

$$(4) \quad Q = \frac{0.173}{3600} \epsilon A \left[\left(\frac{T_s}{100}\right)^4 - \left(\frac{T_e}{100}\right)^4\right]$$
$$+ h_c A(T_s - T_e) \quad ,$$

where

Q = heat loss per lineal foot, Btu/sec·lineal ft,

k = thermal conductivity, Btu/sec·ft^2 (°F/ft),

θ = temperature difference, °F,

D = outside diameter, ft,

D' = inside diameter, ft,

ϵ = emissivity for radiant energy,

A = outside surface area per lineal foot, ft^2/lineal ft,

T_s = temperature of outside surface, °R,

T_e = temperature of environment, °R,

h_c = free convection heat transfer coefficient, Btu/sec·ft^2·°F,

and the subscripts

s = Superex,

$a-s$ = Asbestos-Sponge.

TABLE 13. PROPERTIES OF VARIOUS INSULATING MATERIALS

	DIATOMACEOUS EARTH	SUPEREX	FELTED ASBESTOS-SPONGE
Primary solid constituent	SiO_2	SiO_2	$MgSiO_3$
Density, ρ, lb/ft^3	18	24	30
Density of solid, ρ_s, lb/ft^3	145	145	205
Mean thermal conductivity (air in pores), k, Btu/hr·ft^2 (°F/ft)	0.060	0.070	0.045

TABLE 14. THERMAL CONDUCTIVITIES OF VARIOUS INSULATING MATERIALS

MATERIAL	THERMAL CONDUCTIVITY [Btu/hr·ft^2 (°F/ft)]	
	Solid, k_s	k (helium in pores)
Diatomaceous earth	0.34	0.17
Superex	0.34	0.18
Felted Asbestos-Sponge	0.25	0.13

The free convection heat transfer coefficient is determined from the data of Nusselt,[18] McAdams, and King,[19] who correlated Nusselt's number with Grashof's and Prandtl's numbers (as given by Jakob[14]).

2. For insulating plane shapes, Eqs. 2, 3, and 4 become

$$(5) \quad q = \frac{k_s}{t_s} \theta_s \, ,$$

$$(6) \quad q = \frac{k_{a-s}}{t_{a-s}} \theta_s \, ,$$

$$(7) \quad q = \frac{0.173}{3600} \epsilon \left[\left(\frac{T_s}{100} \right)^4 - \left(\frac{T_e}{100} \right)^4 \right] + h_c (T_s - T_e) \, ,$$

where

q = heat loss per unit area, Btu/sec·ft^2,

t = thickness, ft.

The heat loss per lineal foot of the piping was calculated by using Eqs. 2, 3, and 4. The dimensions of the pipe, annulus, heaters, and insulation of the fuel and NaK piping are given in the following:

OUTSIDE DIAMETER (in.)

Nominal pipe size (IPS)	1	1 1/2	2	2 1/2
Pipe	1.315	1.900	2.375	2.875
Annulus	3.0	3.0	3.5	4.0
Heater	3.94	3.94	4.5	5.25
Superex	7.94	7.94	10	10.75
Asbestos-Sponge	9.94	9.94	12.5	13.25

Table 15 gives the heat loss per lineal foot for a range of heater outside wall temperatures for an emissivity, ϵ, of 0.90 and an ambient temperature, T_e, of 590°R (130°F).

Equations 5, 6, and 7 were used to calculate the heat loss per square foot of a flat surface for various insulation thicknesses and heater outside wall temperatures. Figure 62 shows the heat loss for temperatures of 1150, 1325, and 1500°F for combined insulation thicknesses of from 2 to 6

TABLE 15. HEAT LOSSES FOR VARIOUS TEMPERATURES OF THE HEATER OUTSIDE WALL

TEMPERATURE OF HEATER OUTSIDE WALL (°F)	NOMINAL PIPE DIAMETER (in.)		
	1 to 1½	2	2½
	HEAT LOSS (Btu/sec·lineal ft)		
1150	0.23	0.21	0.23
1325	0.27	0.25	0.27
1500	0.31	0.29	0.31

in.; the thickness of the Superex layer was assumed to be twice the thickness of the Asbestos-Sponge layer. The emissivity and ambient temperature were the same as those used above.

The values calculated above for heat loss through the insulation were used to roughly estimate the heat loss at operating conditions (3-megawatt power output) of the various items of equipment in the three ARE pits (Fig. 63). The results are given in Table 16.

The total heat loss (kw) in each pit is:

Reactor pit	30
Heat exchanger pit	135
Dump tank pit	75
Total	240

REACTOR PREHEATING

The reactor of the ARE, with its large mass of beryllium oxide, has the largest heat capacity of any piece of equipment in the ARE. The reactor must be raised to a high temperature before the system can be filled with fuel carrier, since the fuel carrier has a melting point of approximately 950°F. Figures 9 and 12 show elevation and plan views of the reactor; Fig. 9 shows the reactor and its thermal insulation, which is attached to a metal shell that is separate from the reactor. The heat is supplied by electrical strip heaters strapped to the reactor itself. The procedure for preheating the reactor will be the following:

1. turn the heaters on at a power of 10 kw;
2. increase the heater power as the pressure shell temperature in-
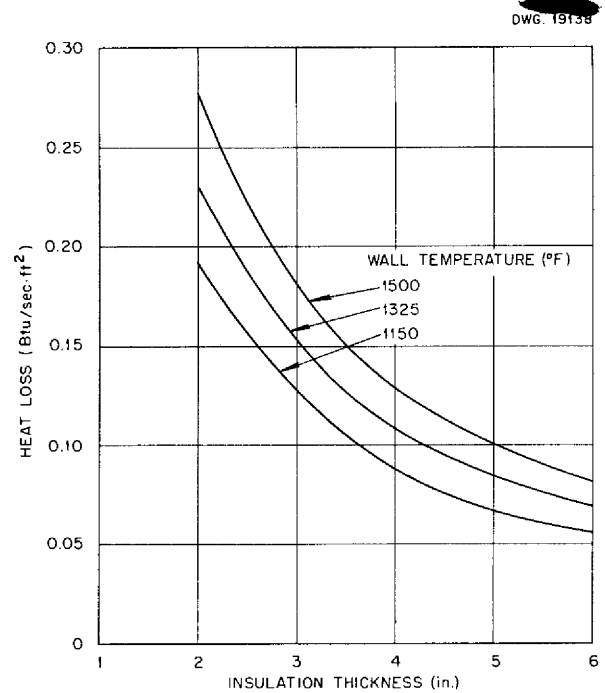
Fig. 62. Heat Loss Through Insulation.

creases so that the heater power is equal to 10 kw plus the heat loss through the insulation;

3. when the pressure shell temperature reaches 1200°F, gradually reduce the heater power to hold the pressure shell temperature at 1200°F.

When no further changes in heater power are required to hold the pressure shell at 1200°F, equilibrium will have been attained and the preheat process completed.

Steps 1 and 2 in the preheat process imply that a constant amount of heat is being added to the reactor, namely, 10 kw. This method of preheating will

81

TABLE 16. HEAT LOSSES IN THE ITEMS IN THE ARE PITS

ITEM	LOCATION	HEAT LOSS (kw)
Reactor and reactor thermal insulation	Reactor pit	15
Fuel system heat exchangers	Heat exchanger pit	5
Fuel system surge tanks	Heat exchanger pit	4
Fuel pumps	Heat exchanger pit	2
Reflector coolant system heat exchangers	Heat exchanger pit	6
Reflector coolant surge tanks	Heat exchanger pit	4
Reflector coolant pumps	Heat exchanger pit	2
Fill and flush tanks	Dump tank pit	25
Fuel dump tank	Dump tank pit	8
Fuel surge tank vapor traps	Heat exchanger pit	2
Fuel dump tank vapor trap	Dump tank pit	2
NaK purification system	Heat exchanger pit	10
Valves	Heat exchanger pit	15
	Dump tank pit	12
Piping	Reactor pit	15
	Heat exchanger pit	85
	Dump tank pit	30

result in a quasi-stationary temperature state being set up in the reactor after some initial period. A quasi-stationary temperature means that the temperature difference between any two points remains constant even though the entire temperature level is rising. The preheating process can therefore be broken up into three periods:

1. the initial period before the quasi-stationary state is obtained,
2. the period when the reactor is in the quasi-stationary temperature state,
3. the period after the pressure shell has reached 1200°F, during which the heater power is being gradually reduced and the quasi-stationary state no longer exists.

The following assumptions were made for the calculation of the reactor preheating:

1. The reactor will be represented by six concentric beryllium oxide shells, 3 ft long and 3.75 in. thick, separated by helium shells 0.050 in. wide.

2. The pressure shell will be constructed of Inconel and will be 48 in. in inside diameter and 2 in. thick.

3. There will be a 1/16 in. helium gap between the pressure shell and outer beryllium oxide cylinder.

4. The heat loss from the ends of the reactor will be considered, but longitudinal heat flow within the reactor will be neglected.

The following physical properties, which represent mean values between 100 and 1200°F, were used in the analysis:

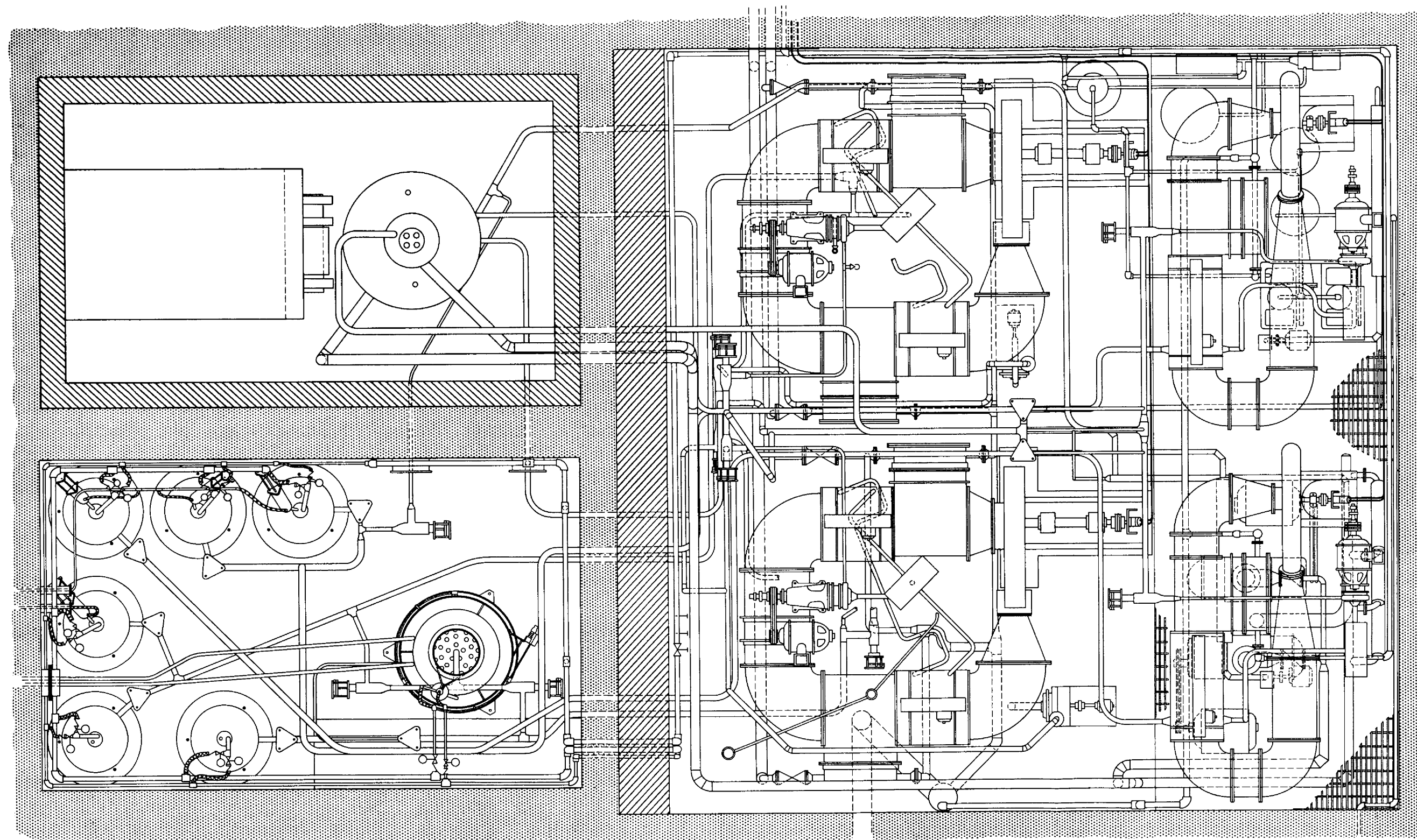|	BeO	INCONEL	HELIUM
Thermal conductivity, Btu/hr·ft² (°F/ft)	10	12	0.13
Density, lb/ft³	184	518	0.0055
Specific heat, Btu/lb·°F	0.38	0.15	1.24

Fig. 63.   Composite Plan View of Piping Inside Shield.

The temperature difference between any radial station in the reactor and the outside of the pressure shell when the reactor is in the quasi-stationary temperature state can be calculated from the following equation:

$$(8) \quad \frac{d\theta}{dt} = \frac{Q}{(Wc_p)_{BeO} + (Wc_p)_{Inc} + (Wc_p)_{He}} \; ,$$

where

$\frac{d\theta}{dt}$ = rate of temperature rise, °F/hr, of any point in the reactor (in the quasi-stationary temperature state),

Q = heater input to the reactor, Btu/hr,

W = weight of material in the reactor, lb,

c_p = specific heat, Btu/lb·°F,

and the subscripts

BeO = beryllium oxide,

Inc = Inconel,

He = helium.

The weight of the beryllium oxide in the reactor is approximately 5800 lb; the Inconel in the pressure shell weighs about 7900 lb; the helium weight can be neglected. From Eq. 8,

$$\frac{d\theta}{dt} = \frac{34,100}{5800 \times 0.38 + 7900 \times 0.15}$$

$$= 10.1°F/hr \; .$$

The temperature difference across any of the cylindrical shells may be approximated in the following manner:

$$(9) \quad \Delta\theta_n = \frac{q_n \ln \dfrac{r_{n+1}}{r_n}}{2\pi k_n L} \; ,$$

$$(10) \quad q_n = 34,100 - \sum_{i=1}^{n-1} (Wc_p)_i \frac{d\theta}{dt} \; ,$$

where

$\Delta\theta$ = radial temperature differential across a shell (in the quasi-stationary temperature state), °F,

q = heat entering shell, Btu/hr,

r = outside radius of shell, ft,

k = thermal conductivity of shell, Btu/hr·ft² (°F/ft),

L = length of shell, ft,

and the subscript n refers to the number of the shells, counting inward from the outside. (For a more accurate estimate, the fact that all the q_n in Eq. 10 is not transferred across shell n should be considered. The above approach is a conservative simplification, however, because it leads to larger values of $\Delta\theta_n$.)

The results of the solution of Eqs. 9 and 10 are shown in Fig. 64, which gives the difference in temperature (in the quasi-stationary state) between the outside of the pressure shell and any radial position. The difference between the outside of the pressure shell and the center of the reactor is 162°F.

The time required to reach the quasi-stationary temperature state may be readily calculated. The reactor is originally at some uniform temperature θ_0. The quasi-stationary state is reached while the temperature of the center of the reactor remains fixed at θ_0 and the outer shells heat up to a temperature of

$$(11) \quad \theta_{n_1} = \theta_0 + \sum_{i=n+1}^{N} \Delta\theta_i + \frac{1}{2} \Delta\theta_n \; ,$$

where

θ_{n_1} = temperature of the nth shell at the beginning of the quasi-stationary state,

N = total number of shells.

The time required to reach the quasi-stationary temperature state is,
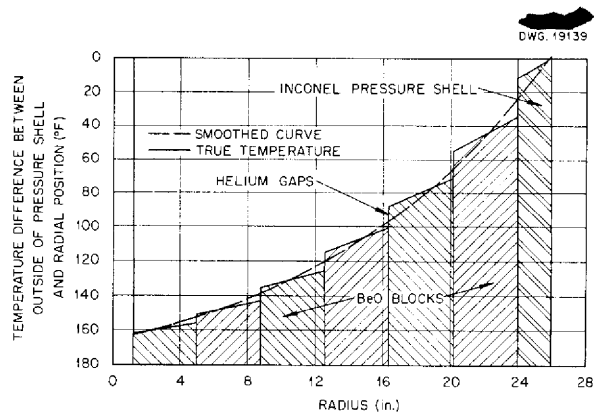

Fig. 64. Temperature Profile of Reactor Core and Pressure Shell (Quasi-Stationary State).

therefore,

$$(12) \qquad t_1 = \frac{\sum_{i=1}^{N} (Wc_p)_i \ (\theta_{i_1} - \theta_0)}{Q} \ ,$$

where t_1 is the time required to reach the quasi-stationary temperature state in hours. This time was calculated from Eq. 12 to be about 10.0 hours. Thus, after about 10 hr, the temperature of the outside of the pressure shell will be at about 162°F above ambient temperature, while the center of the core will still be at about ambient temperature. The actual ambient temperature in the pits will probably vary during the preheating period; most of the calculations of this report assume an ambient temperature of 130°F in the pit. It was assumed for these calculations that the reactor and pit were both, at the

until the reactor pressure shell outer temperature reaches 1200°F. During this period, the temperatures are in the quasi-stationary state, and every temperature in the reactor is raised uniformly at the rate of 10.1°F/hr:

$$(13) \qquad t_2 - t_1 = \frac{1200 - 292}{10.1} = 89.9 \ hr,$$

where t_2 is the time at the end of the quasi-stationary state. During this period, the electrical heater power must be continually increased as the pressure shell temperature increases to maintain a constant rate of heat flow into the reactor. The heater power must therefore be equal to 10 kw plus the heat loss through the insulation. The heat loss through the insulation may be calculated as a function of reactor pressure shell outer temperature from the following equations:

$$(14) \qquad q = h_1 A_1 \ (T_1 - T_{He}) + \frac{0.173}{3600} \frac{A_1}{\frac{1}{\epsilon_1} + \frac{A_1}{A_2}\left(\frac{1}{\epsilon_2} - 1\right)} \left[\left(\frac{T_1}{100}\right)^4 - \left(\frac{T_2}{100}\right)^4\right] ,$$

$$(15) \qquad q = h_2 A_2 \ (T_{He} - T_2) + \frac{0.173}{3600} \frac{A_1}{\frac{1}{\epsilon_1} + \frac{A_1}{A_2}\left(\frac{1}{\epsilon_2} - 1\right)} \left[\left(\frac{T_1}{100}\right)^4 - \left(\frac{T_2}{100}\right)^4\right] ,$$

$$(16) \qquad q = \frac{k_I}{\tau_I} A_I \ (T_2 - T_3) ,$$

$$(17) \qquad q = h_3 A_3 \ (T_3 - T_a) + \frac{0.173}{3600} \epsilon_3 A_3 \left[\left(\frac{T_3}{100}\right)^4 - \left(\frac{T_a}{100}\right)^4\right] ,$$

start, at a temperature of 130°F. The time required to raise the mean temperature of the reactor from 70 to 130°F is about 6 hours. It may therefore be considered that t_1 is really about 16 hr and that at the end of the 16-hr period the reactor pressure shell outer temperature will be about 292°F and the center-line temperature will be about 130°F.

The next period of the preheating process is the heating of the reactor

where

q = heat loss through insulation, Btu/sec,

h = heat transfer coefficient, Btu/sec·ft^2·°F,

A = heat transfer area, ft^2,

T = temperature, °R,

k = thermal conductivity, Btu/sec·ft^2 (°F/ft),

τ = thickness, ft,

ϵ = emissivity,

and the subscripts

1 = outside of reactor pressure shell,
2 = inside of thermal insulation,
3 = outside of thermal insulation,
I = insulation,
He = helium between pressure shell and thermal insulation,
a = ambient.

Equations 14 through 17 and the following data were used to calculate the heat loss through the insulation for various pressure shell temperatures:

1. $\epsilon = 1.0$.
2. The data of King[19] were used to evaluate h_1.
3. The dimensions of thermal insulation were:

Outside diameter	76.25 in.
Outside length	80.5 in.
Thickness	6 in. (4 in. of Superex, 2 in. of Asbestos-Sponge)

4. The thermal conductivity value for the insulation, as found in the previous section on "Heat Loss Through Insulation," was used.

The results of the calculation are shown in Fig. 65, where the heat loss through the insulation is plotted against the reactor pressure shell outer temperature. Temperatures at other points in the reactor thermal insulation are shown by the dotted line.

The last portion of the preheating process, that is, when the heater power is reduced to maintain the pressure shell outer temperature at 1200°F, is evaluated by a graphical method developed by Schmidt.[20] As a simplification, each helium shell is divided between adjacent beryllium oxide shells, and the Inconel pressure shell is replaced by an equivalent thickness of beryllium oxide. The reactor is then treated as a homogeneous cylinder with a thermal conductivity equal to the average thermal conductivity of the composite beryllium oxide and helium shells. A plot of the temperatures in the reactor for the first 8 hr of the last portion of the preheating period is shown in Fig. 66.
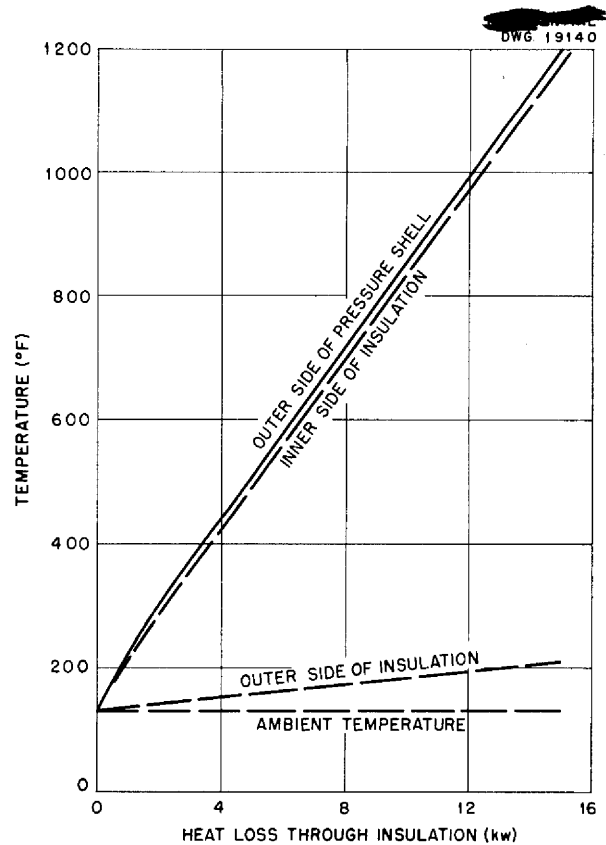
Fig. 65. Temperature of Outer Side of Pressure Shell vs. Heat Loss Through Insulation.

After 8 hr, the temperature of the core center line is about 1125°F.

A summary of the temperatures and powers in the entire preheating period is shown in Fig. 67.

The maximum temperature gradient in the pressure shell at any time is approximately 6°F/inch.

HELIUM LEAKAGE THROUGH CLEARANCE HOLES IN THE REACTOR THERMAL SHIELD

The tubes which contain the control rods and fission chambers pierce the reactor thermal insulation at both the top and bottom, and there are six such tubes. Figure 68 shows a sketch of a typical tube and the passage through the reactor thermal shield. The helium inside the reactor thermal shield, being at a higher temperature than the room helium, will flow through the clearance holes in the reactor thermal insulation and consequently will add

87
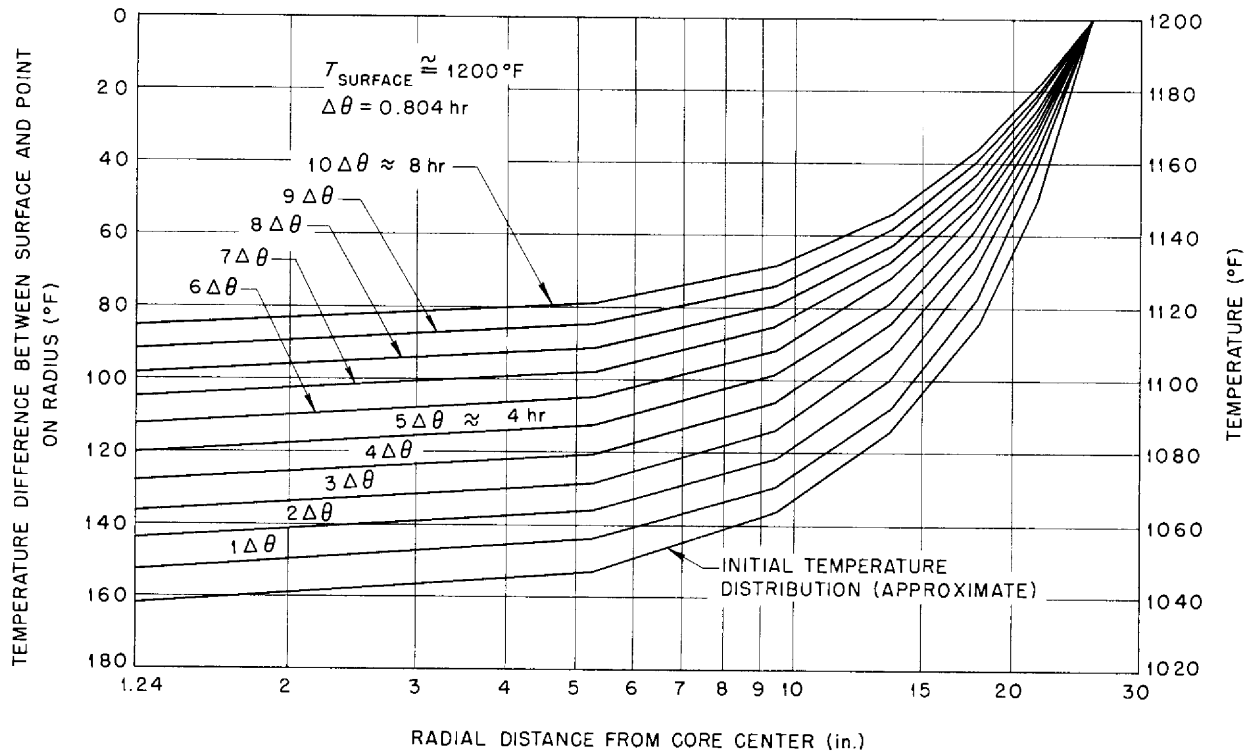
Fig. 66. Temperature vs. Time Relationship for Reactor Core and Pressure Shell.

to the room cooling requirements and the reactor electric heater requirements.

It was assumed that the flow through the bottom clearance holes was negligible and that the flow through the upper clearance holes was that due to the difference in head between the helium in the clearance holes and room helium. The head available for flow is, then,

$$(18) \qquad P = h(\rho_a - \rho_c) ,$$

where

P = pressure head, lb/ft^2,

ρ_a = density of ambient helium, lb/ft^3,

ρ_c = density of helium in clearance hole, lb/ft^3,

h = height of clearance hole, ft.

To be conservative, it was assumed that the temperature of the helium in the clearance hole was 1200°F; the room temperature was taken as about 130°F. Thus

$$P = \frac{6.125}{12} \times (0.0092 - 0.00335)$$

$$= 0.00299 \ lb/ft^2 .$$

The loss in pressure head in a gas flowing through an annulus in laminar flow is

$$(19) \qquad P = \frac{12\mu GL}{y^2 g_c \rho} ,$$

where

μ = viscosity, $lb/hr \cdot ft$,

G = flow, $lb/hr \cdot ft^2$,

L = length = height of clearance hole, ft,

y = annulus gap, ft,

g_c = gravitational constant, ft/hr^2,

ρ = gas density, lb/ft^3.

88
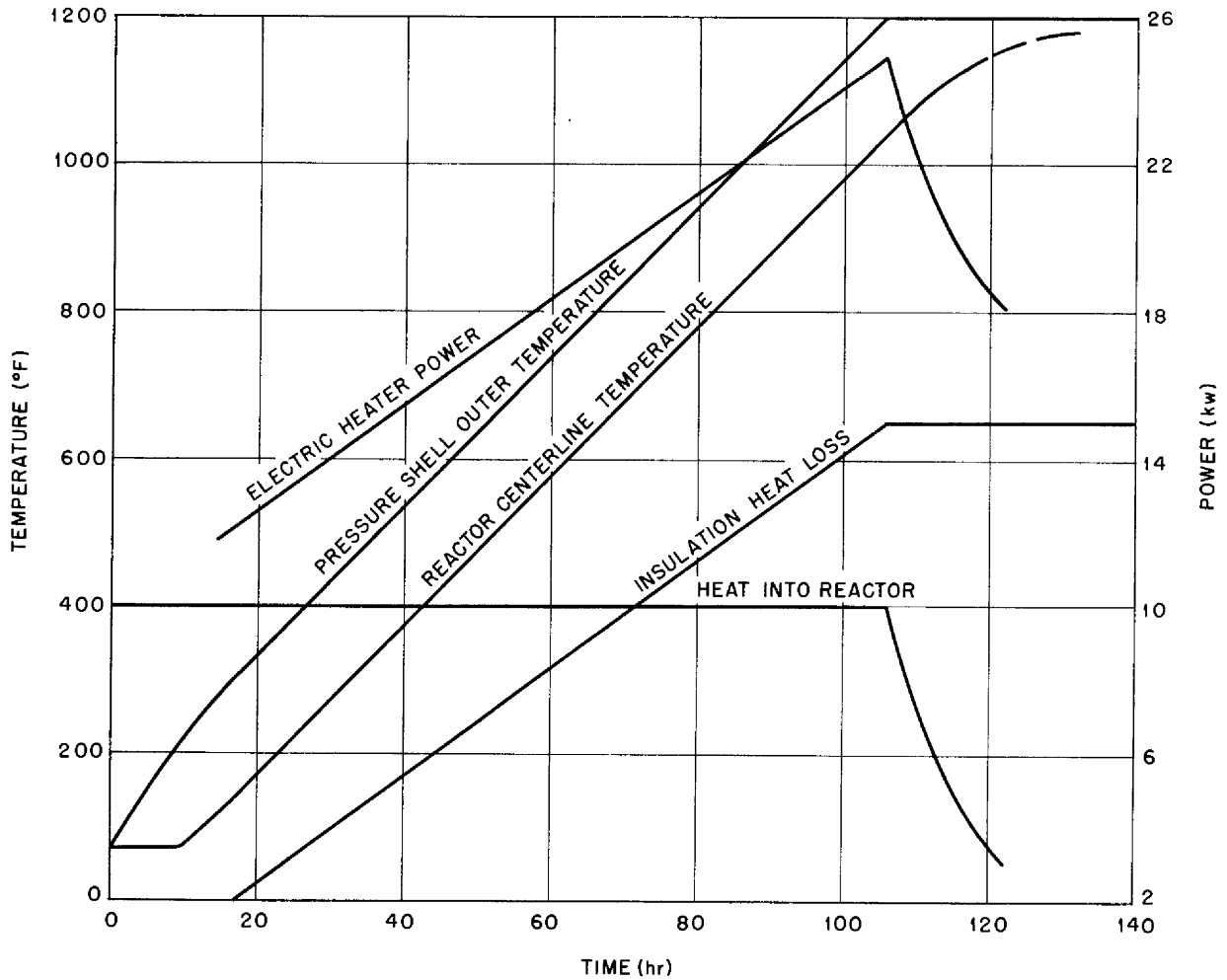
Fig. 67. Summary of Temperature and Power in Entire Preheating Period.

An evaluation of Eq. 19 gives

$$P = \frac{12 \times 0.102 \times G \times \dfrac{6.125}{12}}{\left(\dfrac{0.39}{12}\right)^2 \times 32.2 \times (3600)^2 \times (0.00335)} = 4.24 \times 10^{-4} \ G \ \text{lb/ft}^2 \ .$$

The flow, G, is then evaluated by equating the available pressure head to the loss in head because of flow:

$$G = 7.05 \ \text{lb/hr} \cdot \text{ft}^2 \ .$$

Since there are six identical clearance holes, the total flow area is

$$A = 6 \times \frac{\pi}{4}\left[\left(\frac{3.75}{12}\right)^2 - \left(\frac{2.97}{12}\right)^2\right]$$

$$= 0.1715 \ \text{ft}^2 \ .$$

Therefore the weight flow is

$$W = 0.1715 \times 7.05 = 1.21 \ \text{lb/hr} \ ,$$
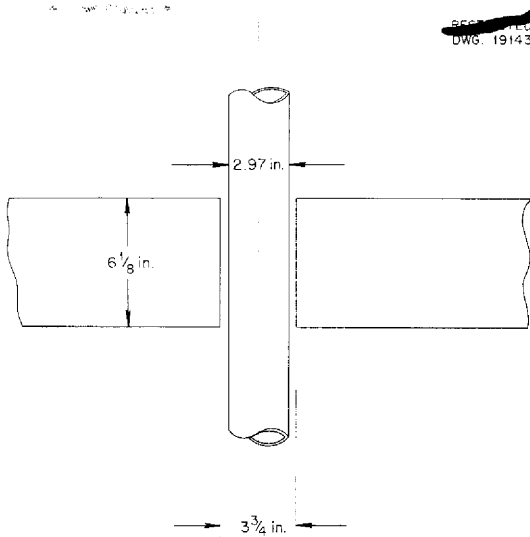
Fig. 68. Rod Sleeve Through Thermal Shield.

and the heat loss is

$$Q = Wc_p(T_c - T_a) = 1.21 \times 1.24 \ (1200 - 130)$$

$$= 1605 \ \text{Btu/hr}$$

$$= 0.446 \ \text{Btu/sec} \ ,$$

where

T_c = temperature in clearance hole, °F,

T_a = ambient temperature, °F.

The heat loss through the clearance holes is therefore approximately 0.45 Btu/sec.

SPACE COOLER PERFORMANCE

The bulk of the equipment of the ARE is contained in three sealed pits, which are kept cool by the use of space coolers. A typical space cooler is shown in Fig. 69. Each space cooler contains two helium blowers in parallel (total capacity 7200 cfm) and a water cooling coil. The entire unit was supplied by the Trane Co. The cooling coil is a Trane Co., series 93, type S coil, with a 12- by 48-in. face and four rows of tubes longitudinal to the gas flow. The heat transfer coefficient of such a coil, operating with air on one side and water on the other, is given in ref. 21, for various water and air velocities. As used in the ARE, these coils will have helium instead of air on the gas side.

Since it was necessary to convert the performance data from those for air-to-water operation to those for helium-to-water operation, the following equation, from which values can be obtained that are approximately the same as the actual performance data given in ref. 21, was used:

$$(20) \qquad \frac{1}{hA} = \frac{0.00374}{v_w^{0.8}} + \frac{0.189}{v_a^{0.6}} \ ,$$
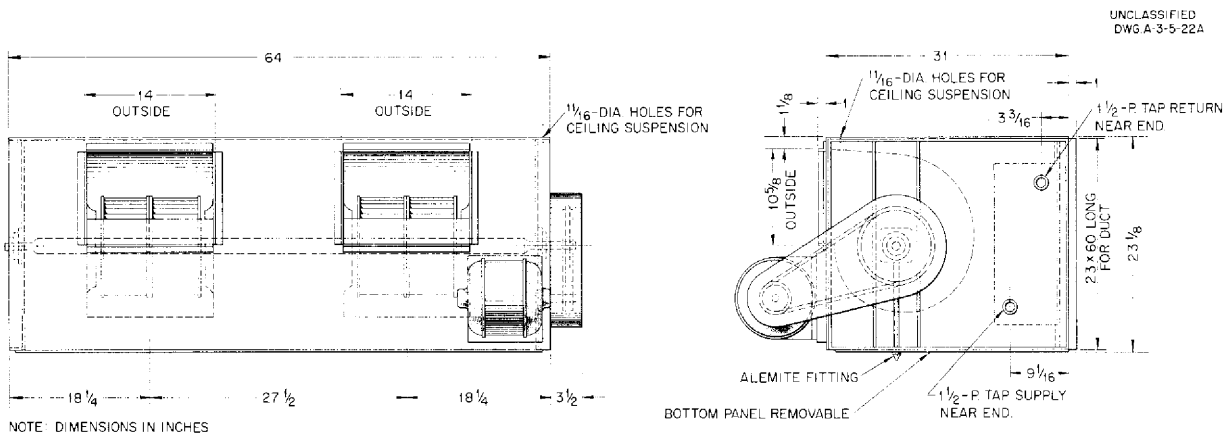
where

h = over-all heat transfer coefficient, Btu/hr·ft^2·°F,

A = heat transfer area per row per square foot of coil face area, ft^2,

v_w = water velocity, ft/sec,

v_a = air velocity, ft/min.

To use Eq. 20, an equivalent air

Fig. 69. Space Cooler.

90

velocity, that is, the air velocity which would give the same heat transfer coefficient as the actual helium velocity, had to be calculated. Since the fin efficiency of the coil fins is very close to 100% at all times (sheet fins of aluminum, 0.012 in. thick, with the tubes on a triangular pitch of approximately 1.2 in.), it may be assumed that the gas-side heat transfer coefficient is a function of the Reynolds' number to the 0.6 power. Since the Prandtl's numbers for air and for helium are about the same at this temperature and since the geometry of the coil is unchanged, the equivalent air velocity can be calculated from the following equation:

$$(21) \quad \frac{h_a}{h_{He}} = 1.0 = \frac{k_a v_a^{0.6} \rho_a^{0.6} \mu_{He}^{0.6}}{k_{He} v_{He}^{0.6} \rho_{He}^{0.6} \mu_a^{0.6}}$$

or

$$\frac{v_a}{v_{He}} = \left(\frac{k_{He}}{k_a}\right)^{1.667} \frac{\rho_{He}}{\rho_a} \frac{\mu_a}{\mu_{He}} ,$$

where

k = thermal conductivity,
ρ = density,
μ = viscosity,
h = heat transfer coefficient,
v_a = equivalent air velocity,
v_{He} = helium velocity.

Since the equivalent air velocity (calculated above) and the water flow are known, the over-all hA can be calculated from Eq. 20.

The equations governing the operation of the space coolers are

$$(22) \quad Q = W_{He} c_{p_{He}} (T'_{He} - T_{He}) ,$$

$$(23) \quad Q = W_w c_{p_w} (T'_w - T_w) ,$$

$$(24) \quad Q = hA\theta ,$$

where

Q = heat transferred, Btu/sec,
θ = log mean temperature difference, °F,
W = weight flow, lb/sec,
c_p = specific heat, Btu/lb·°F,
T' = maximum temperature (also equals ambient temperature), °F,
T = minimum temperature, °F,

and the subscript w refers to water. The system operates under the following restraints and conditions:

1. The helium flow is 7200 cfm at blower temperature.

2. The outlet water temperature is thermostatically controlled to be 100°F.

3. The inlet water temperature varies with the season of the year but is assumed to be 70°F for this calculation.

Equations 20 through 24 and the restraints and condition listed above can be used to evaluate the performance of the space coolers. Figure 70 shows the variation of heat transferred vs. ambient temperature for one of the space coolers. (The heat exchanger pit contains four such units; the other pits each contain two units.) The difference between the maximum helium temperature (ambient) and the minimum helium temperature is small; that is, it varies from about 0.2 deg at a heat load of 25 Btu/sec to about 1.6 deg at a heat load of 200 Btu/sec.

The heat rejected to the ambient atmosphere in the three ARE pits from the various items of equipment in the pits, calculated in the previous section on "Heat Loss Through Insulation," is tabulated in the following:

Reactor pit	30 kw
Heat exchanger pit	135
Dump tank pit	75
Total	240 kw

The three pits are interconnected by passages of relatively small flow area. Therefore the pits will not operate at the same temperature, nor will they operate at the temperatures which would exist if the pits were completely sealed from one another. The pit operating temperatures were calculated for the two extreme cases (pits at the same temperature; pits completely independent) by using the data of Fig. 70, which gives the space cooler performance. It was assumed that the heat loss from the pits to the outside through the concrete walls could be neglected; this is a conservative assumption. Table 17 gives the heat losses in the pits.
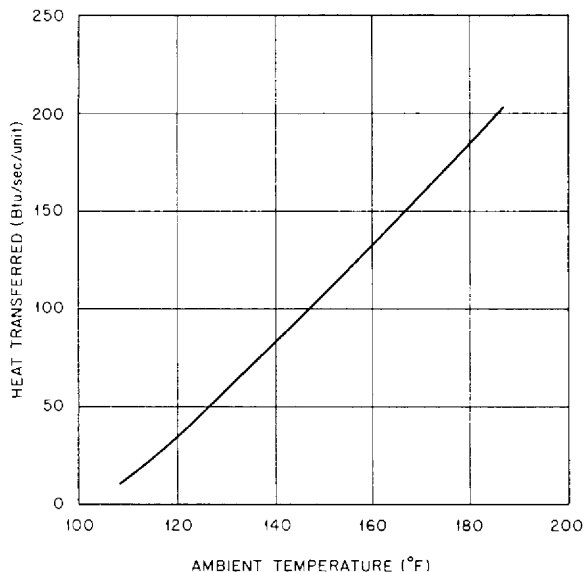
Fig. 70.   Space Cooler Performance.

The pits will therefore operate at a temperature of about 110 to 120°F. It should be noted that all the heat loss calculations in the section on "Heat Loss Through Insulation" were made with an assumed ambient temperature of 130°F. Therefore the heat losses listed in Table 17 are slightly low. The difference is quite small, however, inasmuch as the surface temperature of most of the equipment losing heat is from 1150 to 1500°F.

TEMPERATURE PATTERNS IN THE MONITORING ANNULUS IN THE EVENT OF HEAT FAILURE

The fuel and reflector coolant systems of the ARE are entirely enclosed in a metallic envelope (Fig. 71). This envelope consists of concentric tubing around all the pipes, and conveniently shaped containers around the other items of equipment, such as valves and pumps. Helium is circulated in the space between the metallic envelope and the main systems to serve two purposes. The helium is continuously sampled by instruments which can detect the presence of small quantities of fuel or NaK vapor and thus give warning if a leak develops in the system (hence the name, "monitoring system"). The flowing helium also acts as a distributor of heat in the following manner. Most of the electric heaters of the main system are on the outside of the envelope. Should a heater failure occur, the flowing helium, by transporting heat from the heated to the unheated areas, will tend to make uniform the heat distributed to the systems and, consequently, to reduce the temperature gradients which would otherwise occur.

The locations where the heat distribution function is particularly critical are in the fuel dump-and-fill lines. As may be noted from the position of the valves in Fig. 2, the fuel dump-and-fill lines may stand full of stagnant fuel during the operation of the reactor. Consequently, in the event of a heater failure, it is possible for the fuel carrier to freeze in these lines and make dumping of the reactor impossible. However, a helium bleed line will be connected to the fuel-carrier line to prevent drainage. The temperature patterns that would occur in these fuel-carrier lines and their envelopes if there were a particularly bad heater failure were

TABLE 17.   HEAT LOSSES IN THE PITS

	TOTAL HEAT LOSS (Btu/sec)	NUMBER OF SPACE COOLERS	HEAT LOSS PER COOLER (Btu/sec)	AMBIENT TEMPERATURE (°F)
All pits	228	8	28.4	118
Reactor pit	28.5	2	14.3	111
Heat exchanger pit	128.0	4	32.0	120
Dump tank pit	71.1	2	35.6	121
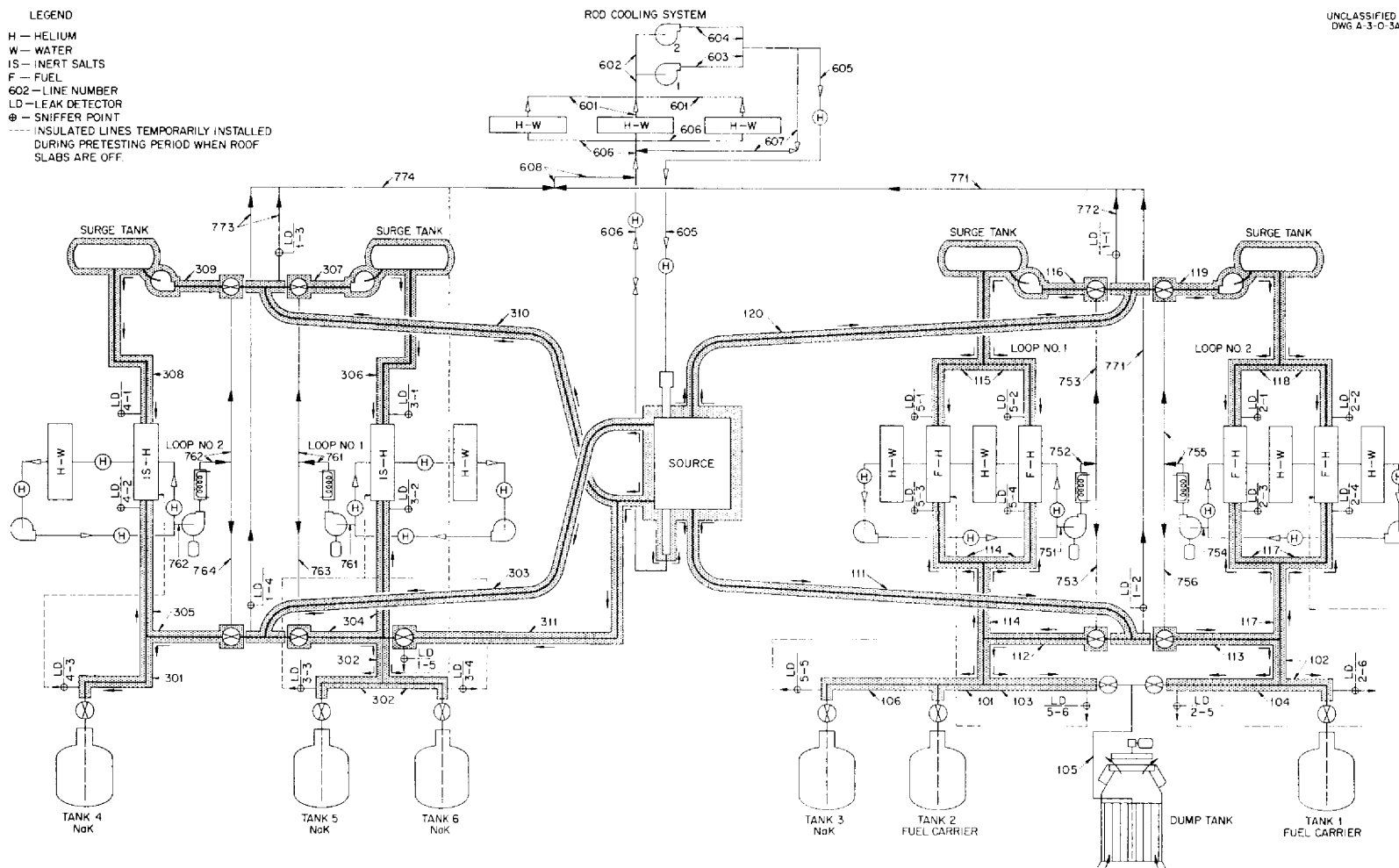
Fig. 71.   Monitoring System Flow Sheet.

COOLEY ELECTRIC CO. UNIT
HEATERS, 650 WATTS, 120 V
CLAM SHELL TYPE, 8 in. LONG

TO OTHER
HEATING UNITS

L3
L2
L1

SECTION "A-A"

DWG. D-13296A

"B"

A"

A"

KEY PLAN

"B"

COOLEY ELECTRIC CO. UNIT
HEATERS, 325 WATTS, 120 V
CLAM SHELL TYPE, 4 in. LONG

L6
L5
L4

SECTION "B-B"

NO. 16 GAGE
STAINLESS STEEL WIRE

DETAIL E
HEATING UNIT HELD IN
PLACE BY NO. 16 GAGE
STAINLESS STEEL WIRE

L2

L1   L2

B
2 WIRE, 3 UNIT. USE ONLY WHEN
NECESSARY FOR 3 UNITS

L1   L3

A
3 WIRE, 9 UNIT DELTA

L1   L2   L3

C
3 WIRE, 6 UNIT. USE ONLY WHEN NECESSARY FOR 6 UNITS

WIRING DIAGRAMS A, B, AND C

HEATING UNIT

DETAIL D
CLAM SHELL HEATING UNIT

PORCELAIN INSULATOR
BUSHING

Fig. 72.   Electrical Wiring Diagram for Monitoring Annulus Heaters.

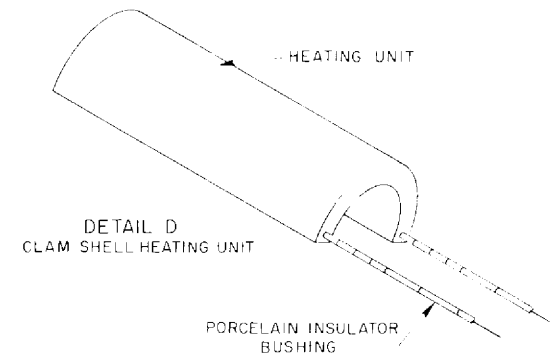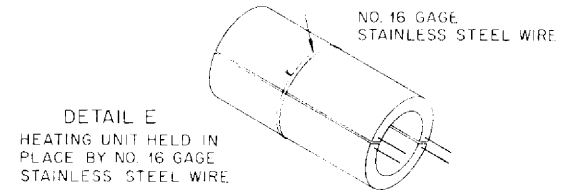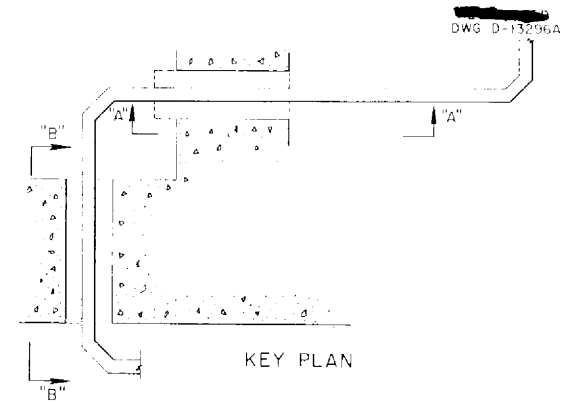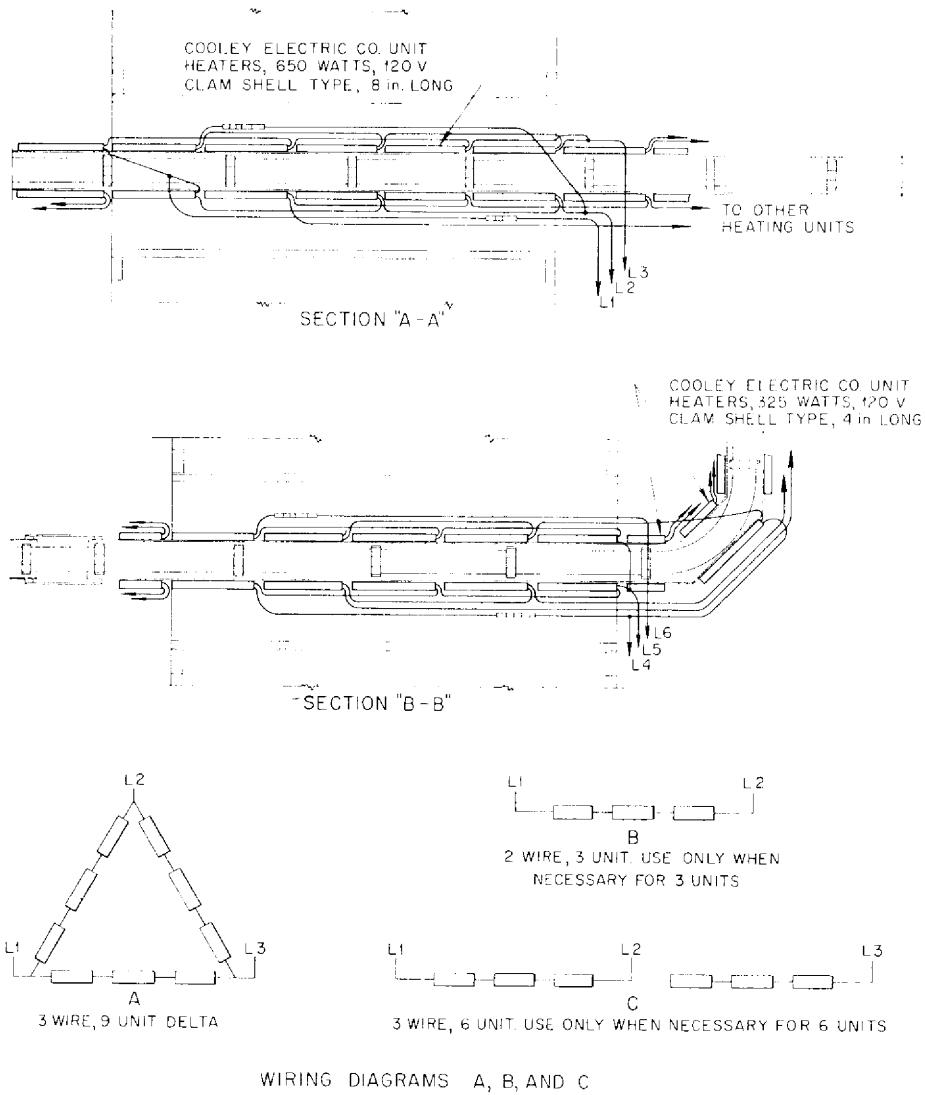investigated for several helium velocities in the monitoring system. For the investigation, it was assumed that the lines were filled with the fuel carrier. Figure 2 shows the pipe line to the fuel dump tank; Fig. 72 shows a wiring diagram of a typical set of electric heaters, which are in the form of half cylinders and surround the lines shown in Fig. 2. It may be noted from Fig. 72 that three sections of electric heater, each consisting of one half cylinder 8 in. long, are connected in series and that the failure of any one heater results in the failure of the other two. The three heaters are separated so that they are not adjacent to one another. For the type of heater failure considered in the following analysis, it is assumed that two sets of heaters fail and that these are exactly opposite each other on the pipe line.

The system, as set up for analysis, is shown in Fig. 73a. For simplicity, the heat produced by the electric heaters is assumed to be generated directly in the wall of the concentric tube which serves as the metallic envelope. The pipe line is divided into seven sections:

1. Sections 1 and 7 are the unaffected areas of the pipe lines upstream and downstream of the area where the heater failures occurred.

2. Sections 2, 4, and 6 are the areas where the heaters on both sides of the pipe failed.

3. Sections 3 and 5 are the areas where the heaters (which separate the failed heaters) are still operative.

In the steady-state condition, the fuel pipe temperature will be equal to the temperature of the flowing helium. Therefore only the heat transfer between the helium, the metallic envelope, and the outside environment needs to be considered. The heat balance in a given section of pipe line in the steady-state condition is given by (Fig. 73b)

(25) $\quad Q_m + Q_g + Q_{He-m} = Q'_m + Q_{m-e}$

and

(26) $\quad Q_{He} = Q'_{He} + Q_{He-m}$,
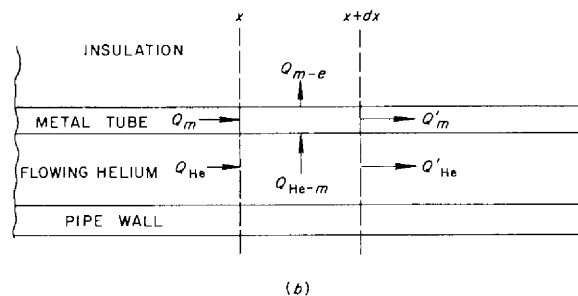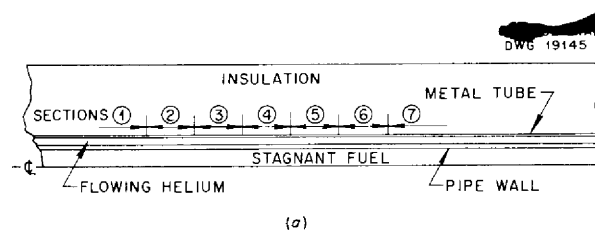
Fig. 73. Sections Showing Fuel Pipe and Annulus Walls.

where Q and Q' are heat transferred in Btu/sec and the subscripts

m = along the metal of the envelope,

He = in the flowing helium,

He-m = from the helium to the metal of the envelope,

m-e = from the metal of the envelope (through the insulation) to the environment,

g = internally generated.

The various terms in Eqs. 25 and 26 are expressed quite readily as follows: From the common equation for one-dimensional heat conduction,

(27) $\quad Q_m - Q'_m = k_m a_m \dfrac{\cdot d^2\theta_m}{dx^2} dx$,

where

θ_m = difference between metal temperature and ambient temperature, °F,

k = thermal conductivity, Btu/sec·ft² (°F/ft),

a = cross-sectional area, ft²,

x = distance from origin, ft (the left end of each section, except section 1, is considered as the origin of that particular section; the right end of section 1 is used as the origin of that section).

The heat gained by the helium

(28) $\quad Q'_{He} - Q_{He} = W_{He} c_{p_{He}} \, d\theta_{He}$,

where

θ_{He} = difference between helium temperature and ambient temperature, °F,

W = weight flow, lb/sec,

c_p = specific heat, Btu/lb·°F.

The heat transferred from the helium to the metal

(29) $\quad Q_{He-m} = h_{He-m} C_m \, dx \, (\theta_{He} - \theta_m)$,

where

h = heat transfer coefficient, Btu/sec·ft²·°F,

C = circumference of inside wall of metallic envelope, ft.

The heat transferred from the metal through the insulation to the environment is a complicated function which was evaluated for various metal temperatures in the section on "Heat Loss Through Insulation," Eqs. 2, 3, and 4, and is shown in Fig. 74. The curve in Fig. 74 can be approximated from about 500 to 1500°F by a straight line for which the formula is

(30) $\quad Q_{m-e} = b\theta_m + d$,

where b and d are constants.

The internal heat generation in the metal is equal to the heat supplied by the electric heaters in those sections in which the heaters are still operative, and it is equal to zero in those
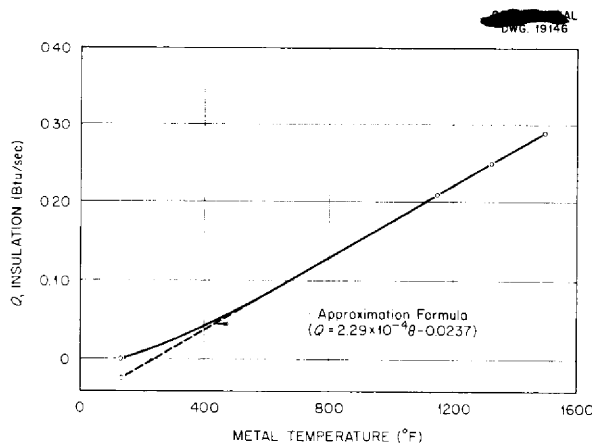
Fig. 74. Heat Loss from Insulated 2-in. Pipe vs. Wall Temperature of the Pipe (Sink Temperature, 130°F).

sections in which the heaters have failed. The heat supplied by the heaters which are still operative can be varied by the operator. At design conditions, the heaters will be operating at about 5/9 capacity; if thermocouple readings indicate that there were heater failures in the line, the adjacent heaters which were still operative could be run at full power. For the following analysis, however, the more dangerous situation will be considered, namely, that the heater failures go unnoticed and the heaters which are still operative remain at their normal power:

(31) $\quad Q_g = q' a_m \, dx = P \, dx$,

for sections 1, 3, 5, and 7, and

$\quad Q_g = q' a_m \, dx = 0$,

for sections 2, 4, and 6, where

q' = unit internal heat generation, Btu/sec·ft³,

P = normal power input to the electric heaters per lineal foot, Btu/sec·lineal ft.

Substitution of Eqs. 27 through 31 in Eqs. 25 and 26 gives

(32) $\quad k_m a_m \dfrac{d^2\theta_m}{dx^2} + q' a_m$

$\qquad + h_{He-m} C_m \, (\theta_{He} - \theta_m) = b\theta_m - d$

and

(33) $\quad W_{He} c_{p_{He}} \dfrac{d\theta_{He}}{dx}$

$\qquad = -h_{He-m} C_m \, (\theta_{He} - \theta_m)$.

Solving Eq. 33 for θ_m and differentiating twice gives

(34) $\quad \theta_m = \theta_{He} + \dfrac{W_{He} c_{p_{He}}}{h_{He-m} C_m} \dfrac{d\theta_{He}}{dx}$

and

(35) $\quad \dfrac{d^2\theta_m}{dx^2} = \dfrac{d^2\theta_{He}}{dx^2} + \dfrac{W_{He} c_{p_{He}}}{h_{He-m} C_m} \dfrac{d^3\theta_{He}}{dx^3}$.

Substitution of Eqs. 34 and 35 in Eq. 32 gives

$$(36) \quad \frac{d^3\theta_{He}}{dx^3} + \frac{h_{He-m}C_m}{W_{He}c_{p_{He}}} \frac{d^2\theta_{He}}{dx^2}$$

$$- \frac{h_{He-m}C_m + b}{k_m a_m} \frac{d\theta}{dx} - \frac{h_{He-m}C_m \, b}{k_m a_m W_{He}c_{p_{He}}} \theta$$

$$= \frac{h_{He-m}C_m}{k_m W_{He}c_{p_{He}}} \left(\frac{d}{a_m} - q' \right) \ ,$$

which may be solved quite readily. It is first necessary to evaluate the constant in Eq. 36 for the conditions of the problem. Three different helium velocities were considered: 1, 3, and 10 ft/sec. For these three different velocities, the values of the constants of Eq. 36 are tabulated in the following:

	1	3	10
Helium velocity, ft/sec	1	3	10
h_{He-m}, Btu/sec·ft²·°F	3.03×10^{-4}	4.97×10^{-4}	8.54×10^{-4}
C_m, ft		0.899	
W_{He}, lb/sec	1.03×10^{-4}	3.09×10^{-4}	10.30×10^{-4}
k_m, Btu/sec·ft² (°F/ft)		0.00333	
a_m, ft²		0.00487	
b		2.29×10^{-4}	
d		-0.0237	
q', Btu/sec·ft³		45.5	(sections 1, 3, 5, and 7)
		0	(sections 2, 4, and 6)
$\dfrac{h_{He-m}C_m}{W_{He}c_{p_{He}}}$	2.13	1.17	0.601
$\dfrac{h_{He-m}C_m + b}{k_m a_m}$	30.9	41.6	61.5
$\dfrac{h_{He-m}C_m \, b}{k_m a_m W_{He}c_{p_{He}}}$	30.1	16.5	8.48
$\dfrac{h_{He-m}C_m}{k_m W_{He}c_{p_{He}}} \left(\dfrac{d}{a_m} - q' \right)$			
For sections 1, 3, 5, and 7	$-32,300$	$-17,600$	-9090
For sections 2, 4, and 6	-3120	-1700	-879

The helium heat transfer coefficient, h_{He-m}, may be evaluated from the following formula:[14]

$$(37) \quad h_{He-m} = 1.02 \frac{k_{He}}{D_{He}} Re_{He}^{0.45} Pr_{He}^{0.5} \left(\frac{\mu}{\mu_s} \right)_{He}^{0.14} \left(\frac{D_{He}}{L_{He}} \right)^{0.4} \left(\frac{D_o}{D_i} \right)^{0.8} Gr_{He}^{0.05} \ ,$$

where

D = equivalent diameter, ft,

D_o = outside diameter of helium annulus, ft,

D_i = inside diameter of helium annulus, ft,

Re = Reynolds' number,

Pr = Prandtl's number,

$\dfrac{\mu}{\mu_s}$ = ratio of viscosity at bulk temperature to viscosity at surface temperature,

L = length of passage, ft,

Gr = Grashof's number.

Having evaluated the constants in Eq. 36, the solution of the equation is straightforward. Once an expression for θ_{He} is found, θ_m can be evaluated from Eq. 34. The solutions for helium velocities of 1, 3, and 10 ft/sec follow:

1. For a helium velocity of 1 ft/sec,

$$(38) \quad \theta_{He} = n_1\, e^{5.10x} + n_2\, e^{-6.29x}$$
$$+ n_3\, e^{-0.941x} + K$$

and

$$(39) \quad \theta_m = 3.39\, n_1\, e^{5.10x} - 1.95\, n_2\, e^{-6.29x}$$
$$+ 0.559\, e^{-0.941x} + K \; ,$$

where

n = arbitrary constant,

K = 1070 for sections 1, 3, 5, and 7
= 104 for sections 2, 4, and 6.

2. For a helium velocity of 3 ft/sec,

$$(40) \quad \theta_{He} = n_4\, e^{6.10x} + n_5\, e^{-6.87x}$$
$$+ n_6\, e^{-0.392x} + K$$

and

$$(41) \quad \theta_m = 6.23\, n_4\, e^{6.10x} - 4.90\, n_5\, e^{-6.87x}$$
$$+ 0.664\, n_6\, e^{-0.392x} + K \; .$$

3. For a helium velocity of 10 ft/sec,

$$(42) \quad \theta_{He} = n_7\, e^{7.62x} + n_8\, e^{-8.08x}$$
$$+ n_9\, e^{-0.137x} + K$$

and

$$(43) \quad \theta_m = 13.7\, n_7\, e^{7.62x} - 12.4\, n_8\, e^{-8.08x}$$
$$+ 0.772\, n_9\, e^{-0.137x} + K \; .$$

There are nine arbitrary constants in Eqs. 38 through 43. These constants have a different value in each of the seven sections; there are therefore, altogether, 63 arbitrary constants. These may be evaluated by means of the following boundary conditions, which apply to all three helium velocities:

$$(44) \quad \lim_{x_1 \to -\infty} \theta_{He}$$

is bounded. Since each section has a different origin (see definition of x, following Eq. 27), the subscript on x refers to the number of the section being considered. Thus

$$(45) \quad \theta_{He}\Big|_{x_1 = 0} = \theta_{He}\Big|_{x_2 = 0} \; ,$$

$$(46) \quad \theta_m\Big|_{x_1 = 0} = \theta_m\Big|_{x_2 = 0} \; ,$$

$$(47) \quad \frac{d\theta_m}{dx}\Big|_{x_1 = 0} = \frac{d\theta_m}{dx}\Big|_{x_2 = 0} \; ,$$

$$(48) \quad \theta_{He}\Big|_{x_r = 2/3} = \theta_{He}\Big|_{x_{r+1} = 0} \; ,$$
$$r = 2, 3, 4, 5, 6 \; ,$$

$$(49) \quad \theta_m\Big|_{x_r = 2/3} = \theta_{He}\Big|_{x_{r+1} = 0} \; ,$$
$$r = 2, 3, 4, 5, 6 \; ,$$

$$(50) \quad \frac{d\theta_m}{dx}\Big|_{x_r = 2/3} = \frac{d\theta_m}{dx}\Big|_{x_{r+1} = 0} \; ,$$
$$r = 2, 3, 4, 5, 6 \; ,$$

$$(51) \quad \lim_{x_7 \to \infty} \theta_{He}$$

is bounded.

Equations 44 through 51 were used to evaluate the nine arbitrary constants, n_1 to n_9, for each of the seven sections. The results of the evaluation are given in Table 18.

The values of the arbitrary constants and Eqs. 38 through 43 were used to calculate the temperatures of the helium and the metallic envelope for all positions along the pipe line for the three helium velocities. The results are shown in Figs. 75, 76, and 77. The minimum helium temperature
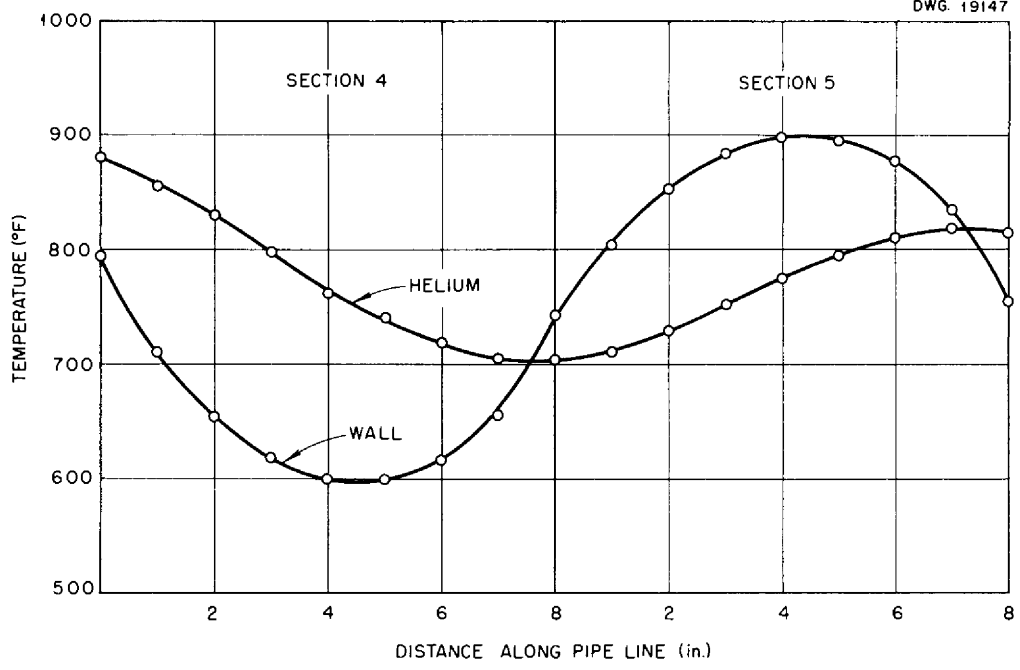
Fig. 75. Temperature Patterns of Helium and Wall of Monitoring Annulus.
Helium velocity of 1 ft/sec.
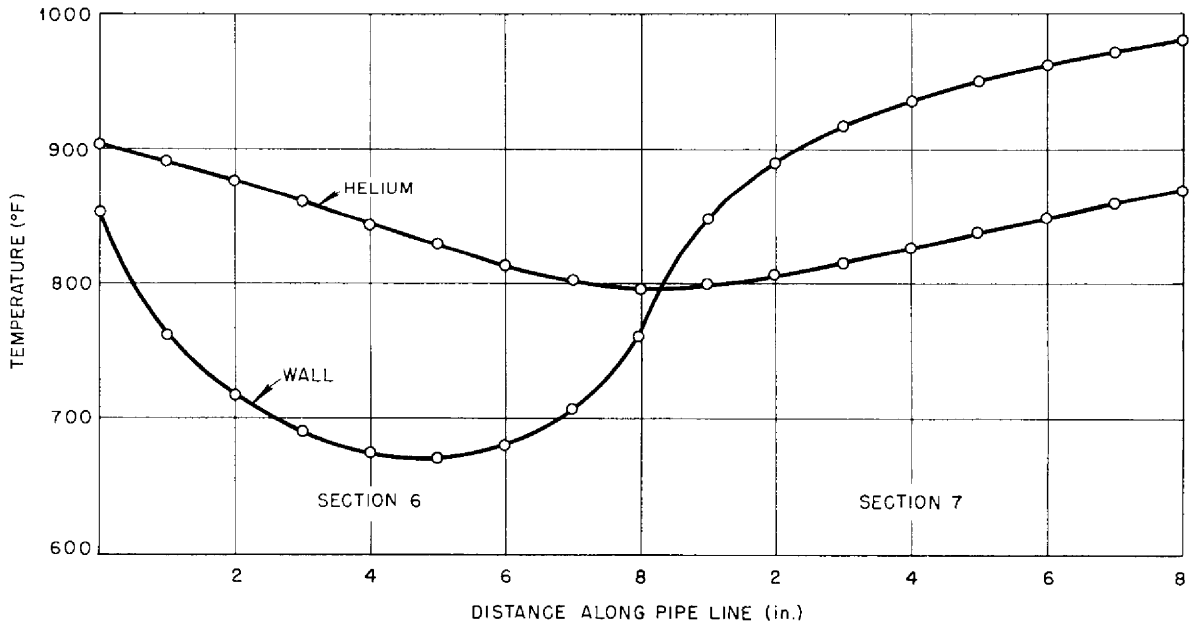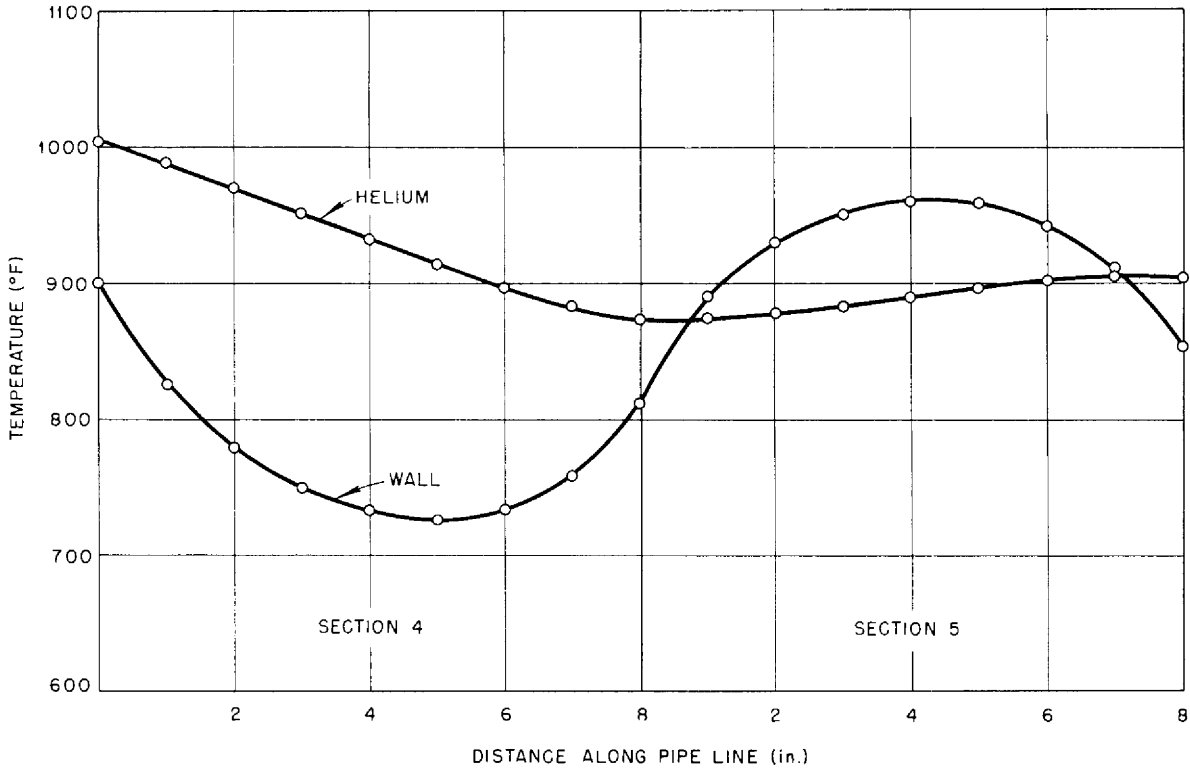
Fig. 76. Temperature Patterns of Helium and Wall of Monitoring Annulus. Helium velocity of 3 ft/sec.
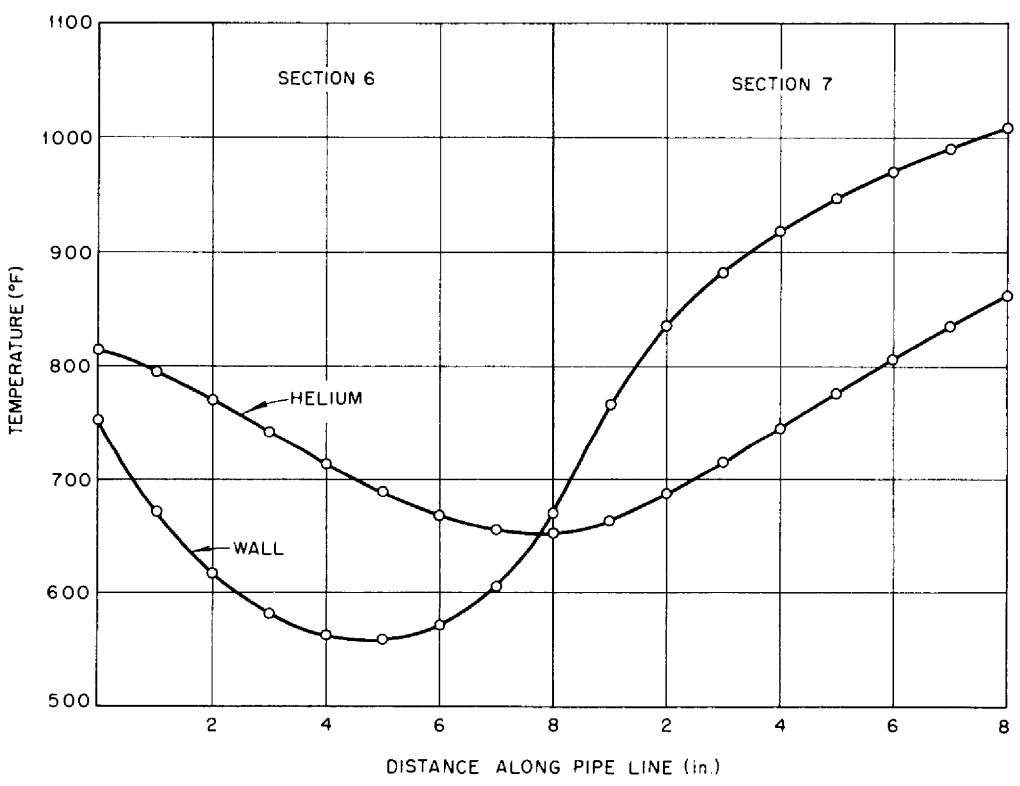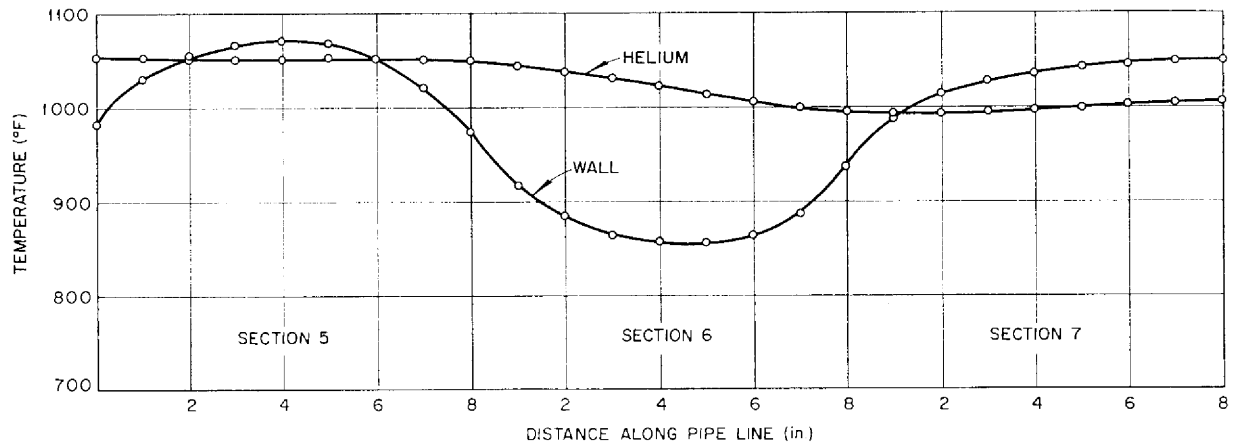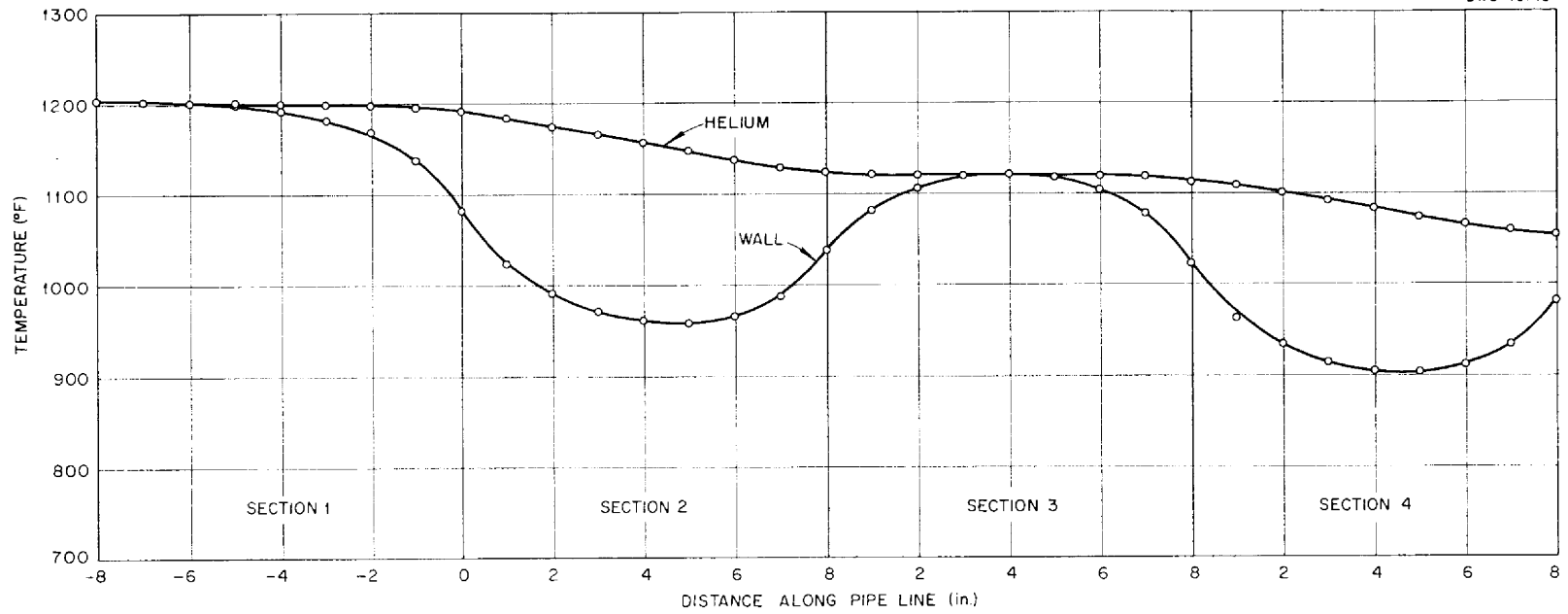
Fig. 77. Temperature Patterns of Helium and Wall of Monitoring Annulus. Helium velocity of 10 ft/sec.

TABLE 18. VALUES OF THE ARBITRARY CONSTANTS

	SECTION NUMBER						
	1	2	3	4	5	6	7
n_1	−80.6	2.69	−2.72	2.88	−2.70	2.38	0
n_2	0	−76.1	75.5	−76.6	75.6	−75.7	89.5
n_3	0	960	−447	722	−575	654	−637
n_4	−30.5	0.476	−0.459	0.467	−0.461	0.473	0
n_5	0	−27.6	27.7	−27.5	28.0	−27.6	27.9
n_6	0	965	−222	796	−354	695	−431
n_7	−8.64	0.0554	−0.0537	0.0546	−0.0538	0.0548	0
n_8	0	−8.20	8.19	−7.95	8.05	−7.96	8.04
n_9	0	968	−84.2	891	−155	826	−213

and the minimum metallic envelope temperature have been plotted against helium velocity in Fig. 78. Since the temperature of the fuel in the pipe line is equal to the helium temperature and since the fuel melts in the vicinity of 950°F, it can be seen from Fig. 78 that the fuel will remain molten, in this particular case, if the helium velocity exceeds about 8 ft/sec.
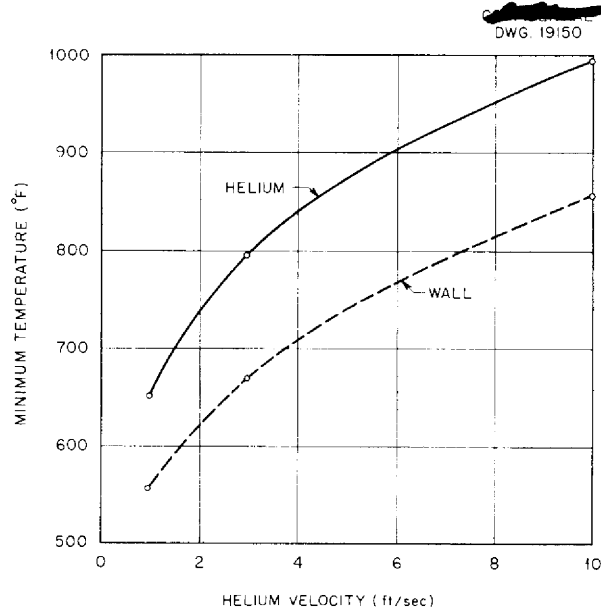
Fig. 78. Minimum Wall and Helium Temperatures vs. Helium Flow in Monitoring Annulus.

Chapter 7
HELIUM SUPPLY AND VENTING SYSTEM

TRUE HOLDUP OF FISSION GASES IN TANKS

The fission gases removed along with helium through the various gas vents in the fuel circuit are held up in the pipes and tanks of the off-gas system (Fig. 79) until the activity in the fission gases is reduced sufficiently to permit their being discharged into the stack. The holdup time of the gases in pipe lines or similar shapes of large length-to-diameter ratio is readily calculated as the pipe volume divided by the gas volume flow rate. All the gas is held up substantially the same amount of time. In large tanks or similar shapes of small length-to-diameter ratio, the average gas holdup time is the same as in a pipe line of similar volume. However, because of the mixing of the gas in the tank, not all the gas is held up for substantially equal periods; that is, some of the gas leaving the holdup tank is held up for much less than average time and some for much more than average. The true activity of the gases leaving the holdup tank (Fig. 80) of the off-gas system has been calculated and compared with the activity which would be present if all gases were held up for equal periods.

The mixing of the gas in the tank is due to convective and diffusive forces and occurs fairly rapidly compared with the average holdup time in the tank. The reasonably conservative assumption was made that the gas entering the tank mixes instantaneously with the gas in the tank. The following definitions were made for the calculations:

N = flow rate of gas, cfm,
V = tank volume, ft^3,
$C(t)$ = concentration of gases of age t, that is, $C(t)\, dt$ equals the ratio of the volume of gas with age from t to $t + dt$ compared with the total tank volume, V (age is used here to

mean time measured from the time the gases enter the off-gas system),

t = time, min.

Then,

$$(1) \quad C(t + dt)\, dt = C(t)\, dt - C(t)\, dt\, \frac{N}{V}\, dt ,$$

$$(2) \quad \frac{C(t + dt) - C(t)}{dt} = - C(t)\, \frac{N}{V} ,$$

$$(3) \quad \frac{dC(t)}{dt} = - C(t)\, \frac{N}{V} ,$$

$$(4) \quad C(t) = K\, e^{-(N/V)t} ,$$

where K is an arbitrary constant.

When $t = t_0$, where t_0 is the age of the youngest gases in the tank,

$$(5) \quad C(t)\, dt = \frac{N}{V}\, dt$$

and

$$(6) \quad C(t_0) = \frac{N}{V} .$$

Substituting Eq. 6 in Eq. 4 and solving for K gives

$$(7) \quad \frac{N}{V} = K\, e^{-(N/V)t_0} ,$$

$$(8) \quad K = \frac{N}{V}\, e^{(N/V)t_0} ,$$

$$(9) \quad C(t) = \frac{N}{V}\, e^{-(N/V)(t - t_0)} .$$

The energy, $E(t)$, in the fission gases xenon and krypton (bromine and iodine removed previously) at time t is plotted against t in Figs. 81, 82, and 83 for the separate xenon and krypton isotopes and for the total of these isotopes. For the determination of $E(t)$, it was considered that there had been 200 hr of reactor operation prior to time zero and that the fission gases had subsequently decayed time t.

MATERIAL AND MATERIAL SPECIFICATIONS

ITEM NO	QTY	NAME	SIZE	MATERIAL
1	2	KINNEY VAC PUMP NO Y26166	1½ hp	
2	2	DRUMS	55 gal	SS
3	1	VAPOR TRAP, NaK	55 gal	SS
4	1	VAPOR TRAP, SUMP	55 gal	SS
5	2	SURGE TANK VAPOR TRAP	55 gal	SS
6	13	FLEXIBLE HOSE	½ in. x 3 ft-0 in. LG.	SS
7	6	RESEARCH CONT CO VALVE	¼ in IPS	SS
8	AS REQ	MANIFOLD, VAC	2 in. IPS SCH 40	WS
9	AS REQ	AIRLINE FROM 10 cfm BLOWER	2 in. IPS SCH 40	WS
10	6	SWING CHECK VALVES	2 in IPS	SS
11	6	VALVE		
12	1	OIL CATCH BASIN	6 in IPS x 24 in	SS
13	10	CHECK VALVE		SS
14	5	SOLENOID VALVES	1 in. IPS-SCREW	BRASS
15	AS REQ	VAC PUMP LINES	1 in IPS SCH 40	
16	1	FULFLO FILTER		
17	2	RADIATION MONITORS AND SHIELD		
24	3	PACKLESS VALVE	¼ in BAR STOCK	SS
27	AS REQ	VAC LINE	½ in IPS SCH 40	WS
33	2	MASON NEILAN VALVE	¼ in. (TYPE 108)	SS
34	6	SOLENOID VALVES	½ in IPS	SS
35	1	DUMP TANK VAPOR TRAP		
36	2	SWING CHECK VALVE	1¼ in IPS	SS
37	1	MONITORING SYSTEM HEATERS		
38	1	RELIEF VALVE	¾ in. IPS	BRASS

BULKHEAD

TEST PIT

FUEL SURGE TANK NO 1

FUEL SURGE TANK NO 2

FUEL ENRICHING SYSTEM TANKS

TANK NO 4   TANK NO 5   TANK NO 6

DUMP TANK

FILL AND FLUSH TANKS
(SAME TYPE VALVES AND HOSE ON EACH TANK)

TANK NO 3

TANK NO 2   TANK NO 1

SLEEVE NO 1

10 cfm BLOWER

STACK
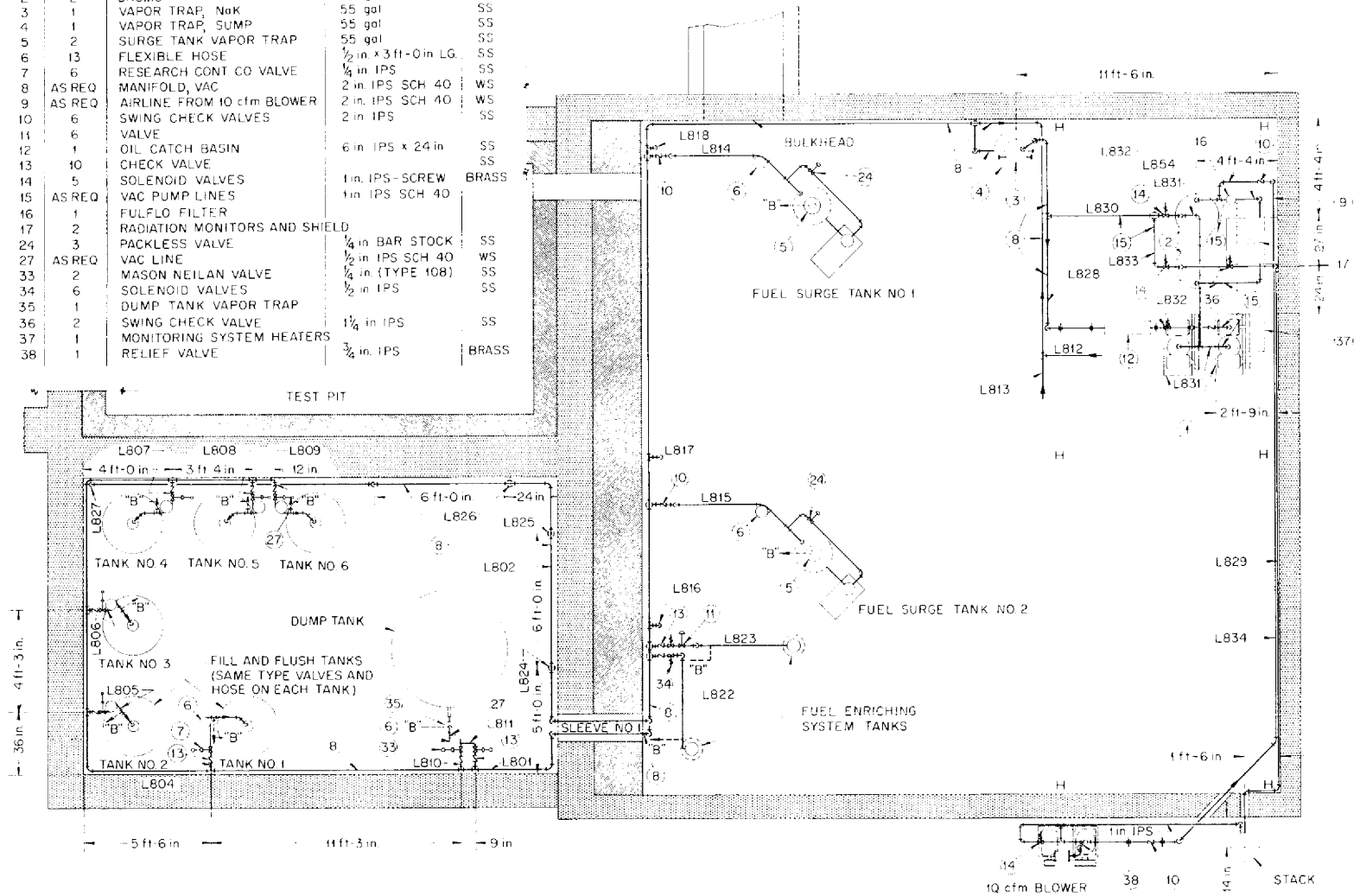
Fig. 79.   Off-Gas Disposal System.
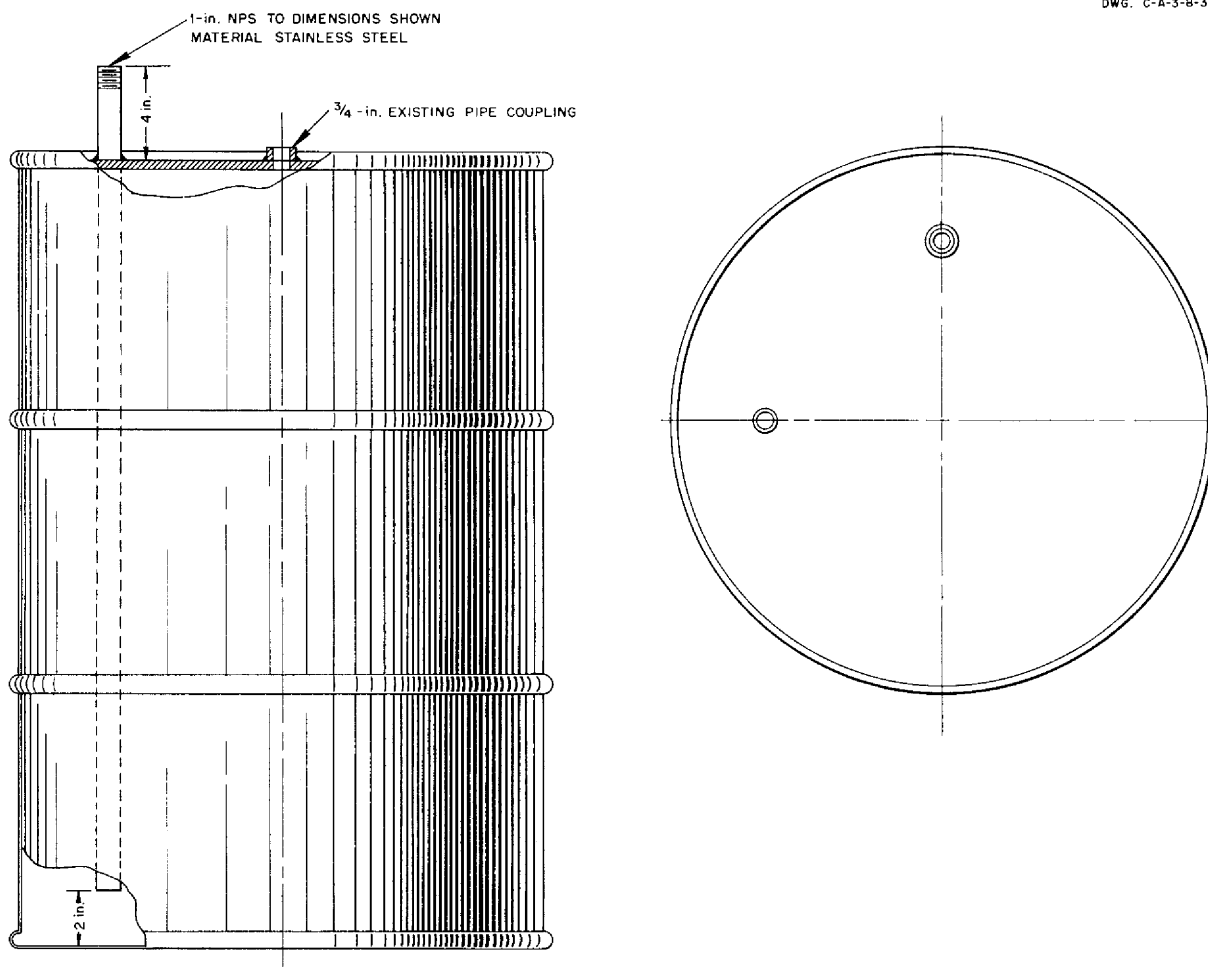
Fig. 80. Off-Gas Disposal System Drum.

If R is the ratio of the true activity of the gases leaving the holdup tank to the activity which would be present if all the gases were held up equally,

$$(10) \quad R = \frac{\displaystyle\int_{t_0}^{t_p} \frac{N}{V} e^{-(N/V)(t-t_0)} E(t)\, dt}{E\left(t_0 + \dfrac{V}{N}\right)},$$

where t_p is the age of the oldest gases in the tank. The total energy in all the fission gases developed may be used since the final answer desired is a ratio.

It is important to note that for Eq. 10 it is assumed that all the gases in the tank contain equal amounts of fission gases. This is obviously not true of the gas originally in the tank. Thus, at the beginning of operation, the value of R is actually less than is predicted by Eq. 10. The highest possible values of R will occur after long periods of operation, and Eq. 10 will therefore be evaluated with t_p sufficiently large for the contribution to the total activity of the gases of age greater than t_p to be neglected.

The curve of $E(t)$ vs. t shown in Fig. 83 for the total energy of all xenon and krypton isotopes was broken up into a series of M segments between t_0 and t_p, and an equation of exponential form was fitted to each segment.

105
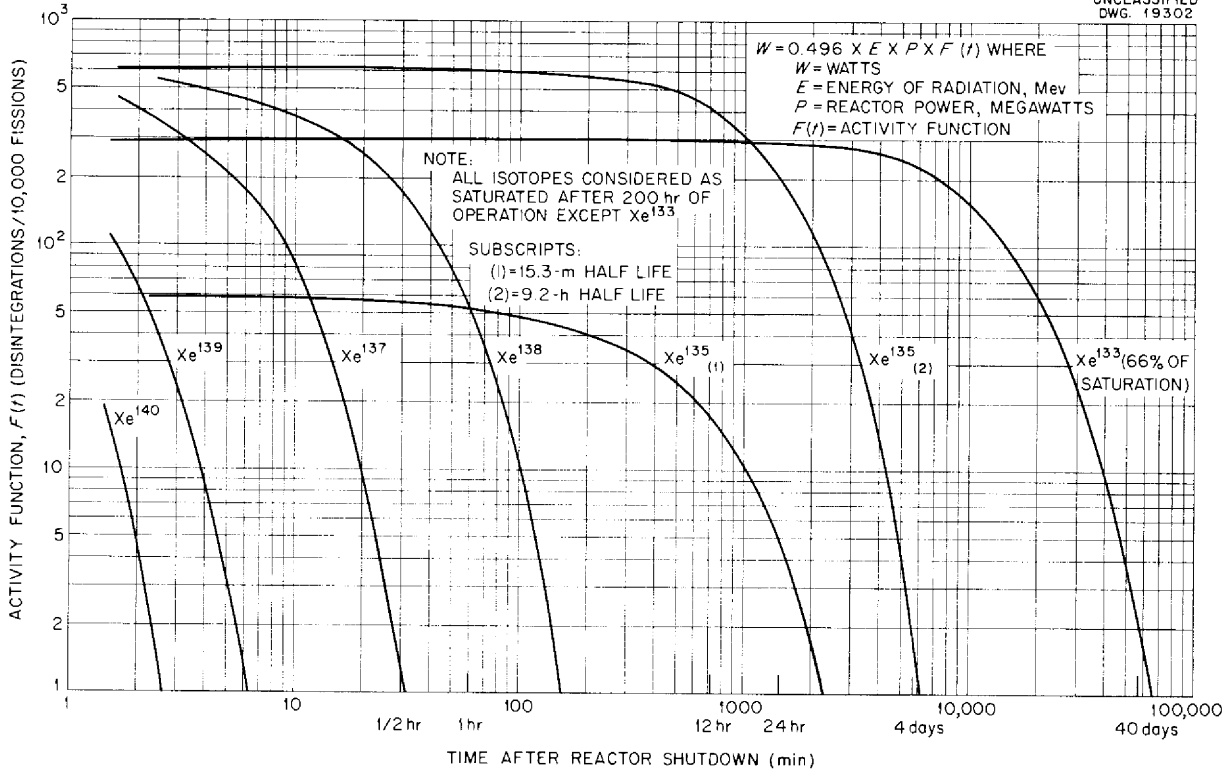
Fig. 81. Integrated Xenon Activity, $F(t)$, vs. Time after Reactor Shutdown.

Thus, for the nth segment,

$$(11) \qquad E_n(t) = A_n \, e^{-b_n t}, \qquad t_{n-1} \leqslant t < t_n,$$

and then

$$(12) \qquad R = \frac{\displaystyle\sum_{n=1}^{M} \int_{t_{n-1}}^{t_n} \frac{N}{V} \, e^{-(N/V)(t-t_0)} \, A_n \, e^{-b_n t} \, dt}{E\left(t_0 + \dfrac{V}{N}\right)},$$

where $t_M = t_p$,

$$(13) \qquad R = \frac{1}{E\left(t_0 + \dfrac{V}{N}\right)} \sum_{n=1}^{M} A_n \frac{N}{V} \int_{t_{n-1}}^{t_n} e^{-\left[(N/V)+b_n\right]t + (N/V)t_0} \, dt,$$

$$(14) \qquad R = \frac{1}{E\left(t_0 + \dfrac{V}{N}\right)} \sum_{n=1}^{M} -\frac{A_n \dfrac{N}{V}}{\dfrac{N}{V} + b_n} \left[e^{-\left[(N/V)+b_n\right]t + (N/V)t_0} \right]_{t_{n-1}}^{t_n},$$

$$R = \frac{\dfrac{N}{V} e^{(N/V)t_0}}{E\left(t_0 + \dfrac{V}{N}\right)} \sum_{n=1}^{M} -\frac{A_n}{\dfrac{N}{V} + b_n} \left[e^{-\left[(N/V)+b_n\right]t_n} - e^{-\left[(N/V)+b_n\right]t_{n-1}} \right].$$

106
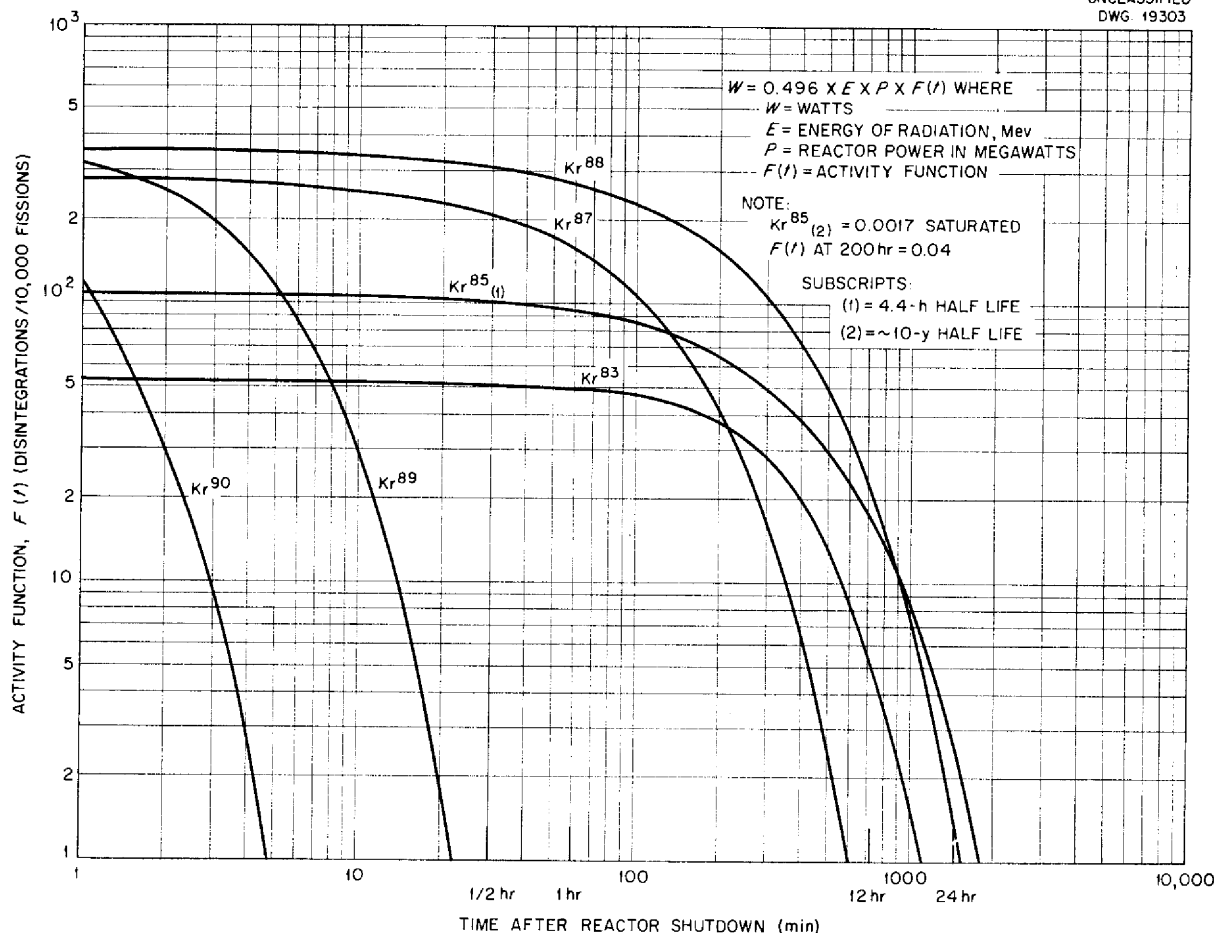
Fig. 82. Integrated Krypton Activity, $F(t)$, vs. Time after Reactor Shutdown.

The data and results of the calculations for the particular problem of the first holdup tank in the off-gas system are given in Table 19.

As a check on whether the intervals selected were small enough, the interval between t_0 and t_1 was divided into two parts. Recalculation of the data for the smaller intervals is given in Table 20.

The value of 295 checks very closely with the value of 296 calculated for the original intervals, and thus the intervals selected were probably small enough.

The final answer, then, is that the actual activity of the gases coming out of the tank is 23% greater than the activity which would be present if all the gases were held up for equal periods.

TEMPERATURES IN THE HELIUM VENT LINES CONTAINING FISSION GASES

The off-gas system carries gases from the surge tanks, the dump tank, and the pits to the exhaust stack (Fig. 79). At times, a portion of these gases will be radioactive fission products. The gas flow rate is generally quite low, and the question arises as to what temperatures will exist on the off-gas system with essentially stagnant radioactive gases in the system. The total energy of all the fission gases produced after 200 hr of reactor operation at 3 megawatts is about 14.8 Btu/sec for a delay time of 1 1/2 minutes.[22] The

Data:

t_0 = holdup time in off-gas system before reaching tanks
= 6 hr = 360 min

N = gas flow
= 1/2 cfh = 1/120 cfm

V = tank volume
= 7.5 ft^3

$\dfrac{V}{N}$ = 900 min

$E\left(t_0 + \dfrac{V}{N}\right)$ = $E(1260)$ = 350

t_n (min)	$E(t)$	A_n	b_n	$\dfrac{N}{V} e^{(N/V)t_0} \left\{ -\dfrac{A_n}{\dfrac{N}{V}+b_n}\left[e^{-\left[(N/V)+b_n\right]t_n} - e^{-\left[(N/V)+b_n\right]t_{n-1}}\right]\right\}$
t_0 = 360	800			
t_1 = 1,000	419	1152	1.011×10^{-3}	296
t_2 = 2,000	233	752	0.587×10^{-3}	106
t_3 = 4,000	113	480	0.362×10^{-3}	25.7
t_4 = 7,000	56	288	0.234×10^{-3}	1.5
t_5 = 12,000	25	173	0.161×10^{-3}	negligible
t_6 = 20,000	10	99	0.115×10^{-3}	negligible
				Σ = 429.2

$$R = \frac{429.2}{350} = 1.23$$

energy is divided among the fission gases as follows:

	Btu/sec
Xenon	2.2
Krypton	2.0
Bromine	1.4
Iodine	9.2

This energy may be distributed over the gas volume in the surge tanks, which is about 1.3 ft^3, or it may come out of the fuel in the dump tank, in which case it will be distributed over a greater gas diluent volume. The maximum energy release in the off-gas system, which occurs in the release of gases from the surge tanks, is therefore about 11.4 Btu/sec·ft^3.

The fission gases on leaving the surge tanks enter a fuel vapor trap (Fig. 84) and then a 2-in. IPS pipe. The trap and the pipe are the critical points in the off-gas system, since they have the greatest volume-to-surface ratio and since the fission gases are youngest at these points. The energy dissipated per square foot of outside surface by radiation and
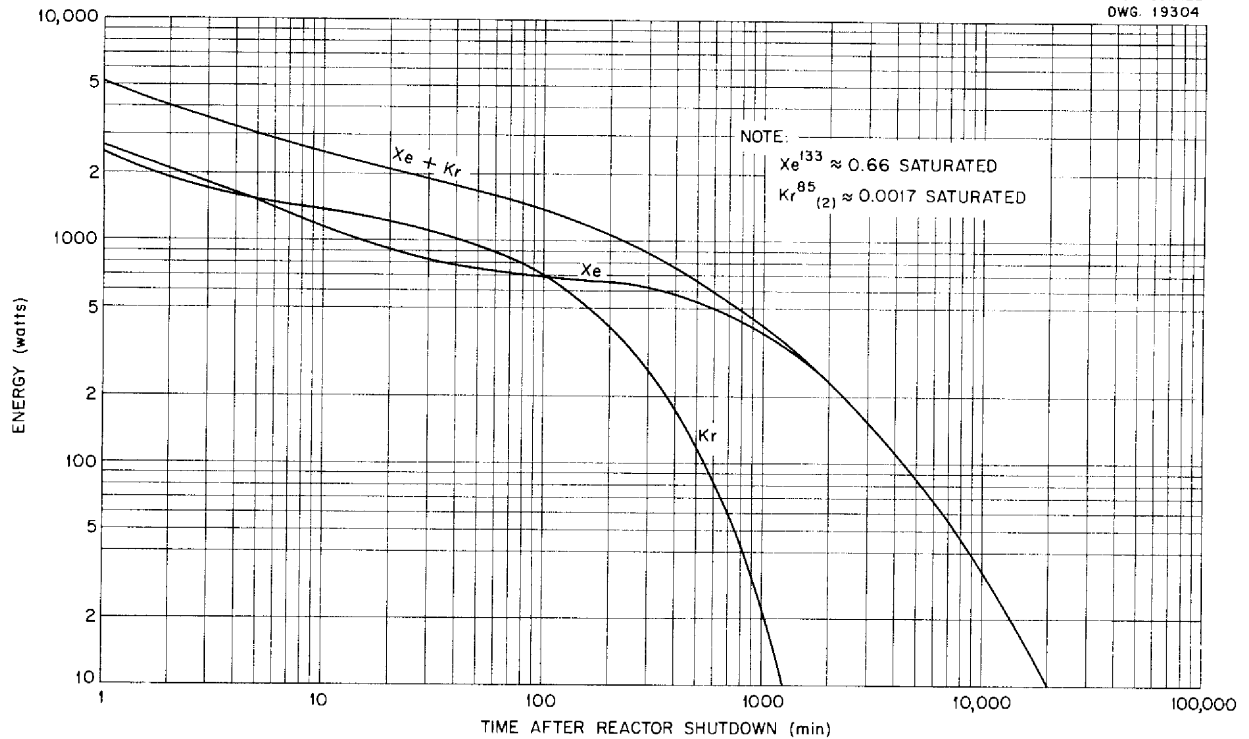
Fig. 83. Energy Emission of Xenon and Krypton after Shutdown from Operation of 200 hr at a Power of 3 Megawatts.

TABLE 20.   RESULTS OF CALCULATION FOR A SMALLER TIME INTERVAL

t_n (min)	$E(t)$	A_n	b_n	$\dfrac{N}{V} e^{(N/V)t_0} \left\{ -\dfrac{A_n}{\dfrac{N}{V} + b_n} \left[e^{-\left[(N/V)+b_n\right]t_n} - e^{-\left[(N/V)+b_n\right]t_{n-1}} \right] \right\}$
$t_0 = 360$	800			
$t_1' = 600$	600	1233	1.20×10^{-3}	159
$t_1 = 1000$	419	1023	0.90×10^{-3}	136
				$\Sigma = 295$

convection may be written in the familiar form

$$(15) \quad Q = \frac{0.173}{3600} \epsilon \left[\left(\frac{T_s}{100}\right)^4 - \left(\frac{T_e}{100}\right)^4 \right] + h_c(T_s - T_e) ,$$

where

Q = heat dissipated, $Btu/sec \cdot ft^2$,
ϵ = emissivity,
T_s = surface temperature, °R,
T_e = environment temperature, °R,
h_c = free convection heat transfer coefficient, $Btu/sec \cdot ft^2 \cdot °F$.

109

He INLET (1/4 - in. SCHEDULE 40 PIPE)

2 ft

2-in. SCHEDULE 40 PIPE CAP

INLET ANNULUS (2-in. SCHEDULE 40 PIPE)

24 in.

FROM SURGE TANK

10 in.

4 in.

VAPOR INLET (1-in. SCHEDULE 40 PIPE)

TO VENT

VENT (1/2 - in. SCHEDULE 40 PIPE)

6-in. SCHEDULE 40 PIPE CAP

1/2 - in. SCHEDULE 40 ELBOW

4-in. SCHEDULE 40 PIPE CAP

MAX. LIQUID LEVEL ON BACK SURGE

MAX. LIQUID LEVEL DURING GAS DISCHARGE

INNER SHELL (4-in. SCHEDULE 40 PIPE)

FILL LEVEL

16 in.

OUTER SHELL (6-in. SCHEDULE 40 PIPE)

V-NOTCHES TO BE APPROX. 1/4 - in. WIDE x 1/4 - in. DEEP

6-in. SCHEDULE 40 PIPE CAP

6.625 in.

ALL MATERIAL TYPE-316 STAINLESS STEEL

Fig. 84. Surge Tank Vapor Trap.

The free convection heat transfer coefficient is determined from the data of Nusselt,[18] McAdams, and W. J. King,[19] who correlated Nusselt's number with Grashof's and Prandtl's numbers (as given by Jakob[14]).

The pertinent physical dimensions and unit energies of the fuel vapor traps and the 2-in. IPS pipe are listed in the following:

	FUEL VAPOR TRAP (per trap)	2-in. IPS PIPE
Gas volume, ft^3	0.13	0.0233 (per ft)
Surface, ft^2	2.6	0.622 (per ft)
Equivalent outside diameter, ft	0.55	0.198
Total energy, Btu/sec	1.48	0.265 (per ft)
Energy per ft^2 of surface, Btu/sec·ft^2	0.246	0.427

For proper operation, the fuel vapor traps must be maintained at 1500°F. The traps are therefore covered with electric heaters and insulated. The heater power is controlled by thermocouples which measure the trap temperature. The heat input required to hold a trap at 1500°F is about 0.71 Btu/sec (cf., chap. 6, section on "Heat Loss Through Insulation"). The energy loss through the insulation would more than be balanced by the energy in the fission gases, and the heaters could be shut off as the fuel vapor trap began to heat up slowly. The heat capacity of the vapor trap, including contained liquid, is about 13.2 Btu/°F. A tabulation of the energy dissipations and of the temperatures of the vapor trap at various times is given in Table 21. The vapor trap temperature would be increased by only about 40°F at the end of 20 min, and the heaters would have to be turned on again as the fission gases further decayed.

The 2-in. IPS pipe is neither heated nor insulated, and therefore Eq. 15 may be used to calculate the pipe outside temperature (the inside temperature is not greatly different). For an emissivity of 0.5, the pipe outside temperature necessary to dissipate 0.265 Btu/sec·lineal ft is about 380°F.

VACUUM PUMP PERFORMANCE

There are two vacuum pumps in the off-gas system (Figs. 79 and 85). They serve many purposes, but their most severe requirement is that they must reduce the pressure in the fuel system sufficiently to permit the boiling off of NaK which cannot be completely drained from this system (NaK is circulated in the fuel system for precleaning and hot testing). Figures 86 and 87 give the experimentally determined performance of the two vacuum pumps. Figure 86 shows the variation of pressure with time in a pump-down test of a 12.3-ft^3 tank; Fig. 87 shows the rate of pressure rise due to leakage after the

TABLE 21. ENERGY DISSIPATIONS AND TEMPERATURES
OF THE VAPOR TRAP AT VARIOUS TIMES

TIME (min)	HEAT IN FISSION GASES (Btu/sec)	HEAT LOSS THROUGH INSULATION (Btu/sec)	HEAT INTO TRAP (Btu/sec)	RATE OF TEMPERATURE RISE IN TRAP (°F/min)	TRAP TEMPERATURE (°F)
1.5*	1.48	0.71	0.77	3.49	1500
10	0.91	0.74	0.17	0.77	1530
20	0.75	0.75	0.0	0	1538

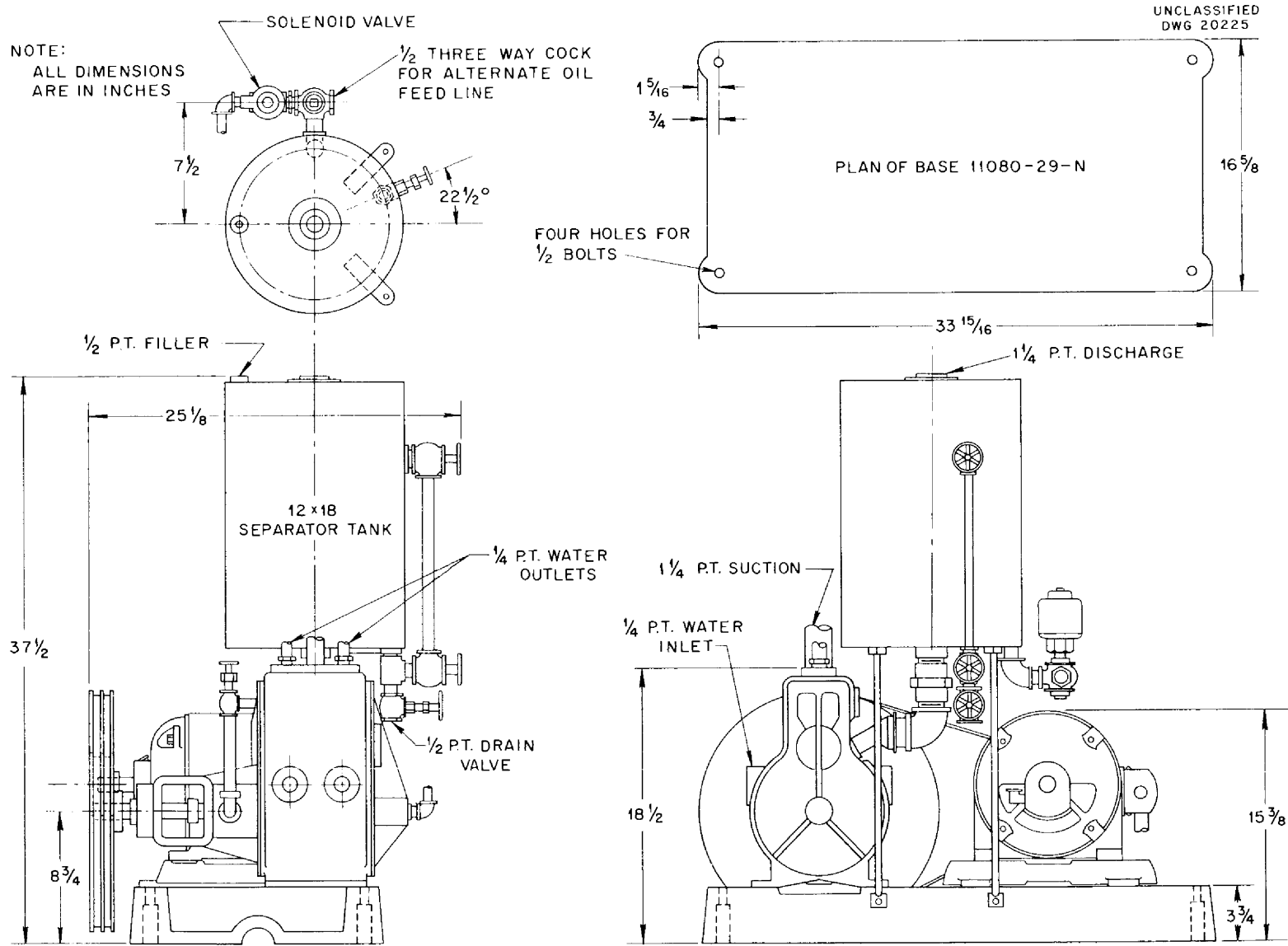*The gas is assumed to enter the trap after a delay of 1.5 minutes.

Fig. 85. Kinney Vacuum Pump.
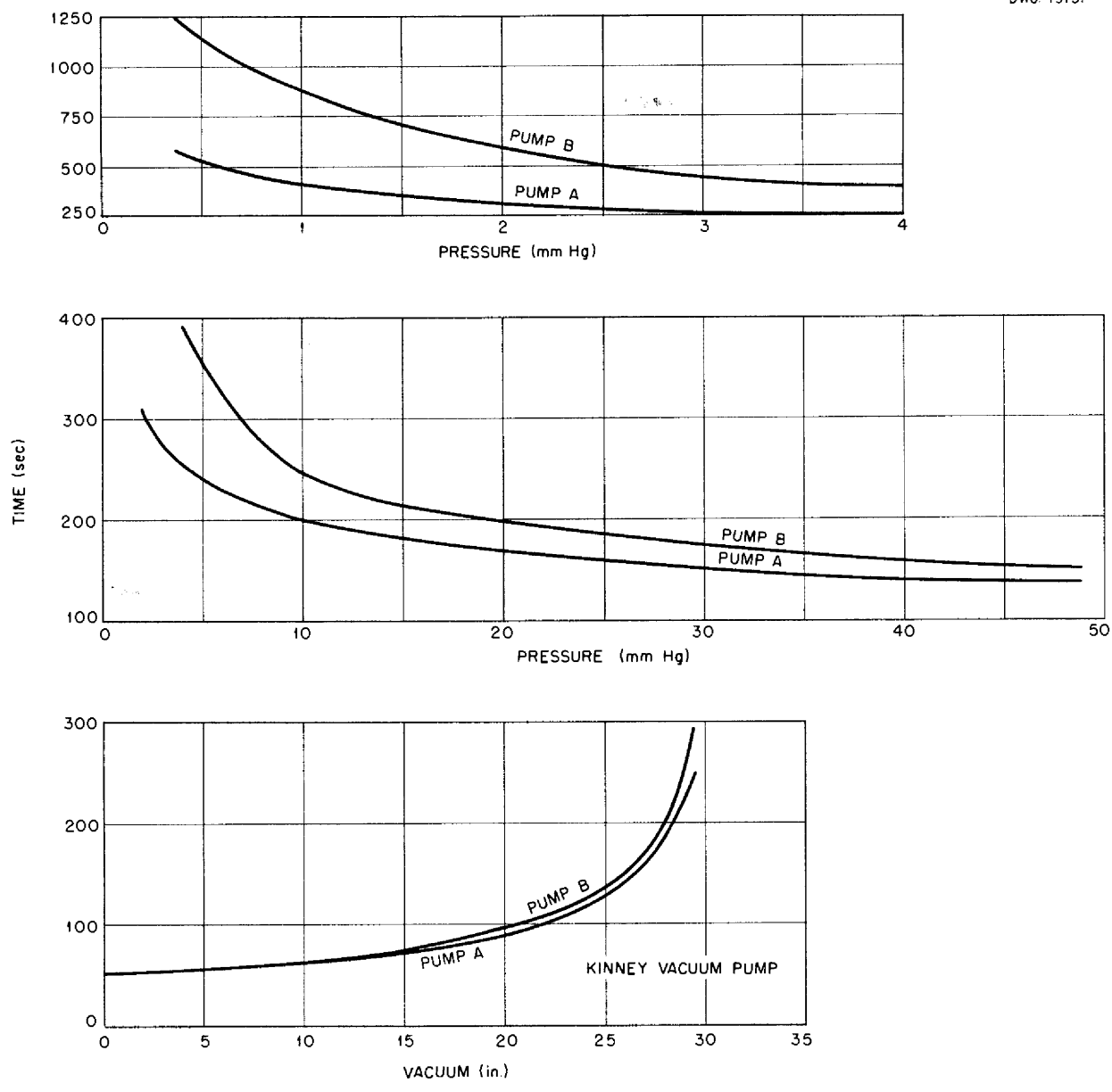
Fig. 86.   Vacuum Pump Performance.

pumps are shut off. From these curves, curves of the variation of rate of change of pressure with pressure were drawn, as shown in Fig. 88.

If a leak develops in the system, it may be desirable to remove all the NaK from the system. In order to boil off NaK at 1200°F, a pressure of about 100 mm Hg or less must be maintained. The following calculations were made to determine the maximum size of leak which might exist and still permit the vacuum pumps to maintain a pressure of 100 mm Hg.

The process of evacuating gas from a tank or containing system is iso-thermal, and therefore

$$(16) \qquad PV = \text{constant} = K$$

or

$$(17) \qquad P = \frac{K}{V},$$

113

where
P = pressure, mm Hg,
V = volume, ft^3,
K = a constant.

Differentiating with respect to time, t, gives

$$(18) \qquad \frac{dP}{dt} = -\frac{K}{V^2}\frac{dV}{dt},$$

and dividing both sides by P gives

$$(19) \qquad \frac{\dfrac{dP}{dt}}{P} = -\frac{K}{PV^2}\frac{dV}{dt}.$$

However, $K = PV$, and therefore

$$(20) \qquad \frac{\dfrac{dP}{dt}}{P} = -\frac{\dfrac{dV}{dt}}{V}.$$

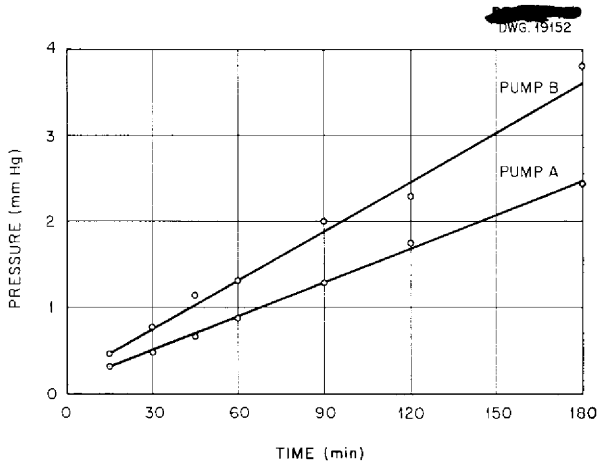Since the volume of the tank tested was 12.3 ft^3, Eq. 20 becomes

Fig. 87. Leakage Test.

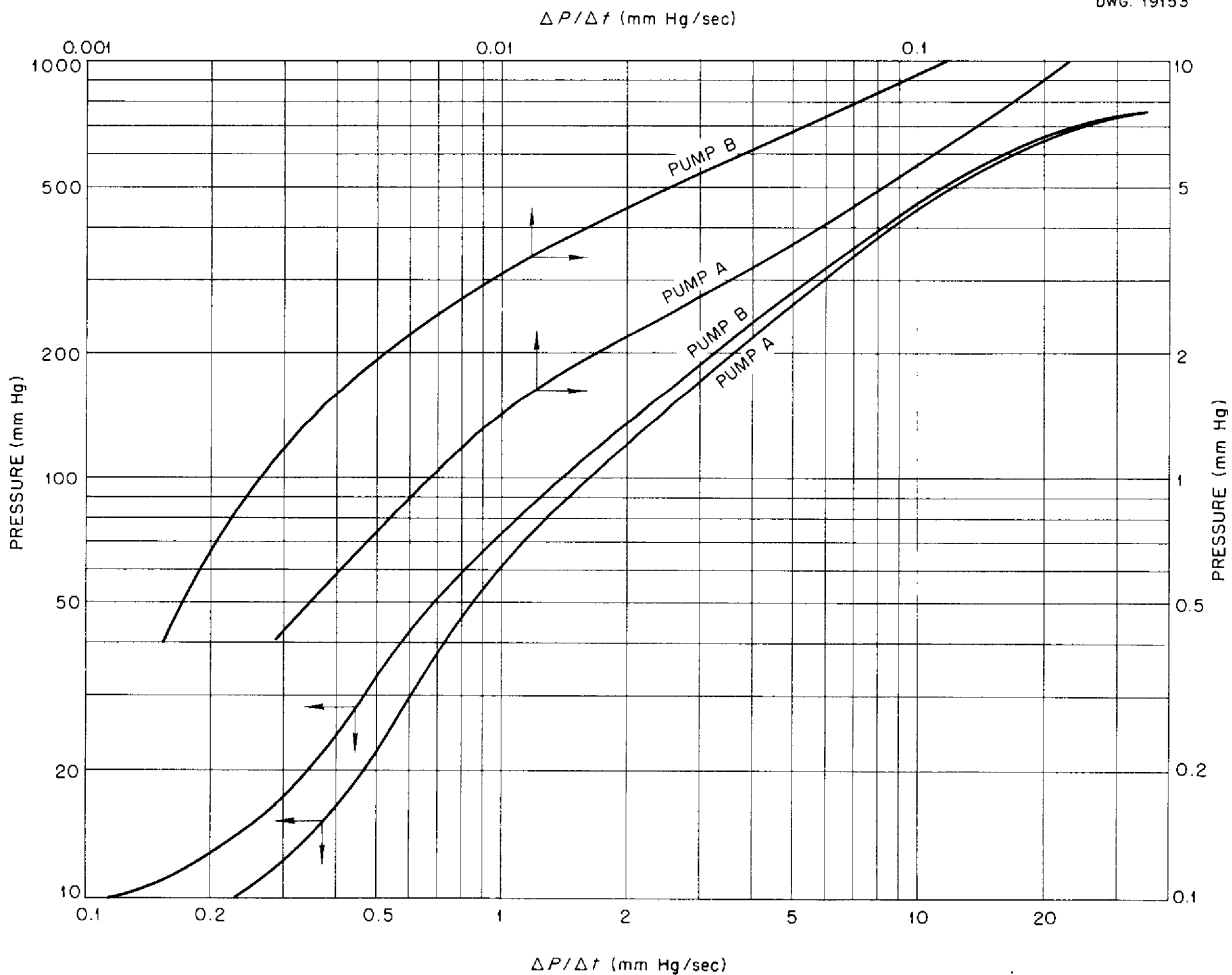Fig. 88. Vacuum Pump Performance. Volume of test system, 12.3 ft^3.

$$(21) \quad \frac{\frac{dP}{dt}}{P} \frac{\frac{dV}{dt}}{12.3} \quad \text{or} \quad \left|\frac{dV}{dt}\right| = \frac{12.3}{P}\left|\frac{dP}{dt}\right| .$$

The values of volumetric flow, dV/dt, as calculated from the pump-down test results, are given in Table 22. The values are for pump inlet conditions; that is, the pressure is equal to the system pressure and the temperature is approximately 560°R, since the gas is cooled before it reaches the vacuum pumps.

The vacuum pumps are of the rotary positive displacement type, and it would therefore be expected that the volumetric flow would decrease slightly with decreasing pressure, since the leakage past the rotor increases. It is apparent from the calculated values of volumetric flow, dV/dt, that the curves of Fig. 88 are probably somewhat inaccurate. The inaccuracy is not entirely unexpected because the information for Fig. 88 was obtained by measuring the slopes of the curves of Fig. 86, and the measurements were not highly accurate. The accuracy is of the order of ±10%, however, which is sufficient for the purpose of the problem.

The values in Table 22 for volumetric flow are for pumping air. The leakage past the rotor when pumping helium may be somewhat higher than when pumping air, but it is probably accurate enough to assume that the volumetric flows are the same for both helium and air.

The volumetric flow of helium through a leak can be approximated by considering a hypothetical "leak" in

the form of a round orifice:

$$(22) \quad \left(\frac{dV}{dt}\right)_{orifice} = CAv ,$$

where

$\left(\dfrac{dV}{dt}\right)_{orifice}$ = orifice volumetric flow, cfs,

C = orifice coefficient = 0.60,

A = orifice area, ft^2,

v = gas velocity in orifice, ft/sec.

The critical pressure ratio for a perfect gas is given by

$$(23) \quad r_c = \left(\frac{2}{\gamma + 1}\right)^{\gamma/(\gamma-1)} ;$$

thus with γ_{He} = ratio of specific heats = 1.67,

$$r_c = 0.487 .$$

The throat pressure for sonic velocity is therefore

$$(24) \quad \rho_{th} = 0.487 \times 760 = 370 \text{ mm Hg}.$$

The throat temperature is

$$(25) \quad T_{th} = T_{amb} (r_c)^{(\gamma-1)/\gamma} ,$$

where

T_{amb} = ambient temperature in the helium monitoring annulus = 1660°R,

T_{th} = throat temperature = 1660 $(0.487)^{(\gamma-1)/\gamma}$ = 1235°R.

For system pressures less than 370 mm Hg, the volumetric flow through the orifice will be constant. The velocity in the throat will always be

TABLE 22.   CALCULATED RESULTS OF THE PUMP-DOWN TEST OF A 12.3-ft^3 TANK

P, SYSTEM (mm Hg)	dP/dt (mm Hg/sec)		dV/dt (cfs)		
	Pump A	Pump B	Pump A	Pump B	Pumps A + B
300	5.95	5.55	0.244	0.277	0.571
150	2.56	2.28	0.210	0.187	0.397
100	1.63	1.41	0.200	0.173	0.373
50	0.86	0.70	0.211	0.172	0.383

sonic velocity, which is given by

$$(26) \qquad v = \sqrt{g\gamma RT} ,$$

where

$g = 32.2 \ \text{ft/sec}^2,$
$\gamma = 1.67,$
$R = \text{gas constant} = 386,$
$T = \text{temperature} = 1235°\text{R},$

and thus

$$v = 5060 \ \text{ft/sec} .$$

Therefore

$$(27) \qquad \left(\frac{dV}{dt}\right)_{\text{orifice}} = 0.60 \ A \times 5060 = 3040 \ A .$$

Chapter 8
DUMP AND FILL SYSTEM

FUEL DUMP TANK COOLING

The heat generated in the fuel after shutdown of the reactor can easily be taken up by the heat capacity of the fuel and the fuel system without overheating. However, once the fuel is in the hot fuel dump tank, it is desirable to keep the temperature of this tank below a reasonable level. Therefore heat is removed by allowing helium to pass through the 91 coolant tubes of the tank (Fig. 89).

It is postulated that the maximum heat removal rate necessary is 50 Btu/sec. The problem of cooling this tank does not lend itself readily to analytical calculation. However, the cooling was analyzed by free-convection calculations and by chimney-effect methods. Both methods are outlined below.

The equation for free convection heat transfer is

$$(1) \qquad Q_c = hA\theta ,$$

where

Q_c = heat removed by convection, Btu/sec,

h = free-convection heat transfer coefficient taken at mean helium temperature, Btu/sec·ft^2·°F,

A = 91 times surface area of inside of a coolant tube, ft^2,

θ = temperature difference between the inside surface of tube and mean helium temperature, °F.

The value of the free-convection heat transfer coefficient for each helium temperature was calculated from the Nusselt's number. The Nusselt's number is given as a function of the product of Grashof's and Prandtl's numbers on p. 525 of ref. 14. It is realized that the length-to-diameter ratio of the coolant tube is too great for use of these correlations; however, they were the only correlations available, and an order of magnitude estimate could be gained by using them.

The inside diameter of each coolant tube is 2.067 in. and the length is 3.1 feet. The temperature of the inside surface was taken to be 1325°F over the entire length of the tube.

Mean temperature values were assumed for the helium in the coolant tube, and from these and Eq. 1, a curve was obtained of heat removed vs. mean helium temperature. The mean temperature corresponding to a heat removal rate of 50 Btu/sec is 1025°F. This corresponds to an outlet temperature of 1920°F, since the inlet temperature was assumed to be 135°F. A lower outlet temperature would mean a greater heat removal rate. Thus, apparently the dump tank will be adequately cooled.

The chimney-effect method makes use of the fact that a buoyant force acts on the air in the coolant tube because of a density difference. This buoyant force is

$$(2) \qquad F = V (\rho_{amb} - \rho_m) ,$$

where

F = buoyant force, lb,

V = volume, ft^3,

ρ_{amb} = density of helium at room temperature, lb/ft^3,

ρ_m = density of helium at mean temperature of helium in tube, lb/ft^3.

From Eq. 2, the pressure acting on the column of helium is

$$(3) \qquad \Delta P = \frac{F}{A},$$

where

ΔP = difference in upward and downward pressures, lb/ft^2,

A = cross-sectional area of coolant tube, ft^2.

The pressure can also be expressed by

$$(4) \qquad \Delta P = 4f \left(\frac{L}{D} \right) \frac{\rho_m v^2}{2g},$$

NOTE:
ALL MATERIAL IS
316 STAINLESS STEEL.

3-in. R, 5 PIPES

$6\frac{7}{8}$-in. R, 12 PIPES

$10\frac{3}{4}$-in. R, 18 PIPES

$14\frac{5}{8}$-in. R, 24 PIPES

$18\frac{1}{2}$-in. R, 30 PIPES

89 COOLING PIPES,
2-in. SCHEDULE NO.
40 x 36-in. LONG

DOUBLE-VEE JOINT WELDED FROM
BOTH SIDES WITH COMPLETE
JOINT PENETRATION

PLAN

3 ft-5 in.

ELBOW, 2-in. SCHEDULE
NO. 40 90° SR ELL

1-in. END PLATE
41-in. DIA

4 in.

3 in.

VENT, 1-in. SCHEDULE NO.
40 x $4\frac{1}{2}$-in. LONG

FILL PIPE, 2-in.
SCHEDULE NO. 40
35-in. LONG

$\frac{1}{2}$-in. TANK WALL PLATE,
128.8 x 34 in.

36 in.

34 in.

45°

1 in.

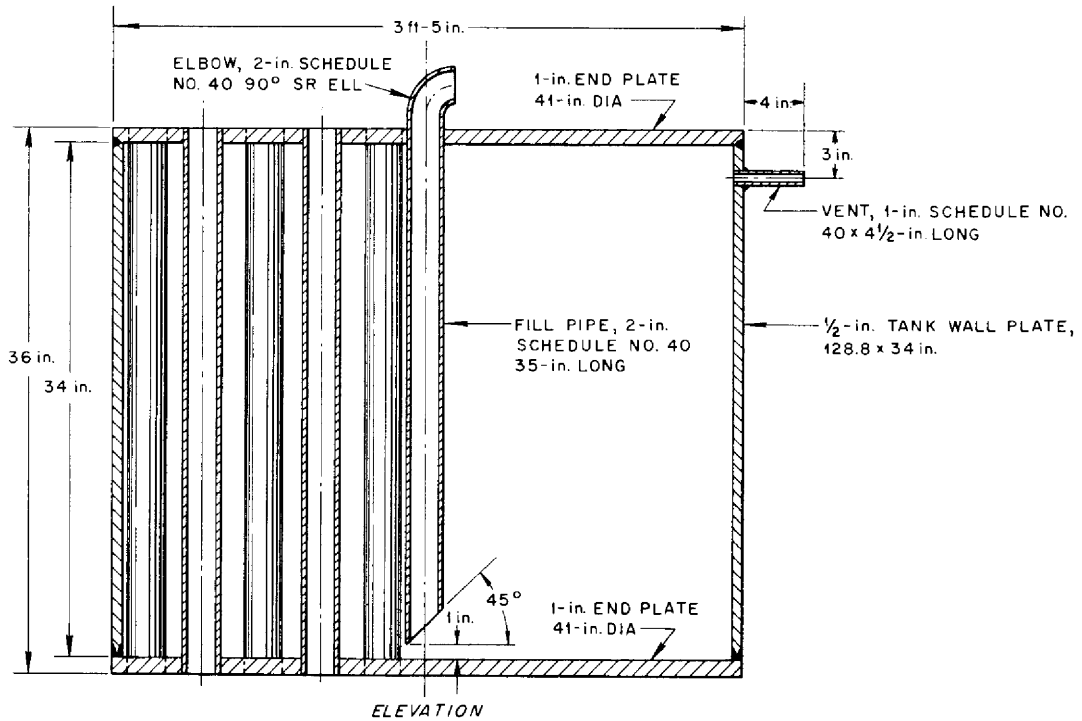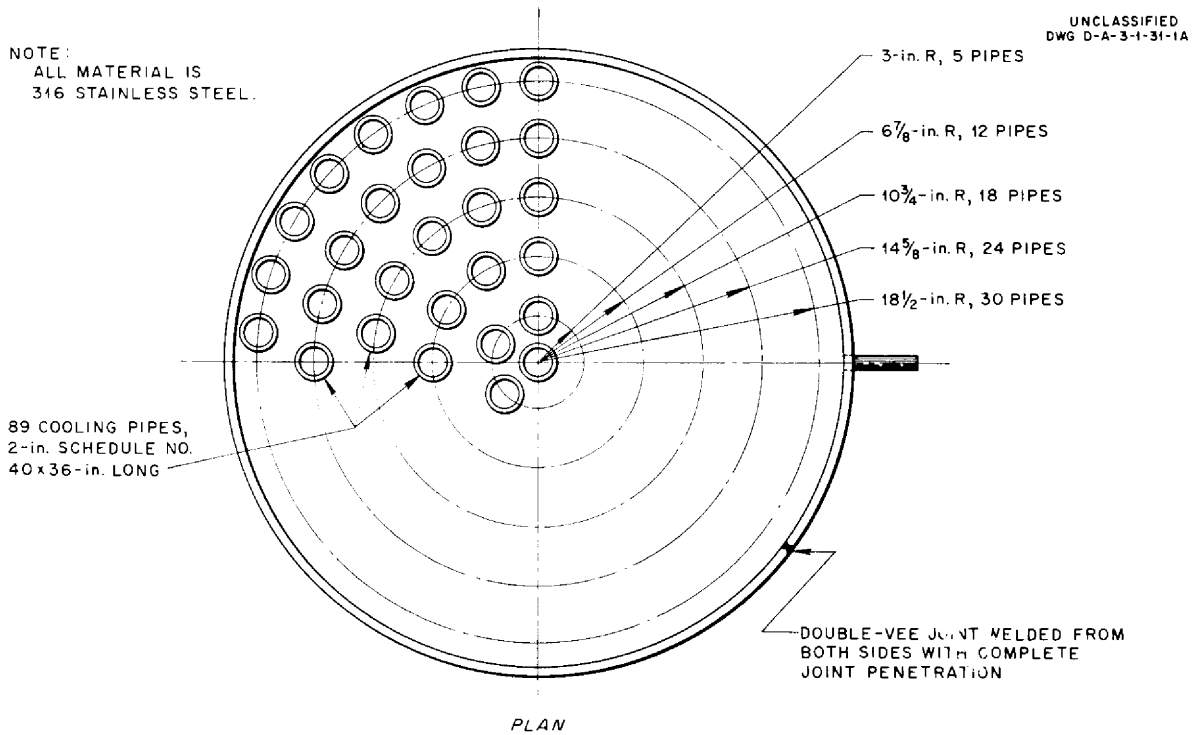1-in. END PLATE
41-in. DIA

ELEVATION

Fig. 89. Fuel Dump Tank.

where

$$f = \frac{16}{N_R}$$

= friction factor for laminar flow, dimensionless,

L = length of coolant tube, ft,

D = equivalent diameter of coolant tube, ft,

v = helium velocity, ft/sec,

g = gravitational acceleration, 32.2 ft/sec^2,

N_R = Reynolds' number, dimensionless,

The velocity of helium through the tube is, from Eq. 4,

$$(5) \qquad v = \left(\frac{2gD}{4fL\rho_m}\right)^{1/2} .$$

The amount of heat removed per tube can be expressed by

$$(6) \qquad Q = wc_p \, \Delta T$$

and

$$(7) \qquad Q = hA_s \theta .$$

In Eqs. 6 and 7,

$$w = vA\rho_m ,$$

and

$$h = 1.86 \, \frac{k}{D}\left(\frac{\mu}{\mu_s}\right)^{0.14}\left(\frac{4wc_p}{\pi k L}\right)^{1/3} ,$$

where

Q = amount of heat removed, Btu/sec,

w = weight flow rate, lb/sec,

c_p = specific heat, Btu/lb·°F,

ΔT = difference between inlet and outlet temperature of helium, °F,

h = heat transfer coefficient, Btu/sec·ft^2·°F,

A_s = surface area of inside of tube, ft^2,

θ = log mean temperature difference,

k = thermal conductivity of helium, Btu/sec·ft^2·°F,

μ = viscosity of helium at mean temperature, lb/sec·ft,

μ_s = viscosity of helium at surface temperature of tube, lb/sec·ft.

Equations 6 and 7 were solved by assuming various helium outlet temper-atures, and the values thus obtained for each equation were plotted against helium outlet temperature. From these curves, the helium outlet temperature was found to be 805°F, the heat removal rate per tube is 0.59 Btu/sec, and the total heat removed is 91 × 0.59 = 53.7 Btu/sec.

HEATING OF FILL TANK WITH CENTRALLY LOCATED DIP TUBE

Upon heating a flush-and-fill tank containing helium, the temperature of the dip tube will lag the temperature of the helium and metal walls of the tank during the heating process (Fig. 90). The temperature of the helium will follow very closely the temperature of the tank walls.

Heat is transmitted to the dip tube by free convection of the helium and by thermal radiation from the wall. The difference in temperature between the dip tube and the wall has been determined at various wall temperatures for certain heating rates.

The net heat input to the tank, excluding loss, is

$$Q = q_T + q_H + q_D ,$$

where

$$q_T = (Wc_p)_T \, \frac{dt}{d\tau} \cong (Wc_p)_T \, \frac{\Delta t}{\Delta \tau} ,$$

and

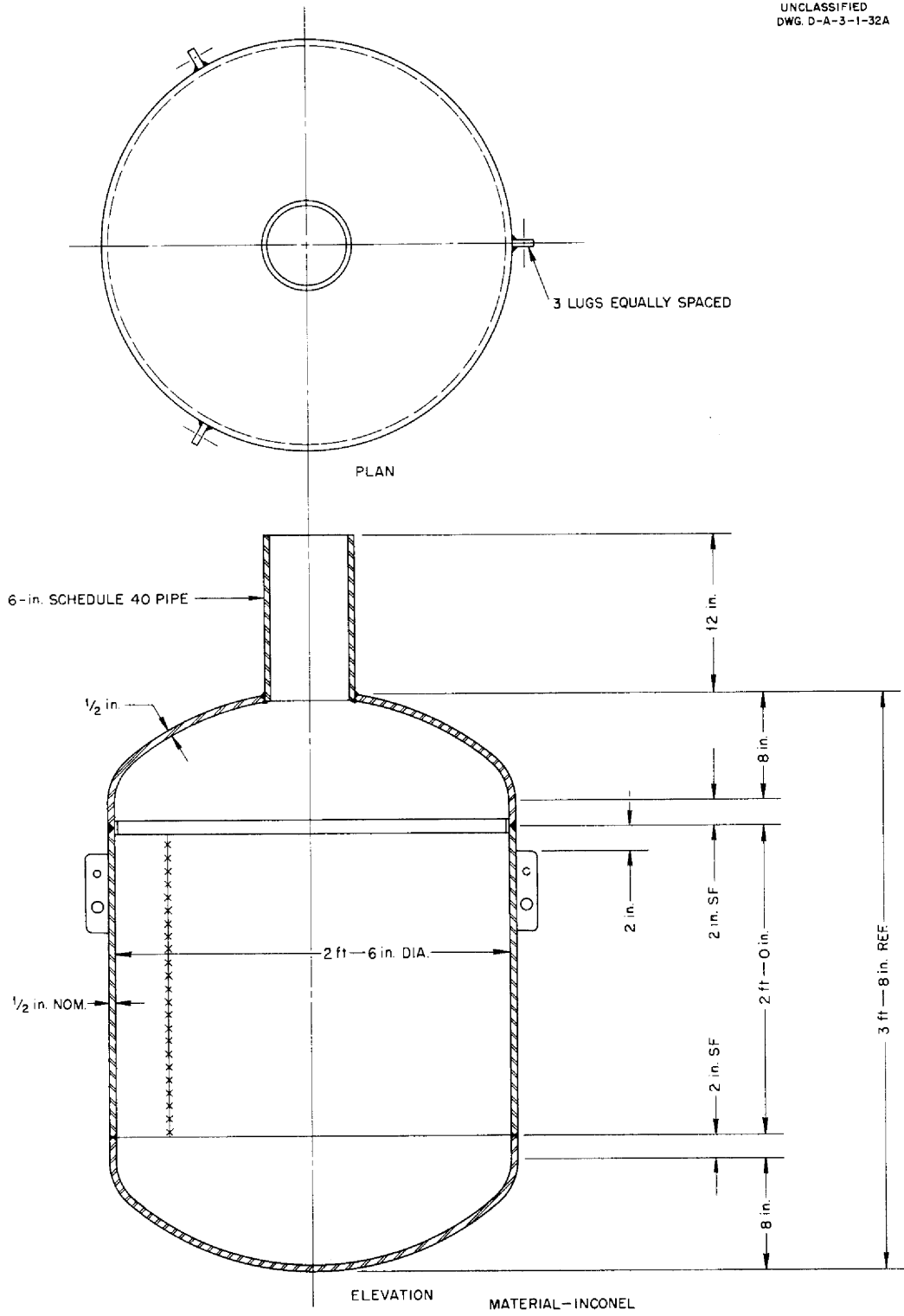$$q_H = (Wc_p)_H \, \frac{dt}{d\tau} \cong (Wc_p)_H \, \frac{\Delta t}{\Delta \tau} .$$

The term $dt/d\tau$ can be replaced by $\Delta t/\Delta \tau$ without much error if $\Delta \tau$ is small.

The value of q_D is given by

$$q_D = hA_D \theta$$
$$+ \frac{0.173}{3600} A_D \epsilon \left[\left(\frac{T_T}{100}\right)^4 - \left(\frac{T_D}{100}\right)^4\right].$$

The emissivity is

$$\epsilon = \frac{1}{\dfrac{1}{\epsilon_D} + \dfrac{D_D}{D_T}\left(\dfrac{1}{\epsilon_T} - 1\right)} .$$

3 LUGS EQUALLY SPACED

PLAN

6-in. SCHEDULE 40 PIPE

12 in.

1/2 in.

8 in.

2 in.

2 in. SF

2 ft—6 in. DIA.

2 in. SF

2 ft—0 in.

3 ft—8 in. REF.

1/2 in. NOM.

8 in.

ELEVATION   MATERIAL—INCONEL

Fig. 90.   Fill Tank.

120

In these equations, the symbols have the following meanings and units:

Q = total net heat input, Btu/sec,
q = heat input of component, Btu/sec,
W = weight of material, lb,
c_p = specific heat of material, Btu/lb·°F,
Δt = temperature change, °F,
$\Delta \tau$ = time interval, sec,
h = free-convection heat transfer coefficient, Btu/sec·ft²·°F,
A_D = outside surface area of dip tube, ft²,
θ = temperature difference between helium and dip tube, °F,
ϵ = radiation emissivity, dimensionless,
T = absolute temperature, °R,
D = diameter, ft,

and the subscripts

T = tank,
H = helium,
D = dip tube.

The free-convection heat transfer coefficient can be calculated from the Nusselt's number. A curve of Nusselt's number vs. the product of Grashof's and Prandtl's numbers is given on p. 525 of ref. 14.

The heat input to the tank wall and the helium is

$$q_T + q_H = Q - q_D \ .$$

Therefore

$$\Delta \tau = \frac{Q - q_D}{(Wc_p)_H \ \Delta t + (Wc_p)_T \ \Delta t} \ ;$$

the change in temperature of the dip tube is

$$\Delta t_D = \frac{q_D \Delta \tau}{(Wc_p)_D} \ ;$$

and the temperature at any time is

(19) $$t_D = t_1 + \Delta t_D \ ,$$

where t_1 is the temperature at the beginning of the time interval (°F).

The emissivity of the tank wall was taken to be the same as that of the dip tube. The value used in making the calculation was

$$\epsilon_T = \epsilon_D = 0.50 \ .$$

The dip tube was taken to be a 2-in., schedule 40 pipe that extended to the bottom of the tank.

In calculating the temperature differences between the wall and the dip tube, net input heat rates of 50, 12, and 8 Btu/sec were used. The results of these calculations are shown in Fig. 91.
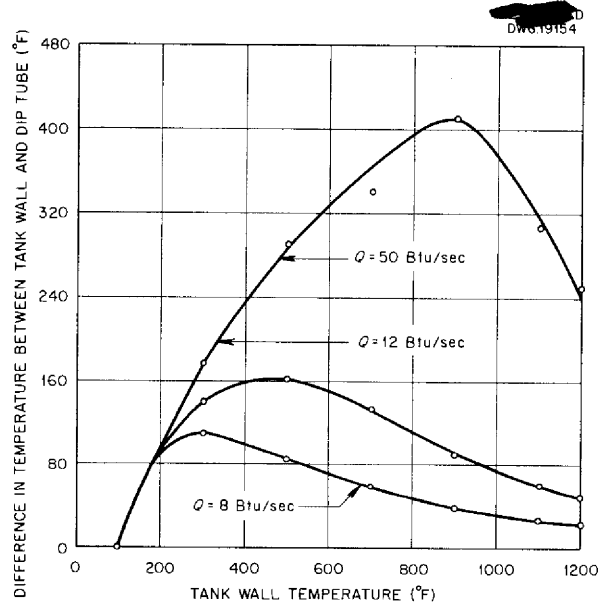

Fig. 91. Results of Fill Tank Preheat Calculations.

121

Chapter 9
OTHER INVESTIGATIONS

AFTERHEAT IN FISSION PRODUCTS

In order to analyze many of the problems which arise in the ARE, it is necessary to know the decay energy of the fission products at various times after reactor shutdown. Reference 23 gives the average disintegration energy of the fission products as a function of time after fission. This curve (ref. 23, Fig. 6a), reproduced as Fig. 92 of this report, cannot be used directly, however, because the fissions in the reactor occur over a considerable period of time and the fission products, consequently, have a wide range of ages. The decay energy of the fission products

may be expressed as

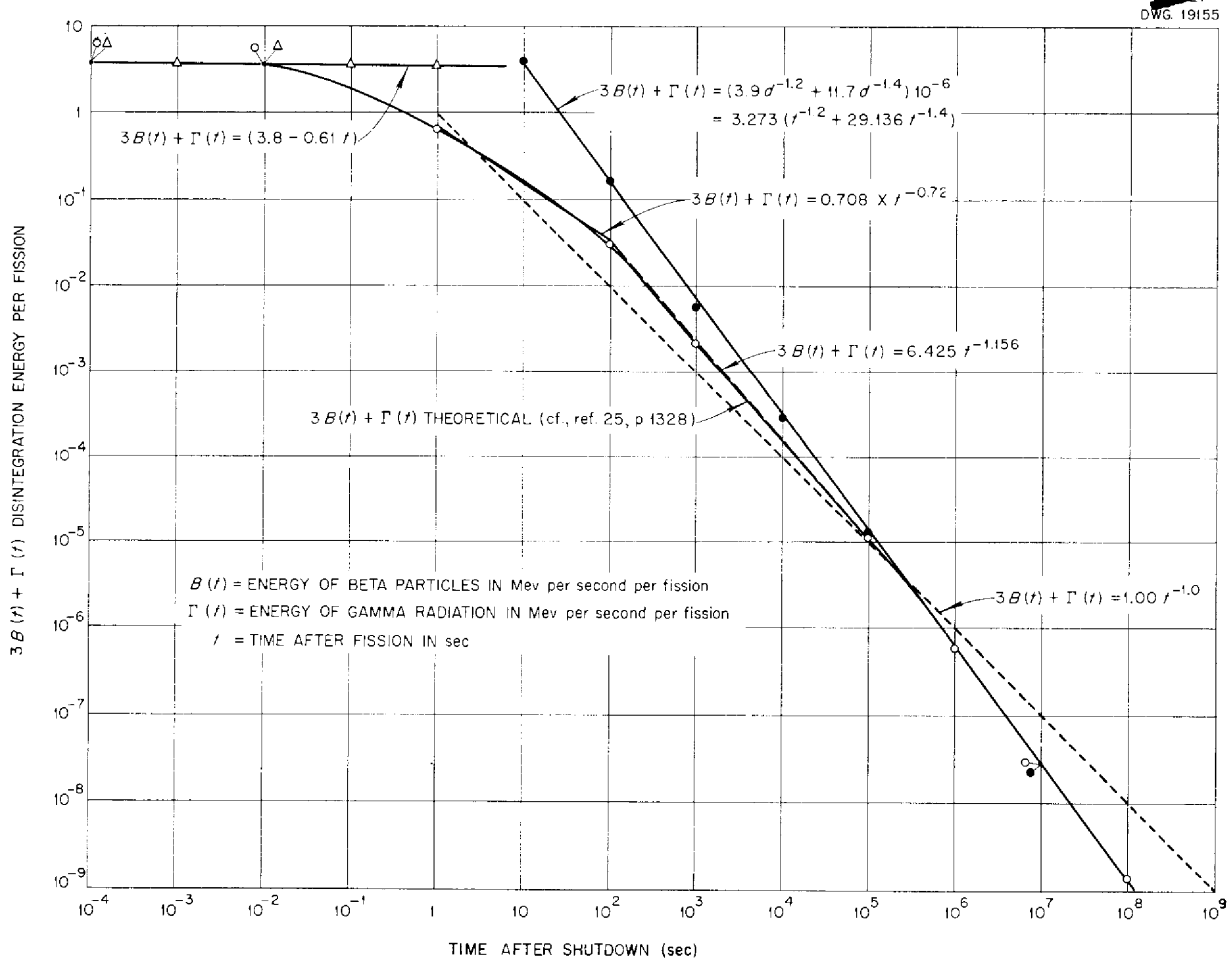$$(1) \qquad Q = K \int_{t_1}^{t_2} q(t) \, P \, dt \ ,$$

where

Q = energy in the fission products, Btu/sec,

$q(t)$ = the average disintegration energy of the fission products as a function of time after fission (Fig. 92), Mev/sec·fission,

P = fission rate in the reactor, fission/sec,

K = a constant for converting Mev/sec to Btu/sec = 1.517×10^{-16},

Fig. 92. Disintegration Energy per Fission vs. Time after Shutdown.

t = age of fission product group under consideration, sec,

t_1 = age of youngest fission products (also equals time since reactor shutdown), sec,

t_2 = age of oldest fission products (also equals time since reactor startup), sec.

For these calculations, it was considered that the power had been constant and equal to 2850 kw, which equals 2700 Btu/sec or 1.78×10^{19} Mev/sec. If it is assumed that there is 190 Mev of energy released per fission, then the fission rate, P, is 9.37×10^{16} fission/sec. Substitution of these values for P and K in Eq. 1 gives

$$(2) \qquad Q = 14.22 \int_{t_1}^{t_2} q(t)\, dt \ .$$

In order to integrate Eq. 2, it is necessary to find a function to fit the curve of $q(t)$ as given in Fig. 92. This was done by dividing the curve into three parts and fitting each of these parts with a different power function. The resulting equations are

$$(3) \qquad q(t) = 0.708\ t^{-0.72} \ ,$$

$$(4) \qquad q(t) = 6.43\ t^{-1.16} \ ,$$

$$(5) \qquad q(t) = 3.27\ t^{-1.2} + 95.4\ t^{-1.4} \ ,$$

(Eq. 5 is the equation recommended in ref. 23 for old fission products).

Equations 3, 4, and 5, were used for integrating Eq. 2 for various values of time after reactor shutdown (t_1) and for 100 hr of reactor operation ($t_2 = t_1 + 3.60 \times 10^5$). The results are tabulated in the following:

TIME AFTER REACTOR SHUTDOWN (sec)	DECAY ENERGY OF THE FISSION PRODUCTS (Btu/sec)
10^2	207
10^3	119
10^4	58.8
10^5	17.7
3.16×10^5	4.1
10^6	1.4
10^7	0.1

These values of decay energy include the energy carried by neutrinos. The energy of the neutrinos is essentially unabsorbable and, consequently, the actual absorbable decay energy of the fission products is less than that tabulated above. A rough estimate of the absorbable energy can be obtained by taking one half the total energy,[23] with the results shown in Fig. 93, where the absorbable decay energy in the fission products is plotted as a function of the time after reactor shutdown for the conditions of this case (2850 kw, 100 hr, 190 Mev/fission).

TEMPERATURE DIFFERENCE BETWEEN THERMOCOUPLE ON PIPE WALL AND BULK FLUID

The bulk temperatures of the fluids in the fuel and NaK loops of the ARE are measured by thermocouples welded to the outside of the pipe walls in which the fluid flows. The

$$1 \le t < 100 \ ,$$

$$100 \le t < 3.16 \times 10^5 \ ,$$

$$t > 3.16 \times 10^5$$

difference between the measured temperature and the actual fluid bulk temperature has been calculated for the most serious case, that is, the fuel circuit (Fig. 94).

For the configuration shown, the heat loss per lineal foot, as given in chap. 6, is:

TEMPERATURE OF OUTSIDE OF PIPE WALL (°F)	HEAT LOSS (Btu/sec·lineal ft)
1150	0.23
1500	0.31

The temperature drop across the fuel film is given by
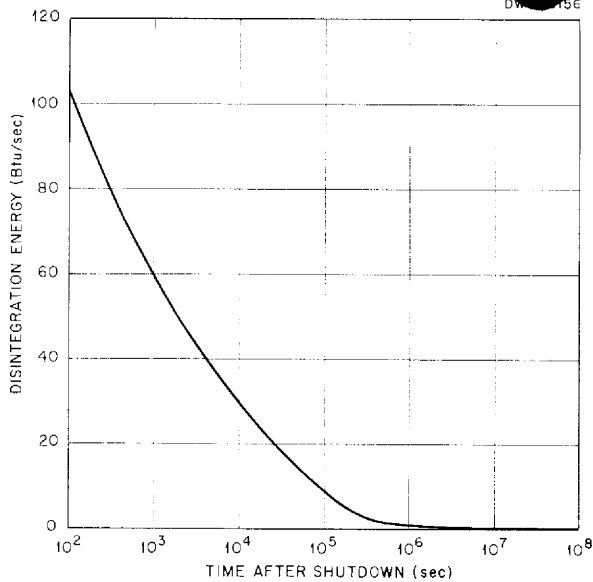
$$\theta = \frac{Q}{hA} \ ,$$

Fig. 93. Disintegration Energy vs. Time after Shutdown.

and the area is given by

$$A = \pi D = \frac{\pi \times 1.049}{12} = 0.275 \ \text{ft}^2/\text{lineal ft},$$

where

θ = temperature difference across fuel film, °F,

Q = heat loss per lineal foot, Btu/sec·lineal ft,

h = fuel heat transfer coefficient, Btu/sec·ft²·°F,

A = heat transfer area per lineal foot, ft²/lineal ft,

D = pipe diameter, ft (1-in., IPS, schedule 40 pipe has an inside diameter of 1.049 in. and an outside diameter of 1.315 in.).

The heat transfer coefficient is given by

$$h = 0.027 \ \frac{k}{D} \text{Re}^{0.8} \ \text{Pr}^{1/3} \left(\frac{\mu}{\mu_s} \right)^{0.14},$$

where

k = fuel thermal conductivity, Btu/sec·ft² (°F/ft),

Re = Reynolds' number,

Pr = Prandtl's number,

μ = viscosity at bulk temperature, lb/hr·ft,

μ_s = viscosity at surface temperature, lb/hr·ft.

For fuel with the properties listed in chap. 1, and a velocity of 6.26 ft/sec,

$$\text{Re}_{1150°\text{F}} = 11,700$$

and

$$\text{Re}_{1500°\text{F}} = 22,300 \ .$$

If it is assumed that $(\mu/\mu_s)^{0.14} \simeq 1$,

$h_{1150°\text{F}} = 0.918 \ \text{Btu/sec·ft}^2 \cdot °\text{F}$,

$h_{1500°\text{F}} = 1.245 \ \text{Btu/sec·ft}^2 \cdot °\text{F}$,

$(hA)_{1150°\text{F}} = 0.253 \ \text{Btu/sec·°F}$,

$(hA)_{1500°\text{F}} = 0.342 \ \text{Btu/sec·°F}$,

$\theta_{1150°\text{F}} = 0.91°\text{F}$,

$\theta_{1500°\text{F}} = 0.91°\text{F}$.

The temperature drop across the pipe wall is

$$\theta_s = \frac{Q \ \ln \dfrac{D_o}{D}}{2\pi k_s},$$

where

θ_s = temperature difference across pipe wall, °F,

D_o = pipe outside diameter, ft,

k_s = thermal conductivity of metal, Btu/sec·ft² (°F/ft),

$\theta_{s,1150°\text{F}} = 2.72°\text{F}$,

$\theta_{s,1500°\text{F}} = 3.67°\text{F}$.

Since the fuel film temperature drop is small and the Reynolds' numbers are high, the difference between the fuel bulk temperature (the so-called "mixing cup" temperature) and the fuel maximum temperature will be very small. The total difference between the fuel bulk temperature and the outside pipe wall temperature is

$$(\theta + \theta_s)_{1150°\text{F}} = 0.91 + 2.72 = 3.63°\text{F},$$

$$(\theta + \theta_s)_{1500°\text{F}} = 0.91 + 3.67 = 4.58°\text{F}.$$

At other thermocouple locations in the fuel circuit, the temperature drop in the fuel film is less than the drop calculated above because the above conditions include the minimum insulation thickness and the minimum Reynolds' number encountered in the system. The temperature drop in the film in the NaK circuit is, of course, very small. The temperature drops
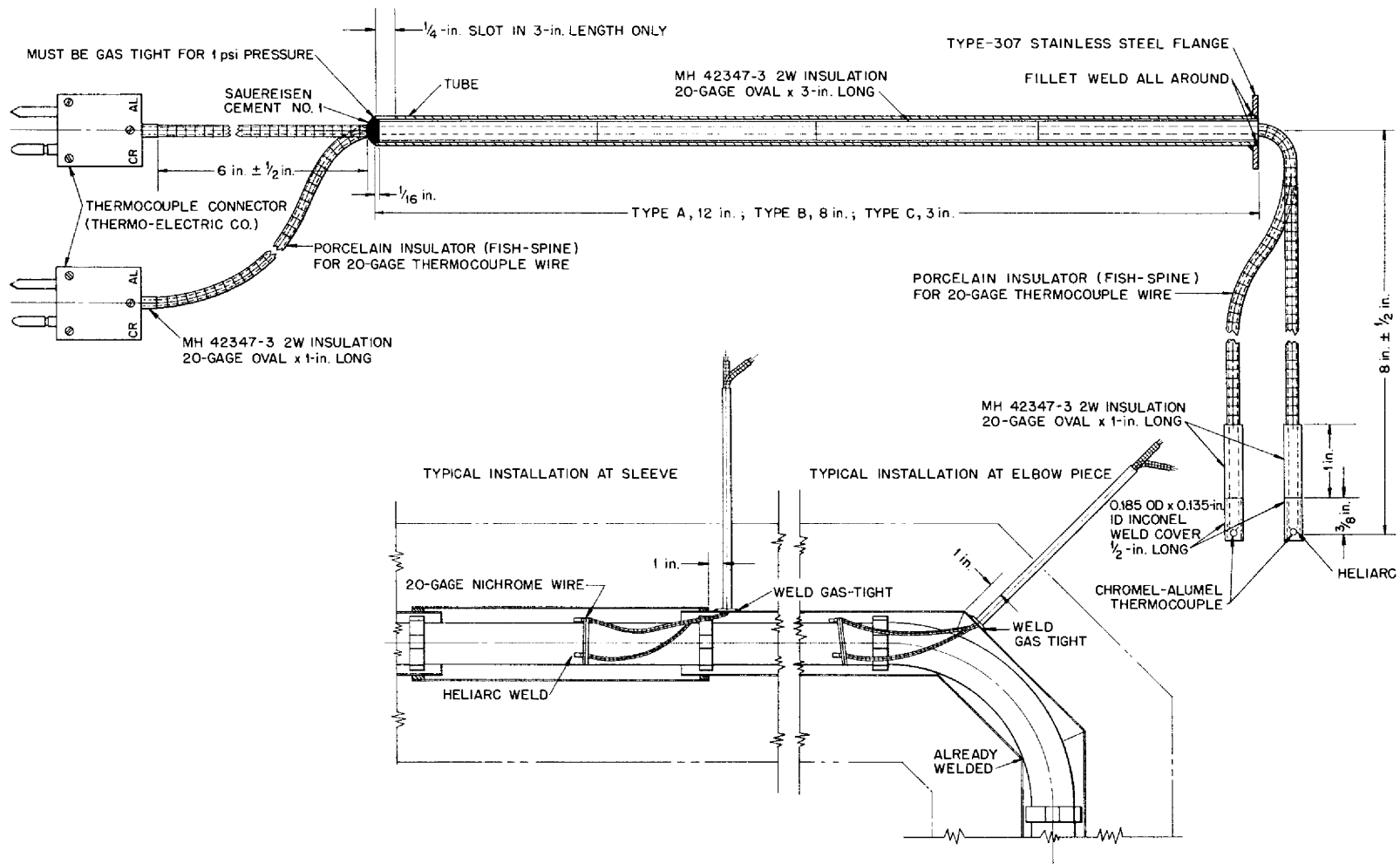
124

Fig. 94. Thermocouple Assembly.

through the pipe wall at various other thermocouple locations are given in Table 23. The maximum temperature differential between the outside of a pipe and the bulk of the fluid is approximately 4.6°F. It is important to note that if the flow rates in either the fuel or NaK circuits are reduced, for some unforseen reason, during operation, the temperature differential between the outside of the pipe wall and the bulk of the fluid will increase. This increase in temperature differential, since it occurs only within the fluid, should not become serious so long as the flow is turbulent; in the laminar region, however, the temperature differential can become great enough to render the thermocouple unreliable.

TABLE 23.   TEMPERATURE DROPS THROUGH THE PIPE WALL AT VARIOUS THERMOCOUPLE LOCATIONS

NOMINAL PIPE DIAMETER (in.)	PIPE WALL TEMPERATURE (°F)	HEAT LOSS (Btu/sec·lineal ft)	θ_m (°F)
1 1/2	1150	0.23	1.98
	1500	0.31	2.67
2	1150	0.21	1.53
	1500	0.29	2.11
2 1/2	1150	0.23	1.73
	1500	0.31	2.33

1. J. H. Keenan and J. Kaye, *Gas Tables*, Wiley, New York, 1948.

2. C. D. Hodgman, *Handbook of Chemistry and Physics*, 31st ed., Chemical Rubber Publishing Co., 1949.

3. M. C. Udy and F. W. Boulger, *The Properties of Beryllium Oxide*, BMI-T-18 (Dec. 15, 1949).

4. *NBS-NACA Tables of Thermal Properties of Gases*, U. S. Department of Commerce, National Bureau of Standards:

H. W. Wooley, Table 6.10, "Helium (Ideal Gas State)," July 1950;

R. L. Nuttall, Table 6.39, "Helium (Coefficient of Viscosity)," December 1950;

R. L. Nuttall, Table 6.42, "Helium (Thermal Conductivity)," December 1950.

5. *The Engineering Properties of Inconel*, International Nickel Co. Tech. Bull. T-7.

6. R. N. Lyon (Editor-in-Chief), *Liquid Metals Handbook*, 2d ed., NAVEXOS P-733 (rev.), June 1952.

7. *Stainless Steel for Elevated Temperature Service*, U.S. Steel Corp.

8. D. Q. Kern, *Process Heat Transfer*, McGraw-Hill, New York, 1950.

9. J. H. Perry, *Chemical Engineers' Handbook*, 3d ed., McGraw-Hill, New York, 1950.

10. H. F. Poppendiek and L. D. Palmer, *Forced Convection Heat Transfer in Pipes with Volume Heat Sources Within the Fluid*, ORNL-1395 (Dec. 2, 1952).

11. W. H. McAdams, *Heat Transmission*, 2d ed. (rev.), McGraw-Hill, New York, 1942.

12. G. N. Cox and F. J. Germano, *Fluid Mechanics*, Van Nostrand, New York, 1941.

13. *Flow of Fluids Through Valves, Fittings, and Pipe*, Crane Co. Tech. Paper No. 409, May 1942.

14. M. Jakob, *Heat Transfer*, Vol. I, Wiley, New York, 1949.

15. E. N. Sieder and G. E. Tate, *Ind. Eng. Chem.* **28**, 1429-1435 (1936).

16. K. A. Gardner, *Trans. Am. Soc. Mech. Engrs.* **67**, 621-631 (1945).

17. A. Y. Gunter and W. A. Shaw, *Trans. Am. Soc. Mech. Engrs.* **67**, 643-660 (1945).

18. W. Nusselt, *Z. Ver. deut. Ing.* **73**, 1475 (1929).

19. W. J. King, *Mech. Eng.* **54**, 347 (1932).

20. E. Schmidt, *Fopp ls Festschrift*, p. 179, Springer, Berlin, 1924; and *Z. Ver. deut. Ing.* **75**, 969 (1931).

21. The Trane Co. Bulletin D-S 365, September 1951.

22. H. L. F. Enlund, personal communication, 1952.

23. K. Way and E. P. Wigner, *Phys. Rev.* **73**, 1318-1330 (1948).

24. S. L. Jameson, *Trans. Am. Soc. Mech. Engrs.* **67**, 633-642 (1945).

25. Johns-Manville Products General Catalog, DS Series 2.

26. M. W. Zemansky, *Heat and Thermodynamics*, 3d ed., McGraw-Hill, New York, 1951.